

# Flapping Foil Propulsion for Cruising and Hovering Autonomous Underwater Vehicles

by

Victor Polidoro

Submitted to the Department of Ocean Engineering  
in partial fulfillment of the requirements for the degree of

Master of Science in Ocean Engineering

at the

MASSACHUSETTS INSTITUTE OF TECHNOLOGY

May 2003

© Massachusetts Institute of Technology 2003. All rights reserved.

Author .....

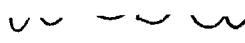


.....

Department of Ocean Engineering  
May 22, 2003


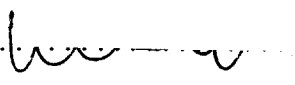
. n

Certified by.....



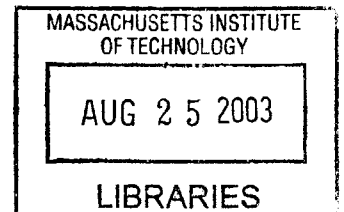
Michael S. Triantafyllou  
Professor of Ocean Engineering  
Thesis Supervisor

Accepted by .....



Michael S. Triantafyllou  
Chairman, Departmental Committee on Graduate Students

BARKER





# Flapping Foil Propulsion for Cruising and Hovering Autonomous Underwater Vehicles

by

Victor Polidoro

Submitted to the Department of Ocean Engineering  
on May 22, 2003, in partial fulfillment of the  
requirements for the degree of  
Master of Science in Ocean Engineering

## Abstract

This thesis describes the design, construction, and testing of an autonomous underwater vehicle capable of high precision positioning and hovering using flapping foils as actuators. The vehicle is 2 m long with an approximate displacement of 157 kg. Four flapping foils, each actuated by two motors, performing a two degree of freedom angular motion (roll and pitch motion) provide the necessary forces for maneuvering and propulsion. The design of the actuators is based on an extensive hydrodynamic database for two and three dimensional foils developed at the Testing Tank and the Propeller Tunnel facilities. The foils have dimensions 0.4 m span and 0.1 m chord and are capable of producing peak lift forces up to 100 N, peak thrust forces up to 70 N, and mean thrust forces up to 37 N. Flapping foils can provide large forces (up to an order of magnitude larger than steadily translating foils) very rapidly.

Experiments were performed with an individual foil actuator over a range of foil sizes ( $s/c = 6, 5, 4, 3$ ) and wake widths ( $1.4 \leq h_0/c \leq 6.3$ ). Planform area thrust coefficients of 7.2 were recorded at a Strouhal number of 1.2. The coefficient of thrust was found to be a strong function of the Strouhal number and maximum angle of attack and a weak function of the wake width in this regime. The size of the foil was the primary factor controlling the trade off between the magnitude and bandwidth of the thrust forces produced.

Thesis Supervisor: Michael S. Triantafyllou  
Title: Professor of Ocean Engineering



## Acknowledgments

I would like to thank my advisor Professor Michael Triantafyllou for his generous support and his kind words of encouragement. His insight into hydrodynamics and controls have changed my perspective of physics. His curiosity and foresight have provided the direction and motivation for this work.

I would like to thank Dr. Franz Hover for introducing me to the Towtank and getting me involved with this vehicle. If I had never met Franz, I definitely would not have attended MIT. Throughout this project Franz has always taken the time to discuss every problem and idea.

All the design and fabrication work for this vehicle was accomplished as a collaborative effort with Stephen Licht. I could not have asked for a better partner on this project. I would have been overwhelmed without him to lean on. Anyone reading this thesis must also read his.

Dave Beal was a great friend and an excellent source of advice. I asked Dave more questions than anyone.

I would like to thank Melissa Flores for the countless hours she worked at the water tunnel gathering data that directly contributes to this vehicle. Be sure to read her thesis as well.

I would like to thank Fred Cote for teaching me nearly everything I know about machining. Fred offered advice and hands on help for almost every part on the vehicle.

I would like to thank Tom Consi for his valuable advice on electronics and for the fabrication materials and computer he contributed to this vehicle.

I would like to thank Jim Bales for his advice on batteries and power management.

I would like to thank Jeff Stettler for his help with the dynamometer and calibration rig.

I would like to thank Justin Manley for his advice on vehicle maintenance and deployment.

I thank Karl McLetchie for his foil molds and his help with  $\text{\LaTeX}2\epsilon$

# Contents

<b>List of Figures</b>	<b>13</b>
<b>List of Tables</b>	<b>15</b>
<b>Nomenclature</b>	<b>17</b>
<b>1 Flapping Foil Propulsion and Biomimetic Design</b>	<b>19</b>
1.1 Hydrodynamics and Mechanics . . . . .	20
1.1.1 Wake Structure . . . . .	24
1.1.2 Kinematics . . . . .	26
1.1.3 Dynamics . . . . .	32
1.1.4 Control . . . . .	34
1.2 Previous Work with Flapping Foil Robotics . . . . .	37
1.2.1 Autonomous Vehicles . . . . .	37
1.2.2 Externally Propelled Robotic Platforms . . . . .	46
<b>2 Design and Fabrication of AUV</b>	<b>51</b>
2.1 Purpose of Vehicle . . . . .	51
2.2 Design Criteria . . . . .	53
2.2.1 Mission Length and Location . . . . .	54
2.2.2 Depth Rating . . . . .	55
2.2.3 Dimensions . . . . .	55
2.3 Vehicle Layout . . . . .	55
2.3.1 Modularity and Scalability . . . . .	55

2.3.2	Planes of Symmetry . . . . .	56
2.3.3	Mass, Hydrostatic Stability and Net Buoyancy . . . . .	56
2.3.4	Added Mass and Drag Considerations . . . . .	57
2.4	Control and Communication . . . . .	57
2.4.1	Single Board Computer Running Linux . . . . .	57
2.4.2	Distributed Motion Control on Ethernet Network . . . . .	59
2.5	Sensors . . . . .	60
2.5.1	Inertial Measurement Unit . . . . .	60
2.5.2	Three Axis Magnetometer . . . . .	61
2.5.3	Leak Detectors . . . . .	62
2.6	Batteries and Power Management . . . . .	62
2.6.1	Diodes for Preventing Accidental Charging or Discharging of the Batteries . . . . .	63
2.6.2	Voltmeter on Batteries . . . . .	63
2.6.3	Ammeter on Power Supply to Each Foil Actuator . . . . .	63
2.6.4	Digital I/O and Relays . . . . .	63
2.6.5	Magnetic Switches and LEDs . . . . .	64
<b>3</b>	<b>Design of Foil Actuators</b>	<b>65</b>
3.1	Single Housing Design . . . . .	68
3.2	Two Housing Design . . . . .	74
<b>4</b>	<b>Force Measurements</b>	<b>81</b>
4.1	Description of Tests . . . . .	84
4.1.1	Setup . . . . .	84
4.1.2	Sensors and Calibration . . . . .	85
4.1.3	Data Acquisition and Control . . . . .	88
4.1.4	Sources of Error . . . . .	88
4.1.5	Testing Procedure . . . . .	90
4.1.6	Postprocessing . . . . .	92
4.2	Cruising Data . . . . .	93



4.3 Discussion of Results . . . . .	108
<b>5 Design Recommendations</b>	<b>109</b>
<b>A Cruising Forces in Time</b>	<b>115</b>



# List of Figures

1-1	Diagram of a reverse von Kármán vortex street . . . . .	24
1-2	Flow visualization of a wake behind a flapping foil . . . . .	25
1-3	Distance from center of roll axis to the root of the foil, $r_0$ . . . . .	28
1-4	Angle of attack diagram . . . . .	29
1-5	Angle of attack distribution over span . . . . .	31
1-6	Periodic lift and thrust forces . . . . .	32
1-7	Tail Section of the RoboPike — John Kumph. . . . .	38
1-8	John Kumph and the RoboPike. . . . .	39
1-9	Draper Laboratory free swimming robotic tuna. . . . .	40
1-10	Drawing of the Draper tuna. — Draper Laboratory . . . . .	41
1-11	Draper tuna at Nickerson State Park. . . . .	41
1-12	Robotic fish with 3DOF pectoral fins. — Naomi Kato . . . . .	42
1-13	The first generation robotic dolphin with pneumatics. — Motomu Nakashima . . . . .	43
1-14	The first generation robotic dolphin with pneumatics. — Motomu Nakashima . . . . .	43
1-15	The second generation robotic dolphin with batteries and an electric motor. — Motomu Nakashima . . . . .	44
1-16	RoboTuna — Dave Barrett. . . . .	45
1-17	RoboTunaII — Dave Beal, Mike Sachinis, Mike Jakuba. . . . .	47
1-18	SeaLion — Craig Martin. . . . .	49
2-1	AUV in the sea turtle configuration. . . . .	52

2-2	AUV power, control, and communication schematic . . . . .	58
3-1	Single housing foil actuator. . . . .	69
3-2	Single housing foil actuator. . . . .	69
3-3	Drawings of single housing foil actuator. . . . .	70
3-4	Inside of single housing foil actuator. . . . .	71
3-5	Drawings of the bellows. . . . .	72
3-6	Drawings of the bellows assembly . . . . .	73
3-7	Two housing foil actuator. . . . .	75
3-8	Drawings of the two housing foil actuator. . . . .	75
3-9	Inside the two housing foil actuator. . . . .	76
3-10	Close up of the roll shaft coupling . . . . .	77
3-11	Drawings of the pitch seal boot. . . . .	78
3-12	Drawings of the pitch seal assembly with shaft seal. . . . .	79
4-1	Two housing foil actuator mounted to the six axis dynamometer. . . . .	85
4-2	Calibration rig used to apply force at the 70% span, $r_{0.7}$ . . . . .	86
4-3	Calibration curve for thrust axis. . . . .	87
4-4	Calibration curve for lift axis. . . . .	87
4-5	Calibration curve for ammeter. . . . .	88
4-6	Spectrum of mechanical vibrations and line noise . . . . .	91
4-7	A typical case: $St = 0.6$ , $\alpha_{max} = 40$ deg, $s = 0.40$ m, $\phi_0 = 40$ deg . . . . .	95
4-8	A high thrust case: $St = 1.2$ , $\alpha_{max} = 40$ deg, $s = 0.40$ m, $\phi_0 = 60$ deg . . . . .	96
4-9	A high efficiency case: $St = 1.0$ , $\alpha_{max} = 30$ deg, $s = 0.40$ m, $\phi_0 = 60$ deg . . . . .	97
4-10	Contour plots for coefficient of thrust $C_T$ : $s = 0.60$ , $\phi_0 = \{60,40,20\}$ . . . . .	99
4-11	Contour plots for coefficient of thrust $C_T$ : $s = 0.50$ , $\phi_0 = \{60,40,20\}$ . . . . .	100
4-12	Contour plots for coefficient of thrust $C_T$ : $s = 0.40$ , $\phi_0 = \{60,40,20\}$ . . . . .	101
4-13	Contour plots for coefficient of thrust: $s = 0.30$ , $\phi_0 = \{60,40,20\}$ . . . . .	102
4-14	Summary of contour plots for coefficient of thrust $C_T$ . . . . .	103
4-15	Summary of contour plots for mean thrust $\bar{F}_x$ [N], with $St$ . . . . .	104

4-16	Summary of contour plots for operational efficiency $\eta_{op}$ , with $St$ . . .	105
4-17	Summary of contour plots for mean thrust $\bar{F}_x$ [N], with $f$ . . . . .	106
4-18	Summary of contour plots for operational efficiency $\eta_{op}$ , with $f$ . . . .	107



# List of Tables

2.1	Mass and buoyancy of major components . . . . .	56
3.1	Specifications of roll and pitch motors . . . . .	67
3.2	List of variables for program running on motion control card. . . . .	68
4.1	Force and moment capacities for six axis dynamometer . . . . .	86





# Nomenclature

$c$	foil chord [ $m$ ]
$s$	foil span [ $m$ ]
$U$	steady vehicle forward velocity, steady towing speed in experiments [ $m/s$ ]
$\rho$	fluid density [ $kg/m^3$ ]
$\nu$	fluid kinematic viscosity [ $m^2/s$ ]
$Re_c$	chord Reynolds number, $Uc/\nu$ [—]
$\alpha_{max}$	maximum angle of attack [ $radians$ ] in equations, [ $degrees$ ] in text
$\theta_0$	amplitude of sinusoidal pitch motion $\theta(t)$ [ $radians$ ] in equations, [ $degrees$ ] in text
$\phi_0$	amplitude of sinusoidal roll motion $\phi(t)$ [ $radians$ ] in equations, [ $degrees$ ] in text
$\psi$	phase between roll and pitch [ $radians$ ]
$r_0$	distance from center of roll axis to root of the foil [ $m$ ]
$r_{0.7}$	distance from center of roll axis to 70% of span, $r_0 + 0.7s$ [ $m$ ]
$r_{0.7}/r_0$	a measure of the range of the angle of attack distribution over span [—]
$2h_0$	wake width at $r_{0.7}$ (arclength), $2r_{0.7}\phi_0$ [ $m$ ]
$h_0/c$	normalized wake width [—]
$f$	frequency of foil motion [ $s^{-1}$ ]
$T$	period of foil motion [ $s$ ]
$\omega$	frequency of foil motion [ $radian/s$ ]
$St$	Strouhal number, $2r_{0.7}\phi_0 f/U$ [—]
$F_x(t)$	thrust force; mean value $\bar{F}_x$ [ $N$ ]

$F_y(t)$	lift force; mean value $\bar{F}_y$ [N]
$C_T$	mean thrust coefficient, $2\bar{F}_x/\rho U^2 cs$ [-]
$C_L$	mean lift coefficient, $2\bar{F}_y/\rho U^2 cs$ [-]
$V$	voltage of power supply (always 24 volts) [V]
$I_{@24}(t)$	current supplied to actuator at 24 volts; mean value $\bar{I}_{@24}$ [A]
$P(t)$	electrical power supplied to actuator, $VI_{@24}(t)$ ; mean value $\bar{P}$ [W]
$\eta_{op}$	operational efficiency, $\bar{F}_x U/\bar{P}$ [-]

# Chapter 1

## Flapping Foil Propulsion and Biomimetic Design

Considerable theoretical, numerical, and experimental work has been done to investigate the physics of swimming and flying [19] [24] [12] [4] [7] [5] [21] [14]. The success of this body of work has greatly improved the general understanding of the hydrodynamics of fish swimming. One of the prime motivations for this body of work was to provide an understanding of hydrodynamics that could be used to improve the design and performance of underwater vehicles. A man-made machine that successfully exploits the hydrodynamics of fishlike swimming could have greatly improved maneuvering and hovering capabilities, while maintaining the ability to cruise efficiently. A simple and robust vehicle of this nature could serve as an extremely powerful mapping and surveying tool for oceanographers and underwater archeologists. Improved maneuvering and hovering capabilities would enable the vehicle to operate in confined spaces, at low speeds, near the surface, and in unsteady flow conditions. Existing AUVs are incapable of operating in such conditions due the limited maneuvering capabilities of vehicles with propellers and conventional lifting surfaces.

The goal of the work presented in this thesis is to apply this knowledge of hydrodynamics to the design of an autonomous underwater vehicle (AUV). Knowledge gained from the design and implementation of this AUV will help transition flapping foil propulsion from the laboratory to the ocean. One of the major hurdles remain-

ing in developing this form of propulsion into a technology that can be implemented in the ocean is to find a mechanical design that is simple and robust enough to be useful. Most of the previous work in designing autonomous flapping foil vehicles [17] [3] has strived to exactly replicate the morphology of a particular species of living fish. While these robots were extremely well designed and well built, they were also too complicated and had too little room for payload instrumentation to be used as a piece of laboratory equipment for oceanography. The focus of the current vehicle was to strive for the simplest design possible to minimize the time and cost for fabrication and maintenance. While the design of this vehicle was not based directly on any particular animal, the location and motion of the foils are similar to a sea turtle. It has a rigid frame to simplify the sealing problems and to make it easier to leave room for payload sensors. This vehicle has four flapping foils that each move with two degrees of freedom.

## 1.1 Hydrodynamics and Mechanics

Flapping foil propulsion is a common mode of locomotion in nature. Birds, flying insects, fish, and cetaceans move with grace and agility. These animals are capable of maneuvers that are currently impossible for machines. Some of these animals are optimal for straight line cruising, while others have an astounding capability to accelerate and turn. Dolphins and tuna are capable of high cruising efficiency [23] [10]. Hummingbirds and dragonflies have stellar hovering capabilities. Sharks and pikes are highly agile and maneuverable predators. All of these animals use some form of flapping foil propulsion. From the perspective of hydrodynamics, aerodynamics, and biology, the investigation of flapping foil propulsion is well justified.

Similarities in the morphologies of various species of fish and cetaceans indicate there is something fundamental in the hydrodynamics of swimming. It was noted that shape and motion of the lunate caudal fin of dolphins and tuna were remarkably similar [19]. The convergence to similar optimal solutions from substantially different initial conditions indicates that there is something universal about these

particular geometries and kinematics. Purely from the perspective of hydrodynamics the optimal design should be expected to be independent of the mechanical means of actuation. However, this view completely disregards the complexities and efficiency losses within the body itself. While there are notable differences between the biomechanics of mammals and fish, these differences are very subtle compared to the differences between machines and animals. Given that the initial conditions for the design of mechanical fish are so drastically different from the initial conditions of animals, it is not safe to assume the design will again converge to the same optimal solution. If this convergence does eventually occur, there will first need to be great advances in artificial muscles.

While it is easy to draw inspiration from the wonders of nature, it is important to remember that animals are made of very different materials than machines. There is certainly no reason to expect that the optimal design in nature will be manifested in the identical form as a machine. The dynamic characteristics of muscles are far different from those of electric motors, combustion engines, and hydraulic pistons. Currently available artificial muscles are very limited by either low bandwidth, low displacement, or low efficiency. The sealing and elastic properties of skin are far superior to the material properties of flexible rubbers and composites. Even primitive animals have a brain and nervous system that is capable of producing highly robust and adaptive behavior. Tissues that are grown can be far more complex than parts that are machined or molded. It is also important to consider that the morphology and behavior of animals are subject multiple evolutionary forces [9]. The aerodynamics of a bird's tail may not be optimal if the size and shape of the tail is also used for attracting a mate [1].

A successful strategy for designing a biomimetic robot should acknowledge the key differences in the fundamental building blocks. A mechanical design that strives to exactly replicate an animal will not be optimal if the properties of the components are drastically different. Design of biomimetic robots is a constrained optimization problem. While the constraints on the biological solutions are far different from the constraints on the mechanical solutions, the optimal design should be expected to

differ. While evolution produces extraordinary solutions, there is no planning or insight in the process. Designers are limited only by their available materials and understanding of physics. Changes between generations of complex machinery are not random, they are the result of deliberate attempts at improving performance or reducing complexity.

The idea of exploiting the hydrodynamics of fishlike swimming to improve the performance of underwater vehicles [24] has been introduced at a time when the requisite technologies for robotics are immature. The performance of future generations of flapping foil vehicles will greatly depend on advances made in artificial muscles, batteries, flow sensors, and controls. The design process is strongly time variant. Clearly the selection of components depends on the availability of materials. Acknowledging the limits on the availability of actuators and materials, the focus of future hydrodynamic research should include a search for kinematics that will be easier for machines to achieve. In order to simplify the mechanical aspects of the problem it is necessary to search for the simplest kinematics with the fewest degrees of freedom that will still result in optimal hydrodynamic forces. Complexity in mechanical design does not scale linearly with the degrees of freedom of motion.

There are many similarities between the current state of flapping foil vehicles and helicopters in the 1920's. The performance of early helicopter designs were greatly limited by the available engines and structural materials. As knowledge of rotary wing aerodynamics rapidly progressed, the performance was restricted mostly by the mechanics. Igor Sikorsky had limited success with his early helicopter designs due to current state of technology in the components. Early helicopters were plagued by lack of power and vibration. Progress depended strongly on the general understanding of metallurgy and combustion. Now, in retrospect, Sikorsky's designs were remarkably modern and sophisticated. He was on the right path and he has received universal recognition as a visionary. There are similarities between the kinematics of rotary wing aerodynamics and flapping foil hydrodynamics. Many of the lessons learned in the design, control, and maintenance of helicopters will provide insight into the design of flapping foil vehicles. There are many ideas in the designs of cyclic and

collective pitch control mechanisms on helicopters that could be applied to flapping foil actuators.

Due to the tremendous success of previous research in the hydrodynamics of flapping foil propulsion, the performance of flapping foil vehicles is now mostly limited by the general understanding of the mechanical and control aspects of the problem. Some of the most daunting tasks in the mechanics and controls could be simplified through research in hydrodynamics. There are certainly many issues that remain to be explored in hydrodynamics. These areas involve three dimensional flow effects, the geometry and compliance of the foil, methods for manipulating upstream vorticity, and cavitation. In addition to these areas, the direction for future research into the hydrodynamics of flapping foil propulsion should be directed towards reducing the complexity of the kinematics and finding regimes with the greatest forgiveness to errors in the angle of attack profile. Due to the necessity of the flow velocity in calculating the kinematics, the performance of flapping foil propulsion will be highly sensitive to the accuracy of the estimated or measured value of the incoming flow velocity upstream of the foils. Flapping foil propulsion could be applied to a much wider variety of vehicles if this knowledge of the incoming flow velocity was not necessary. The technological impact of flapping foil propulsion would be much greater if flapping foil actuators could effectively be used for propulsion and maneuvering without knowledge of the local flow velocity.

Progress in flapping foil propulsion will depend on the availability of advanced artificial muscles, batteries, and velocimeters. Specifically we need batteries with greater power density and actuators with dynamic characteristics like fast twitch muscles. In order to take full advantage of the potential of flapping foil propulsion, the powertrain needs to be able to deliver rapid bursts of energy. Fast starts require large forces quickly. The majority of muscle tissue in fish is only used for quick bursts of energy to rapidly accelerate or turn [25], while a very small portion of the muscles have the endurance for cruising. A highly advanced flapping foil vehicle would have two types of artificial muscles or motors in parallel. One type of actuator would deliver the explosive power for rapid starts and aggressive maneuvers and the other

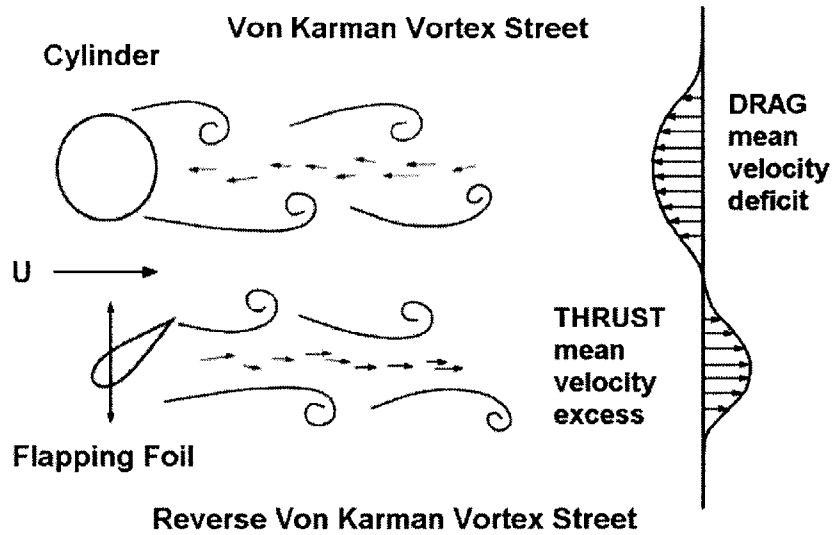


Figure 1-1: Diagram of a reverse von Kármán vortex street. The foil motion repositions the vortices in the wake to form a thrust jet.

would be used for cruising with high efficiency.

### 1.1.1 Wake Structure

One of the major hydrodynamic benefits of flapping foil propulsion is that the wake structure is very simple and natural, it is the reverse of a common drag wake known as a von Kármán vortex street. In a von Kármán street the vortices are shed in an alternating pattern that results in a mean velocity deficit behind the body. For a steady upstream flow, this velocity deficit is manifested as a reduction of the momentum flux in the streamwise direction. By conservation of momentum, a decrease in the streamwise momentum of the fluid must result in a net drag force on the body.

The beauty of flapping foil propulsion is that the motion of the foil is simply reversing the shedding pattern of the vortices in the von Kármán street to result in a net velocity excess behind the body. As the foil imparts additional downstream momentum into the fluid, there is a net thrust force on the body. This is a very simple and elegant means of transforming drag into thrust.



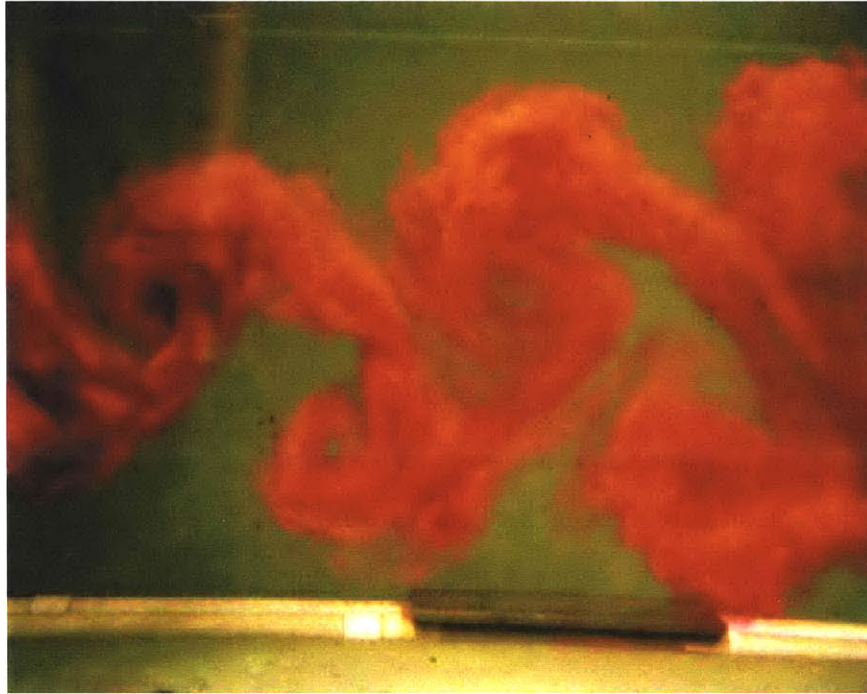


Figure 1-2: Flow visualization of a wake behind a flapping foil -Øyvind Haugsdal [14]

One of the major benefits of a simple wake structure is that it now becomes possible to devise control strategies to superimpose existing upstream vorticity with the downstream wake in such a way that the foil can recover energy from the flow [2] [8]. With existing upstream vorticity in the flow, a flapping foil actuator could achieve hydrodynamic efficiency greater than 100% by extracting some of the existing kinetic energy from the flow. This is how rainbow trout are able to swim upstream so efficiently [18]. The ability to manipulate upstream vorticity gives flapping foil propulsion enormous potential for improving the efficiency of underwater vehicles. While this aspect of flapping foil propulsion is too complicated to implement on a vehicle in the short term, a vehicle that is able to manipulate upstream vorticity will have greatly improved efficiency in the wake of another vehicle. This strategy could give AUVs the ability to exhibit schooling to cruise to a survey sight. The net efficiency of the group of vehicles could be greatly improved if the downstream vehicles could recover energy from the wakes of upstream vehicles. Manipulating upstream vorticity may also give AUVs the capability of operating in the surf zone.

The most common form of propulsion in marine applications is obviously the propeller. The wake structure of a propeller is far more complex than the wake behind a flapping foil. The geometry of a propeller is more complex and difficult to manufacture than a foil. The major advantage that propellers currently have over flapping foils is that the drivetrain supplying power to the propeller is drastically simpler and more efficient than the existing designs for drivetrains of flapping foils. The drivetrain is defined to be every component that transfers either electrical or mechanical energy. Engines and electric motors perform best when turning at a constant speed, which makes them ideally suited to supply energy to a propeller. The other advantage that propellers currently have is that their performance for straight cruising is not as sensitive to the knowledge of the incoming flow.

### 1.1.2 Kinematics

In this work foils are moved with two rotational motions. The large displacement flapping motion of the wing is referred to as the roll motion. The twisting or feathering of the wing is referred to as the pitch motion. The terms roll and pitch were selected to be consistent with conventional ship and vehicle notation. Linear motions and the yaw rotational motion are not used to minimize the complexity of the mechanical design.

#### Equations of motion for three dimensional kinematics

The roll and pitch motions of the foil are both sinusoidal, and this is sometimes referred to as simple harmonics.

The roll position of the foil is defined as,

$$\phi(t) = \phi_0 \sin(\omega t) + \phi_{bias} \tag{1.1}$$

where  $\phi_0$  is the roll amplitude in radians and  $\omega$  is the frequency of the foil motion in radians per second.  $\phi_{bias}$  is a static roll bias used to change the mean roll position

of the foil.  $\phi_{bias}$  is normally zero, but may be used, for example, to prevent a downstream foil from intercepting an upstream wake.

The pitch position of the foil is defined as,

$$\theta(t) = \theta_0 \sin(\omega t + \psi) + \theta_{bias} \quad (1.2)$$

where  $\theta_0$  is the pitch amplitude in radians and  $\psi$  is the phase angle between pitch and roll in radians.  $\theta_{bias}$  is a static pitch bias used for maneuvering, and is normally equal to zero. For this work the phase angle  $\psi$  is always  $\pi/2$ <sup>1</sup> and we can therefore write  $\theta(t)$  as,

$$\theta(t) = \theta_0 \cos(\omega t) + \theta_{bias} \quad (1.3)$$

A rolling and pitching foil is referred to as having three dimensional kinematics because the angle of attack varies over the span of the foil, refer to Figure 1-5. The heaving and pitching kinematics used in previous work [21] [14] is referred to as two dimensional because the angle of attack is constant over the span of the foil. The three dimensional (rolling and pitching) kinematics are collapsed to two dimensions (heaving and pitching) at one span location on the foil. This location was selected to be 70% from the root of the foil. This location was selected because it is close to the effective center of hydrodynamic force on the foil and also to be consistent with conventional propeller notation. This location is referred to as  $r_{0.7}$ , and is defined,

$$r_{0.7} = r_0 + 0.7s \quad (1.4)$$

where  $r_0$  is the distance from the center of the roll axis to the root of the foil, and  $s$  is the span of the foil, refer to Figure 1-3.

---

<sup>1</sup>This phase angle was selected based on the results of Doug Read's experiments with a heaving and pitching foil.[21]

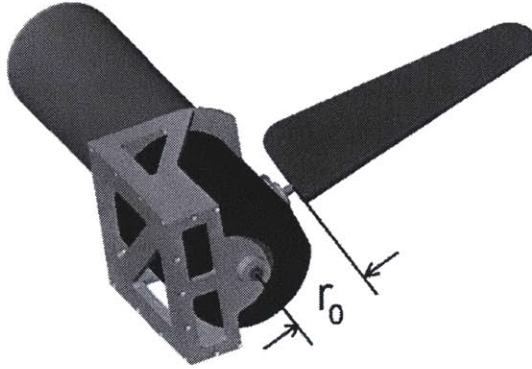


Figure 1-3: Distance from center of roll axis to the root of the foil,  $r_0$

The amplitude of heave motion (arclength) at  $r_{0.7}$  is referred to as  $h_0$ , and is defined,

$$h_0 = r_{0.7}\phi_0 \quad (1.5)$$

The heave motion is defined as

$$h(t) = h_0 \sin(\omega t) \quad (1.6)$$

For two dimensional kinematics the angle of attack is defined as,

$$\alpha(t) = -\arctan\left(\frac{\dot{h}(t)}{U}\right) + \theta(t) \quad (1.7)$$

where  $U$  is the forward speed of the foil, and  $\dot{h}$  is the heave velocity,

$$\dot{h}(t) = \omega h_0 \cos(\omega t) \quad (1.8)$$

Using our definition of  $h_0$ ,

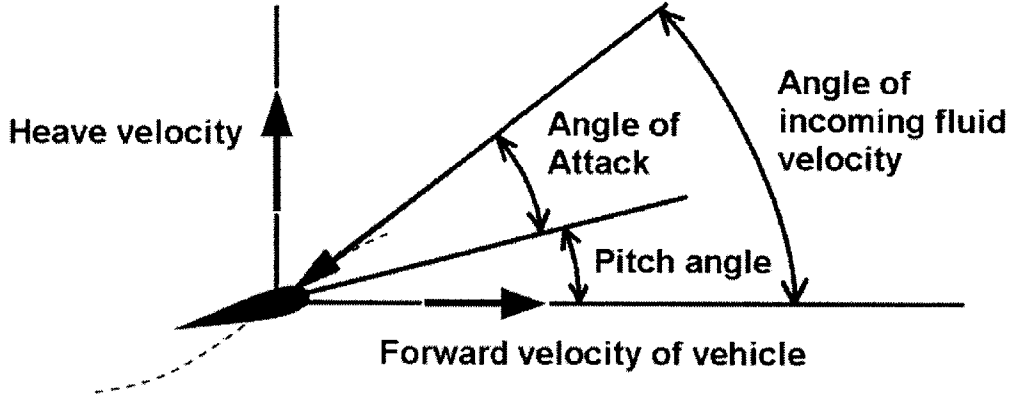


Figure 1-4: Angle of attack at one span location — The angle of attack has two components, one due to the ratio of two velocities, and another due to the instantaneous pitch position of the foil.

$$\dot{h}(t) = \omega r_{0.7} \phi_0 \cos(\omega t) = r_{0.7} \dot{\phi}(t) \quad (1.9)$$

Now for three dimensional kinematics we can express the angle of attack as,

$$\alpha(t) = \underbrace{-\arctan\left(\frac{\omega r_{0.7} \phi_0 \cos(\omega t)}{U}\right)}_{\text{roll induced}} + \underbrace{\theta_0 \cos(\omega t) + \theta_{bias}}_{\text{pitch induced}} \quad (1.10)$$

Note that for positive  $\theta_0$  the pitch motion is selected to reduce the maximum angle of attack, which is the case for vast majority of the motions that produce thrust. In these cases the leading edge of the foil is rotated towards the direction of incoming flow.  $\theta_{bias}$  is used to make the mean angle of attack nonzero, and therefore the mean lift force nonzero.[21] Nonzero lift forces allow for the thrust vector to be rotated out of the surge direction in order to produce maneuvering forces on the vehicle.

The maximum angle of attack is calculated at  $r_{0.7}$ ,

$$\alpha_{max} = \max[\alpha(t)] \quad (1.11)$$

## Dimensionless parameters in kinematics

In order to make the knowledge gained from experiments as general as possible, scaling analysis is applied to the results. Scaling analysis involves finding dimensionless numbers through Buckingham  $\pi$  theory. The relationships between the correct dimensionless parameters reveals fundamental aspects of the physics.

The most important dimensionless parameter in flapping foil propulsion is the Strouhal number [23]. The Strouhal number,  $St$ , can be thought of in two ways. The Strouhal number is the normalized heave velocity. The Strouhal number also describes the geometric spacing of the vortices in the wake.

For three dimensional kinematics, the Strouhal number is defined,

$$St = \frac{2r_{0.7}\phi_0 f}{U} \quad (1.12)$$

Since a radian is dimensionless, the maximum angle of attack is also a dimensionless parameter. For a particular geometry, the  $St$  and  $\alpha_{max}$  together capture the physics of the foil motion.

$$\alpha_{max} \quad (1.13)$$

The wake width is determined mostly by the amplitude of the heave motion. The amplitude of heave motion is nondimensionalized by the chord of the foil,

$$\frac{h_0}{c} \quad (1.14)$$

The distribution of the angle of attack profile, as seen in Figure 1-5, could be described by the ratio of the heave velocities at two locations. Likewise it could simply be described by the ratio of two radii,

$$\frac{r_{0.7}}{r_0} \quad (1.15)$$

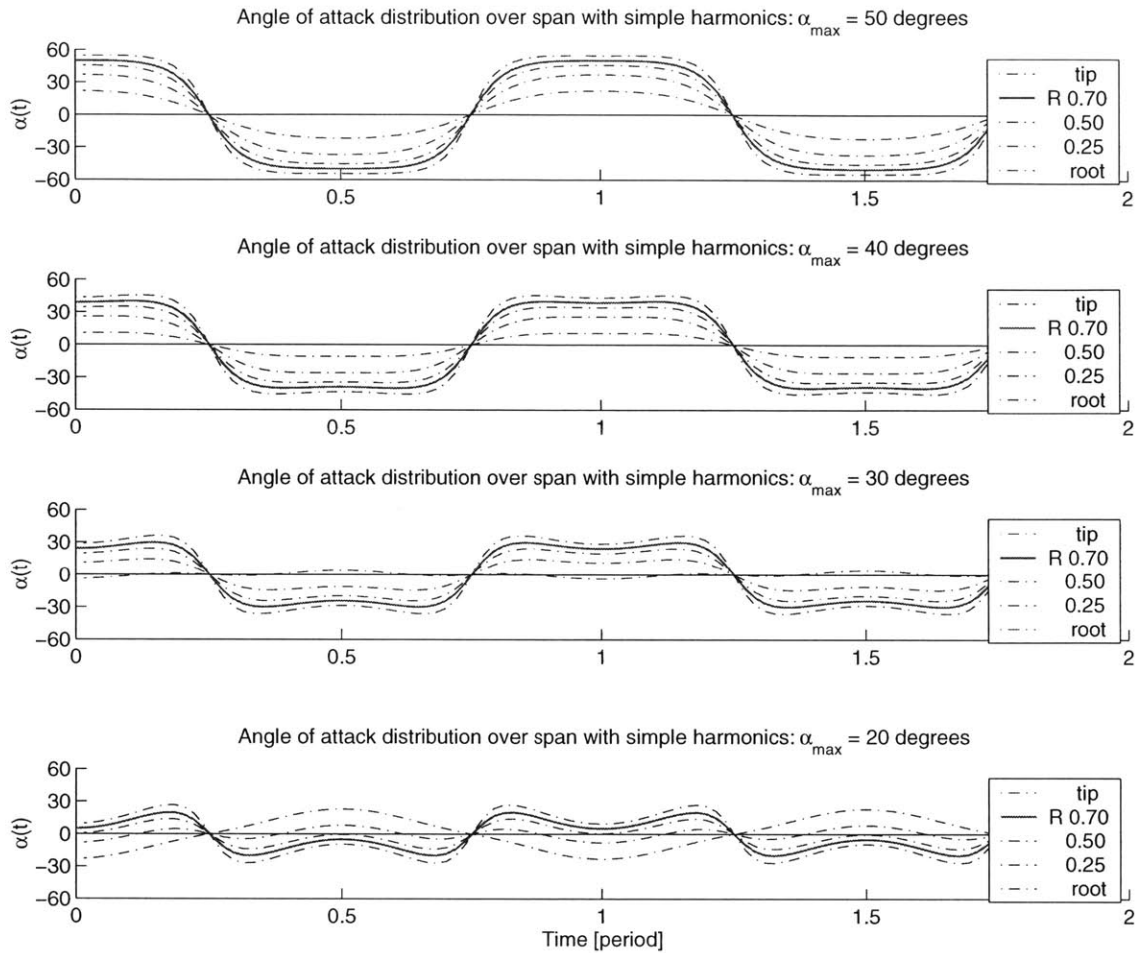


Figure 1-5: Angle of attack distribution over span. The only parameter that changes between these four plots is the amplitude of pitch motion. Lower  $\alpha_{max}$  correspond to larger pitch motions. Note that  $\alpha_{max}$  is always computed at  $r_{0.7}$ . Simple harmonics is referring to the sine in the roll motion and the cosine in the pitch motion. Heave velocity increases with radius because it is proportional to the arclength. Locations near the tip of the foil are farther from the centerline of the roll axis, so the heave velocity is higher near the tip. The angle of attack is larger near the tip of the foil due to the increased heave velocity. The pitch motion is constant over the span. For low  $\alpha_{max}$  the large pitch motions cause the the local angle of attack to be negative near the root of the foil. An analysis from the 2D perspective would indicate that a change in the sign of the angle of attack in the spanwise direction would degrade thrust. This problem is fully 3D and this 2D analysis may not be valid. A compliant foil may allow the sign of the angle of attack to be constant over the span. Actively twisting the pitch of the foil over the span would allow for better control of this distribution. This is similar to the reason helicopter rotor blades are twisted. The orientation of the twist for a helicopter rotor blade is fixed because there is a preferred direction for lift. For a flapping foil the orientation of the twist would need to flip every half cycle.

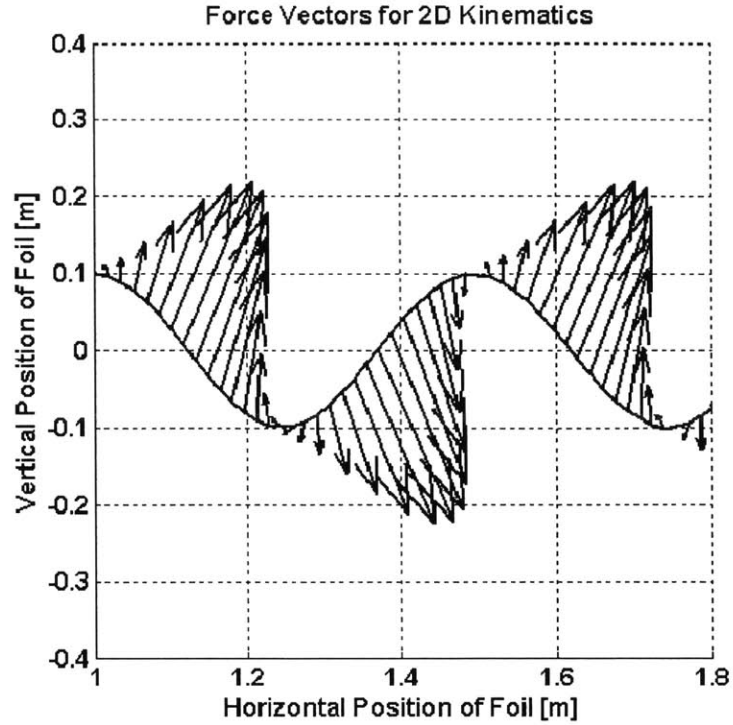


Figure 1-6: Periodic lift and thrust forces. Figure made with Doug Read’s data [21].

### 1.1.3 Dynamics

Considerable experimental work has been done to map foil motions to forces [21] [14] [11]. Experimental force data is presented in Chapter 4.

The hydrodynamic forces produced by flapping foils are periodic. For most kinematics used there are either two or four vortices shed per cycle of foil motion. The lift force varies at the frequency of foil motion, and the thrust force varies at twice that frequency. Typically the magnitude of the lift force is higher than the thrust force. For symmetric geometries and kinematics the mean lift force over an integer number of cycles is zero and the mean thrust force is nonzero. Thrust vectoring is achieved by breaking the symmetry in the kinematics. This is normally accomplished by adding a static DC offset to the pitch motion.

Flapping foils need reciprocating motions with coordinated velocity trajectories



on multiple axes. In order to achieve oscillatory motion, energy must be spent to accelerate the mass of the solid moving parts. Passive mechanical springs or magnets may be used to minimize the energy spent on inertial forces of the solid moving parts, at the cost of added complexity in the mechanics and controls. If the stiffness of the spring or magnet results in a fundamental resonant frequency of vibration that is coincident with the desired frequency of motion, the motors and active control will only need to supply energy to offset the damping in steady state. The closer the passive dynamics of the system are to the desired motion, the lesser the energy that will be required by active control. The biomechanics of animals take great advantage of this. There are passive elastic materials at the base of the wings of dragonflies. When they are not gliding, some species of dragonflies (e.g. *Sympetrum sanguineum*) flap their wings within a very small range of frequencies centered about 39 Hz, which suggests they are storing the inertial energy in the elastic structures. [26] [27] In this case the desired frequency of the flapping wings is coincident with the natural frequency of the wing mass and elastic structure.

There is another strategy that does not require a spring. Some insects, for example some butterflies and some *Drosophila* species, have no elastic structures and spend no net energy on inertia [27]. This is a special case of insect flight where the net inertial power is less than the aerodynamic power. These cases correspond to relatively large wings and low wingbeat frequencies. The net inertial power is zero for these insects because the energy required to accelerate during the beginning half-stroke will be recovered when the fluid is used to decelerate the wing at the end half-stroke [27]. The kinetic energy stored in the solid material is transferred to the fluid during the deceleration phase. If it is determined that the hydrodynamic power is greater than the inertial power (which will be the case for a substantially large foil), then perhaps commanding a small or zero torque for a portion of the cycle of motion would enable our flapping foil actuators to achieve zero net inertial power. For a heavy actuator design, the zero torque strategy would only work for a relatively large foil, and the frequency of foil motion would be low, resulting in a low thrust vectoring bandwidth. In light of the knowledge gained from these insects, one of the considerations for

selecting an appropriate foil size should be that the hydrodynamic power is greater than the inertial power in order to allow for control strategies to recover energy spent on solid mass in the absence of a spring.

#### 1.1.4 Control

There are nontrivial control problems to be solved on the lowest level. There is typically a large inertial term in the solid dynamics of the foil actuator and a large damping term in the hydrodynamics. As the desired frequency of motion is increased, the torque on the roll motor will saturate in the acceleration phase or the velocity phase, depending on the foil size and amplitude of motion. A PD controller with velocity feed forward is sufficient to track the requisite sinusoidal velocity trajectories. With a spring, a higher level controller could be used to slide the desired frequency to lock onto the resonant mode.

The physical constraints on the frequency of foil motion limit the frequency of thrust vectoring bandwidth. Lags at the low level will contribute to phase loss in the higher body level control. There will be additional lags at the foil level due to the hydrodynamic and mechanical constraints on the rate of transition between velocity profiles. Discontinuities in the velocity trajectories will likely cause unfavorable vortex shedding and will certainly cause large inertial forces. There are physical constraints on the rate at which the desired thrust vectors can be updated. The bandwidth on the thrust vectoring rate will be key in determining the maneuvering capabilities of the vehicle.

High bandwidth, low magnitude forces may be achieved with high frequency pitch motions and chordwise flexibility. This style of motion would be useful for hovering and making minor adjustments in the body position at low speeds. The two degree of freedom large amplitude flapping foil motion will be used for accelerating the vehicle and cruising at moderate to high speeds.

Once the foil motion control has been pushed to the highest bandwidth possible (currently in the absence of a spring), the next major control problem will be to find paths in the kinematics parameter space to scale the magnitude of the thrust force for

a given geometry and vehicle speed. There is redundancy in the kinematics, which will allow for a constrained optimization problem. Certainly the most desirable parameter to optimize will be efficiency. So the problem will be to find paths in the kinematics parameter space that will satisfy a specific coefficient of thrust while maximizing the operational efficiency. It may be possible that the frequency of foil motion always remains the same to simplify the central body motion control. As larger forces are needed the amplitude of motion could be increased.

In order to implement flapping foil propulsion on a vehicle there need to be sensors that measure the incoming velocity upstream of the foil, or this velocity must be estimated with a mathematical model running in real time on the vehicle control system. Errors in the measured or estimated fluid velocity will translate directly to errors in the foil kinematics, and therefore into the hydrodynamic forces and body dynamics. For this reason, regimes with great forgiveness to errors in the angle of attack profile are desirable to minimize the effect of error in the fluid velocity. These errors in the fluid velocity will also effect the hydrodynamic efficiency. If the kinematics are incorrectly computed, the forces may deviate from the plateau of high hydrodynamic efficiency. While accurate high bandwidth velocimeters are available, they consume power and space, and add to the cost of the vehicle.

One of the unique control problems for flapping foil vehicles will be to develop an algorithm that accepts as inputs the desired thrust vectors and the measured or estimated local flow velocity, and outputs the necessary kinematics for the foils to achieve the desired forces. The algorithm must be robust in the presence of uncertainties in the upstream velocity, uncertainties in the hydrodynamic interactions between individual foils and interactions between the foils and the body, and constraints of the motions attainable by the machine. The robustness of this algorithm will be fundamental in determining the performance of this and future vehicles. This is at the core of the control problem for flapping foil propulsion, and this vehicle will provide the opportunity begin developing this algorithm.

Beyond vehicle body motion control, there are higher level control problems that must be solved to obtain a robust and useful tool for oceanography or deep water

archeology. This is a very rough overview of the control hierarchy for an flapping foil AUV that is to be deployed in the ocean:

1. Start with high level mission objectives such as building a map of the ocean floor, or locating an object within a search area, or sampling temperature, salinity, and chemistry of the water column. Simultaneously perform high level error handling in regard to the vehicle status involving leaks, battery capacity, collisions, etc. Perhaps given robust machine vision algorithms and hovering capability, a higher resolution map could be made in the vicinity of a potential object of interest. Likewise if the payload sensors detect other events such as the presence of a particular chemistry in the water, a large disturbance in the magnetic field revealing the presence of a metal object, or particular sound pattern, other high level mission objectives could occur.
2. Perform concurrent mapping and localization to navigate the vehicle along a desired trajectory to meet the objectives.
3. Given the desired vehicle body position, measure linear accelerations and angular velocities of the body. Additional orientation information will be available from a magnetometer. Additional body and fluid velocity information may be available from a doppler velocity log. Additional position data may be available from a sonar, digital camera, or perhaps laser. Using a Kalman Filter estimate the vehicle body velocity and position, and the hydrodynamic and hydrostatic forces on the body.
4. Given the full vehicle state, calculate the desired thrust vectors for each foil given the estimated hydrodynamic, hydrostatic, and solid dynamic forces.
5. Given a desired thrust vector at each actuator, the velocity of the vehicle body, and possibly the local velocity of the fluid, calculate the necessary kinematics for the foils to result in the desired thrust vector at each actuator. Command velocity trajectories for each axis of foil motion.

6. Given desired velocity trajectories for the foils, implement closed loop motion control locally at each foil.

## 1.2 Previous Work with Flapping Foil Robotics

Flapping foil propulsion is very attractive in terms of hydrodynamics, but it presents great difficulties in the mechanics and controls. Previous work with robotic fish [3] [6] [17] has resulted in extraordinarily complex and beautiful machines with limited performance compared to the animals on which they were based. While these machines have provided further insight in the hydrodynamic and mechanical aspects of the problem, they have also served as an indication that the elegant solutions that exist in nature will be extraordinarily difficult to implement as machines. In order to simplify the mechanical aspects of the problem it is necessary to search for the simplest kinematics with the fewest degrees of freedom that will still result in optimal hydrodynamic forces. Complexity in mechanical design does not scale linearly with the degrees of freedom of motion.

### 1.2.1 Autonomous Vehicles

#### **RoboPike**

The RoboPike was the first autonomous robotic fish built at MIT [17]. It was designed and fabricated by John Kumph in 1994. This robot is remarkably small with a length of 0.81 meters and a displacement of 3.6 kilograms. The depth rating is approximately 2 meters. The top speed is approximately 0.2 body lengths per second. This robot has five degrees of freedom. Two servomotors control the curvature of the body and tail sections, and a third servomotor controls the angle of the caudal fin. The two pectoral fins are each controlled by another servomotor.

The frame is made of links of Delrin. The links are connected by stainless steel ball bearings that are direct contact with water. There are two helical springs made of fiberglass and epoxy that surround the body of the vehicle. The skin is made of

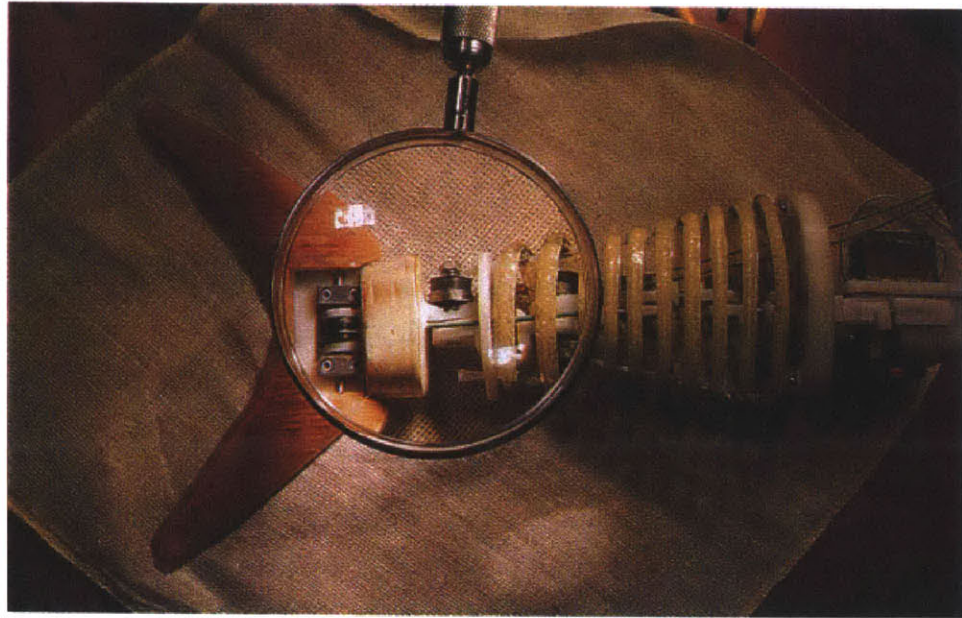


Figure 1-7: Tail Section of the RoboPike — John Kumph.

Lycra. With the exception of the head, the rest of the vehicle is flooded. Buoyancy is obtained with small pieces of PVC foam that are placed to trim the vehicle and provide a small hydrostatic righting moment. Each of the motors are individually sealed with a butyl rubber coating. There are a small pack of nickel cadmium batteries that give the vehicle a mission life of less than an hour.

There is a small dry volume in the head that contains an Onset model 8 computer. This computer has a 32 bit processor that runs a C program that sends pulse width modulation signals to each of the servos. Each servo receives a square wave signal. The duty cycle of the square wave determines the position of the servo. All commands are sent open loop. This robot is simply running a predetermined set of kinematics that have been hard coded by the user.

In the past nine years a series of modifications have been made to the RoboPike to incorporate a wireless modem, three axis magnetometer, and two pressure sensors. The wireless modem was used to communicate with a laptop on the bench, but it has recently been removed to make space in the head for new sensors. The two pressure sensors measure depth and approximate forward velocity. Once incorporated

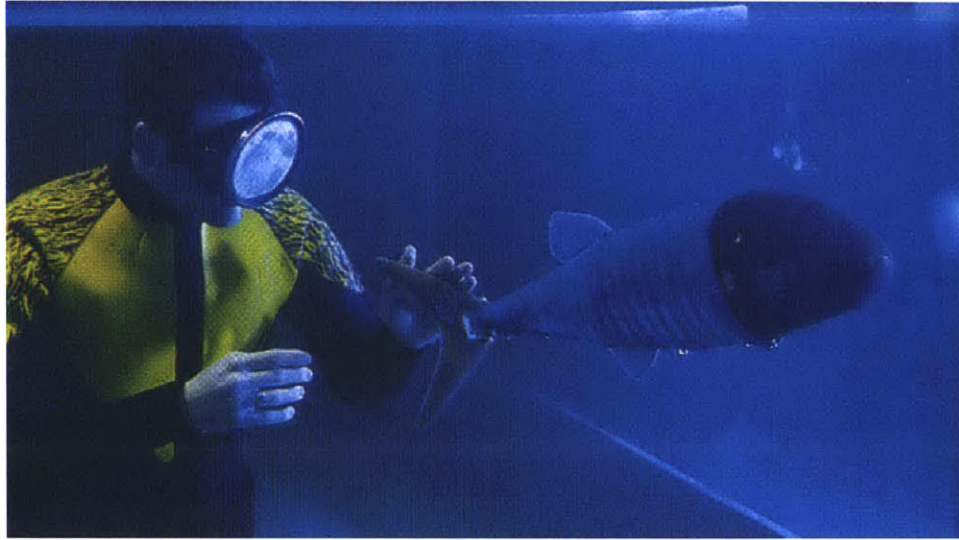


Figure 1-8: John Kumph and the RoboPike.

into a vehicle body control system, the three axis magnetometer and two pressure sensors will give the robot the ability to maintain a heading and to navigate by dead reckoning. The RoboPike is not currently operational, but is being worked on by Cosimo Malesci, an undergraduate at MIT.

### **Draper Laboratory Robotic Tuna (VCUUV)**

The Vorticity Control Unmanned Underwater Vehicle (VCUUV) is a free swimming robotic tuna fish that was designed and fabricated by Jamie Anderson and her colleagues at Draper Laboratory [3] in 1997. This robot is near the practical upper limit of what is currently possible for a flexible hull free swimming robotic fish given the constraints on available batteries and actuators. The vehicle has a length of 2.4 meters and a displacement of 136 kilograms. It has a 10 meter depth rating and a top speed of 0.5 body lengths per second with a tailbeat frequency of 1 Hertz.

This robot has maneuvering capabilities that far exceed traditional cylindrical shaped AUV's. While a typical cylindrical AUV has a turning radius of 3.5 body lengths, this vehicle has a turning radius of 0.5 body lengths. This vehicle has a maximum yaw velocity of 30 degrees per second, in comparison to a typical value of

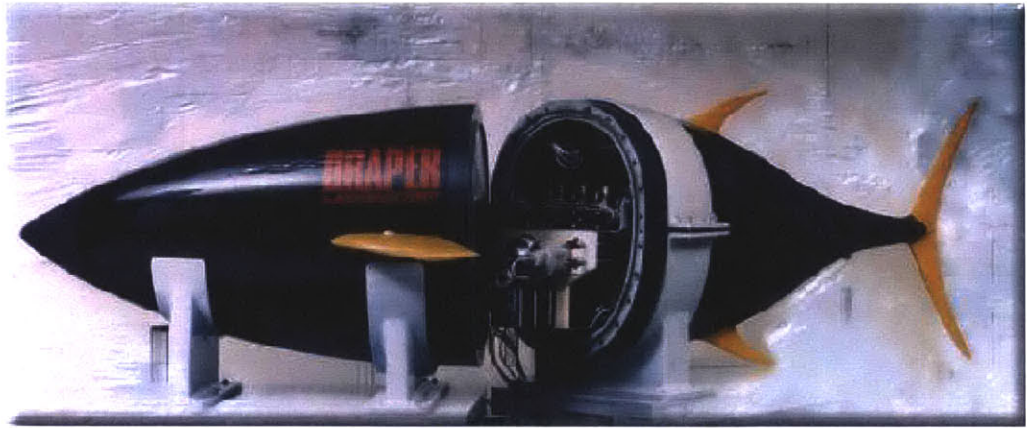


Figure 1-9: Draper Laboratory free swimming robotic tuna.

7 degrees per second for a cylindrical vehicle. This yaw rate enables the vehicle to make a full 90 degree turn every 10 seconds.

This robotic fish has a total of six degrees of freedom, four in the tail section and two in the pectoral fins. The tail section and caudal fin are actuated by hydraulics and rigid links. The hydraulic pump is powered by an electric motor that is connected to 29.5 kilograms of sealed lead acid batteries. There is a total of 800 watt-hours of battery capacity that result in a mission life of 3 hours. The pectoral fins are driven by servomotors.

The Draper tuna is capable of closed loop body control with a six axis inertial navigation unit, three axis magnetometer, and depth sensor. The body motion control system receives feedback from the drivetrain in the form of force and positions of the hydraulic pistons, electric motor speed, and pressure in the hydraulic reservoir. The error handling algorithm is aided by measurements from leak detectors and thermocouples.

The design of VCUUV has been demonstrated to be mechanically robust and reliable, with over one hundred deployments in swimming pools and fresh water ponds.



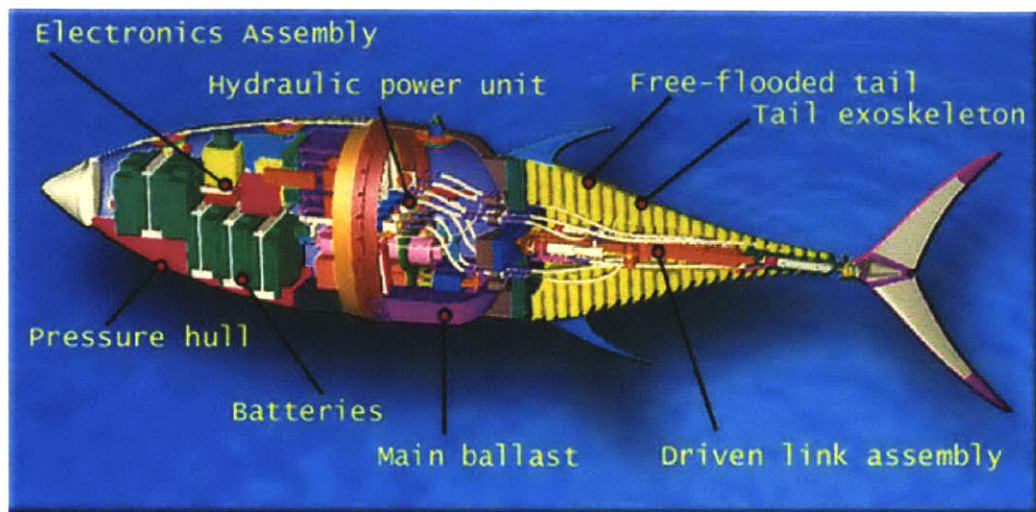


Figure 1-10: Drawing of the Draper tuna. — Draper Laboratory



Figure 1-11: Draper tuna at Nickerson State Park.

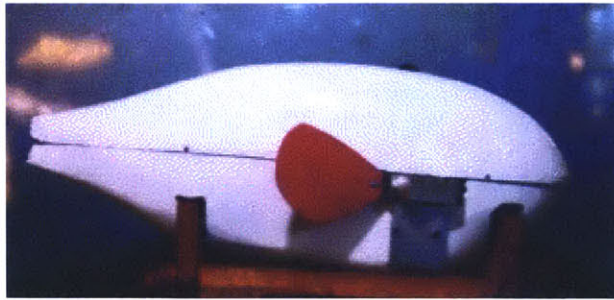


Figure 1-12: Robotic fish with 3DOF pectoral fins. – Naomi Kato

### **Bass Robot at Tokai University**

Naomi Kato and his colleagues at the Department of Marine Design and Engineering at Tokai University built two generations of robotic fish with two pectoral fins. Each pectoral fin is driven by three servos. The fins are moved to perform a drag based form of propulsion, similar to rowing. The vehicle is 2 m long and has a displacement of 105.7 kg. This vehicle is capable of cruising and turning in the horizontal plane.[16]

### **Robotic Dolphins at Tokyo Institute of Technology**

Motomu Nakashima and his colleagues at Tokyo Institute of Technology have built two robotic dolphins. The first design was powered by a pneumatic motor attached a crankshaft and spring mechanism in the tail section. The robotic dolphin was propelled by a caudal fin that moved with two degrees of freedom. The robot was constrained to operate at the free surface due to the large buoyancy resulting from the pneumatics. The mission life was on the order of one minute due to the limited compressed air in the tank. The second design incorporated motors and batteries to enable the vehicle to be submerged and achieve a substantially longer mission life.



Figure 1-13: The first generation robotic dolphin with pneumatics. – Motomu Nakashima

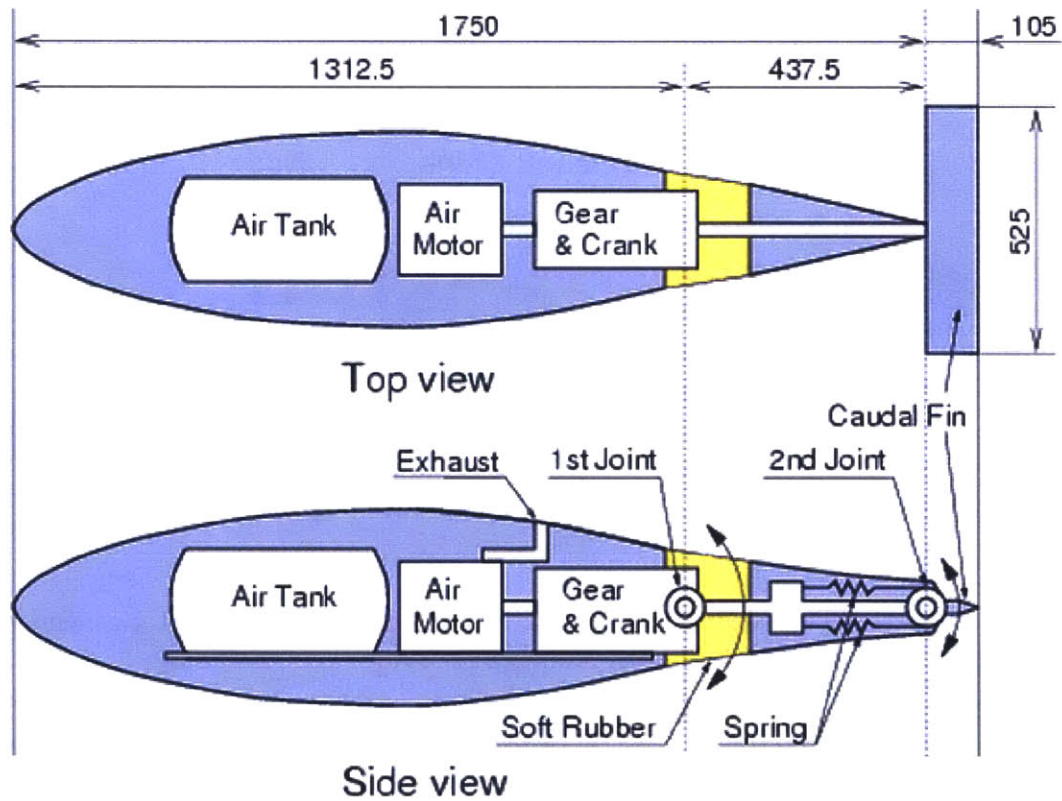


Figure 1-14: The first generation robotic dolphin with pneumatics. – Motomu Nakashima

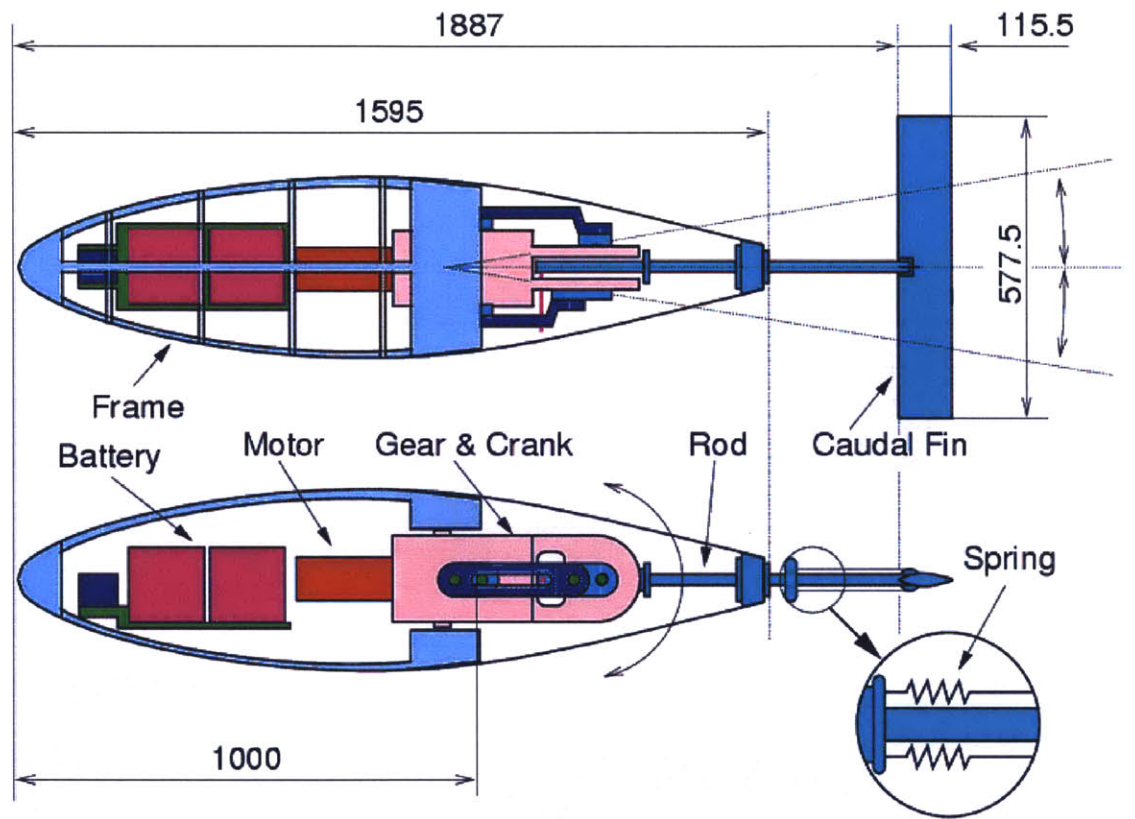


Figure 1-15: The second generation robotic dolphin with batteries and an electric motor. – Motomu Nakashima

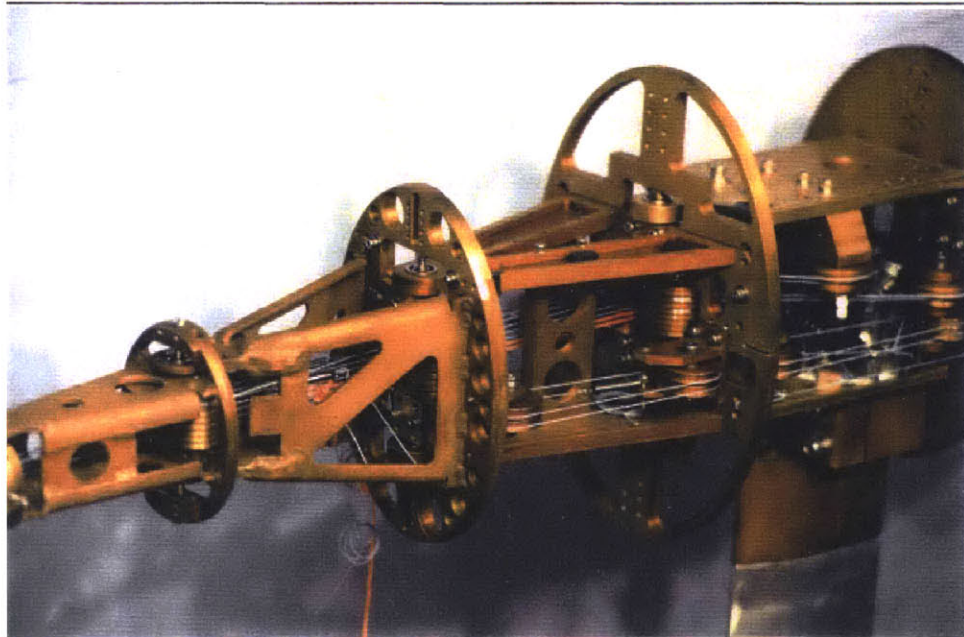
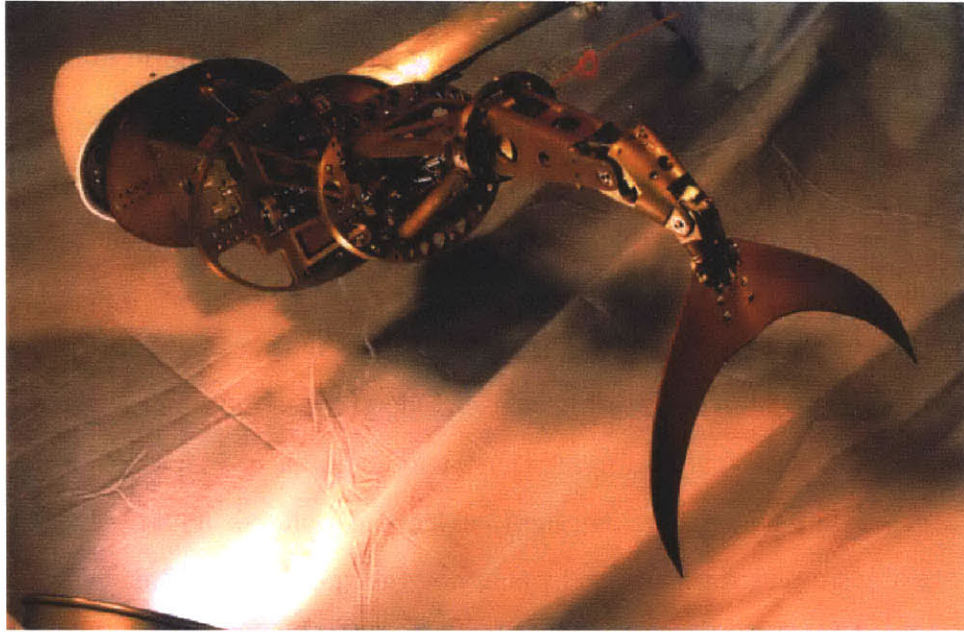


Figure 1-16: RoboTuna — Dave Barrett.

## 1.2.2 Externally Propelled Robotic Platforms

### RoboTuna

The RoboTuna was designed and constructed by Dave Barrett at MIT in 1994. [6][7]. The RoboTuna was a robotic platform for investigating the hydrodynamics of fish swimming. The body had six degrees of freedom that were actuated with cables and pulleys connected to motors above the water. This apparatus demonstrated drag reduction on an undulating body.

The RoboTuna was externally mounted to an overhead carriage system that contained the motors, amps, power, and control. The hull was flexible and flooded. There was no dry space underwater for sensors, electronics, motors, or batteries. However the nose cone was rigid and water tight, and could have been sealed with a bulkhead.

Actuation was achieved through cables and pulleys. These cable tendon drives drastically simplified the design by enabling the motors to be removed from the flexible submerged body. This offered a nice simple solution for keeping the electronics and motors dry and out of the way of moving parts. The cable tendon drives had relatively low backlash and the forces in individual cables could be measured with strain gauges, which enabled measurement of the power input with the known velocities from the servomotors. The drive ratio for the cable tendon drives could be easily modified by changing the diameter of the drums. The cables could deliver very large forces into small places. This cable tendon drive arrangement also allowed the mechanical fish to be removed and replaced by another body with a different geometry or design.

### RoboTuna II

RoboTuna II was the next generation, constructed by Dave Beal, Mike Sachinis, and Mike Jakuba in 2000. [8] [22] [15] As with the first tuna, it was mounted to a carriage with external power and control. One of the major improvements for this generation was that the cables and pulleys were arranged to decouple the motion of the links which simplified the control.

The goal of RoboTuna II was to use pressure sensors along the lateral line of the

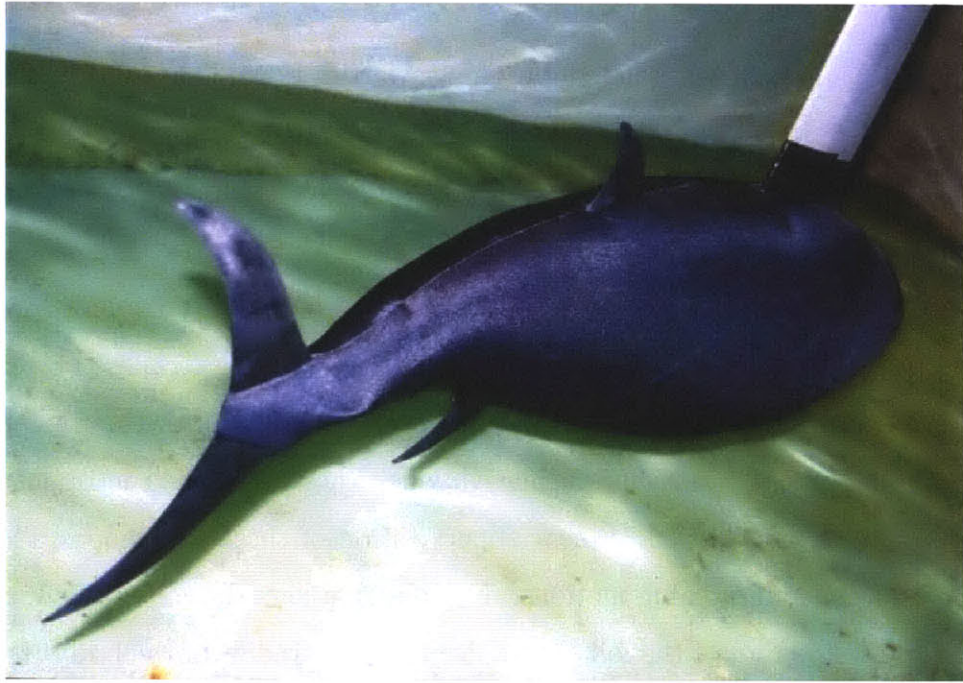


Figure 1-17: RoboTunaII — Dave Beal, Mike Sachinis, Mike Jakuba.

flexible body as input to a control system that could manipulate upstream vorticity being generated by a half cylinder ahead of the body. Results from those experiments were published by Mike Sachinis [22].

## SeaLion

The SeaLion was constructed by Craig Martin at MIT in 2001 [20]. This robot was also carriage mounted and received external power and control. There was a considerable dry volume underwater for motors and sensors. There was a single foil that was moved with two degrees of freedom.

The purpose of this apparatus was to measure hydrodynamic forces on a rolling and pitching foil. There are two motors with collinear centerlines. Power is transmitted from the motors to the foil through bevel gears. When the motors are turned the same direction roll motion is achieved, when they are turned in opposite directions pitch motion is achieved. Linear superposition of these two modes allows for combined rolling and pitching motions. This design allows the centerline of the motors to be close to the root of the foil, which decreases the radius of the body. If the backlash in the bevel gears could be eliminated, this design certainly has potential that should be explored.



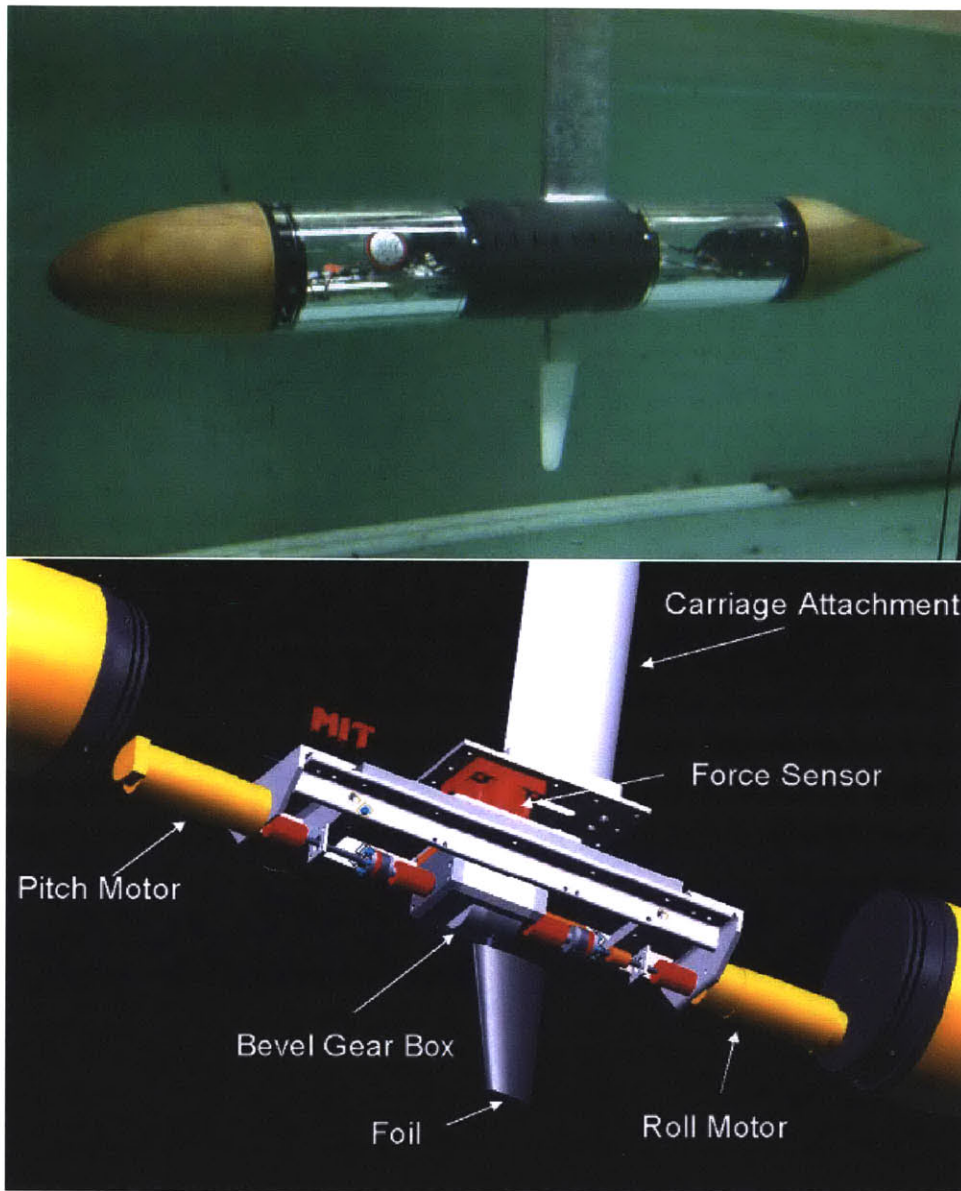


Figure 1-18: SeaLion — Craig Martin.



# Chapter 2

## Design and Fabrication of AUV

### 2.1 Purpose of Vehicle

This AUV will be a platform for research in hydrodynamics and controls. The design and fabrication of this vehicle serves as an opportunity to identify and address the key design considerations for rigid hull, flapping foil, autonomous underwater vehicles. Knowledge gained from the major problems in the mechanics and controls of this vehicle will provide feedback for the direction of future hydrodynamic research that will help maximize the performance and minimize the complexity of flapping foil propulsion.

There is considerable knowledge to be gained from the design process, the dynamic characterization of the foil actuators, and data from the navigation sensors on the vehicle. Individual foil actuators are useful for flow visualization, hydrodynamic force measurements, and testing motion control algorithms. Four foils on a vehicle with sensors and data acquisition, will serve as a valuable test platform for hydrodynamics and controls research. The acceleration of the vehicle and good estimates of the hydrodynamic coefficients of the vehicle body will give insight into the forces produced by the foils in unsteady or accelerating flow. This AUV will be useful for testing body motion control strategies for a vehicle with highly unsteady propulsive forces.

The open loop dynamic characterization of the vehicle will help in the design of the closed loop foil and body control systems. The closed loop dynamic characterization

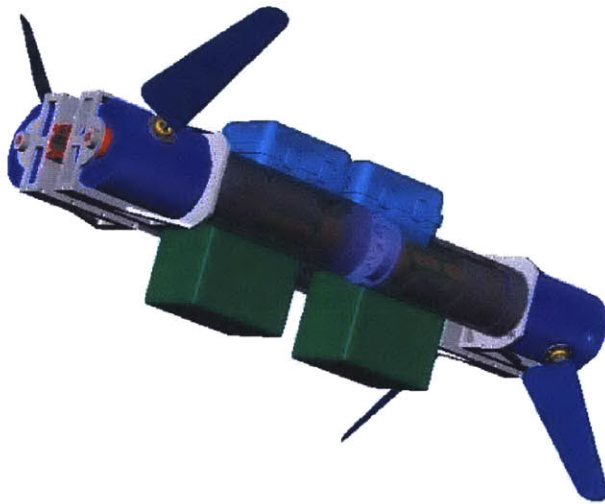
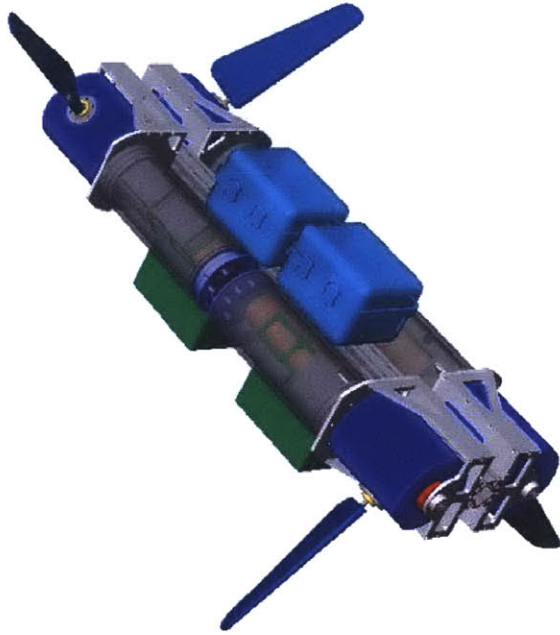


Figure 2-1: AUV in the sea turtle configuration.

will provide quantitative estimates of the capabilities of a next generation vehicle. If this vehicle has far better hovering than cruising capabilities, the next generation design should be specifically tailored for missions that require mostly hovering. Likewise if this vehicle has a far superior ability to cruise than hover, the next generation design should be highly streamlined.

Ultimately the goal will be to develop a vehicle that has superior hovering agility and cruising efficiency. It is not crucial for the current vehicle to obtain these capabilities. The purpose of the current vehicle is to provide information to make the ultimate goals more obtainable, and also to demonstrate that two degree of freedom flapping foil propulsion can be used to propel and control a vehicle. As the development of the mechanics and controls becomes more advanced, it will become more evident which aspects of flapping foil propulsion can be leveraged to provide new capabilities for oceanographic research.

Knowledge gained in hydrodynamics will endure. Knowledge gained in mechanical design will need to be adapted to developments in materials, fabrication techniques, and actuators. Likewise the knowledge gained in the controls that is particular to physics will persist, and knowledge that is particular to hardware and software will need to be adapted to the advancements in the available computers, solid state memory, sensors, motion control cards, digital I/O and data acquisition cards, servomotors, amps, waterproof cables and connectors, wireless and underwater modems, and batteries. Advances in electronics occur at a fast rate, and each new generation vehicle should take full advantage of the components that become affordable and practical to implement.

## **2.2 Design Criteria**

This vehicle was designed to primarily operate in confined shallow water spaces such as swimming pools, large tanks, and perhaps in a small pond or quarry. The first deployments of this vehicle will be with open loop body motion control. For these initial runs the vehicle will not have the capability of navigating or performing high

level error handling and behaviors such as collision avoidance. With such limited high level control functionality the vehicle must be confined to protected waters where there will be no chance of the vehicle becoming lost or sunk.

One of the highest priorities in the design was modularity. A highly modular design minimizes the cost and difficulty in changing the location and number of foils. For this modular design, all the electronics, motors, and mechanical components required to add a foil to the vehicle are contained in a single, stand alone module. These individual foil modules receive power and communication, and are capable of operating independently from the rest of the vehicle. Any individual foil module can be operated with a 24 volt power supply and any computer with an Ethernet card. These individual foil modules can be operated in a variety of testing facilities such as a propeller tunnel or towing tank, which makes them very valuable for hydrodynamic force measurements and flow visualization.

### **2.2.1 Mission Length and Location**

The two 12 volt sealed lead acid batteries have a total capacity of 31.3 amp-hours at 24 volts.<sup>1</sup> With all four foils moving continuously and aggressively, this would result in approximately 2 hours of battery life. For the preliminary open loop runs, battery life will not be the limiting factor on mission life. Without the ability to navigate or perform collision avoidance, the preliminary open loop mission life will be limited by the size of the pool or tank and the commanded open loop kinematics.

The first several deployments will be used to characterize the open loop dynamics of the vehicle. With short bursts of acceleration on each linear and rotational axis, the vehicle will not travel any considerable distance. The first test will be done at the MIT Towing Tank.

---

<sup>1</sup>For these batteries, the amp-hour capacity is a function of the discharge rate. This calculation was made iteratively so that the discharge rate was equal to the battery life. The final amp-hour value used was taken as an average of the capacity ratings for the 3 hour discharge rate and the 1 hour discharge rate.

## **2.2.2 Depth Rating**

This AUV was designed for 30 meter depth rating, however there are custom seals that have an uncertain depth rating.

The safe operating depth will be limited to 5 meters for initial tests. The shaft seals need to be tested in order to give an accurate depth rating. The shallow depth rating will not substantially inhibit the functionality of the vehicle, given its intended purpose.

The shaft seals could be replaced with magnetic couplings in order to eliminate all dynamic seals. With only static seals at the lids and end plugs the depth rating would be drastically increased. The next weakest link on the depth rating will be due to the structural integrity of the housings.

## **2.2.3 Dimensions**

The vehicle is 2.0 m long without a fairing. The fairing will be approximately 2.5 m long and 0.5 m in diameter.

## **2.3 Vehicle Layout**

### **2.3.1 Modularity and Scalability**

The location and number of foils may be changed easily. The communication and power hardware have a capacity for six foil modules with relatively minor changes in the wiring.

As the development of the vehicle advances it may eventually be desirable to add payload instrumentation. There will be room on the frame to add small electronics housings. There will be additional communication ports, power capacity, and data acquisition channels to accept several payload sensors.

### 2.3.2 Planes of Symmetry

Modularity enables to vehicle to be reconfigured with different planes of symmetry. Symmetry in the geometry and kinematics will increase the open loop stability of the vehicle. The foils may be arranged so that the net unsteady lift components will be cancelled by symmetry in order to eliminate the cyclic roll and pitch moments on the vehicle body. Asymmetries in the foil motions could result in large pitch and roll moments for maneuvering.

Initially the vehicle will be configured like a sea turtle. This configuration results in two strong planes of symmetry and one weak plane of symmetry. Weak symmetry simply means that the center of buoyancy will be placed above the center of gravity to result in a net hydrostatic righting moment. The sea turtle configuration should provide control of five degrees of freedom on the body (surge, heave, pitch, roll, yaw). A static roll bias can be used to change the orientation of the lift vector on a foil, and this may enable control of the full six body motions with the sea turtle configuration.

Another useful four foil configuration for the vehicle would be similar to a boxfish, with two pectoral fins near the front of the vehicle and a vertical anal and dorsal fin near the rear of the vehicle. The boxfish configuration may allow control of all six degrees of freedom. The disadvantage of this configuration would be less open loop stability, resulting in more complex body dynamics and thus more closed loop body control activity.

### 2.3.3 Mass, Hydrostatic Stability and Net Buoyancy

Component	Mass	Net Buoyancy
Total Vehicle (Approximate)	157 kg (345 lbs)	1.0 kg (2.2 lbs)
Two Housing Actuator	4 X [27.4 kg (60.5 lbs)]	4 X [-9.3 kg (-20.5 lbs)]
Lead Acid Batteries	2 X [17.1 kg (31 lbs)]	2 X [-9.0 kg (-19.8 lbs)]
Frame (Approximate)	7.1 kg (15.6 lbs)	-5.0 kg (-11 lbs)
Electronics Housings (Approximate)	6 kg (13.2 lbs)	12.5 kg (27.5 lbs)
Flotation Required (Approximate)		48.7 kg (107.1 lbs)

Table 2.1: Mass and buoyancy of major components



There is a trade off between passive stability and maneuverability. Many fish are passively unstable in order to perform quick starts and turns. A low or negative hydrostatic righting moment allows the body to be rolled or pitched rapidly. The location of the batteries and electronics housings can be adjusted to trim the vehicle and to adjust the hydrostatic stability.

The vehicle will always be trimmed a few kilograms positively buoyant so that the vehicle will rise to the surface in the event of a power failure or small leak. A large leak could certainly be catastrophic. One strategy for recovering from a large leak would be to carry dead weight that could be dropped with a magnet. Another strategy would be to attach a piston to a pin on a  $CO_2$  canister to inflate a small volume.

### **2.3.4 Added Mass and Drag Considerations**

In order to retain the ability to quickly and easily relocate the foils for the open loop runs, there will initially be no external fairing on the vehicle. Without a fairing, the bluff body drag on the batteries and housings will be very high the added mass of the batteries and housings will be slightly increased. This will greatly decrease the speed of the vehicle and will only be the case for the initial runs.

Once a foil arrangement has been settled upon, a highly streamlined fairing will be fabricated. Ideally the fairing would be modular to retain the ability to relocate the foils. A simple fairing shape (elliptical or cylindrical) is desirable to simplify the computations to estimate the hydrodynamic coefficients.

## **2.4 Control and Communication**

### **2.4.1 Single Board Computer Running Linux**

The single board computer is the Octagon Systems model PC680. This computer is a state of the art embedded PC made for vehicles operating in extreme environments. This computer fits the EBX form factor, which simply means that the size of the

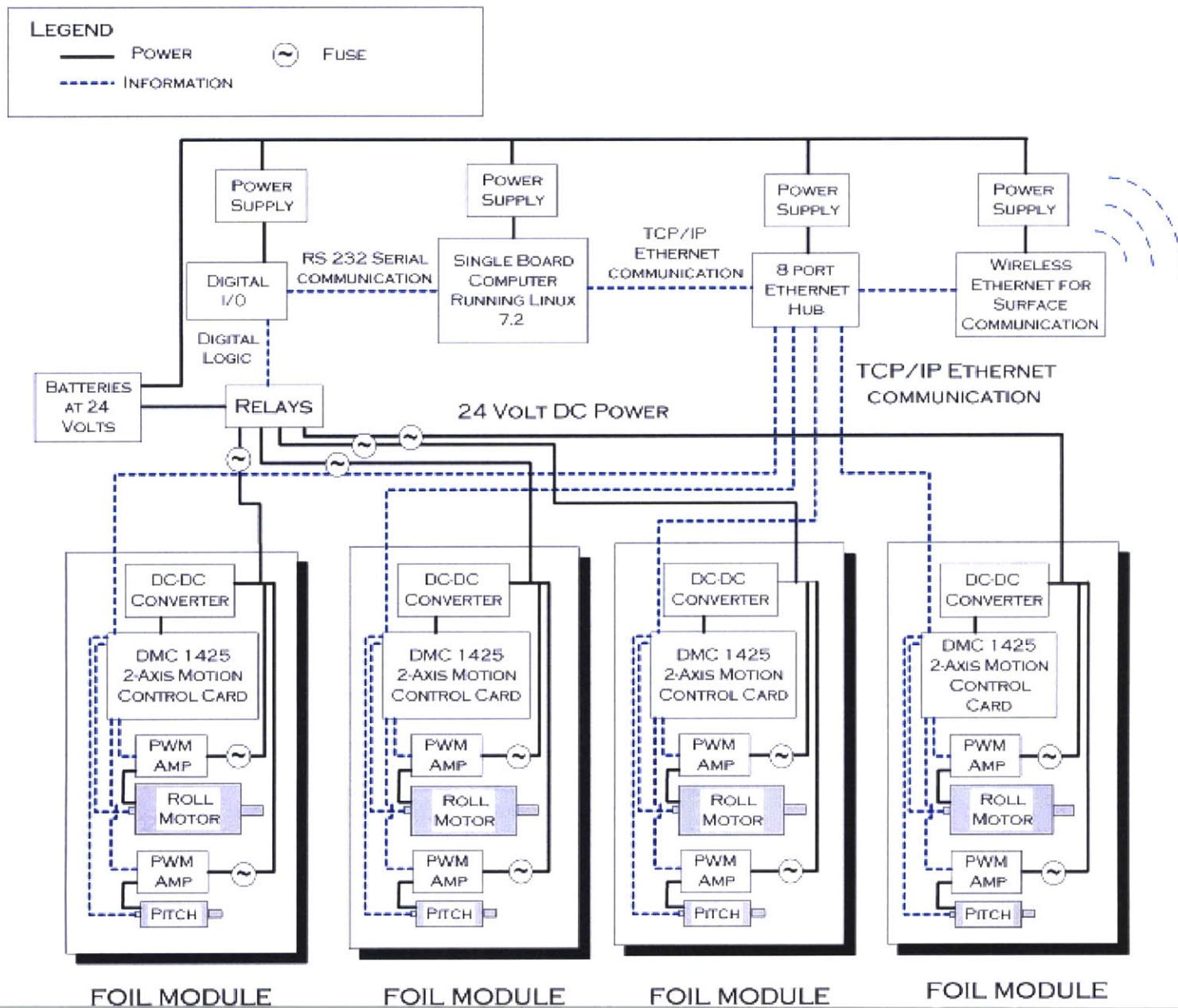


Figure 2-2: AUV power, control, and communication schematic

board is 14.6 cm x 20.3 cm. It has a Intel Pentium 166 MHz processor with 32 MB of SDRAM. There are two two operating systems loaded on the computer. The primary operating system is Red Hat Linux 7.2, which is installed on a 20 GB IDE hard drive. The secondary operating system is Datalight ROM-DOS v.6.22, loaded onto a 32 MB solid state Flash memory chip. The BIOS is loaded onto 512 KB of solid state EEPROM memory. There is a programable watchdog timer that can automatically reboot the computer and execute a program in the event of a system lock up.

This computer has 6 serial ports, 2 parallel ports, 2 USB ports, a 10T/100Tx Ethernet card, 32 channels of 32 bit digital I/O, PCI and ISA bus. It has a built in video card and support for PS-2 keyboard and mouse, so it can function as a normal desktop PC. It supports all 8 and 16 bit PC/104 expansion boards, so it should be completely compatible with the hardware used on the Odyssey class AUVs.

All components except the hard drive can withstand  $-40^{\circ}$  to  $85^{\circ}\text{C}$  operating temperature, 5% to 95% relative humidity, 40g shock, and 6g vibration. It has onboard support for up 128 MB of solid state memory, so the hard drive could be completely removed.

The power supply accepts 10-36 volt DC power. The operating voltage of the vehicle is 24 volt, so it is extremely unlikely that a voltage dip on the batteries caused by a draw from the foil actuators, could reboot the computer.

Software and technical references for this computer are available at

*<http://www.octagon.systems.com>*

## **2.4.2 Distributed Motion Control on Ethernet Network**

There is a two axis motion control card located within each foil module. Each motion control card has a processor with solid state memory and an Ethernet card with a unique IP address. There is a simple program running locally on each motion control card. This program executes closed loop motion control for sinusoidal velocity trajectories and computes transitions between desired motions. Kinematics commands are sent from the single board computer in the form of amplitudes, phases, and frequencies. Refer to Table 3.2 and Figure 2-2.

In the center of the Ethernet network is a hub. A laptop could be connected to this hub either directly or via a wireless Ethernet modem. The laptop would enable a user to communicate with the single board computer, or directly with one of the foil modules. This communication setup will enable a user to change the gains, torque limits, or error limits for an individual foil without communicating with the single board computer.

The motion control cards are the Galil Motion Control model DMC-1425.

Software and technical references for the motion control cards are available at <http://www.galilmc.com>

## **2.5 Sensors**

Data will be logged with through serial ports and a data acquisition card. The data acquisition card will connect to the single board computer on either the PCI bus or on one of the USB ports.

### **2.5.1 Inertial Measurement Unit**

The inertial measurement unit is a Crossbow IMU VG300CB-100. It measures three linear accelerations on orthogonal axes and three angular rotations rates about orthogonal axes. The range on the acceleration measurement is  $\pm 2g$  and the range on the rotation rates is  $\pm 100$  degrees/second. This sensor has an RS232 serial link and 10 analogue outputs. It has an onboard CPU with solid state EEPROM memory that executes a calibration algorithm. This sensor does not require calibration after shipment from the factory.

The data from this sensor will be the most crucial in determining the dynamics of the vehicle body. This sensor will provide the most valuable data and it is critical to thoroughly understand its output. Once a closed loop body motion control system is implemented, the inertial measurement unit will be used to measure the vehicle body

attitude and short term perturbations.

## Factory Calibration Data for IMU

Serial Number: 111278

Current firmware version: DMU VGX REV.B.04

### Accelerometer Calibration Data:

Axis	Range (g)	Sensitivity (g/V)	Null Offset (V)
X	2.000	1.037	2.584
Y	2.000	0.981	2.599
Z	2.000	1.008	2.547

### Gyro Calibration Data:

Axis	Range (deg/sec)	Sensitivity (deg/sec/V)	Null Offset (V)
X	100.000	49.847	2.525
Y	100.000	50.077	2.519
Z	100.000	49.847	2.520

Software and technical references for the IMU are available at <http://www.xbow.com>

## 2.5.2 Three Axis Magnetometer

The three axis magnetometer is a Precision Navigation model TCM2. It has built in tilt and roll sensors to correct the compass heading for tilt. This sensor communicates via RS232 on a serial port.

Dimensions	6.35 cm X 5.08 cm X 2.79 cm
Heading	$0 - 359.9^{\circ} \pm 0.1^{\circ}$
Tilt	$\pm 50^{\circ} \pm 0.4^{\circ}$
Magnetic Field	$\pm 80\mu T \pm 0.2\mu T$
Sampling Rate	16 to 30 Hz

Technical references for the magnetometer are available at  
*<http://www.pcweb.com/pni/TCM2.HTM>*

### **2.5.3 Leak Detectors**

There will be leak detectors in every electronics housing and foil actuator. The leak detector simply measures the resistance between two probes. In the event of a leak, the water will provide a current path between the two probes and the detector will sound an alarm or alert the central control system. The design for these leak detectors is the simple flood alarm from the Encyclopedia of Electronic Circuits Volume 5. The design consists of two 2N3904 transistors and two 1  $k\Omega$  resistors.

## **2.6 Batteries and Power Management**

The operating voltage for the vehicle is 24 volts. There are two sealed lead acid 12 volt batteries, MK Systems model 8G22NF. The mass of each battery is 17.1 kg. At a 2 hour discharge rate the batteries have 31.3 amp-hours of capacity. These batteries can be deep cycled (100 % discharge) 500 times, a lower discharge will greatly increase the cycling capacity.

These batteries would never be used on an ocean going vehicle. They have a large block shape (23.8 cm x 14.0 cm x 23.5 cm) that will be difficult to incorporate into a streamlined fairing. Compared to state of the art AUV battery technology, they have low power density 22 watt-hour/kg (vs. 150 watt-hour/kg for state of the art).

These batteries were selected as a temporary solution because they are very cheap and can sustain a massive current draw (120 amp) with a low voltage dip. As the central control system becomes more advanced, these batteries will eventually be replaced with a pack of nickel metal hydride or lithium ion batteries.

Technical references for the batteries are available at  
*<http://www.mkbattery.com>*

### **2.6.1 Diodes for Preventing Accidental Charging or Discharging of the Batteries**

There will be two diodes to ensure that the batteries will not be accidentally charged while connected to shore power, and also to guarantee the user will not be shocked while connecting shore power. The voltage drop across these diodes will consume battery power. While these diodes waste approximately 5 % of the battery power, they provide a crucial safety measure.

### **2.6.2 Voltmeter on Batteries**

In order to monitor the remaining battery life, a voltmeter will be installed in parallel across the two batteries in series. As the batteries are discharged the voltage will drop. When the remaining battery life reaches a critical value the vehicle will surface.

### **2.6.3 Ammeter on Power Supply to Each Foil Actuator**

There will be an ammeter monitoring the electrical current delivered to each individual foil actuator. With an estimate of the thrust produced by a foil, this will provide an estimate of the operating efficiency of the actuators on the vehicle. Conversely with an estimate of the operational efficiency, the power consumption will provide a measure of the thrust produced by a foil. If the foil actuators are retrofitted with springs, these ammeters will enable a low level control system to sweep the frequency of foil motion to lock onto the resonant mode.

### **2.6.4 Digital I/O and Relays**

The digital I/O and relays enable each of the foil actuators to be individually powered on by a program running on the single board computer. Individual power control will enable the vehicle to conserve power in a dormant state during shore communication or as part of mission objective that requires idling. If one of the foil actuators is leaking or overheating, it can be powered down in an effort to protect the electronics.

Powering on individual foil actuators may be useful for debugging. Power control and wireless Ethernet will enable a user to communicate directly with an individual foil actuator, independently of the single board computer.

### **2.6.5 Magnetic Switches and LEDs**

The magnetic switches will enable a user to power on the vehicle without opening an electronics housing. This will greatly simplify the deployment and operation of the vehicle. There could be multiple switches to define a vehicle power state, such as computer and sensors on with all foil actuators off. The LEDs would be used to indicate the vehicle power state and status. Individual foil actuators could have red and green status LEDs for leaking, overheating, and communication.



## Chapter 3

# Design of Foil Actuators

The foil actuators make this AUV unique. Most of the design effort for the vehicle was concentrated on the foil actuators. In order to maximize the reliability of the vehicle, more emphasis was placed on simplicity and robustness than on performance. To achieve a modular design, a single foil actuator contains all the components necessary to add one foil to the vehicle. There are two DC brush motors, a two axis motion control card, two PWM amps, gears, bearings, and frame enclosed in waterproof plastic housings.

There are two generations of foil actuator designs. In the first design, all the components were placed in a single housing. While the mechanical actuation and wiring were simple with a single housing, the sealing was complex. The dynamic seal between the foil and housing limited the depth of operation, range of motion, and the fatigue life.

The first design was improved to increase the depth rating of the actuator and the range of roll motion of the foil. The design was changed to be contained in two independently sealed housings, one that remains stationary with respect to the vehicle and a second that rotates about one axis with respect to the other housing. Having two independently rotating housings drastically simplified the sealing problem, which improved the robustness of the seals and the range of motion on the roll axis. The major problem with the second design is that the mass of the solid moving parts is relatively high, which increases the energy wasted on inertia and decreases the

bandwidth of thrust vectoring.

A future design should be substantially smaller and lighter. Smaller amps and motion control cards should be available. Two smaller motors on the roll axis could be used to completely eliminate the backlash and to increase the torque. A passive mechanical spring on the roll axis would improve the operational efficiency and bandwidth. Direct drive on the pitch axis would decrease the size of the pitch housing, and enable higher frequency motions on the pitch axis. Currently the torque on the pitch axis is limited by the shaft couplings and not by the power of the motor.

There are two rotational motions about orthogonal axes. One motor is dedicated to each axis so the motions are decoupled. The roll motor is a Litton Polyscientific model C34-L60-W10, with the HEDS 5600-500 rotary encoder. The pitch motor is a Litton Polyscientific model C13-L19-W20, with the HEDS 5500-500 rotary encoder. Refer to Table 3.1 for more detail.

Technical references for these motors are available at *<http://www.polysci.com>*

There is a two axis motion control card located within each foil module. Each motion control card has a processor with solid state memory and an Ethernet card with a unique IP address. There is a simple program running locally on each motion control card. This program executes closed loop motion control for sinusoidal velocity trajectories and computes transitions between desired motions. Kinematics commands are sent from the single board computer in the form of amplitudes, phases, and frequencies. Refer to Figure 2-2 for a power, communication, and control schematic.

The motion control cards are the Galil Motion Control model DMC-1425.

Software and technical references for the motion control cards are available at *<http://www.galilmc.com>*

The PWM amps are Advanced Motion Controls series 25A model 12A8. They accept a reference voltage from the motion control card and output a current to the

	ROLL MOTOR	PITCH MOTOR
Rated Terminal Voltage	12-30 V	6-24 V
Rated Current	8.20 A	1.8 A
Torque Sensitivity	0.08 N-m/A	0.0242 N-m/A
Back EMF	0.08 V/rad/s	0.0242 V/rad/s
Terminal Resistance	0.43 $\Omega$	2.30 $\Omega$
Terminal Inductance	0.90 mH	0.84 mH
Rotor Inertia	2118.45 g-cm <sup>2</sup>	18.4 g-cm <sup>2</sup>
Stiction Torque	0.11 N-m	0.01 N-m
Damping	0.02 N-m/KRPM	0.001 N-m/KRPM
	ROLL GEARHEAD	PITCH GEARHEAD
Gear Reduction	two stage 25.01:1	three stage 50.89:1
Efficiency	75%	70%
Maximum Backlash	1.5 <sup>0</sup>	2.5 <sup>0</sup>
Shaft Inertia	0.125 g-cm <sup>2</sup>	1.49 g-cm <sup>2</sup>
Maximum Torque	60 N-m	4.5 N-m
Maximum Axial Load	120 N	30 N
Maximum Radial Load	600 N	100 N
	ROLL PWM AMP	PITCH PWM AMP
Operating Voltage	24 V	24 V
Maximum Continuous Current	6.0 A	6.0 A
Maximum Peak Current (<2.0s)	12.0 A	12.0 A
PWM Switching Frequency	36 kHz	36 kHz
	ROLL ENCODER	PITCH ENCODER
Resolution (including quadrature, excluding gear reduction)	2000 counts/revolution	2000 counts/revolution

Table 3.1: Specifications of roll and pitch motors

motors that is linearly proportional to the reference voltage. The PWM switching frequency is 36 kHz.

Technical references for the PWM amps are available at

<http://www.a-m-c.com>

Variable	Description	Default Value
AMX	Roll Amplitude [deg]	
AMY	Pitch Amplitude [deg]	
PHIX	Roll Phase [deg]	0
PHIY	Pitch Phase [deg]	-90
FR	Frequency [Hz]	
TRNRATE	Number of Cycles to Transition Motion	2
BIASX	Static Roll Bias (Relative Adjustment) [deg]	0
BIASY	Static Pitch Bias (Relative Adjustment) [deg]	0
CHANGE	Set value to 1 to update motion	0
STOP	Set value to 1 to stop motion	0

Table 3.2: List of variables for program running on motion control card.

### 3.1 Single Housing Design

The single housing design is very simple. There is an aluminum frame inside a Lexan housing. The roll motor is face mounted to a bulkhead, as seen in Figure 3-3. The pitch motor and the pillow blocks constraining the foil are attached to a plate. Refer to Figure 3-4. That plate is cradled between the shaft on the roll motor and large double roller taper bearing. The PWM amps and the motion control card are mounted beside the roll motor.

There is one dynamic seal and four static seals in this design. The dynamic seal is a large flexible cone shaped bellows, as seen in Figure 3-5. The bellows forms a rotary shaft seal at the base of the foil and a static o-ring seal at the side of the Lexan housing. There is an o-ring seal at the lid of the housing.

Power and communication are sent to the module through two waterproof cables and connectors. These cables and connectors were purchased from Impulse Electronics, as seen in Figure 3-2

Closed loop foil motion control is achieved with two servomotors and a two axis motion control card. There is a program running locally on the motion control card, which minimizes the communication required to operate the module.

This actuator was used by Melissa Flores for measurements of hydrodynamic force data and flow visualizations. The results of those experiments are detailed in her thesis [11].

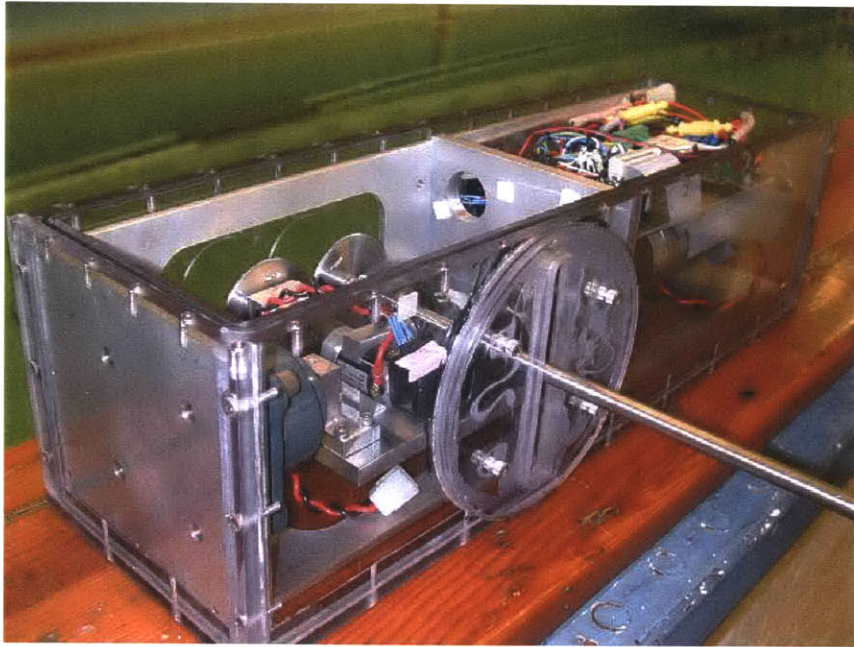


Figure 3-1: Single housing foil actuator.

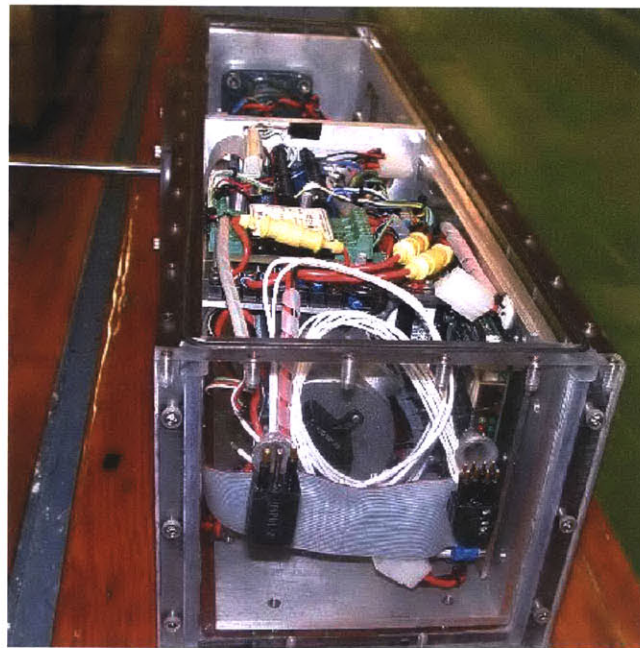


Figure 3-2: Single housing foil actuator.

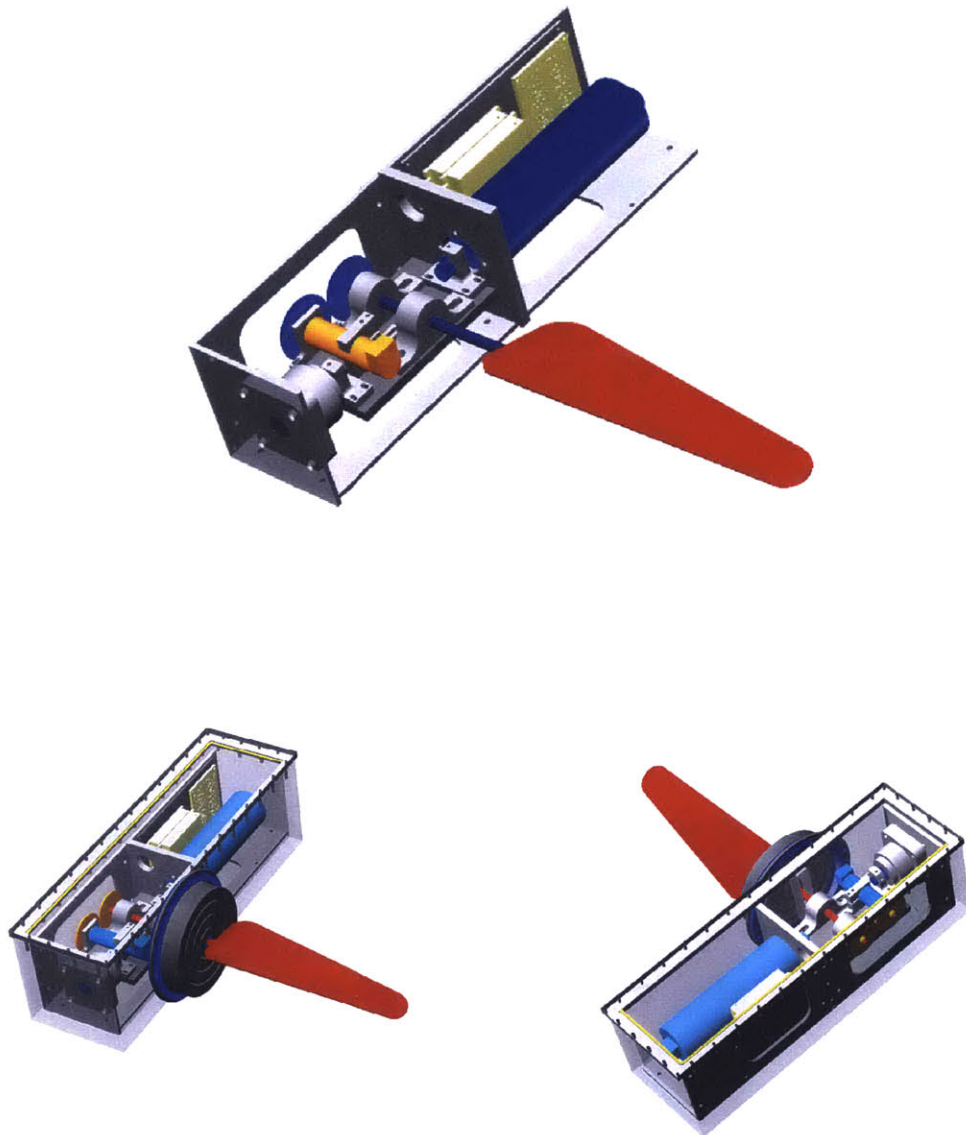


Figure 3-3: Drawings of single housing foil actuator. The center line of the roll axis crosses the center line of the pitch axis. There are radial ball bearings in the pillow blocks that constrain the shaft attached to the foil. There are set screws on the inner collar of the radial ball bearings that constrain the shaft in the axial direction. The large bearing attached to the vertical plate at the far end is a double roller taper bearing. This bearing can take large radial and axial forces, and large moments about the pitch and yaw axes. This design is highly over constrained, which allows no motion on axes other than pitch and roll. The range of motion on the pitch axis is 360 degrees. The total range of motion on the roll axis is 26 degrees due to the stiffness of the bellows. The limited range of motion on the roll axis and the poor robustness of the bellows were the major problems with this design.

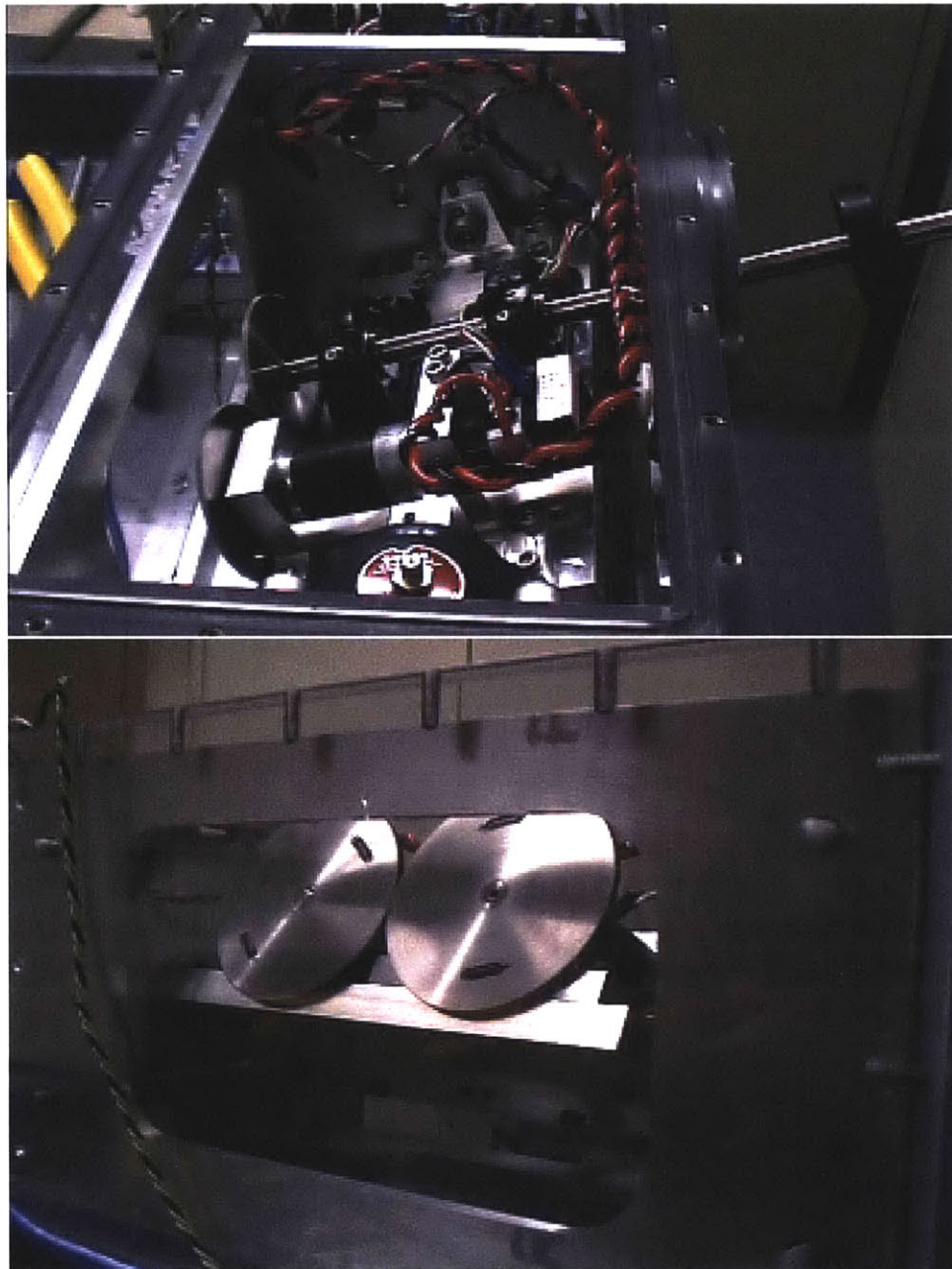


Figure 3-4: Inside of single housing foil actuator. The pitch actuation is achieved with a small DC brush motor with a three stage gear reduction, resulting in a drive ratio of 50.89:1. Power is transmitted from the pitch motor to the shaft through two stainless steel anti-backlash gears. The anti-backlash gears are actually two pairs of gears with a very fine teeth that are loaded against each other with two pairs of springs. As the pitch motion is reversed the torque that is immediately transmitted is proportional to the tension in the springs. The gears are attached to the shafts with set screws on a flat and a spring pin. While these anti-backlash gears did have near zero backlash, they were only capable of transmitting about 1.5 newton-meters of torque.

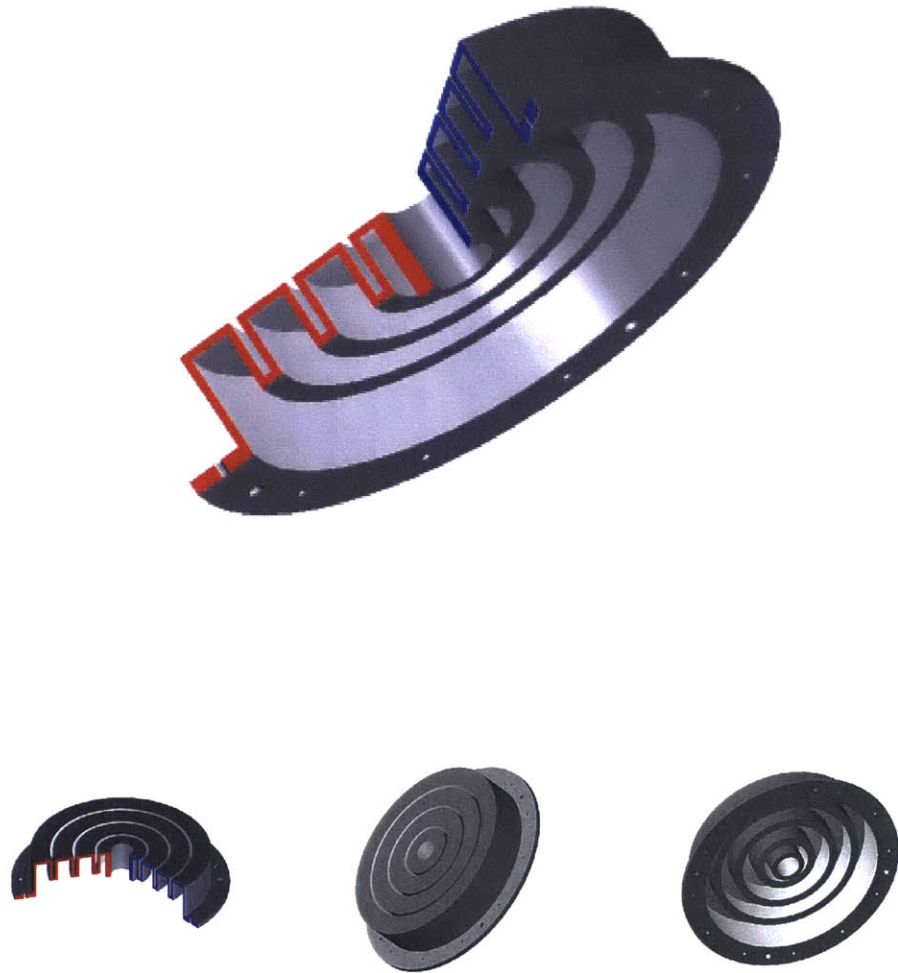


Figure 3-5: Drawings of the bellows. The bellows is made of a flexible urethane and Kevlar composite. The urethane has a Shore A hardness of 30. The Kevlar was cut to form overlapping triangular sheets. This cross-section made the bellows much stiffer in compression than in tension. A better design would a cross-section more like a sine wave with a duty cycle of 0.5, however a mold for that design would be very complicated to machine or very expensive to buy. The fatigue life of this design was measured to be about 60,000 cycles. This fatigue life would need to be increased by at least a factor of 10 to be useful on a vehicle.



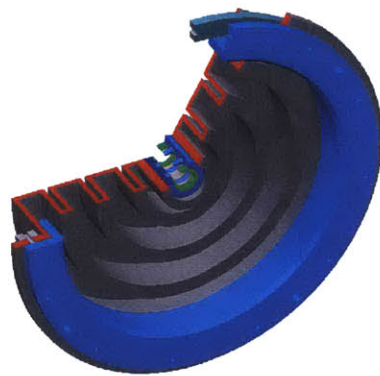
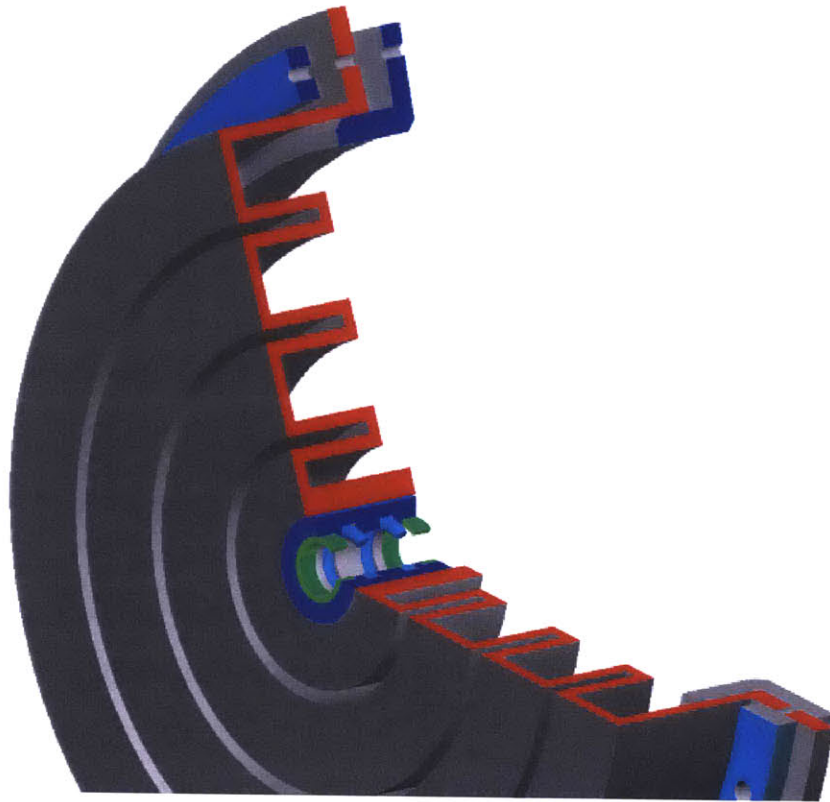


Figure 3-6: Drawings of the bellows assembly with shaft seal and retaining rings. The shaft seal has two buna-n o-rings and two teflon bushings. The larger inner retaining ring bolted to the side of the Lexan housing, and mated with an o-ring on the inner radial face. The smaller outer retaining ring compressed the bellows on the outermost planar surface to form a gasket seal.

## 3.2 Two Housing Design

In order to eliminate the bellows seal the pitch motor and pillow blocks were moved into a separate housing. With two housings there are two dynamic seals that function as conventional rotary shaft seals, and nine static seals. Refer to Figure 3-8.

The roll motor and electronics are contained in a PVC tube. The roll motor is face mounted to a bracket attached to a circular plate. Refer to Figure 3-10. The PWM amps and motion control card are mounted to an L bracket that is cantilevered from the same base circular plate. Power and communication are sent through Impulse cables penetrating the end plug on the PVC housing.

The pitch motor and pillow blocks are housed in a cylindrical block of Delrin, as seen in Figure 3-9. Power and communication for the pitch motor are received via two waterproof cables connecting the housings. The pitch motor is connected to the foil shaft with sprockets and chains. The sprockets and chains have zero backlash and can transfer 2.5 N-m of torque. The sprockets and chains were purchased from W.M. Berg. Refer to <http://www.wmberg.com> for more detail on these components.

The two housing actuator is mounted to the vehicle frame with a large aluminum C bracket. There is a wet bearing at one end of the C bracket that constrains the pitch housing. The wet bearing is made of a composite material called Rulon, and has low friction and high strength. The other end of the C bracket is attached to the circular plate that constrains the roll motor, electronics, and PVC tube.

Torque is transmitted from the roll motor to the pitch housing through a stainless steel bracket bolted to the Delrin housing. This bracket is clamped to the shaft on the roll motor with a large shaft coupling, as seen in Figure 3-10.

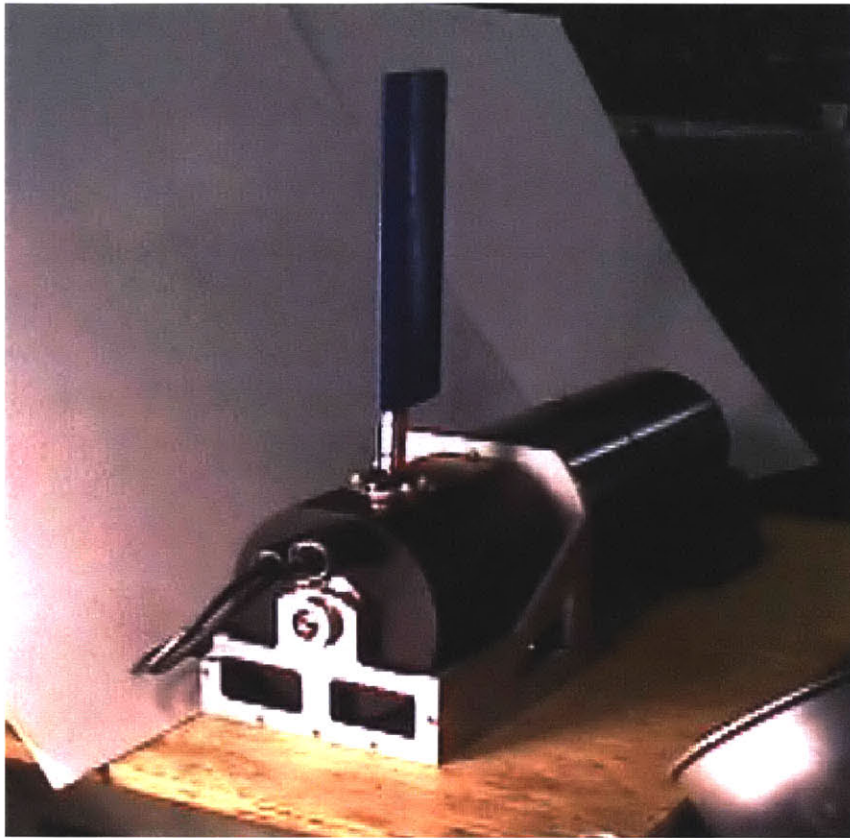


Figure 3-7: Two housing foil actuator.

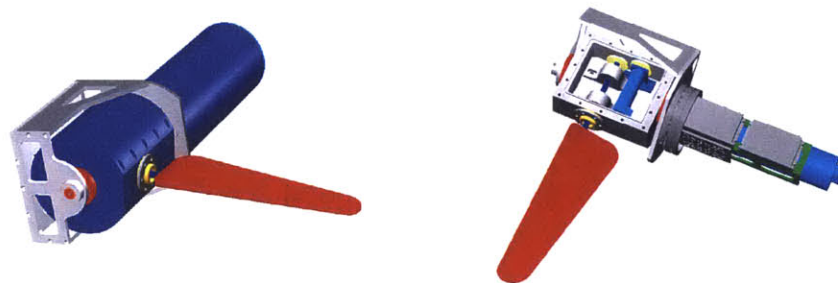


Figure 3-8: Drawings of the two housing foil actuator.

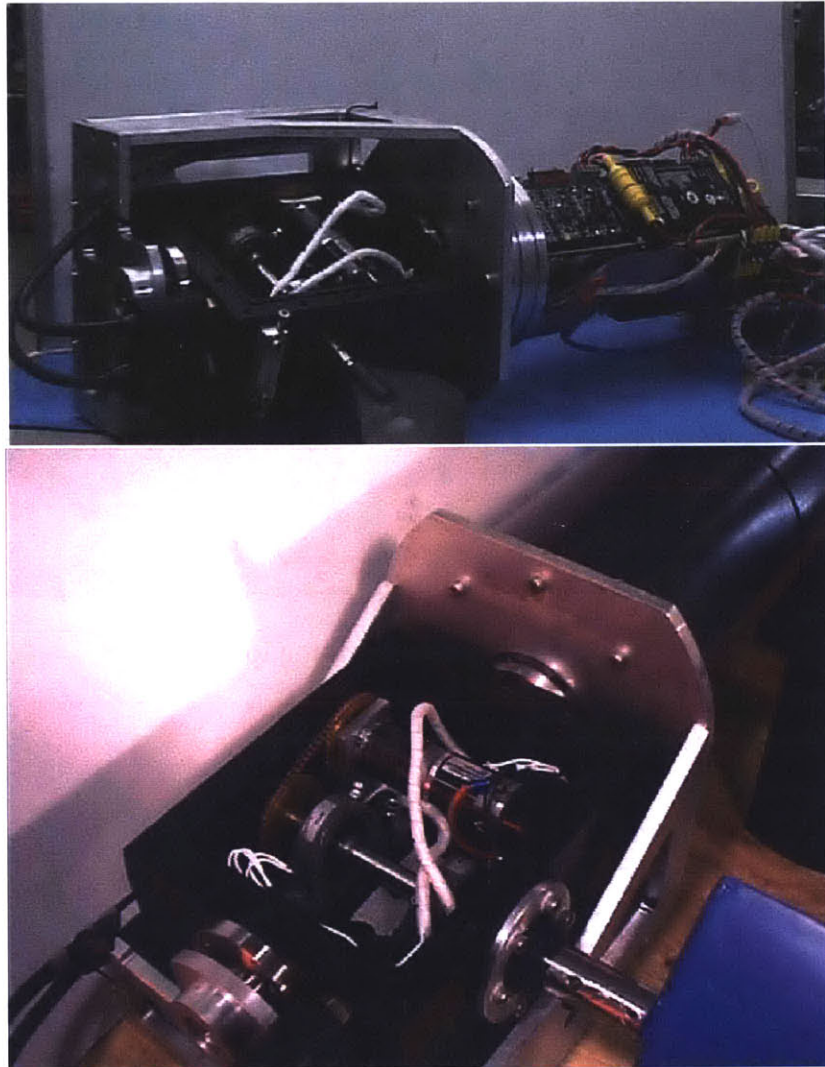


Figure 3-9: Inside the two housing foil actuator.

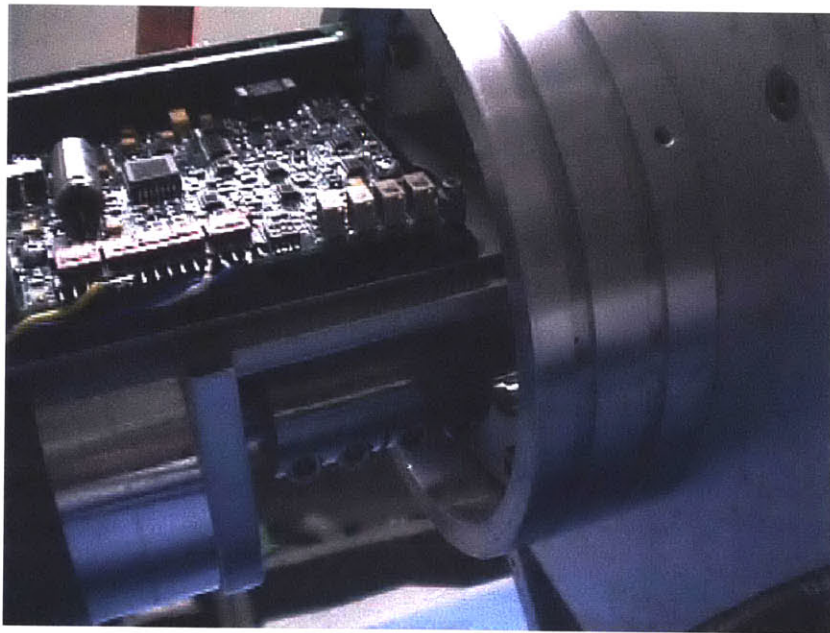


Figure 3-10: Close up of the roll shaft coupling and one of the PWM amps in the two housing actuator



Figure 3-11: Drawings of the pitch seal boot. The large lift and thrust forces cantilevered out on the foil result in radial deflections of the shaft attached to the foil. In order to prevent these radial deflections of the shaft from transmitting large loads to the shaft seal, this seal boot allows the shaft seal to ride on the shaft and the deflections are taken up in the compliance of the boot. These deflections are on the order of several millimeters. While these deflections may seem small, o-ring seals need tolerances on the order of 0.01 millimeters. These seal boots are made of a flexible urethane with a Shore A hardness of 70. The depth rating for this seal has not been measured, but it will be on the order of 10 meters. Fatigue is not an issue with these seals because the small motions of the boot.

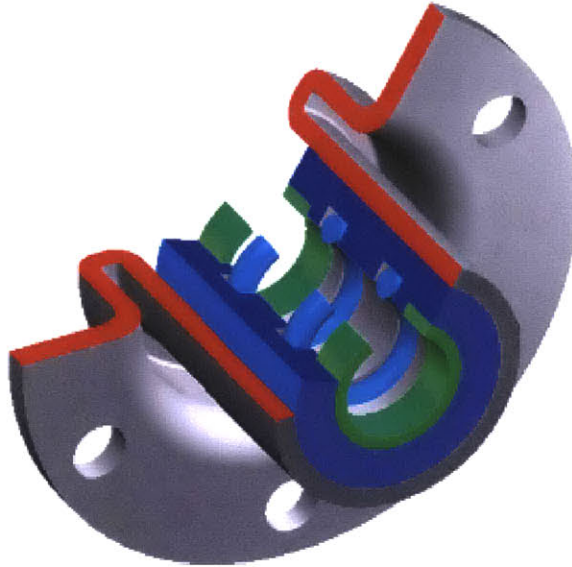


Figure 3-12: Drawings of the pitch seal assembly with shaft seal. These shaft seals are identical to the shaft seals used in the bellows. There are two buna-n o-rings and two teflon bushings. The purpose of the teflon bushings is to transmit radial loads and to prevent compression set from occurring in the o-rings. There is an aluminum ring that is used to hold the seal boot to the Delrin pitch housing. There is a gasket seal formed between the planar surface of the seal boot and a planar surface on the pitch housing. The compliance in this boot also allows the dimensional tolerances on the location and alignment of the pillow blocks to be drastically relaxed. Reducing these tolerances greatly simplified the fabrication and assembly of the actuator.





# Chapter 4

## Force Measurements

There were six reasons for taking force data with one of the two housing foil actuators:

1. To make a preliminary map of the hydrodynamic forces over a broad range in the parameter space for a rolling and pitching foil.
2. To determine how sensitive the scaling analysis is to perturbations in geometric similarity.
3. To determine how well the spanwise distribution of the angle of attack profile predicts thrust.
4. To find an appropriate foil size for this particular actuator design.
5. To determine how large the inertial forces are compared to the hydrodynamic forces for this design.
6. To run an actuator for enough time to identify any major problems in the design before assembling the vehicle.

Experimental hydrodynamic force data will always contain some artifacts, however small, of the mechanical apparatus used to make the measurements. These artifacts will be manifested as boundaries in the parameter space of the kinematics, mechanical vibration, and electrical noise. In order to predict the performance of future designs, it will be necessary to understand the interactions between the water and machine.

The boundaries of the parameter space are due to the torque limits of the motors and the strength of the components in the power transmission such as the chains, sprockets, gears, shaft couplings, and shear pins. Signals from most sensors are on the order of millivolts. These low level signals are corrupted by the magnetic fields surrounding motors, amps, and power supplies. There is an additional component in the electrical noise due to the fluctuations in motor torques in response to the inertial forces of the vibrating solid parts, refer to Figure 4-6.

Highly unsteady hydrodynamic forces excite structural modes in the rig containing the sensors. Given that the sampling frequency is higher than twice the lowest structural mode, which should be the case in order to prevent aliasing in the absence of an analogue filter, there will be certain regions in the spectrum of the force data that are highly dependent on the machine used to measure the forces. This component of the signal is normally filtered in order to generalize the knowledge beyond the specific experimental apparatus. The strong presence of these mechanical vibrations in hydrodynamic force data for flapping foil propulsion serves as an indication that mechanical vibrations will be a serious design consideration for flapping foil vehicles. Great care must be taken by the designers of flapping foil vehicles in order drive the lowest frequency of the structural modes well above the excitation frequency of the propulsion forces. Data from accelerometers will be highly sensitive to vibrations in the frame. For a high performance design, the bandwidth of thrust vectoring may be limited by structural vibrations in the frame.

Flapping foil propulsion has the potential to improve both the maneuverability and the efficiency of AUVs, this work is focused on maneuvering rather than efficiency. Previous work [21] [14] [4] has shown that flapping foil propulsion may have the potential to exceed the hydrodynamic efficiency of screw propellers, but this aspect of the propulsion is much more difficult to exploit in practice. The only useful measure of efficiency on a vehicle must include all losses of energy from the batteries to the water. Hydrodynamic efficiency only accounts for the losses in the water. There are losses in the drivetrain for existing designs of flapping foil actuators that do not exist for screw propellers. For the two housing actuator design, a typical value for the

operating efficiency,

$$\eta_{op} = \frac{\overline{F}_x U}{V \overline{I}_{@24}} \quad (4.1)$$

was 10%, with a maximum of 20%. This measure of efficiency is different from the hydrodynamic efficiency, and these findings do not conflict with any of the previous work cited in this thesis. Operational efficiency includes all the losses in the machine, and therefore will enable designers to benchmark the efficiencies of various flapping foil actuator designs. This is a necessary metric to optimize the performance at the vehicle level. A design that incorporates mechanical springs and a higher operating voltage could drastically improve these values. The springs would be used to minimize the energy spent on inertial forces and the increased voltage would reduce the losses due to the impedances in the electronics. Magnetic couplings could be used to eliminate the need for dynamic shaft seals, thus removing the high damping in the seals due to the necessary o-ring squeeze and resulting friction. These magnetic couplings would also enable the vehicle to operate to much greater depths.

Measuring hydrodynamic efficiency is extremely desirable, but it was not possible to measure directly with this experimental setup. In order to make an accurate measurement of the hydrodynamic efficiency there must be an accurate measure of the power input into the water. Normally this power is calculated using torques, forces, and velocities measured directly at the foil. There were no torque sensors available for these experiments. In these experiments the power input was calculated using the voltage and current delivered to the actuator. The hydrodynamic efficiency can not be directly computed using this data, but an approximation could be found with good estimates of the mechanical and electrical losses in the actuator. The mechanical losses are due to the inertia of solid moving parts, friction in the seals, gears, and bearings, and impedances in the amps, wires, connectors, and motors, and the power consumption of the motion control card and encoders.

The thrust coefficient was calculated using the projected area of the foil,

$$C_T = \frac{2\overline{F}_x}{\rho U^2 c s} \quad (4.2)$$

## 4.1 Description of Tests

Cruising tests were done at a forward speed,  $U$ , of 0.5 m/s. Data was taken over a wide range, with large steps, in the parameter space. Measurements were taken at  $St = \{0.2, 0.4, 0.6, 0.8, 1.0, 1.2\}$ ,  $\alpha_{max} = \{50, 40, 30, 20\}$ ,  $s = \{0.6, 0.5, 0.4, 0.3\}$ , and  $\phi_0 = \{60, 40, 20\}$ . In all of the previously cited work, data was taken over a smaller range in the parameter space with higher resolution. This is a preliminary mapping of the parameter space for a rolling and pitching foil. Future work should certainly be done to map out the details of the space where the best performance was found.

Measurements were done over a variety of spans and wake widths. This data could also be used to determine how well scale analysis and nondimensional parameters are able to capture the physics of flapping foil propulsion when geometric similarity is not maintained. This data will help determine how well the measured thrust and lift coefficients from one design can be applied to a design with different  $r_0$  and  $s$ .

### 4.1.1 Setup

#### Description of Tank

Tests were performed at the MIT Towing Tank in March 2003. The tank is 30 meters long, 2.5 meters wide, and 1.1 meters deep.

#### Description of Foil

The distance between the centerline of the roll axis and the root of the foil,  $r_0$  was 0.178 m. The foil was a NACA 0012 with  $\{0.6, 0.5, 0.4, 0.3\}$  m span and 0.1 m chord. The foil was made of a rigid Shore D 50 urethane. There was a 1 cm x 3 cm aluminum frame inside the foil. The frame was not precisely located in the center of the foil, which resulted in a slight asymmetry of the bending stiffness of the foil. This may

have caused some asymmetry in the lift force under heavy loading.



Figure 4-1: Two housing foil actuator mounted to the six axis dynamometer.

#### 4.1.2 Sensors and Calibration

Forces were measured with a six axis strain gauge dynamometer. The dynamometer is an Advanced Mechanical Technology Inc. model MC3A-6-100. This sensor had an appropriate linear force capacity for these tests, but the moment capacity was an order of magnitude too small, refer to Table 4.1. In order to use this sensor it was necessary to constrain the roll and pitch moments about the sensor. To protect the sensor on the moment axes, there were two plates with four threaded rods used to constrain the sensor. Basically the idea is that the threaded rods are compliant in bending and stiff in tension. The rods are placed were in tension to prevent buckling. The nuts on the threaded rods were very tight to prevent slipping and friction. The deformation of the rods was nearly linear elastic, so the sensor could be calibrated with a linear curve fit. Constraining the dynamometer resulted in a slight nonlinearity, refer to Figure

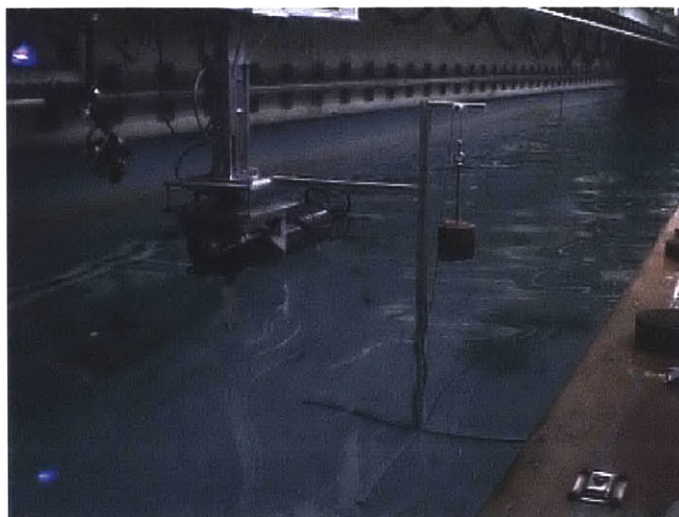


Figure 4-2: Calibration rig used to apply force at the 70% span,  $r_{0.7}$ .

4-3 and 4-4. It would not have been possible to use this sensor without constraining the moments.

Axis	Capacity
F <sub>x</sub> and F <sub>y</sub>	220 N (50 lbs)
F <sub>z</sub>	440 N (100 lbs)
M <sub>x</sub> and M <sub>y</sub>	11 N-m (100 in-lbs)
M <sub>z</sub>	5.6 N-m (50 in-lbs)

Table 4.1: Force and moment capacities for six axis dynamometer

Technical references are available for the dynamometer at  
<http://www.amtiweb.com>

The electrical current delivered to the actuator was measured with a hall-effect current sensor. The sensor was an F.W. Bell model BB-25/100 type 155150. This sensor has a  $\pm 25$  amp range and outputs a signal in the  $\pm 1$  volt range.

Technical references are available of this sensor at  
<http://www.fwbell.com>

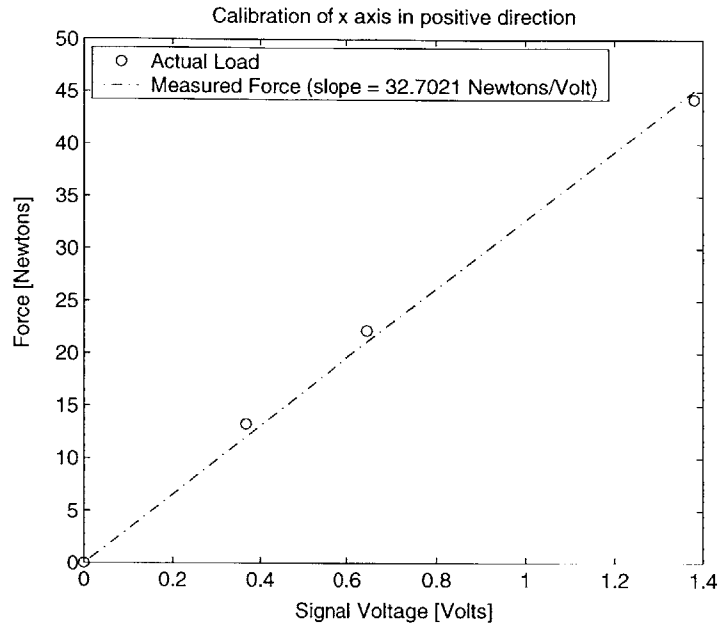


Figure 4-3: Calibration curve for thrust axis. The slight nonlinearity of the sensor is due to the rig used to reduce the roll and pitch sensitivity.

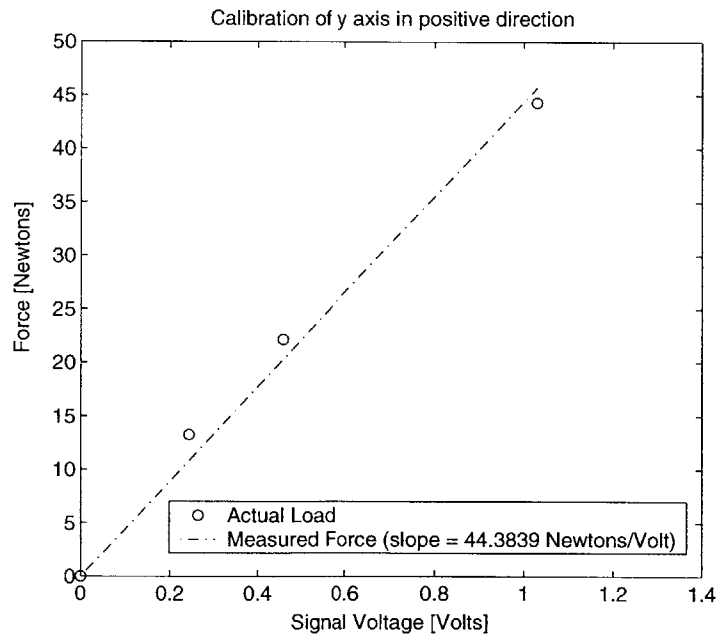


Figure 4-4: Calibration curve for lift axis. The slight nonlinearity of the sensor is due to the rig used to reduce the roll and pitch sensitivity.

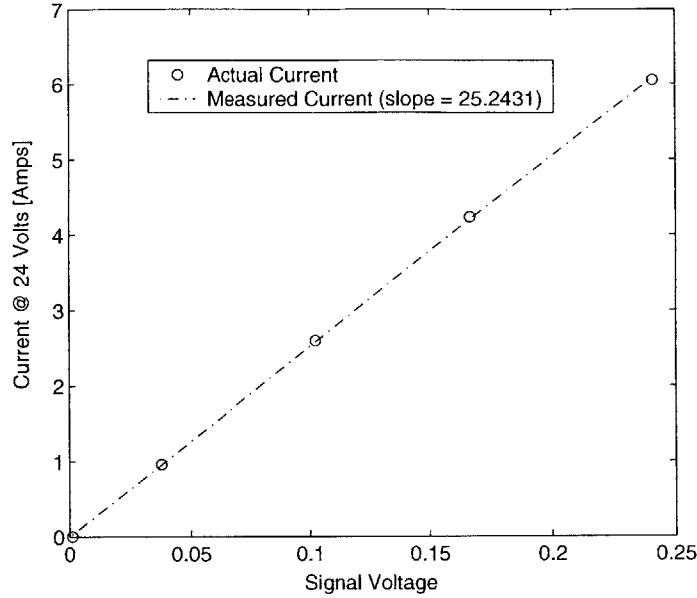


Figure 4-5: Calibration curve for ammeter.

### 4.1.3 Data Acquisition and Control

Data was logged at a sampling rate of 100.040 Hz using a 16 channel 12 bit data acquisition card. The input range on the data acquisition card was set to  $\pm 10V$  on every channel.<sup>1</sup> The foil was controlled with a program running on the motion control card in the foil actuator. The amplitudes, phases, and frequency were input by the user with a laptop via Ethernet. The forward motion of the foil was achieved with a servomotor pulling a carriage along a rail down the tank.

### 4.1.4 Sources of Error

1. Wave action and free surface effects were present. Instead of using a streamlined fairing, the foil actuator was mounted above the water to avoid the bluff body drag on the housings. The root of the foil was approximately 5 cm below the free surface of the water. Substantial wave action was observed for high Strouhal

---

<sup>1</sup>The firmware for this data acquisition card forces every channel to have the same range. The resolution is inversely proportional to the range. Ideally the ranges could be set independently to maximize the resolution for the output of each sensor.



numbers.

2. Structural vibrations in the rig containing the dynamometer were present, refer to Figure 4-6. The motions due to vibration were on the order of 1 mm.
3. Asymmetry in the frame of the foil may have resulted in asymmetry in the lift and thrust forces.
4. The projected area of the foil was rectangular. The sharp corners on the foil reduced the hydrodynamic efficiency and thus the operational efficiency.
5. The actual position of the foil was not recorded. The position data was not used for any calculations, but the actual foil position could have varied from the desired foil position by several degrees for highly aggressive kinematics. The error on the axes was queried regularly during the runs. The error on the pitch axis was typically on the order of 0.1 degrees (not including backlash), and the error on the roll axis was on the order of 2 degrees (not including backlash).
6. Each measurement was repeated twice. The contour plots were made with the mean of the two runs. In the majority of the test matrix the values would vary by less than 7%. For kinematics with large  $St$  and large  $\alpha_{max}$  the values varied by as much as 12%.
7. The water was allowed to settle while the carriage returned to the starting end of the tank. The total time between consecutive runs was about three minutes. It takes fifteen minutes for the tank to completely settle. The shorter settling time was used to enable the full test matrix to be completed in one week.
8. The rig used to constrain the moments on the dynamometer resulted in a slightly nonlinear response, refer to Figure 4-3 and Figure 4-4.
9. The voltage of the power supply was not measured. The power supply had a maximum power output of 500 watts. The foil actuator never drew more than 200 watts and would typically draw 50 watts, so a substantial voltage dip

is unlikely. An unmeasured voltage dip would result in an apparent decrease in the operating efficiency. For example, if the voltage of the power supply dipped by one volt under a heavy load and the measured operating efficiency was 10%, the actual operating efficiency would be 10.4%. This error is always conservative.

10. The actual forward velocity of the carriage was not recorded. There is a closed loop motion control system with a tachometer used to control the forward velocity of the carriage. The user would not include the regions of acceleration or deceleration in the region of data points used to compute means.
11. The pitch position was zeroed at the beginning of every day by repeatedly running the carriage down the tank and searching for the position resulting in minimal mean lift. The zero position was checked again at the end of the day. A typical minimum mean lift value obtained corresponded to a lift coefficient of 0.2.<sup>2</sup>

#### 4.1.5 Testing Procedure

The dynamometer and current sensor were calibrated at the start of every testing day. The natural frequencies in the structure were measured at the beginning and end of every day to determine if any screws had worked loose during testing. The pitch position was zeroed at the beginning of every day and checked again at the end of the day.

For a given foil size two measurements were taken at every Strouhal number, maximum angle of attack, and roll amplitude. The following day the foil was removed from the actuator, cut to the next span length, and the new sharp edges were slightly

---

<sup>2</sup>This nonzero value for lift is likely due to the interaction between the backlash on the pitch axis and the munk moment on the foil. This interaction between the backlash and munk moment would be very sensitive to the stiction in the pitch seal. It is also important to consider that very small forces are difficult to measure due to electrical noise, and the resolution of the dynamometer and data acquisition card.

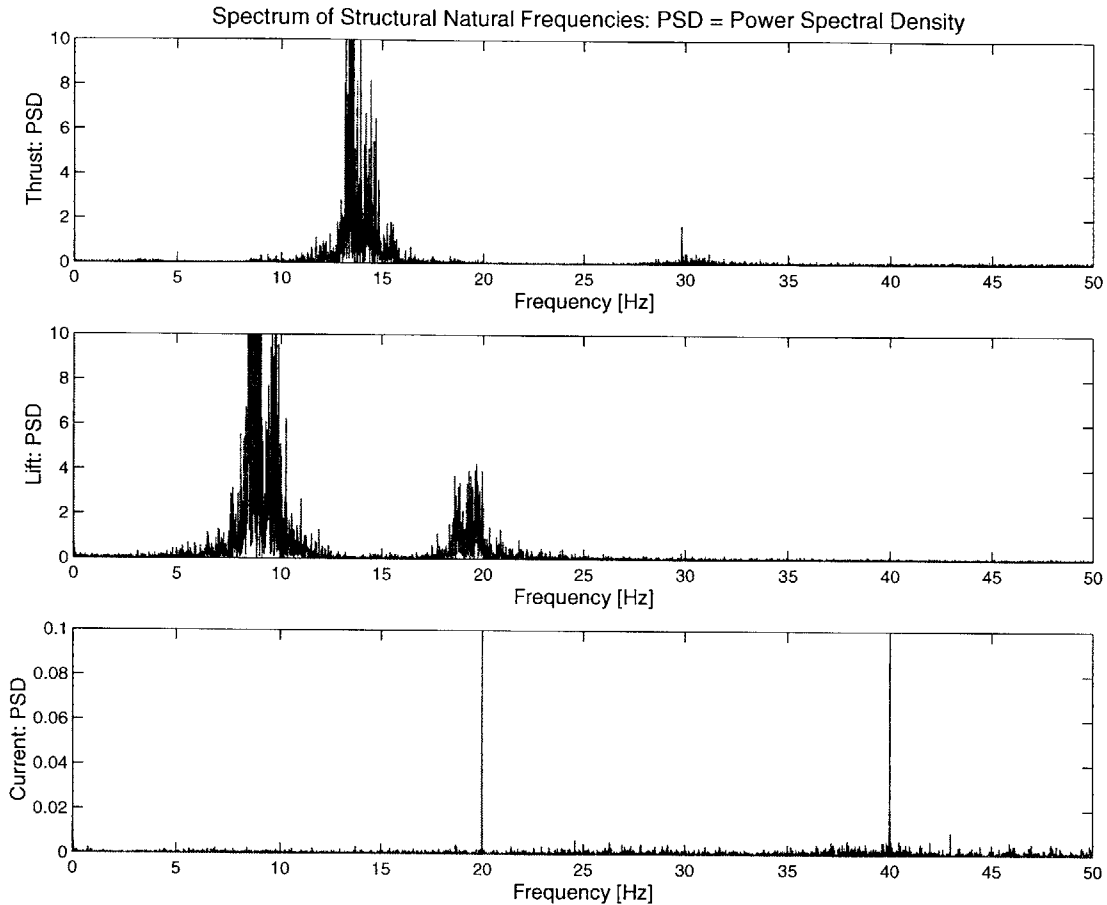


Figure 4-6: Spectrum of mechanical vibrations and line noise. The natural frequencies were measured by repeatedly jarring the structure constraining the dynamometer, with the motors and sensors on. The motors were commanded to maintain a zero position. The structure was hit in many different directions, with forces of varying magnitude. Data from the dynamometer and current sensor was logged at 100.040 Hz for several minutes, while the structure was perturbed approximately every 10 seconds. The dominant structural mode (7 - 10 Hz on the lift axis) was due to the cantilevered mass of the actuator, refer to Fig 4-1. The mechanical vibrations on the thrust axis were at a higher frequency because the structure has a greater stiffness in that direction. The magnitude of the deflections due to vibration were on the order of 1 mm. The motion of the foil in the water was minimal due to the backlash on the roll axis. The backlash on the roll axis minimized the effect of the added mass of the water on the foil, and as a result the frequencies of these vibrations were not effected by the size of the foil. The two sharp peaks in the current signal are due to aliasing of electromagnetic interference from 60 Hz 120 volt AC power and 180 Hz three phase 220 volt power. In postprocessing the hydrodynamic force data, the raw data was filtered by convolution at 6 Hz on the lift and current axes, and 8 Hz on the thrust axis. The current signal was filtered at 6 Hz because in some runs there was a strong 7 - 10 Hz component in the current signal due to mechanical vibrations on the lift axis. Means were computed with both the filtered and unfiltered data, and values were consistent within 1.5%, typically varying by 0.5%.

rounded (approximately 2 mm radius round on the edges near the tip of the foil). The sensors would be calibrated and the next block of experiments were conducted.

The forward speed of the carriage was 0.5 m/s and the return speed was 0.2 m/s. The return speed was selected to allow for a moderate settling time between runs. The carriage would be stationary for less than 10 seconds between runs.

In order to find the boundaries of where the actuator could operate in the kinematics parameter space, increasingly aggressive (higher Strouhal number) kinematics were attempted until the saturation of roll torque resulted in a position error on the roll axis greater than approximately ten degrees, or the spring pin would shear on the pitch axis. There was no torque limit enforced on the roll axis. The torque limit on the pitch axis was lowered three times in an effort to increase the fatigue lifetime of the spring pin. The final torque limit used on the pitch axis was 0.9 V (voltage of command sent from motion control card), which corresponds to approximately 1.3 N-m of torque after gear reduction. The design has since been retrofitted with substantially stronger pins, which will enable the full 2.5 N-m to be transferred on the pitch axis. If the two housing actuators are routinely operated at Strouhal numbers greater than 1.0, there will be fatigue problems on the pitch axis. No problems were ever encountered on the roll axis in over 110 hours of testing.

#### **4.1.6 Postprocessing**

All postprocessing was done in Matlab. The file used to process the data was called `postcruise.m` and is located on the Towtank server at `/Vic/Documents/Matlab/`.

To remove the effect of the structural vibrations and electrical noise, the data was filtered at 6 Hz on the lift and current axes and 8 Hz on the thrust axis, refer to Figure 4-6. The filtering was done by convolution, which resulted in zero distortion, attenuation, or phase shift in the pass band.

Means were computed over an integer number of cycles. The number of data points for the integer cycles was computed using the period of foil motion and the sampling rate. The user was prompted to visually inspect the data and select the zero region and load region. For every run the means were computed with both the

filtered and unfiltered data, and the values were consistent within 1.5%, typically varying by 0.5%.

## 4.2 Cruising Data

Figure 4-7 represents a typical case for the time history of the forces and current recorded. The lift force varies at the frequency of foil motion and is very nearly symmetric about zero. The thrust force varies at twice the frequency of foil motion, and the mean is positive. For good thrust producing kinematics, the current is qualitatively similar to the thrust. In regimes with useful thrust kinematics, the measured current may provide a good estimate of the thrust produced on a vehicle given an estimate for the operational efficiency. The distribution of the angle of attack profile is calculated analytically using the commanded motion of the foil and is not synchronized with the measured data. The distribution of the angle of attack profile is presented to enable the reader to make a qualitative assessment of the dependency of the hydrodynamic forces on the spanwise distribution of the angle of attack profile.

Figure 4-8 is a time trace of the maximum thrust force encountered in the test matrix, at  $St$  of 1.2,  $\alpha_{max}$  of 40 degrees, and a span of 0.40 m. The mean thrust force was 37 N, which corresponds to a thrust coefficient of 7.2. The maximum lift force for this run is 100 N. These kinematics correspond to the condition where the mean of the angle of attack at  $r_{07}$  over a half cycle of motion is nearly maximum. The angle of attack profile at  $r_{07}$  is qualitatively similar to a low order Fourier series approximation of a square wave. Under these heavy loading conditions there are substantial cantilevered deflections of the foil. The asymmetry in the thrust force is likely due to the asymmetry in the bending stiffness of the foil due to an asymmetry in the frame. For this run it is notable that the current is qualitatively similar to the thrust.

Figure 4-9 is a time trace of the run with the maximum operational efficiency, 20%. The high operational efficiency corresponds to a mean thrust force of 22 N, and a thrust coefficient of 4.8. These kinematics correspond to the condition when the

angle of attack at the root of the foil is nearly zero for the full cycle of motion.

INPUT: U 0.5 [m/s], span 0.40 [m], chord 0.10 [m], roll 40 [deg], St 0.60, MaxAoa 40 [deg], run2 OUTPUT: Ct 1.6, efficiency 0.09

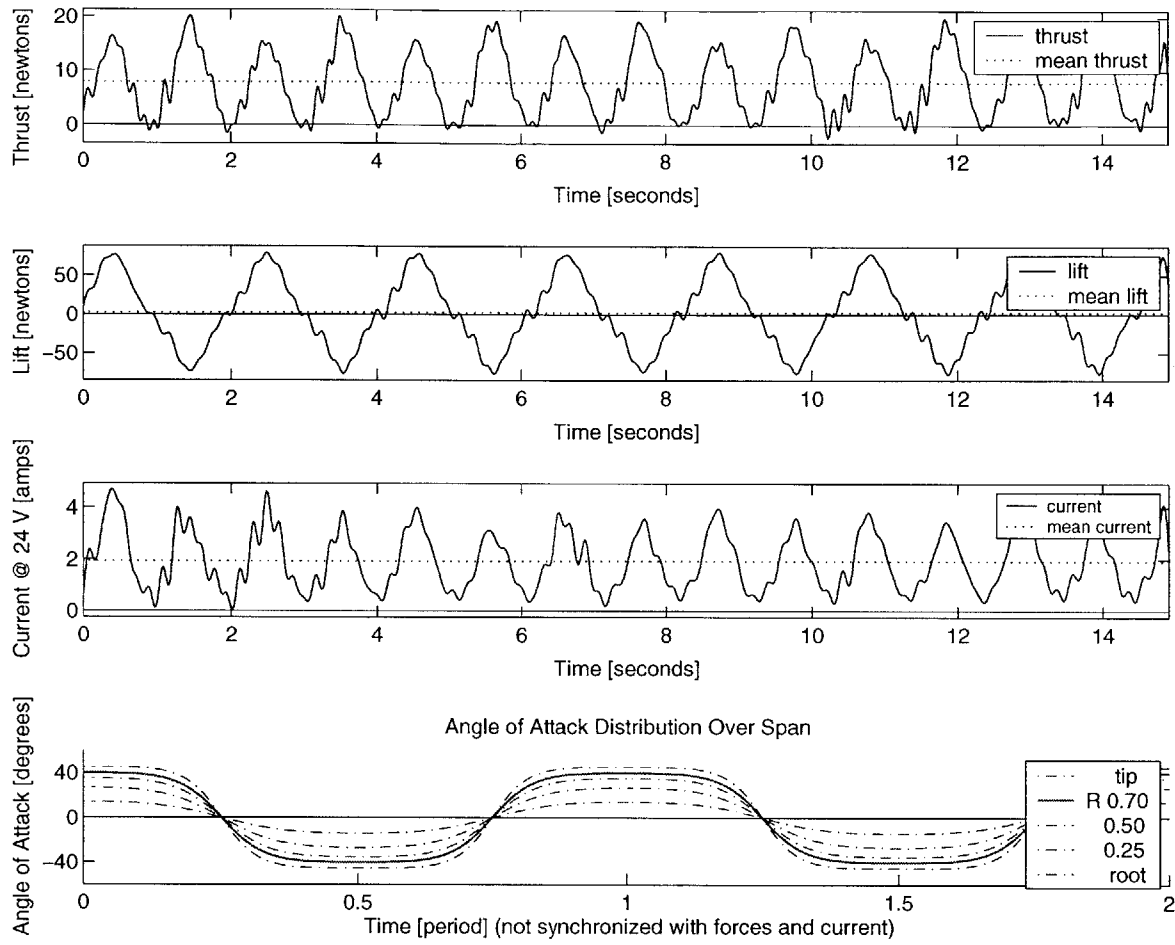


Figure 4-7: A typical case:  $St = 0.6$ ,  $\alpha_{max} = 40$  deg,  $s = 0.40$  m,  $\phi_0 = 40$  deg

INPUT: U 0.5 [m/s], span 0.40 [m], chord 0.10 [m], roll 60 [deg], St 1.20, MaxAoa 40 [deg], run2 OUTPUT: Ct 7.2, efficiency 0.13

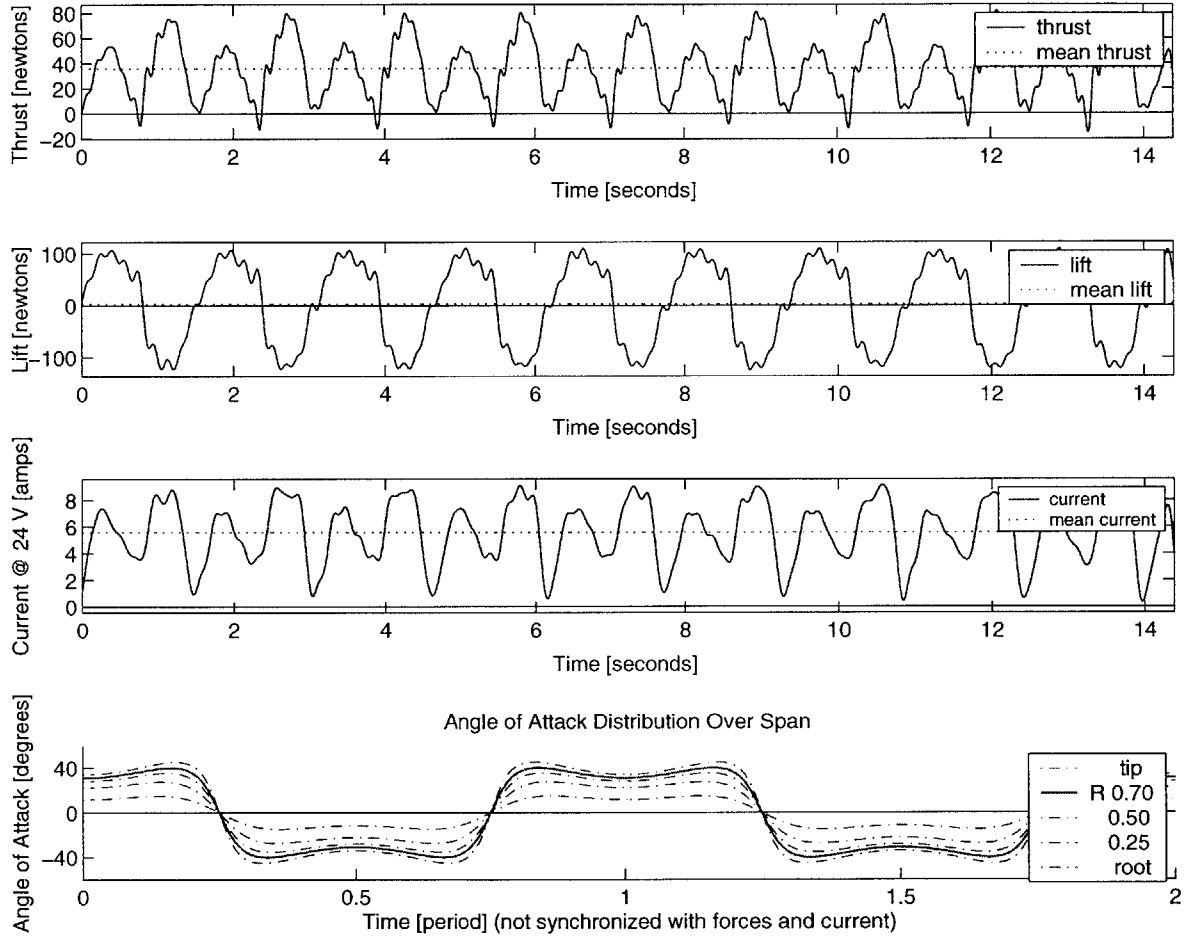


Figure 4-8: A high thrust case:  $St = 1.2$ ,  $\alpha_{max} = 40$  deg,  $s = 0.40$  m,  $\phi_0 = 60$  deg



INPUT: U 0.5 [m/s], span 0.40 [m], chord 0.10 [m], roll 60 [deg], St 1.00, MaxAoa 30 [deg], run1 OUTPUT: Ct 4.8, efficiency 0.20

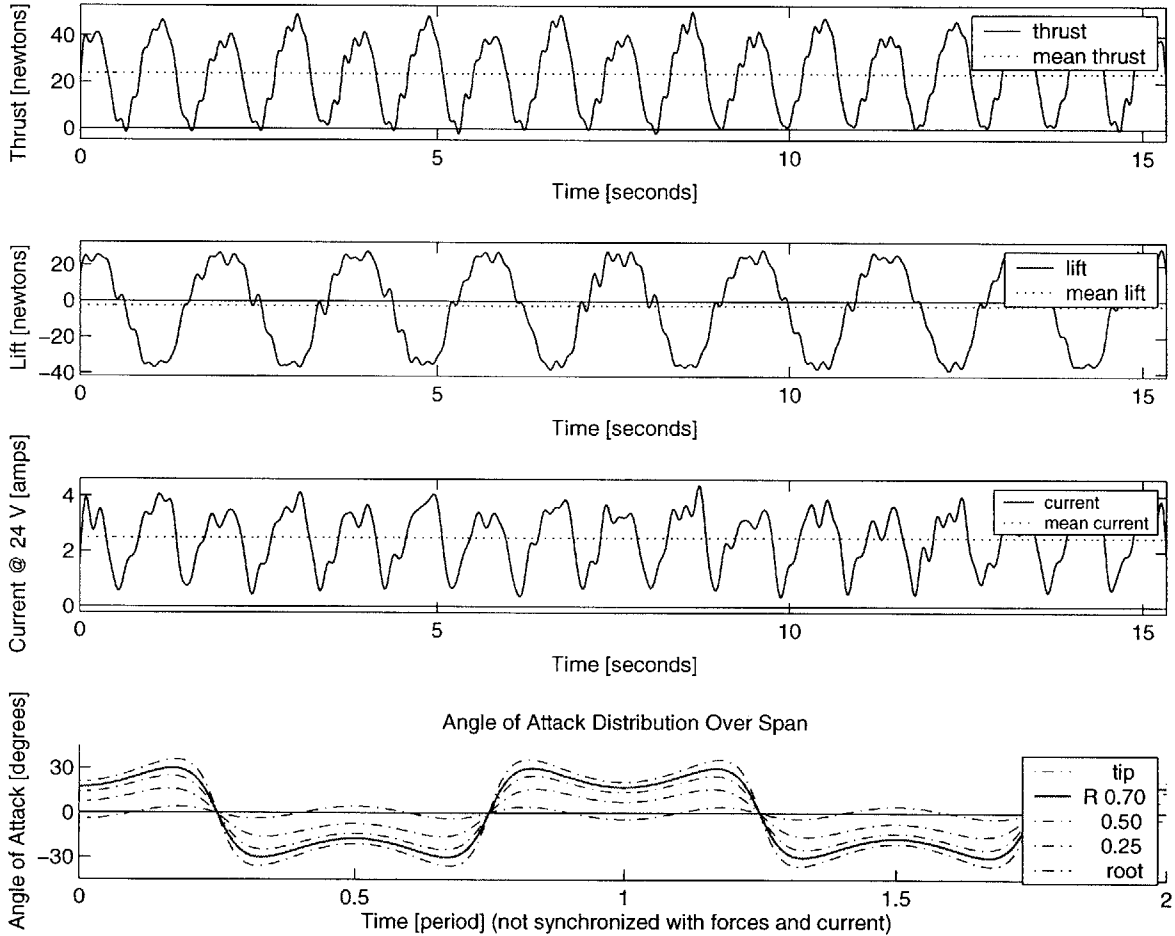


Figure 4-9: A high efficiency case:  $St = 1.0$ ,  $\alpha_{max} = 30$  deg,  $s = 0.40$  m,  $\phi_0 = 60$  deg

Figures 4-10 through 4-13 are contour plots of  $C_T$  as a function of  $St$  and  $\alpha_{max}$ . Each figure represents one foil size. There are three contour plots in each figure, each contour plot corresponds to a roll amplitude,  $\phi_0$ . Higher  $St$  could be achieved at larger  $\phi_0$  because these runs correspond to a larger wake width, when the machine has greater time to accelerate to the maximum velocity. Larger  $\phi_0$  correspond to lower frequencies of foil motion, and therefore lower bandwidth of thrust vectoring capability.

Figure 4-14 is a summary of all 12 coefficient of thrust contour plots on one page. Each column corresponds to a foil size and each row corresponds to a roll amplitude. It is evident from these 12 contour plots that the scaling analysis is robust to perturbations in geometric similarity. The aspect ratio of the foil  $s/c$  varies from 6 to 3, while  $r_0$  is held constant. These geometries and kinematics cover a large range of wake widths ( $1.4 \leq h_0/c \leq 6.3$ ) and a large range of spanwise angle of attack distributions ( $2.18 \leq r_{07}/r_0 \leq 3.36$ ). This is an indication that a designer may apply the nondimensional data from one design to make accurate predictions of the hydrodynamic loads for a future design with a substantially different geometry.

The previous summary of contour plots includes a range of foil sizes, Figure 4-15 provides the same 12 contour plots with the dimensional mean thrust. The dimensional force data is used to find the maximum thrust in the test matrix. The 0.40 m span foil provided the largest thrust forces.

Contour plots of operational efficiency as a function of  $St$  and  $\alpha_{max}$  are presented in Figure 4-16. The 0.40 m span foil provided the largest operational efficiency. The operational efficiency was highest when  $\alpha_{max}$  is close to 30 degrees.

In order to demonstrate the effect of foil size on thrust vectoring bandwidth, the dimensional thrust and operational efficiency are plotted as a function of frequency in Hertz and  $\alpha_{max}$ , as seen in Figures 4-17 and 4-18. The 0.6 m foil and 60 degree roll amplitude correspond to a low frequency of motion, in the 0 to 0.4 Hz range. The 0.3 m span foil with 20 degree roll amplitude corresponds to a frequency range of 0.7 to 1.5 Hz.

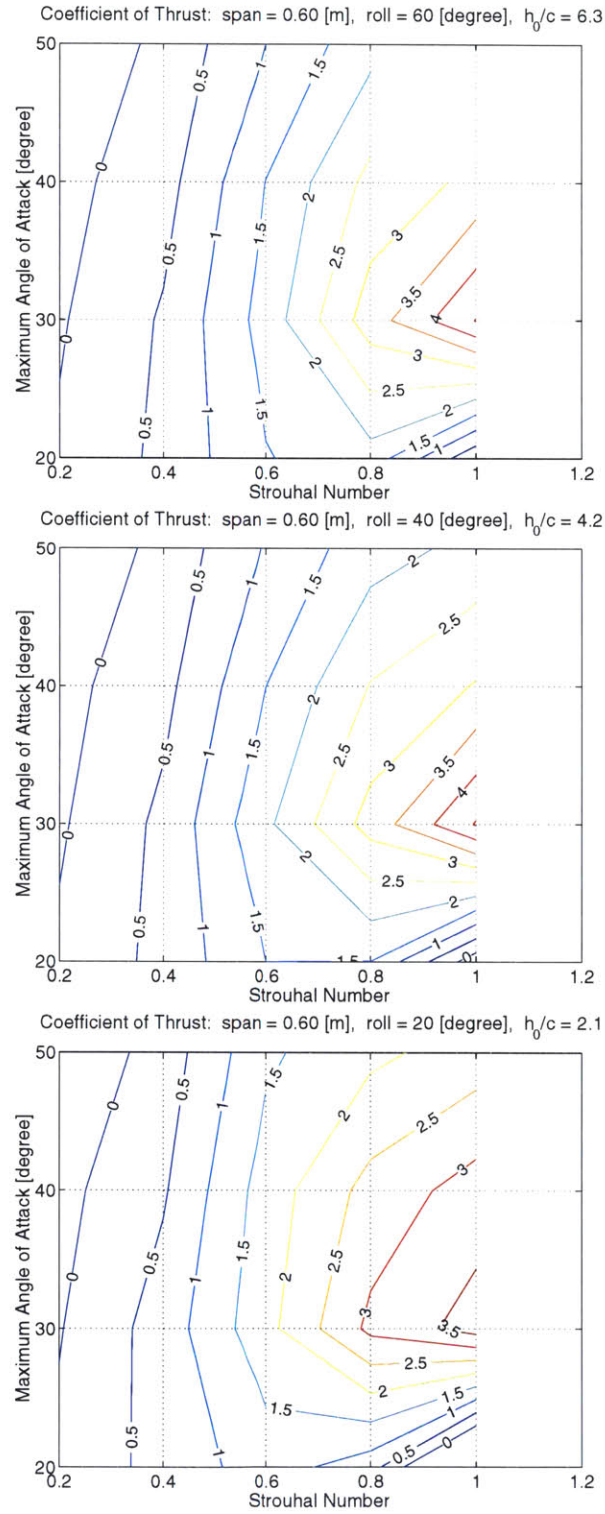


Figure 4-10: Contour plots for coefficient of thrust  $C_T$ :  $s = 0.60$ ,  $\phi_0 = \{60, 40, 20\}$

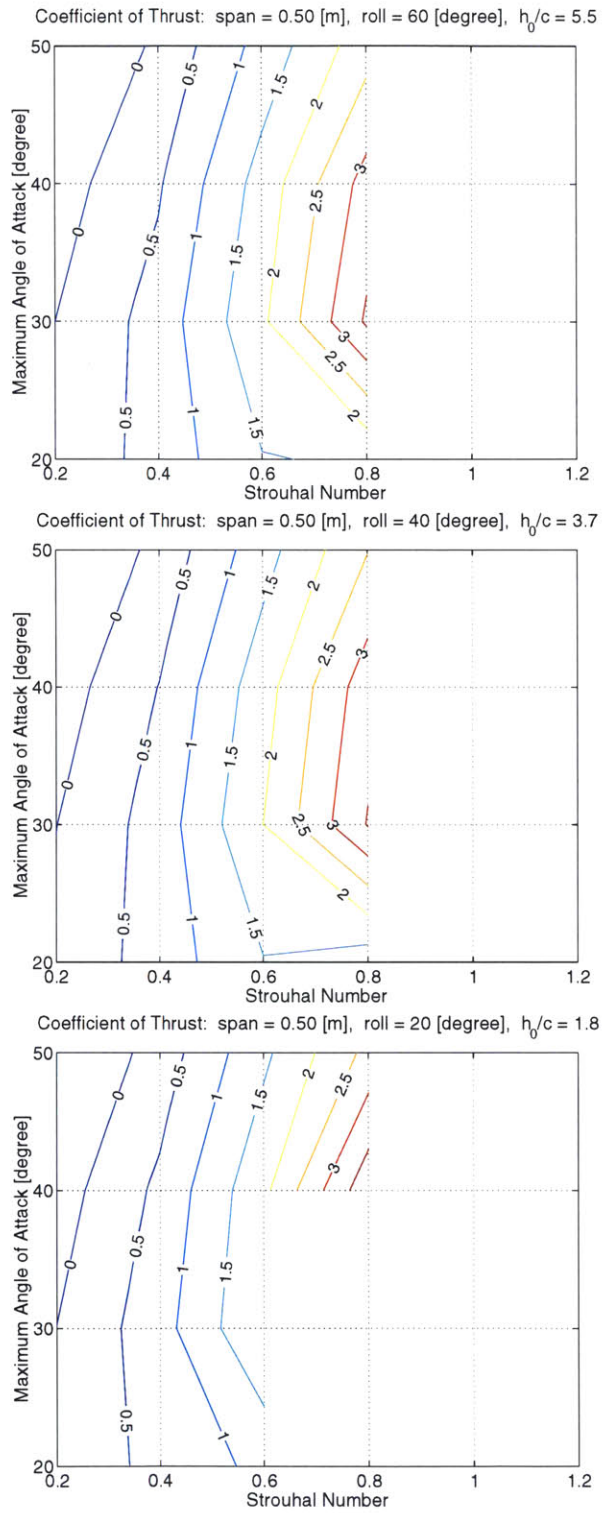


Figure 4-11: Contour plots for coefficient of thrust:  $s = 0.50$ ,  $\phi_0 = \{60,40,20\}$   
 Note: The actuator could have operated up to  $St$  1.0, the data is missing due to over conservative torque limits

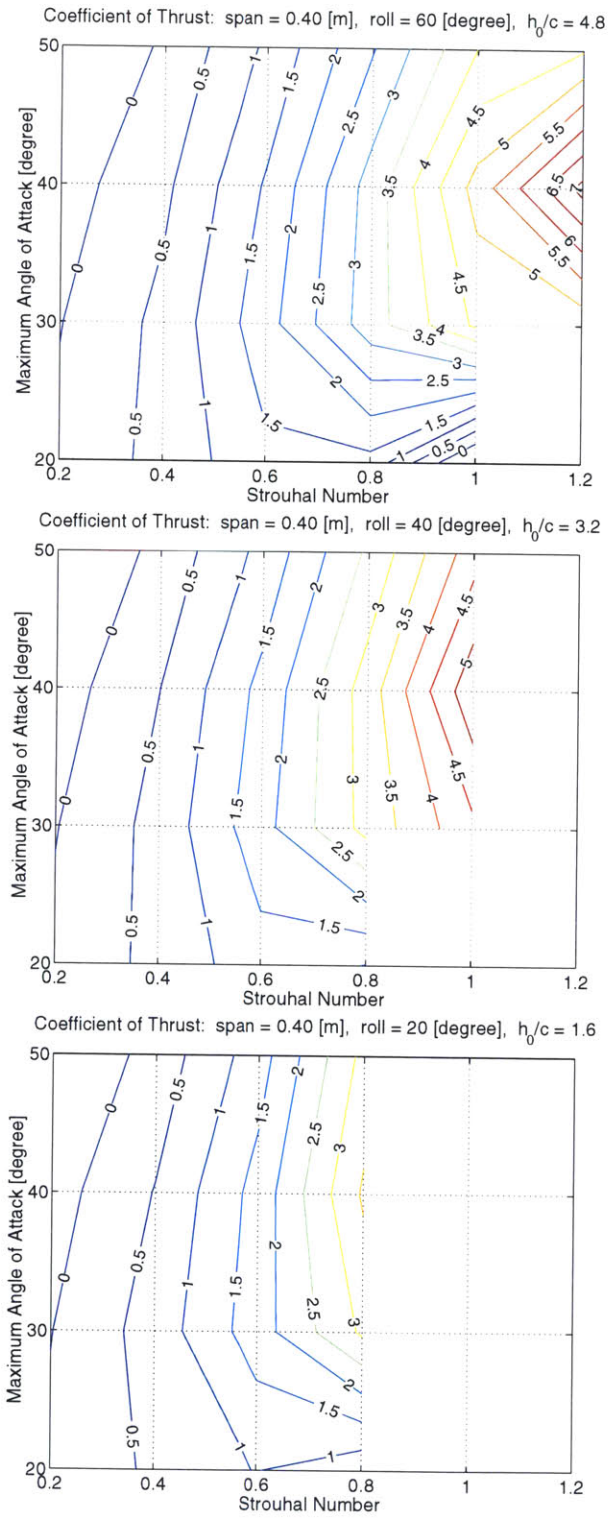


Figure 4-12: Contour plots for coefficient of thrust  $C_T$ :  $s = 0.40$ ,  $\phi_0 = \{60,40,20\}$

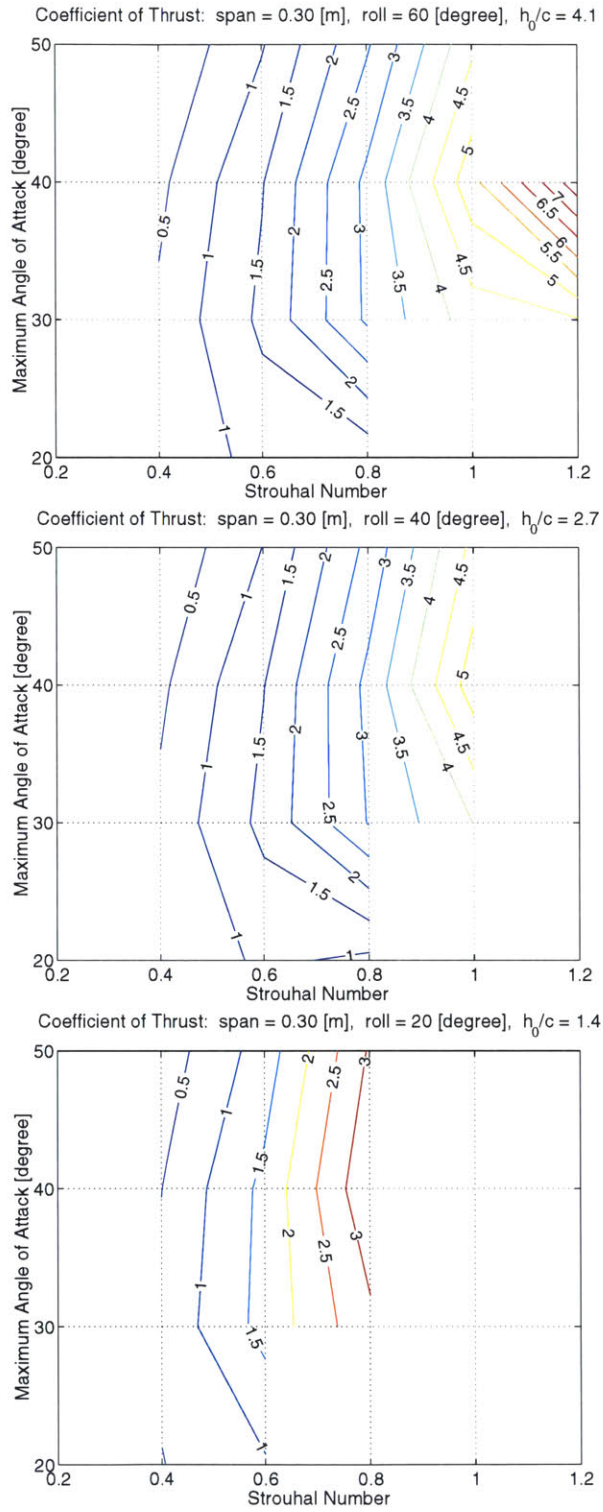


Figure 4-13: Contour plots for coefficient of thrust:  $s = 0.30$ ,  $\phi_0 = \{60, 40, 20\}$

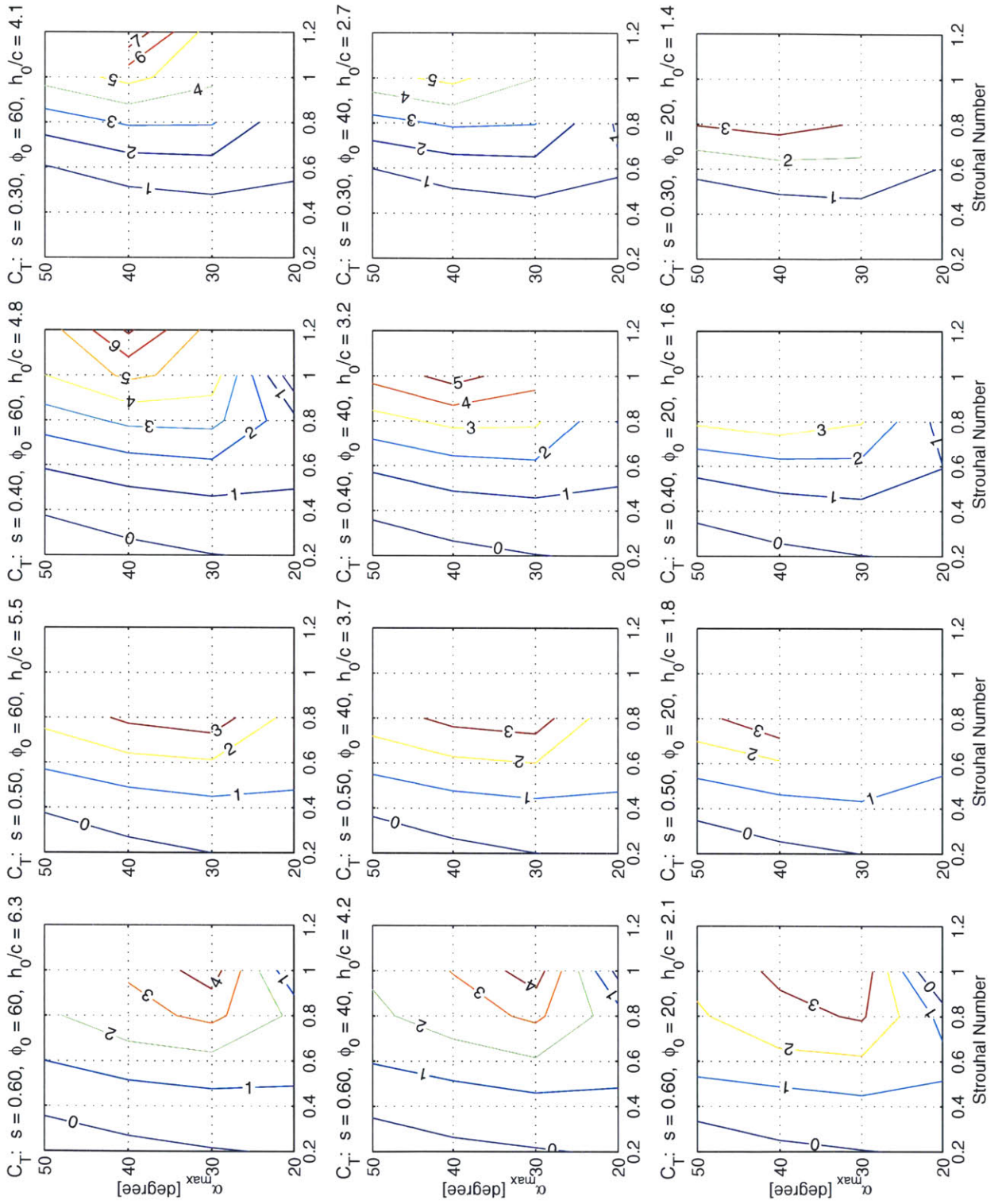


Figure 4-14: Summary of contour plots for coefficient of thrust  $C_T$

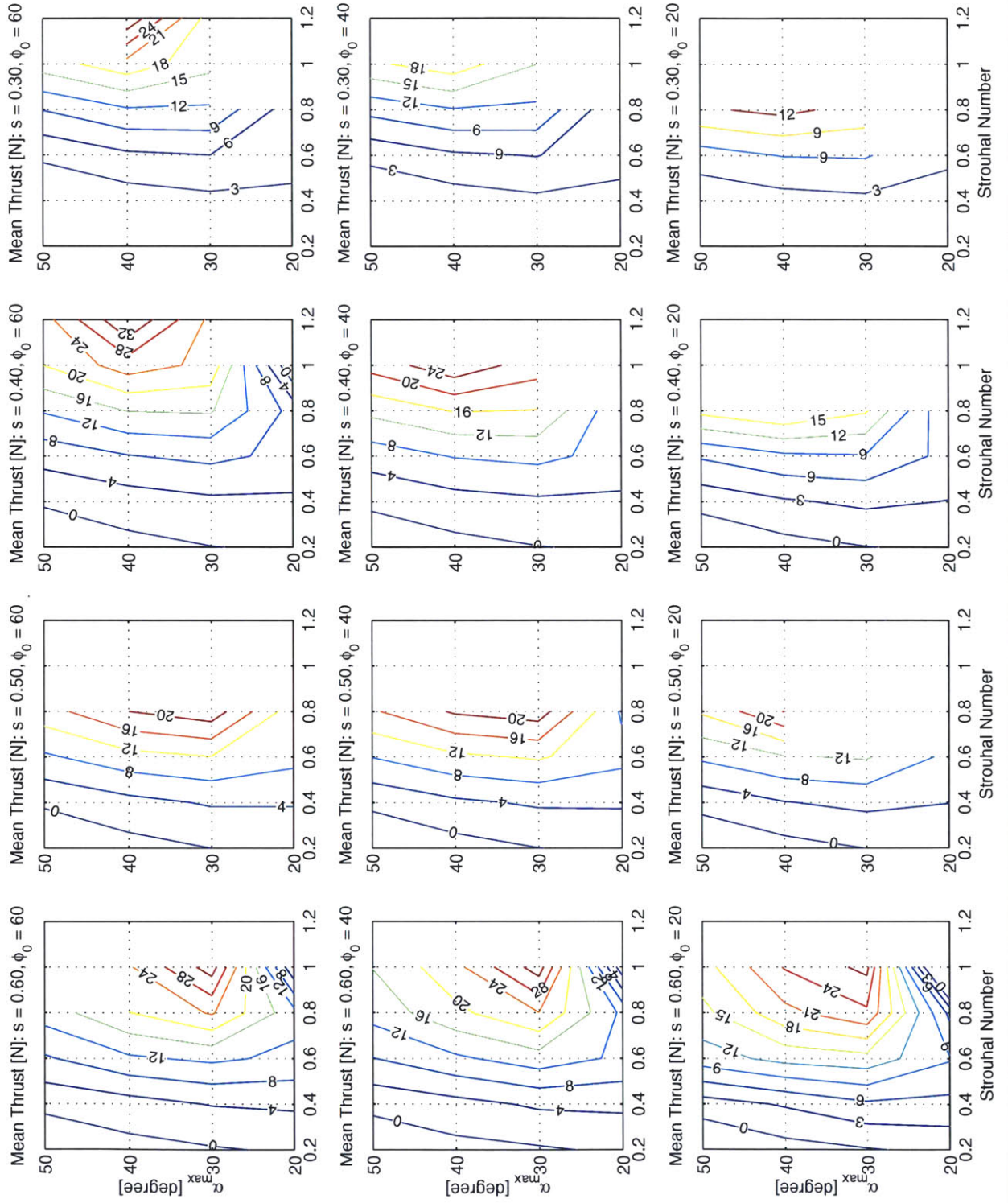


Figure 4-15: Summary of contour plots for mean thrust  $\overline{F}_x$  [N], with  $St$



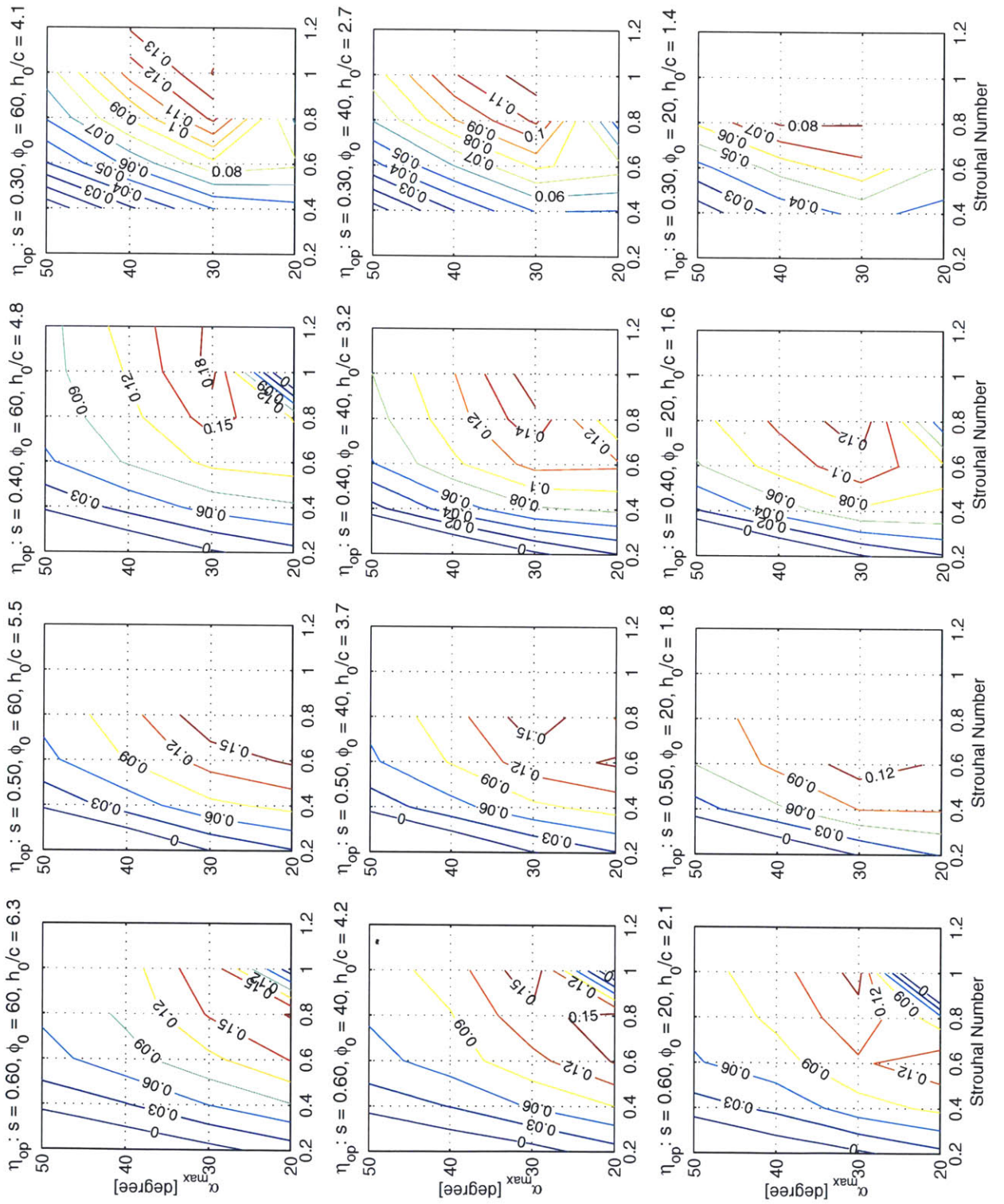


Figure 4-16: Summary of contour plots for operational efficiency  $\eta_{op}$ , with  $St$

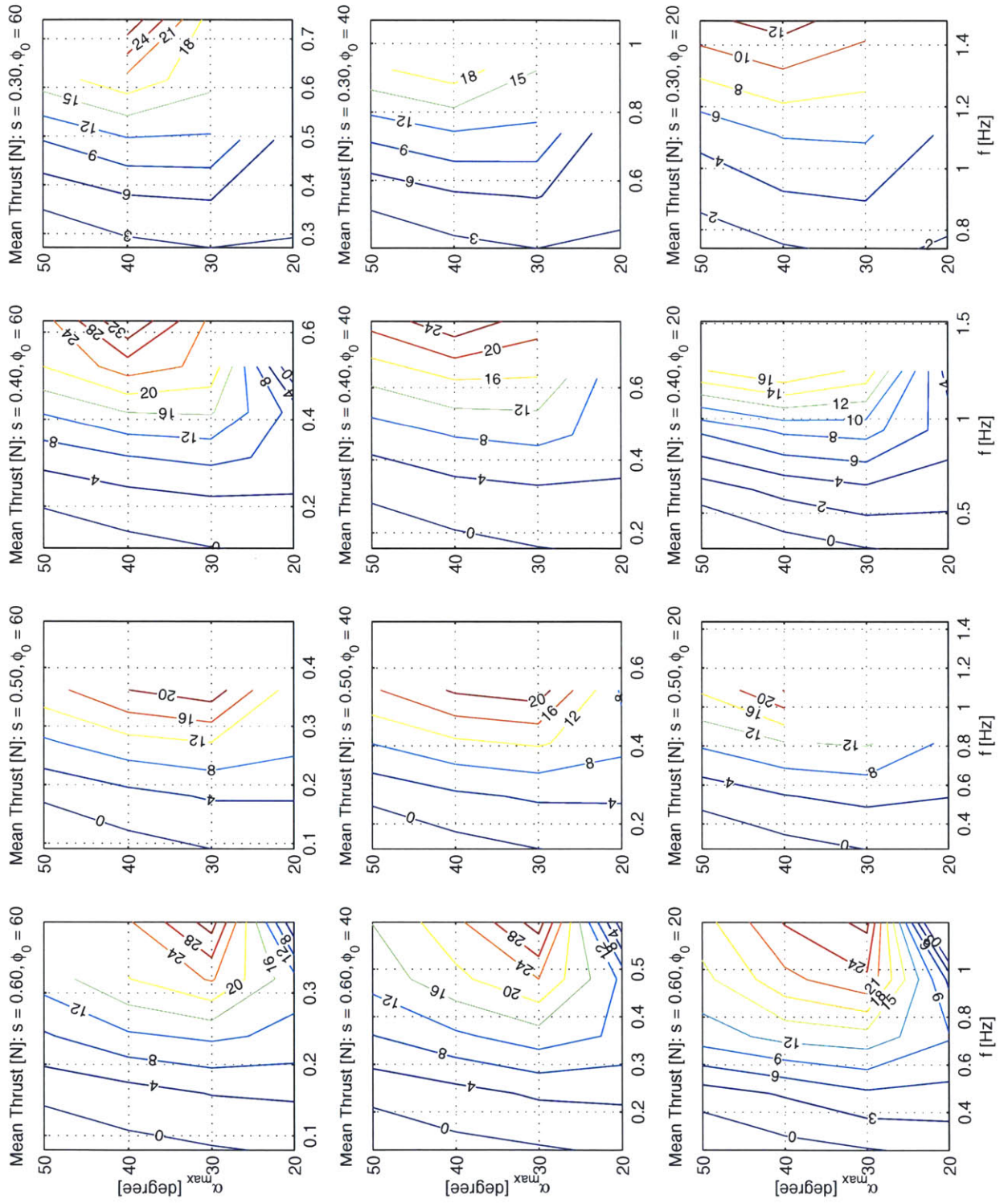


Figure 4-17: Summary of contour plots for mean thrust  $\overline{F}_x$  [N], with  $f$

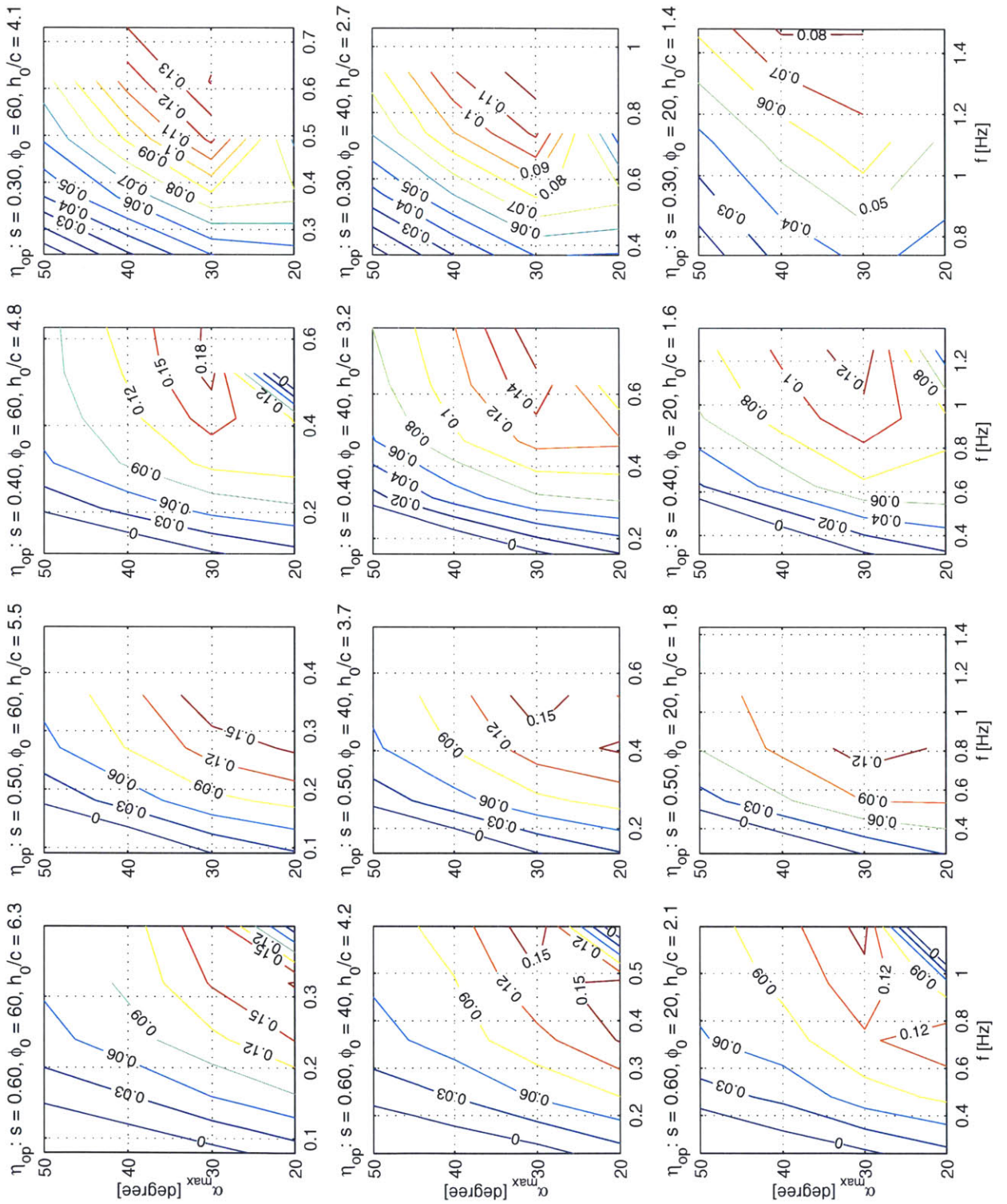


Figure 4-18: Summary of contour plots for operational efficiency  $\eta_{op}$ , with  $f$

## 4.3 Discussion of Results

The scaling analysis was found to be robust to perturbations in geometric similarity. The coefficient of thrust is a strong function of the Strouhal number and maximum angle of attack, and weak function of the wake width in this regime.

The 0.40 m span foil performed best in terms of thrust and operational efficiency. This foil size may have performed best simply due to the constraints of the kinematics parameter space attainable by the machine. However these findings may point to a more general result, which is that the optimal aspect ratio ( $s/c$ ) for a flapping wing is near 4.

Geometric similarities exist between various species of flying animals.[13] For many species of birds, the relationship between wing area and wing length is remarkably consistent. For an enormous variety of birds with wing spans ranging from 0.16 m to 2.4 m, the wing length squared divided by wing area is consistently near 3.86.[13] For a rectangular foil this would result in an optimal aspect ratio of 3.86. The work in this thesis found the optimal aspect ratio to be 4. The similarity between these optimal wing aspect ratios may be an indication that there exist three dimensional flow effects that are optimal when the aspect ratio of the foil is near 4. More work should be done to investigate the relationships between the geometry and aspect ratio of the foil and three dimensional flow effects.

# Chapter 5

## Design Recommendations

Future flapping foil actuator designs should be smaller, lighter, and have a much greater depth rating. Minimize the mass of the solid moving parts. Do not rush the design in early stages. Hold design reviews early and often to discuss multiple strategies for the design. Think the design through to the end before starting fabrication. Be sure all the components and materials will be available. Include long lead times for purchasing in the planning.

Maximize the performance with two degrees of freedom per foil before considering more complicated designs. Avoid extremely complex designs that will be expensive to fabricate and difficult to maintain. A vehicle should be practical and relatively easy to use and maintain.

Consider both the magnitude and bandwidth of the thrust produced. Massive forces delivered at a very low bandwidth are useless. Foil size is the primary factor controlling the trade off between magnitude and bandwidth. A light and powerful design should be able to achieve a thrust vectoring bandwidth of at least 4 Hz. Be sure the pitch axis is powerful enough to use single degree of freedom propulsion kinematics with a flexible foil.

Incorporate a spring or magnet on the roll axis to minimize the inertial power. If incorporating the spring into the design will lead to substantially increased mechanical or fluid damping, the net effect of the spring may decrease efficiency. Simulate the

solid dynamics, hydrodynamics, and control to select an optimal spring stiffness.<sup>1</sup> A large range of motion on the roll axis has many practical benefits in regard to wake interactions and during the deployment and recovery of the vehicle. A low level control system could be used to sweep the frequency and roll amplitude to lock onto the resonant mode. Be sure to consider the interaction between the backlash on the roll axis and the spring. Discontinuities in the velocity trajectory may lead to unfavorable vortex shedding.

Maximize the power density of the motors. Considering the cost of the sensors, custom machined parts, and waterproof cables, additional money spent on extremely high performance motors is well justified. There is a point of diminishing returns on increasing motor size. Multiple small powerful motors in parallel may provide more power density. Think in terms of delivering rapid bursts of energy through the drivetrain. Minimize or eliminate the gear reduction. There has been a recent move in robotics towards high torque direct drive motors to eliminate the backlash and efficiency losses. Investigate advanced servomotors that have the motor, amp, motion control card, and encoder packaged in a single unit. A foil module could consist almost entirely of one or two of these small servomotor packages in waterproof housings. The rest of the design would simply consist of bearings, couplings, and a frame. Be wary of artificial muscles. Rigorously test the actuators before incorporating them into a design. All the artificial muscles available today are seriously limited by the bandwidth, displacement, efficiency, or required operating voltage.

Give sealing a high priority in the design. Consider using magnetic couplings and wet bearings to eliminate the shaft seals. It is very difficult to make reliable dynamic seals on rotating and bending shafts. The friction in the seals wastes considerable amounts of energy. Radial deflections of shafts cause rapid o-ring wear. Buna-n o-rings have good resistance to creep (called compression set in the sealing industry), but they absorb water and swell. Ethylene propylene o-rings are ideal for static seals. Avoid excessive o-ring squeeze in dynamic seals. Read the Parker O-ring Handbook.

---

<sup>1</sup>There is Matlab code of a preliminary simulation for this purpose on the Towtank server at `\Vic\Documents\Matlab\2165\project\`

Teflon and nylon bushings should be used to protect the o-rings from large radial deflections. Pressure compensation should be avoided on a prototype design. The oil adds considerable weight and makes maintenance more difficult.

Give maintenance serious consideration, especially in a prototype design. Make all the housings easy to open and have clear lids if possible. Make all the parts interchangeable. Keep extra fasteners, hardware, electrical connectors (signal, power, communication), o-rings, and fuses organized and on hand. Try to minimize the variety of machine screws in the design. Maintaining a stock of a large variety of screws is very tedious and expensive. Always use a coarse thread in aluminum and plastic. Avoid threading holes into brittle plastics. Avoid helical threaded inserts, they gall and work loose. Always use a copper based lubricant when threading stainless steel screws into stainless steel parts.

Use a higher operating voltage (at least 48 volt) to minimize losses due to impedance. Use more sophisticated batteries (nickel metal hydride or lithium ion). Be aware there are numerous fire and explosion hazards with batteries. Never charge batteries while sealed in housings. Use diodes to guarantee the batteries will not accidentally be charged while connected to shore power. Use diodes to protect the user while wet plugging shore power. Consider using over pressure relief valves in battery housings. Avoid placing switches and relays that spark in the same housings as batteries. Flammable gasses can be trapped in sealed housings with batteries while they are in storage. Manufacturers rarely approve of using batteries in sealed housings.

Teflon and composite materials such as Rulon work well for wet bearings. The dimensional tolerances on conventional packaged bearing units, such as pillow blocks, are very loose. These loose tolerances cause great alignment difficulties with seals and couplings.

The strength of the shaft couplings has been the weakest mechanical component in every design. Consider milling the shafts to have square ends. Coiled spring pins take some effort to replace, but they have worked very well. Clamps have worked well in some applications. Set screws often vibrate loose when there are high derivative gains in the motion control. If set screws are used, drive a cone point into a deep

pocket on the shaft. Use two short set screws in the same hole and drive one into the other. Avoid taper pins. Parts joined with taper pins are not interchangeable because of the tapered reamer. Taper pins vibrate loose very easily.

Sprockets and chains (with two stainless steel cables and urethane coating from W.M. Berg) have worked very well on several designs. Fatigue, strength, and stretching concerns for chains are relatively minor on this scale. Chains rarely break and are very easy to replace. Cable drives have tremendous potential in biomimetic design, but they can be very difficult to adjust and maintain. The cables often slip and break. It is difficult to get the cables in enough tension. Pneumatic pistons are totally impractical for an underwater vehicle. Hydraulics are complicated and have many stages of efficiency losses.

Incorporate an absolute position reference on every axis, (potentiometer, hall-effect, mechanical or optical switch) for homing the foil. It is very important to be able to zero the pitch axis on the foil repeatably. Make sure the pitch axis can rotate a full  $360^{\circ}$ . One of the major advantages of flapping foil propulsion is that there could potentially be no preferred direction for thrust.

Make the foils easy to detach and replace. Do not make the foil detachment point inside a housing. Magnetic couplings would be very convenient for detaching the foils and providing a safety measure. Make all the foils and couplings interchangeable. A foil crash is inevitable. Use torque limits and error limits in the control. Be absolutely sure to include a shear pin, or design failure point to protect the motors and structure. Sharp rigid foils can be dangerous. Flexible foils have many practical benefits as well as hydrodynamic benefits. Foils that bend before they break will be much more robust. It is almost impossible to maintain a pristine trailing edge on a rigid foil once the actuator is getting some serious use.

Give major consideration to the number of waterproof cables and connectors when deciding which components will reside in which housings. Waterproof cables and connectors are very expensive and unreliable. Do not send the encoder signal for the roll axis through a waterproof cable without a limit switch. Encoder signals are routinely lost and a crash on the roll axis could cause major damage. The least



reliable components have always been the custom cables and connectors. This is true in many robotics applications. Communication problems are almost always due to a faulty connector. Take the extra time to make extremely high quality cables. Always dispose of faulty cables, never return them to storage.

Make the housings easy to open and have clear lids if possible. Nearly every time there is a communication or mechanical problem the housings must be opened. Count on opening the housings several times a day when using the vehicle. End plugs on tubes can be difficult to remove, but this can be avoided with a strong protruding lip on the end plug that can be tapped with a mallet. Be sure that the cables and connectors are not stressed when housing is opened. Use wireless communications between the laptop and vehicle.

Use heat sinks for all the electronics and motors. Be sure to consider the melting temperature of plastic housings. Aluminum or titanium housings would certainly certainly conduct heat into the water much more effectively than plastic housings.

Use corrosion resistant materials. Be aware that anodized parts can be scratched easily. Get samples for any new materials (especially flexible rubbers and composite materials) that are being considered for the design and leave them underwater for several months to observe the rate of deterioration.

Take design measures to minimize structural vibrations in the frame of the vehicle. Make a stiff frame for the vehicle in order to drive the lowest mode well above the excitation frequencies of the highly unsteady hydrodynamic forces. Every flapping foil test rig has experienced heavy mechanical vibrations (normally in the range of 7 to 30 Hz). These test rigs were designed to be very rigid, with size and weight limits that far exceed the constraints for a vehicle frame.

Consider exploiting symmetry in the vehicle design to increase open loop stability. Make the vehicle small and light to ease deployment. Make a modular design and exploit economies of scale in the fabrication. Consider making a prototype for any actuator design before making the full set.



# Appendix A

## Cruising Forces in Time

The data contained in this appendix covers this range in the test matrix:

```
span   = {0.6, 0.4}
roll   = {60, 40, 20}
St     = {0.4, 0.6, 0.8}
MaxAoa = {50, 40, 30, 20}
run    = {1 or 2}
```

These figures, and the remainder that are not published here, are located on the Towntank server at `\Vic\Thesis\Latex\Figures\Matlab\` in `*.eps`, `*.fig`, and `*.jpg` format.

The distance from the centerline of the roll axis to the root of the foil for these tests was

$$r_0 = 0.178 \text{ m}$$

The other dimensions and relevant values needed for calculations are all given in the title of each figure.

All the data presented in these plots was filtered using `ifilt.m` at

6 Hz on the lift and current axes

8 Hz on the thrust axis

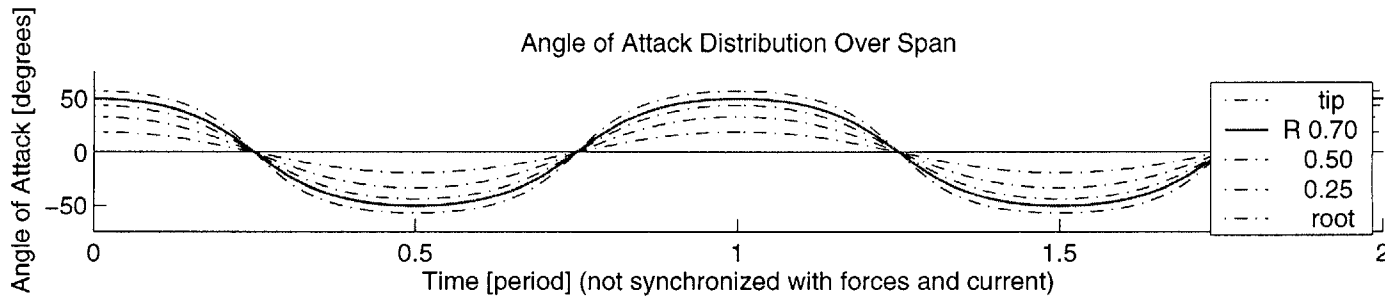
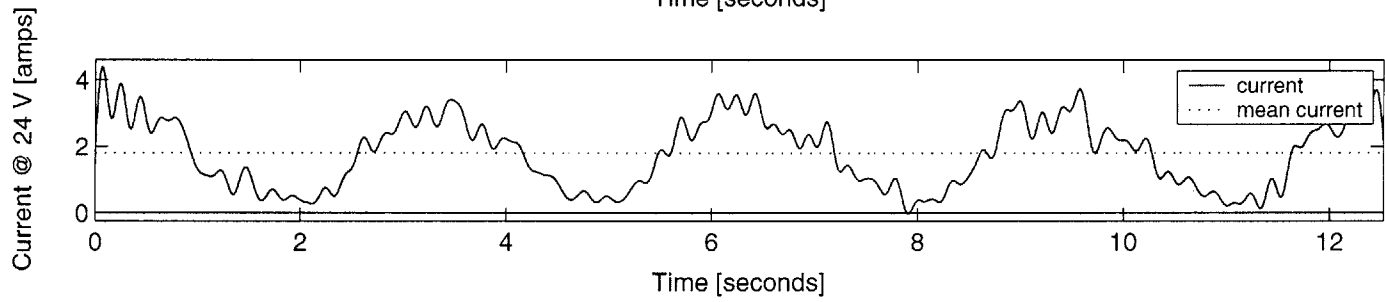
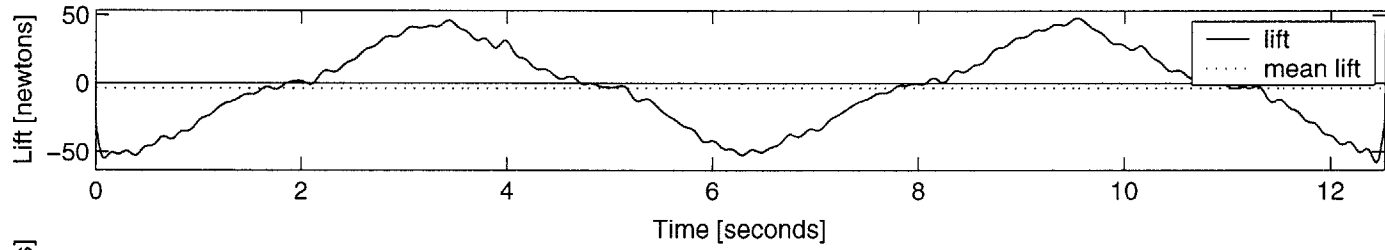
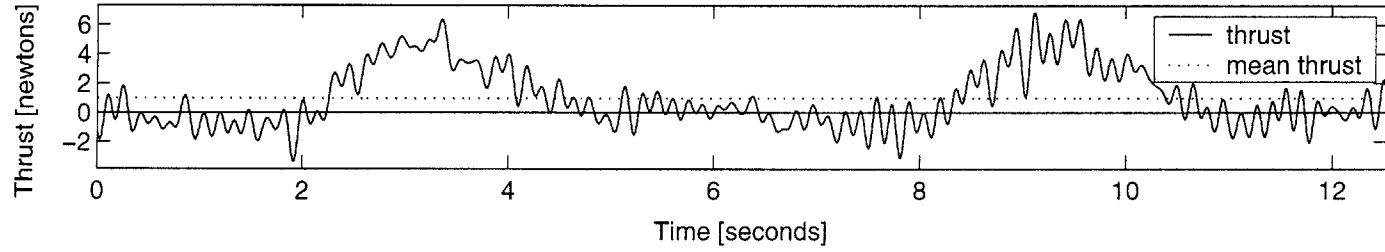
All of the raw data and calibration data is located on the Towtank server at `\Vic\Thesis\Data\`. The data is organized by day. The calibration files always reside in the same folder as the raw data. The calibration data is also loaded into `*.mat` files in the same directory.

The calibration files (`cal_dyno_x_pos.m`, `cal_dyno_y_pos.m`, `cal_ammeter.m`) and postprocessing files (`postcruise.m`, `ifilt.m`, `notch.m`, `notch2.m`, `parsedl2.m`, `postcruise_combo.m`, `plot_spectral_analysis_dyno.m`) are located on the Towtank server at `\Vic\Documents\Matlab\`

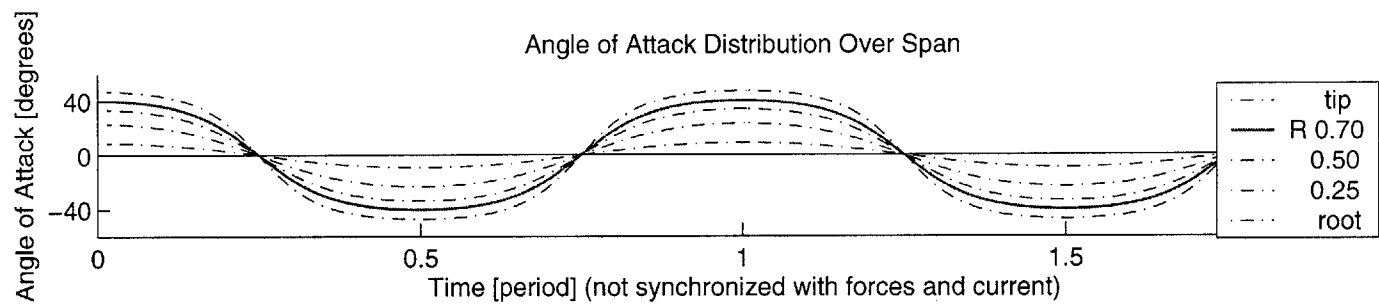
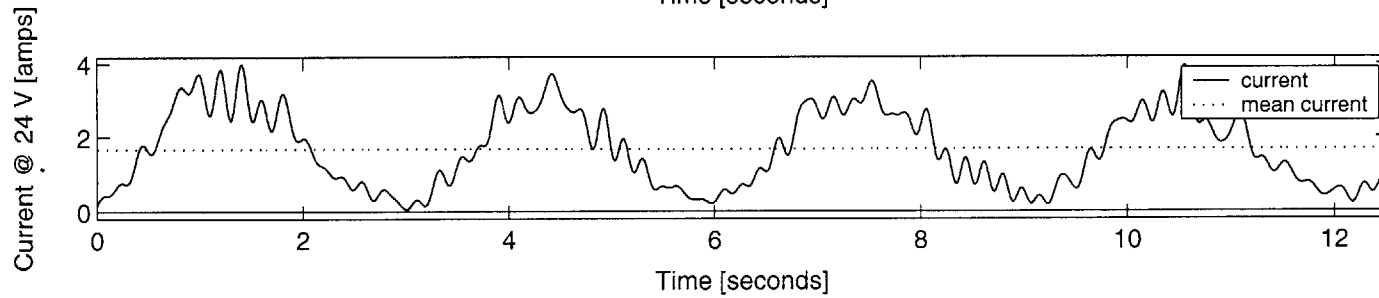
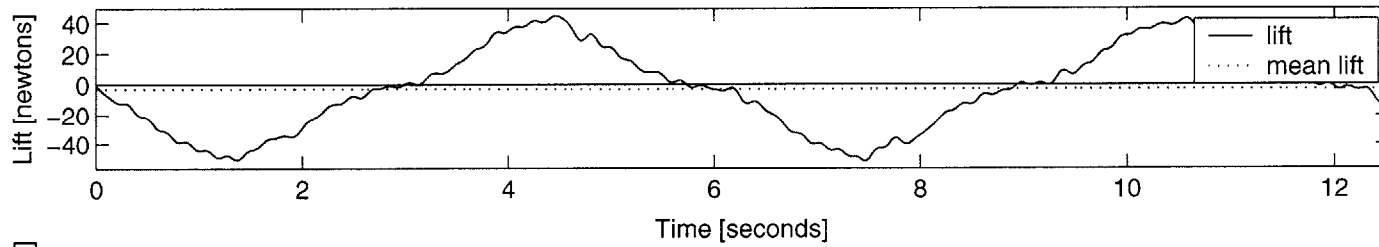
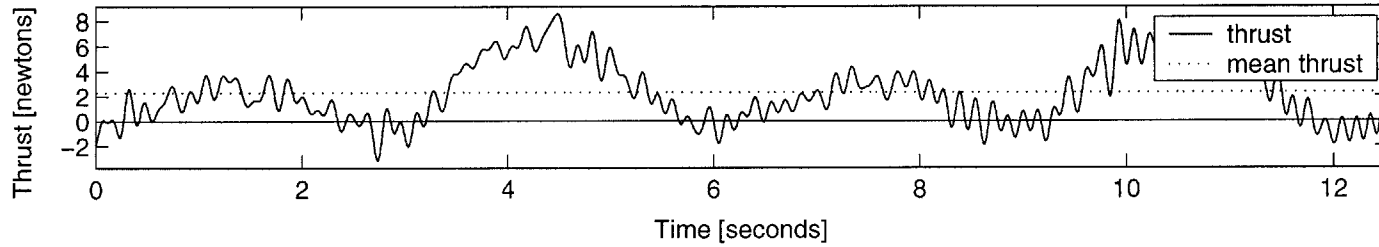
Refer to `cruise_HELP.txt` for a complete explanation of the file naming conventions and specifics of the raw and summarized data files.

All of the mean filtered cruising data (operational efficiency, coefficient of thrust, mean thrust, max thrust, mean current, max current, frequency of foil motion, integer number of cycles used to compute mean, pitch amplitude) is stored in a large data structure called `cruising_testmatrix()` written in `cruise_matrix_mat.mat` on the Towtank server at `\Vic\Thesis\Data\`. There is a help file called `cruise_HELP.txt` in that directory to explain the arguments and output of the data structure. There are additional help files located with the raw data.

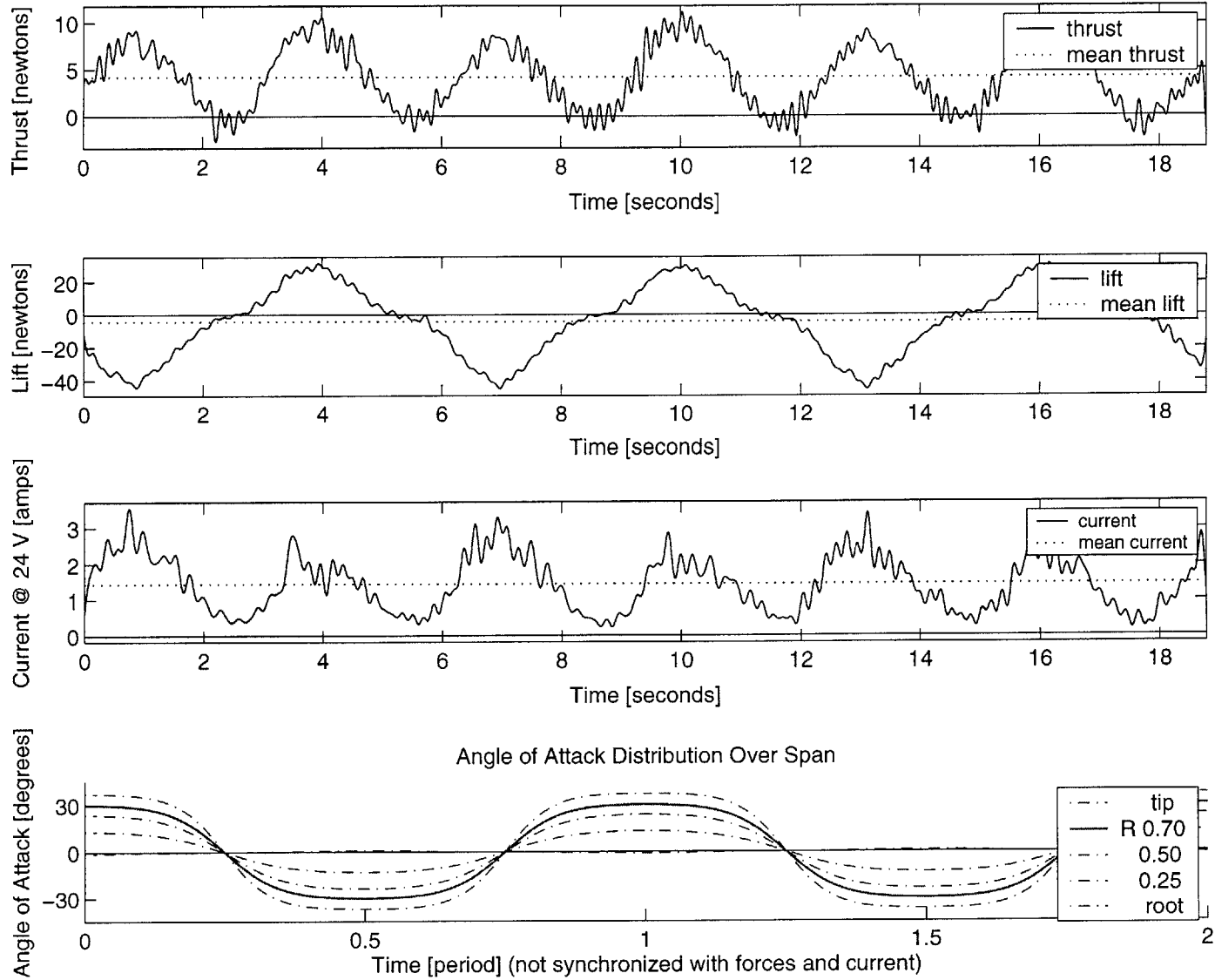
INPUT: U 0.5 [m/s], span 0.60 [m], chord 0.10 [m], roll 60 [deg], St 0.40, MaxAoa 50 [deg], run2 OUTPUT: Ct 0.1, efficiency 0.01



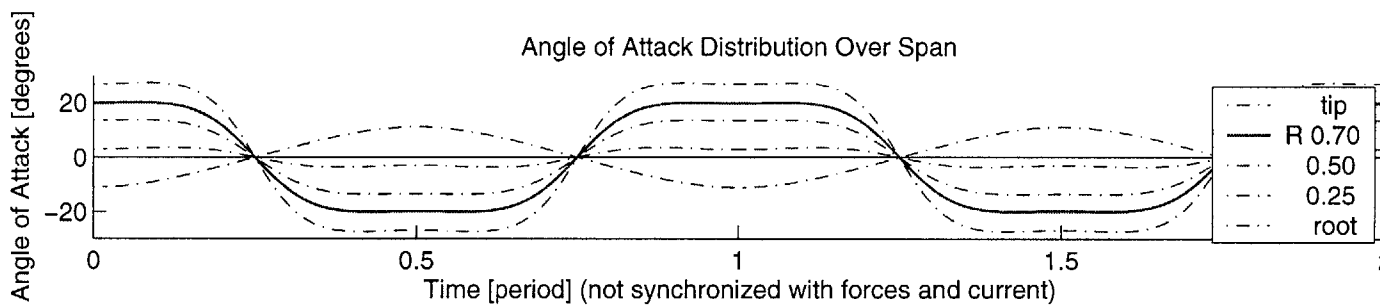
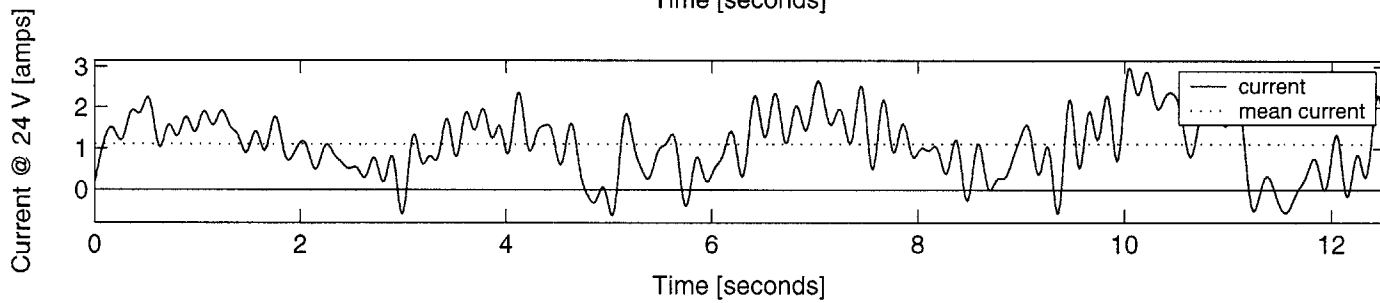
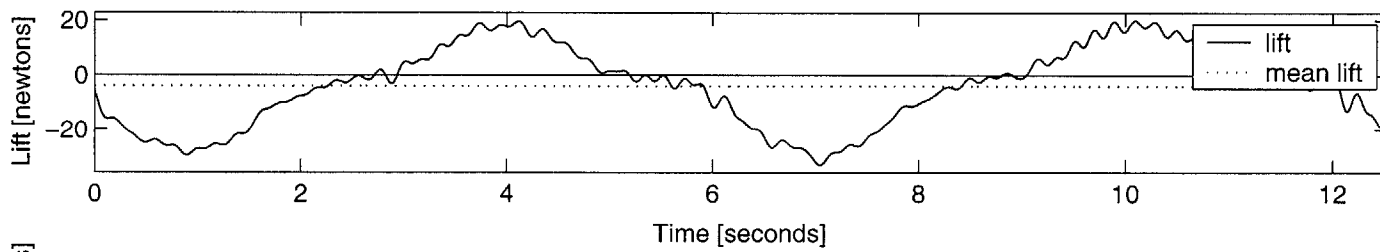
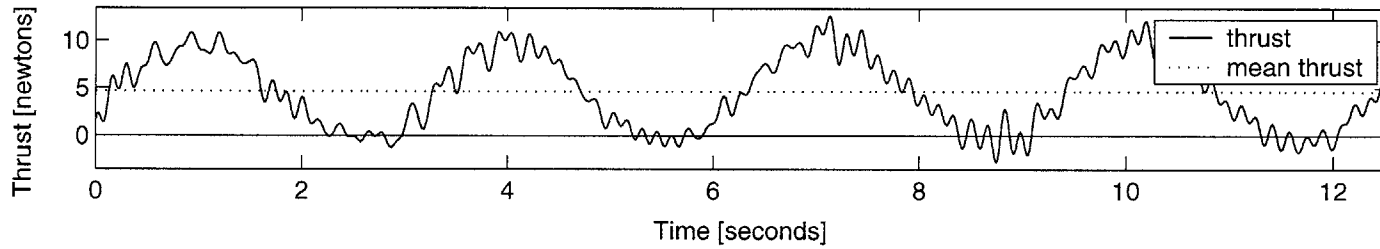
INPUT: U 0.5 [m/s], span 0.60 [m], chord 0.10 [m], roll 60 [deg], St 0.40, MaxAoa 40 [deg], run2 OUTPUT: Ct 0.3, efficiency 0.03



INPUT: U 0.5 [m/s], span 0.60 [m], chord 0.10 [m], roll 60 [deg], St 0.40, MaxAoa 30 [deg], run2 OUTPUT: Ct 0.6, efficiency 0.06

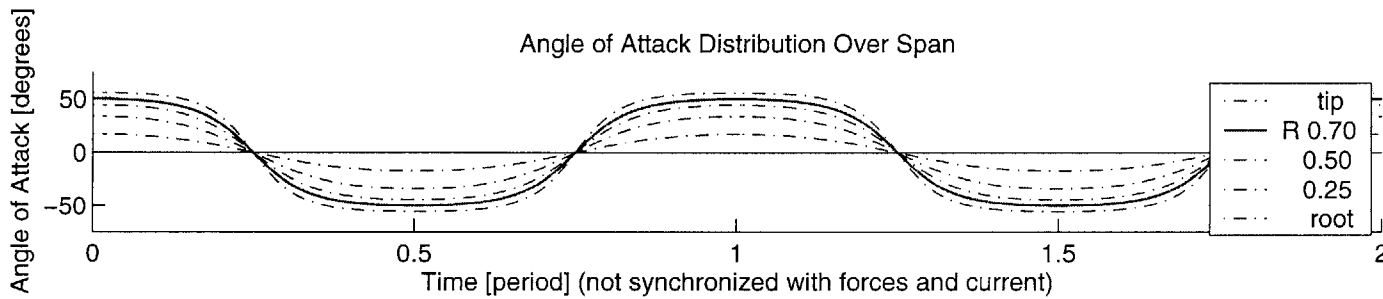
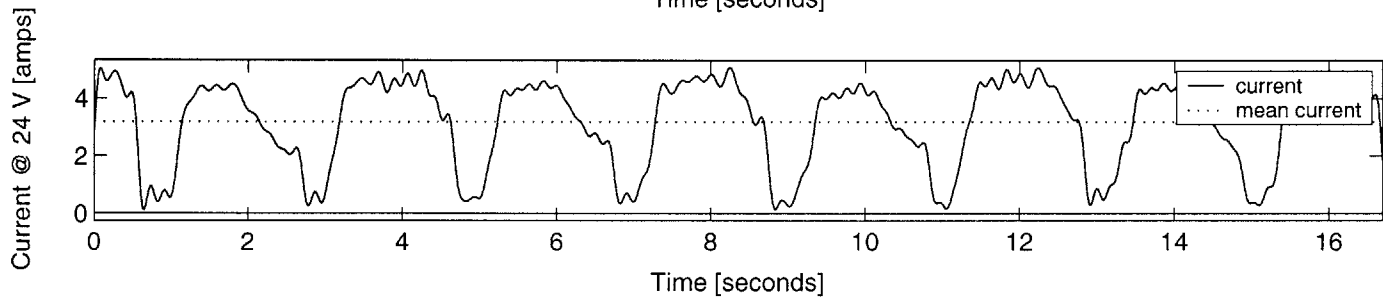
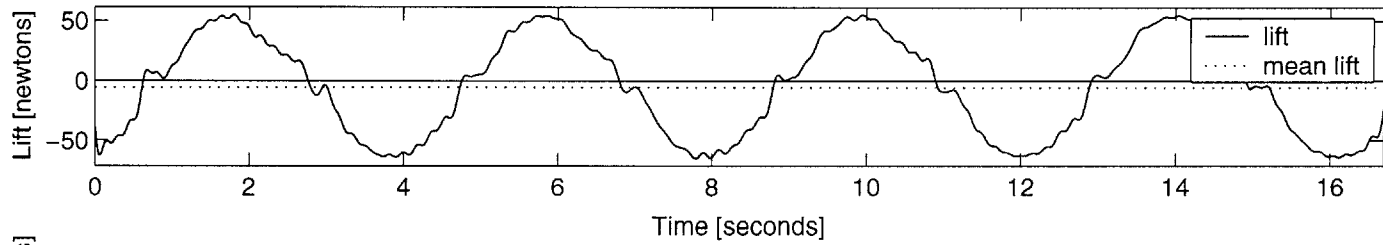
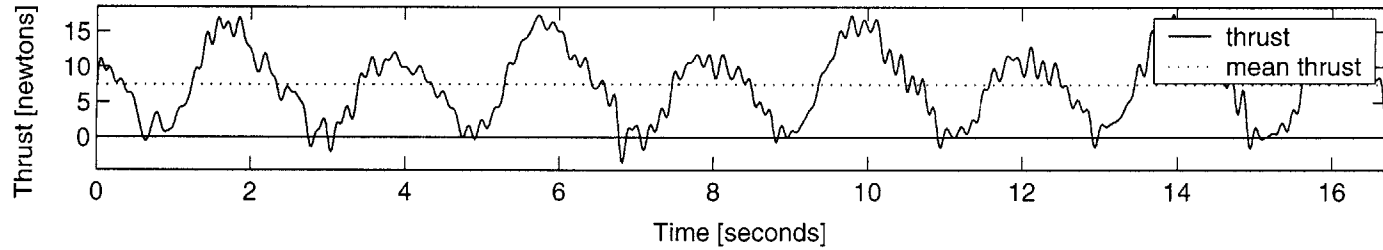


INPUT: U 0.5 [m/s], span 0.60 [m], chord 0.10 [m], roll 60 [deg], St 0.40, MaxAoa 20 [deg], run2 OUTPUT: Ct 0.6, efficiency 0.09

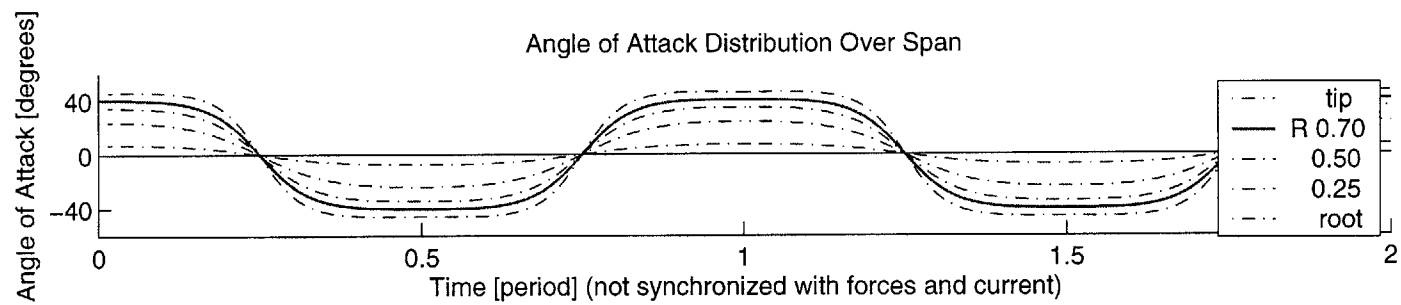
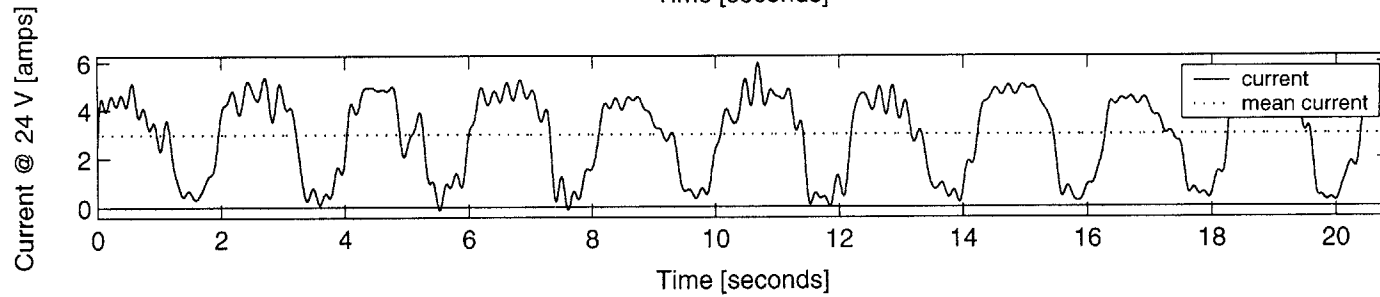
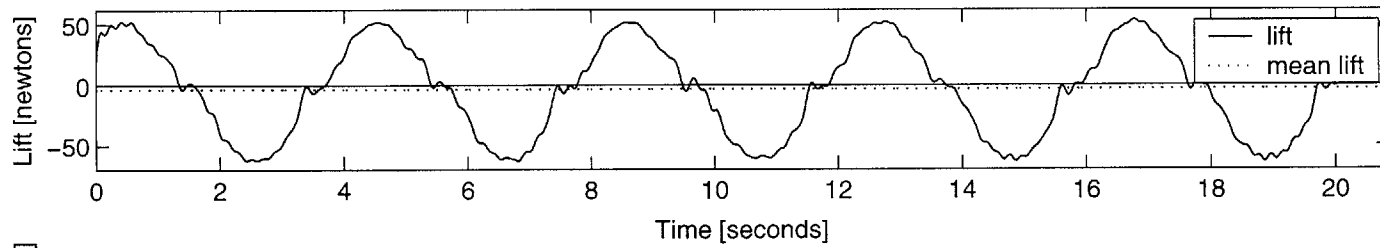
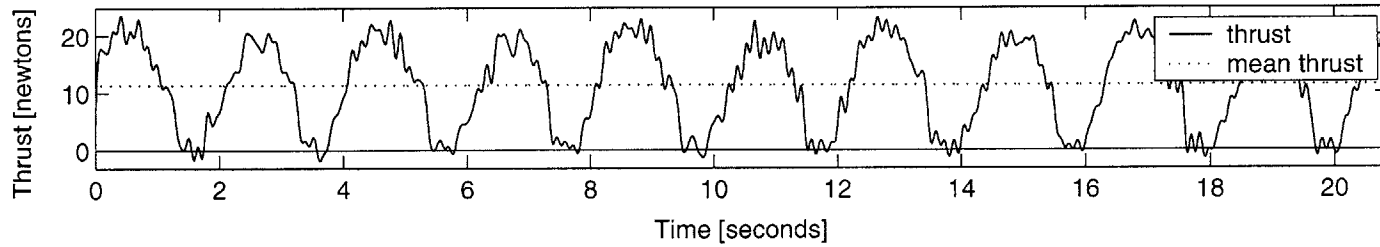




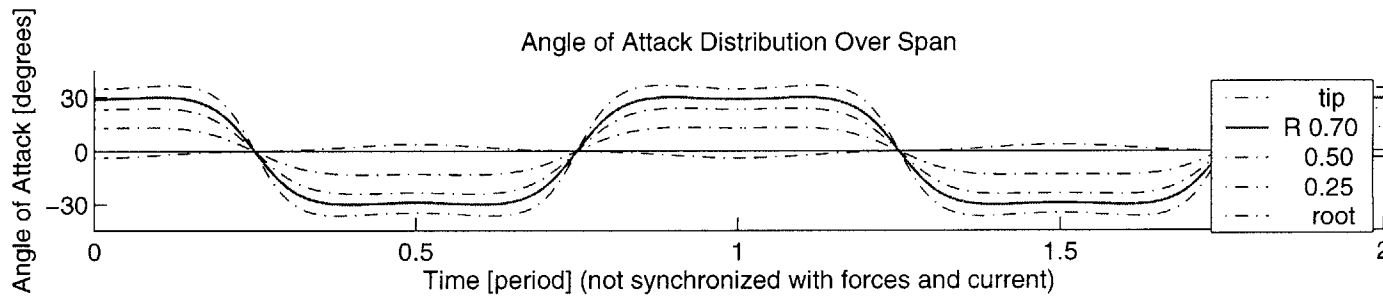
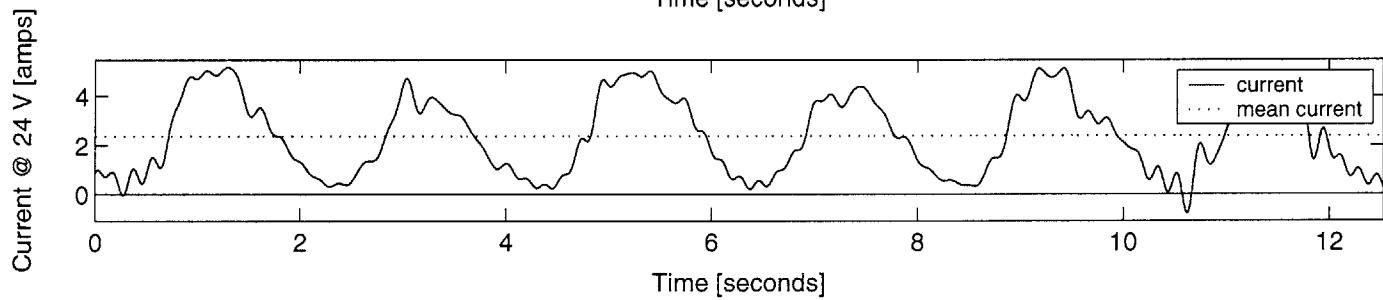
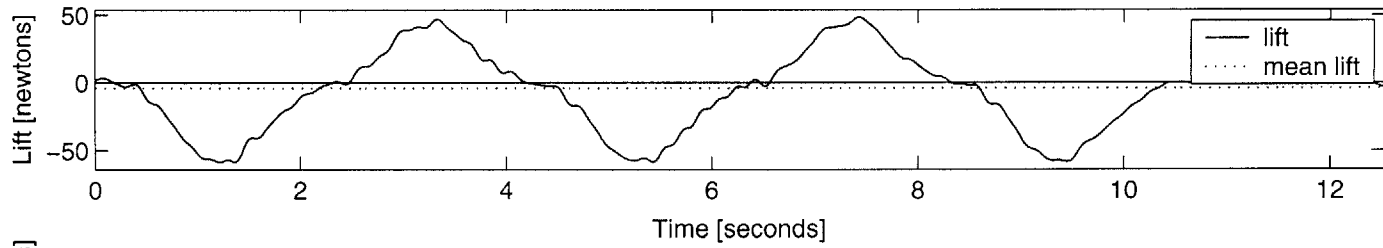
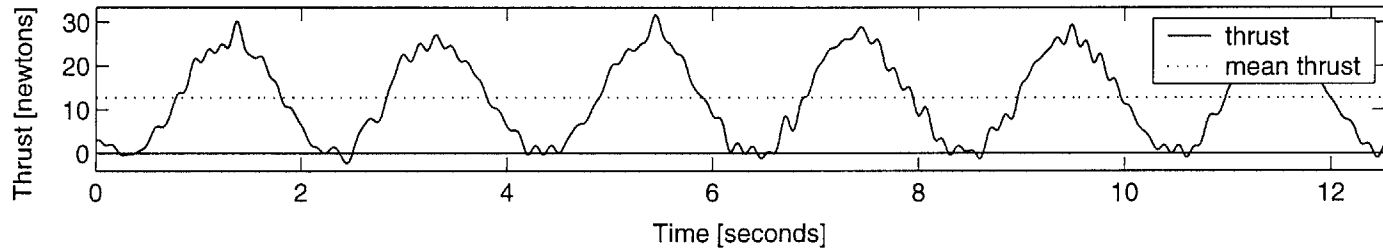
INPUT: U 0.5 [m/s], span 0.60 [m], chord 0.10 [m], roll 60 [deg], St 0.60, MaxAoa 50 [deg], run2 OUTPUT: Ct 1.0, efficiency 0.05



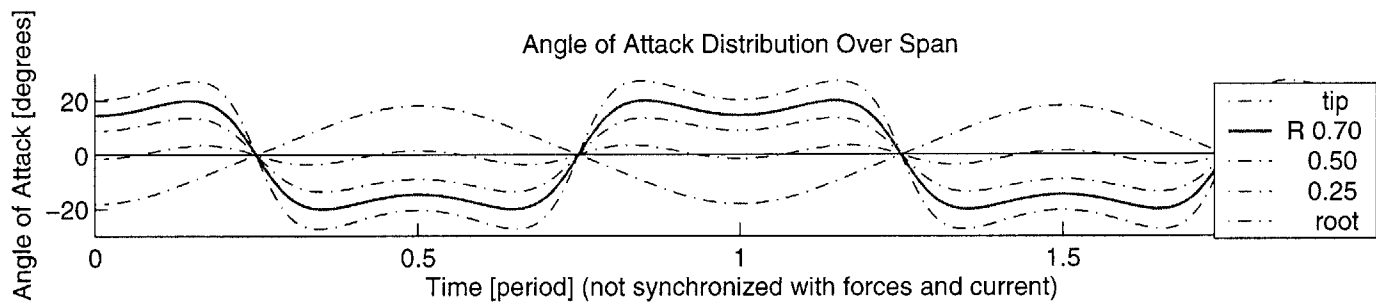
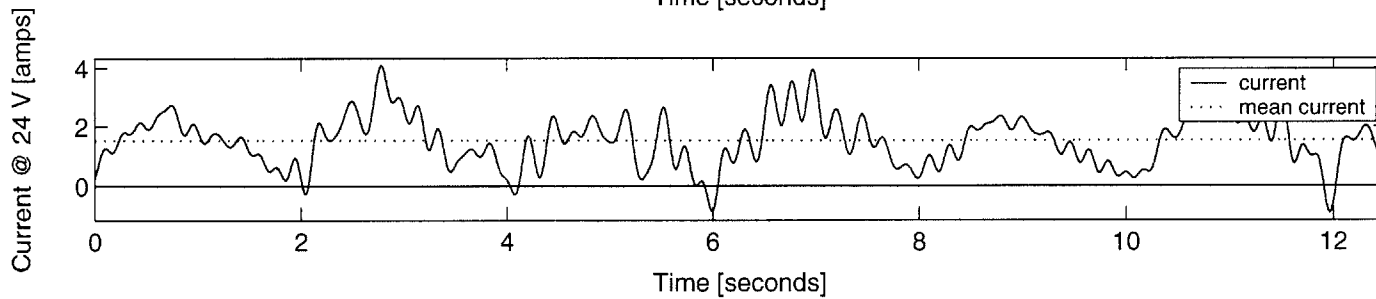
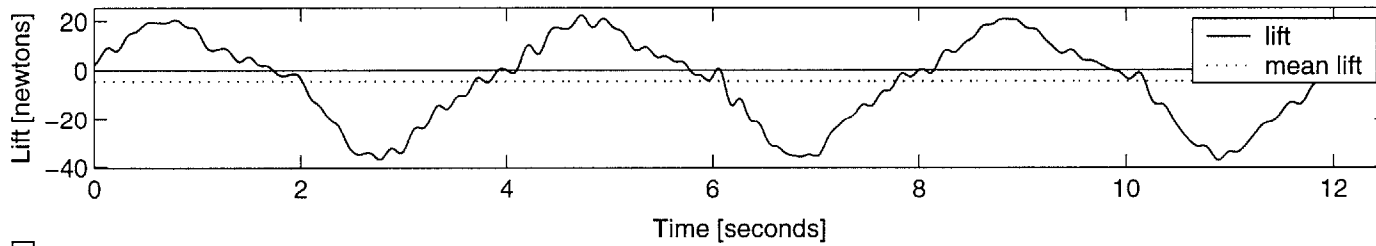
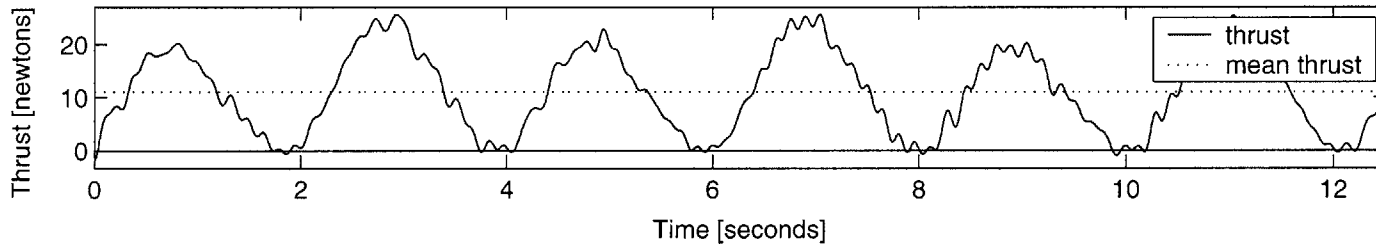
INPUT: U 0.5 [m/s], span 0.60 [m], chord 0.10 [m], roll 60 [deg], St 0.60, MaxAoa 40 [deg], run2 OUTPUT: Ct 1.5, efficiency 0.08



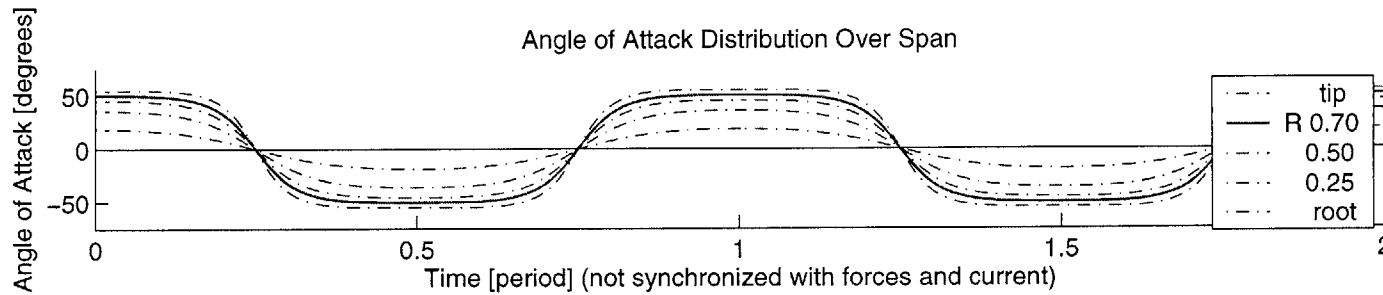
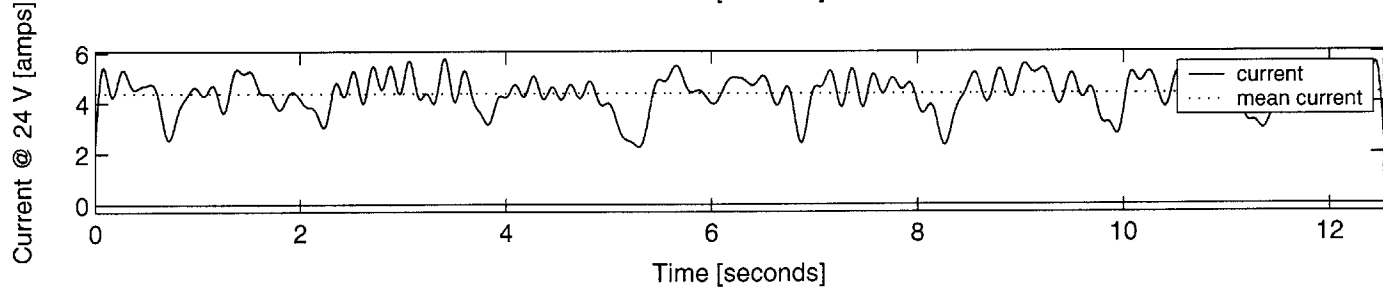
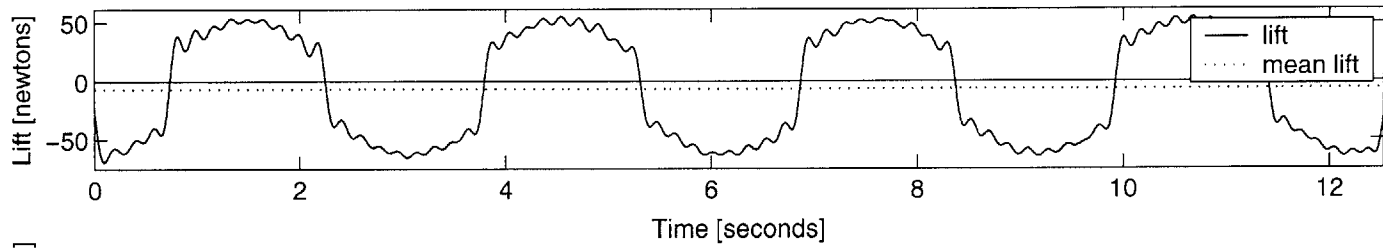
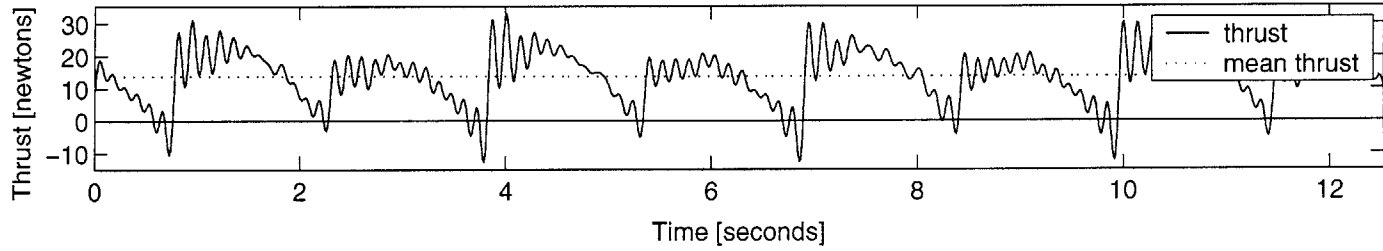
INPUT: U 0.5 [m/s], span 0.60 [m], chord 0.10 [m], roll 60 [deg], St 0.60, MaxAoa 30 [deg], run2 OUTPUT: Ct 1.7, efficiency 0.11



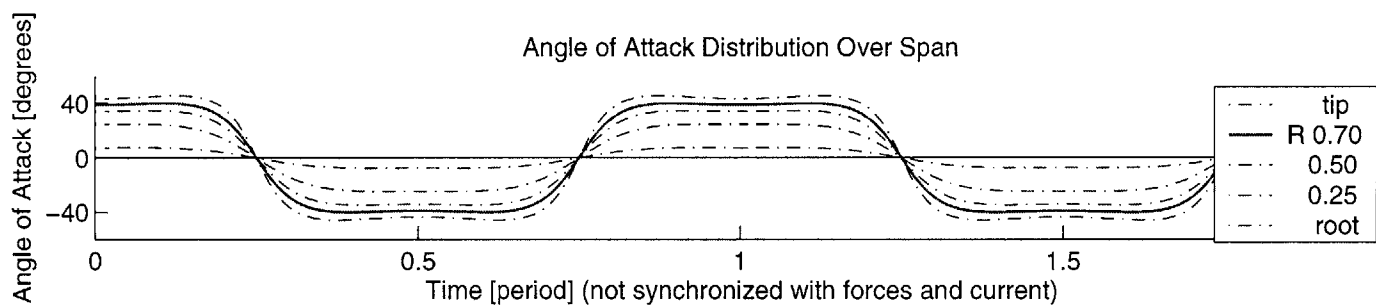
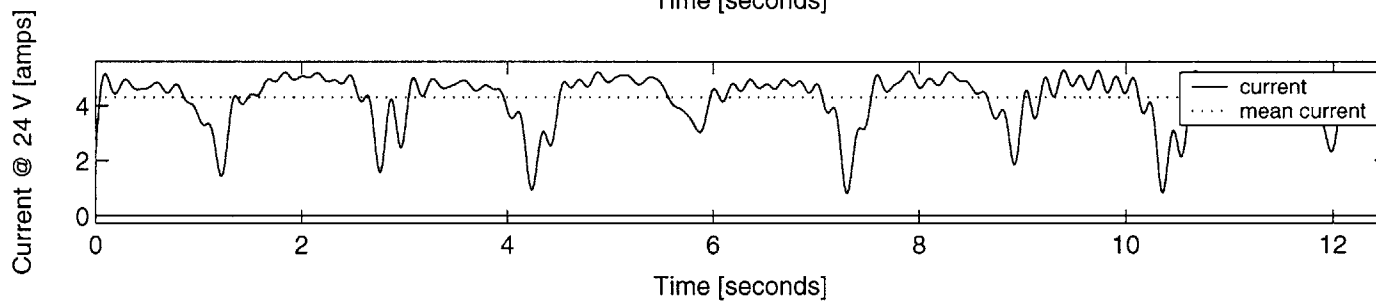
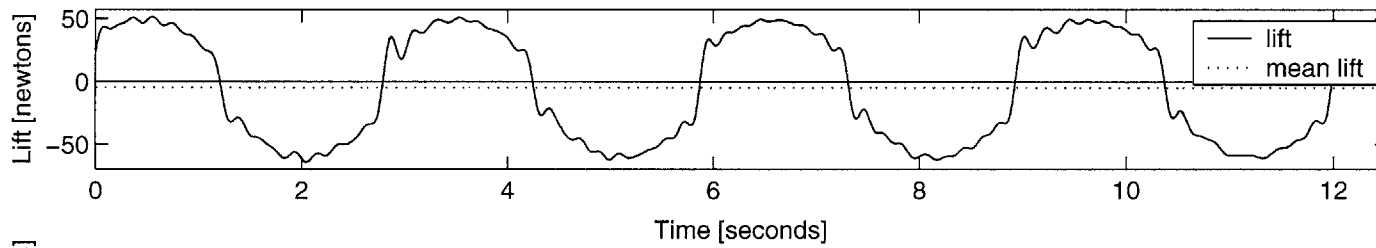
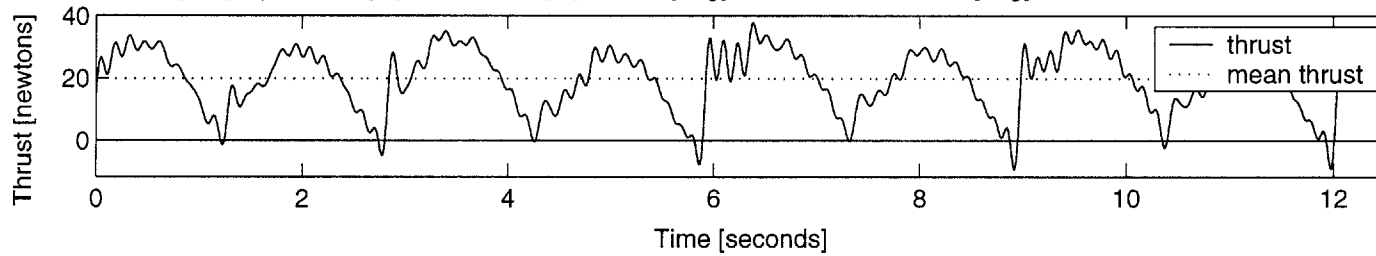
INPUT: U 0.5 [m/s], span 0.60 [m], chord 0.10 [m], roll 60 [deg], St 0.60, MaxAoa 20 [deg], run2 OUTPUT: Ct 1.5, efficiency 0.15



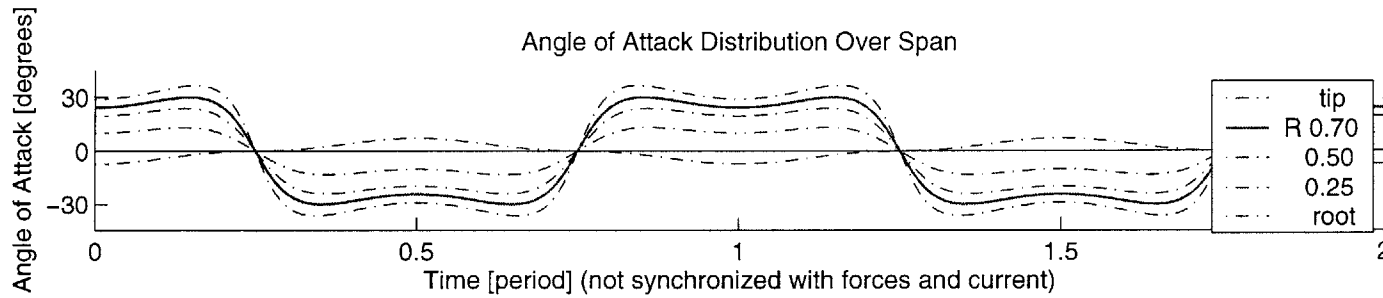
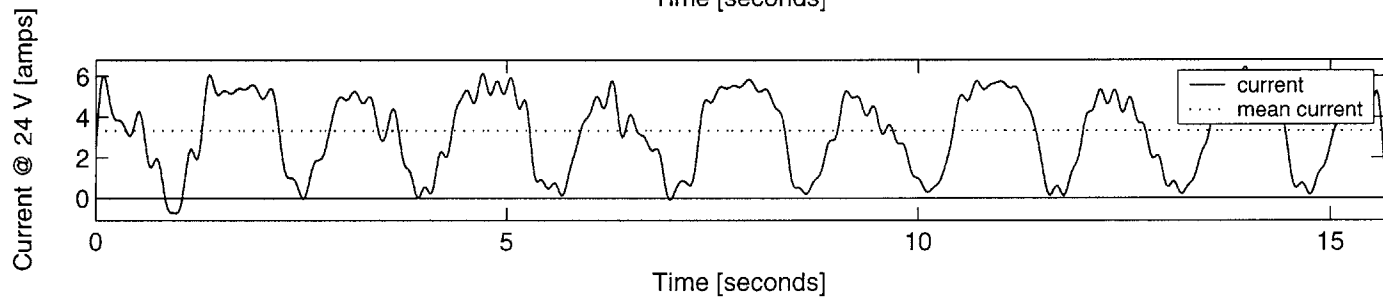
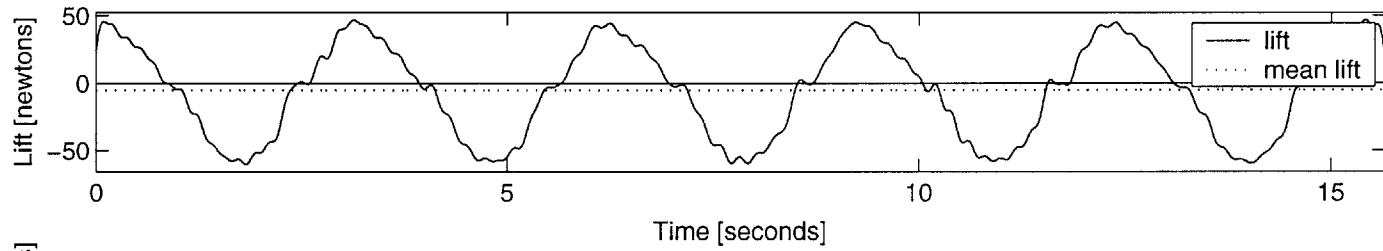
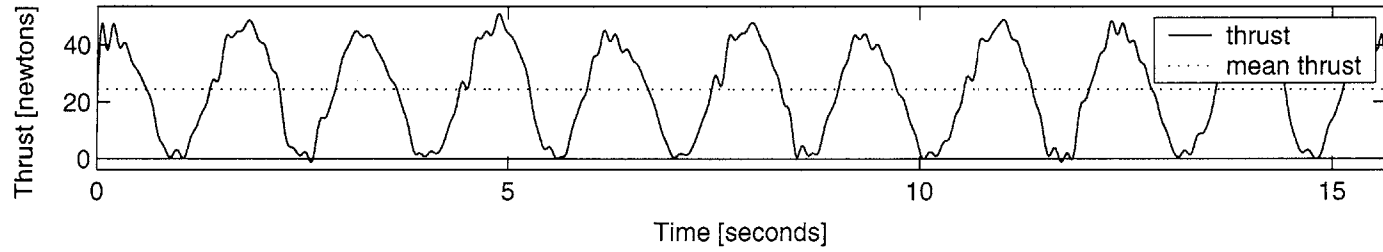
INPUT: U 0.5 [m/s], span 0.60 [m], chord 0.10 [m], roll 60 [deg], St 0.80, MaxAoa 50 [deg], run2 OUTPUT: Ct 1.8, efficiency 0.07



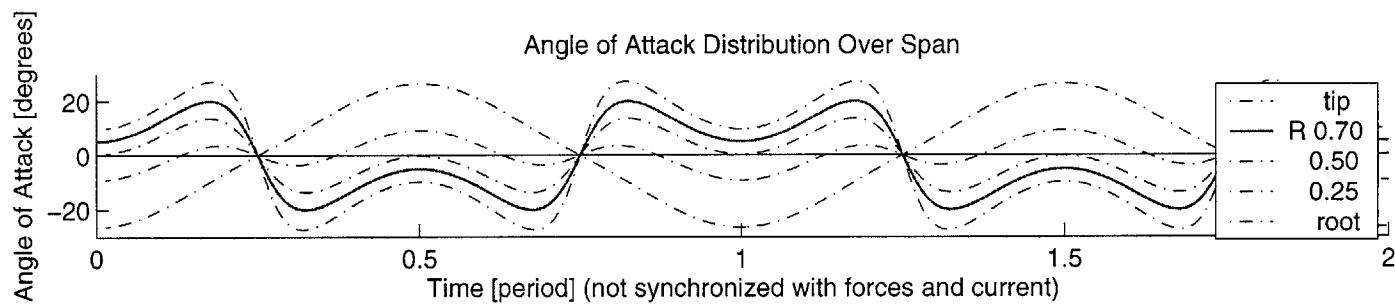
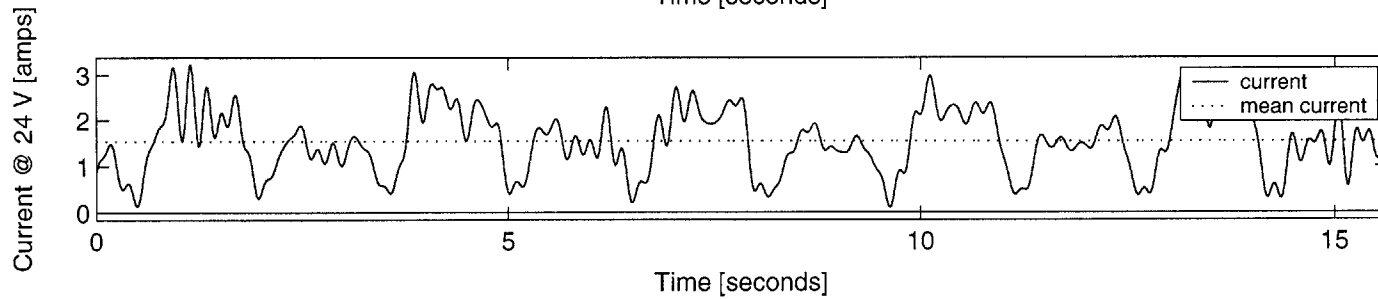
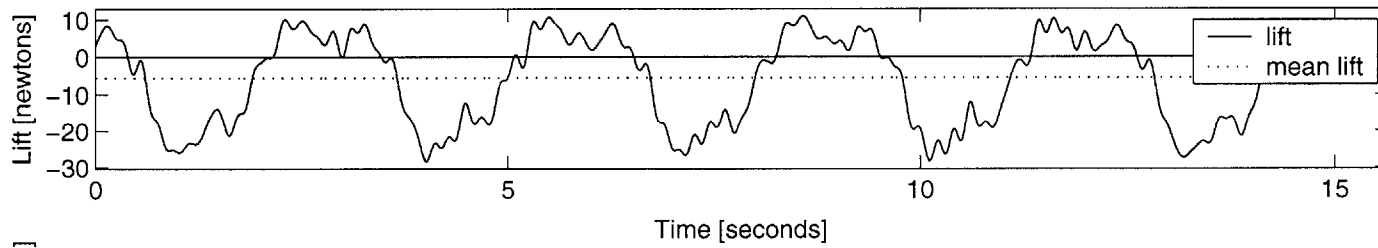
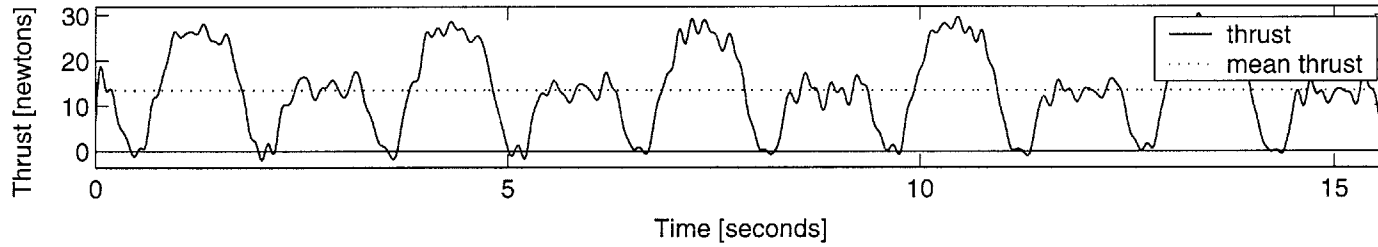
INPUT: U 0.5 [m/s], span 0.60 [m], chord 0.10 [m], roll 60 [deg], St 0.80, MaxAoa 40 [deg], run2 OUTPUT: Ct 2.6, efficiency 0.10



INPUT: U 0.5 [m/s], span 0.60 [m], chord 0.10 [m], roll 60 [deg], St 0.80, MaxAoa 30 [deg], run2 OUTPUT: Ct 3.3, efficiency 0.15

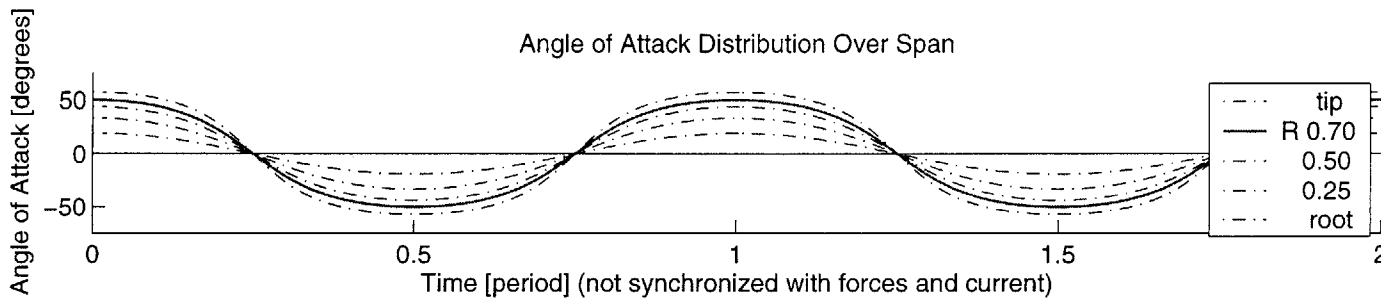
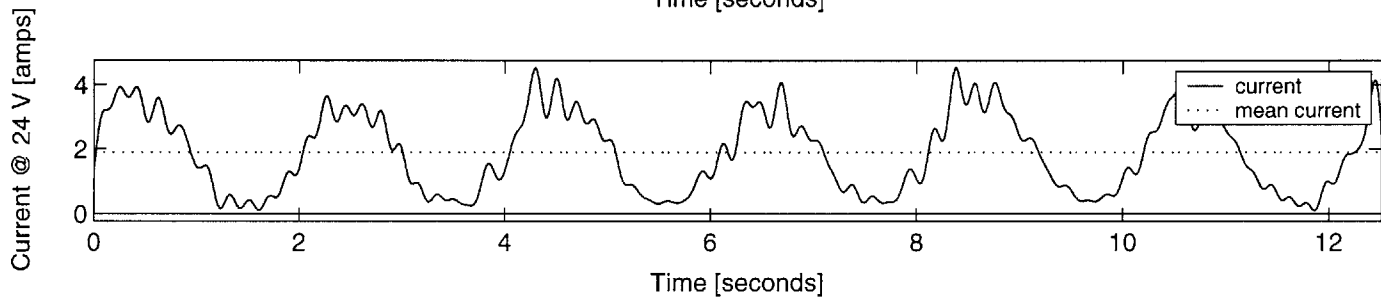
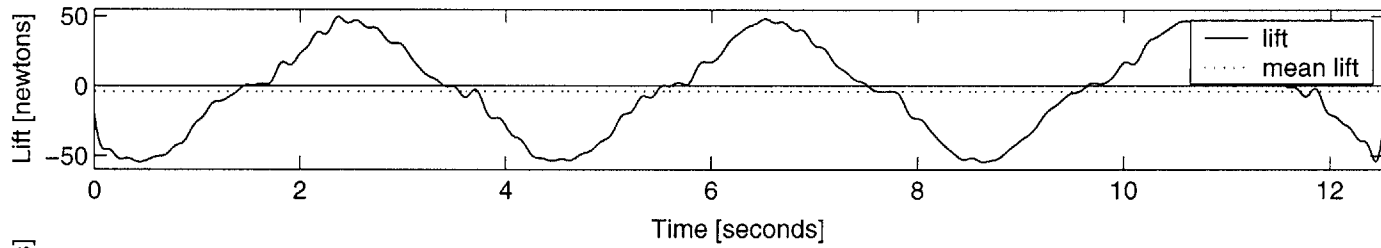
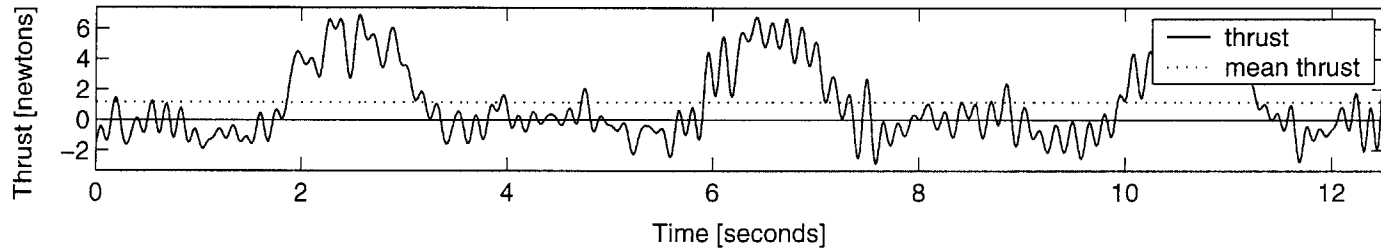


INPUT: U 0.5 [m/s], span 0.60 [m], chord 0.10 [m], roll 60 [deg], St 0.80, MaxAoa 20 [deg], run2 OUTPUT: Ct 1.8, efficiency 0.18

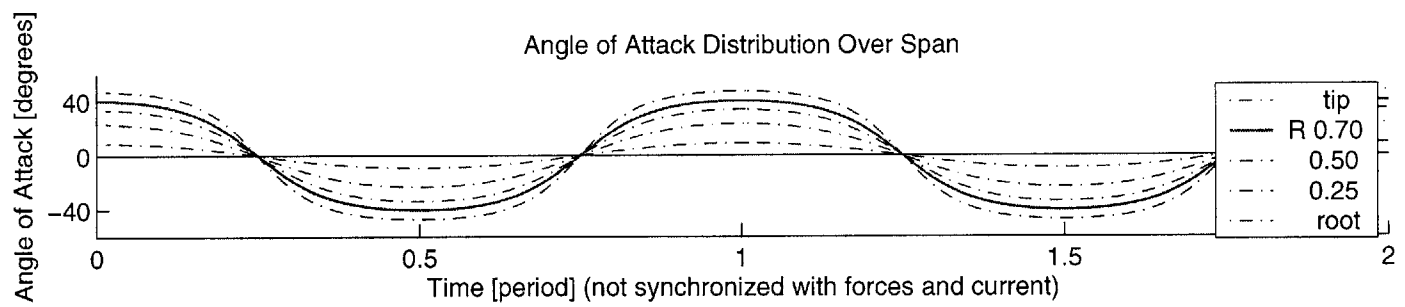
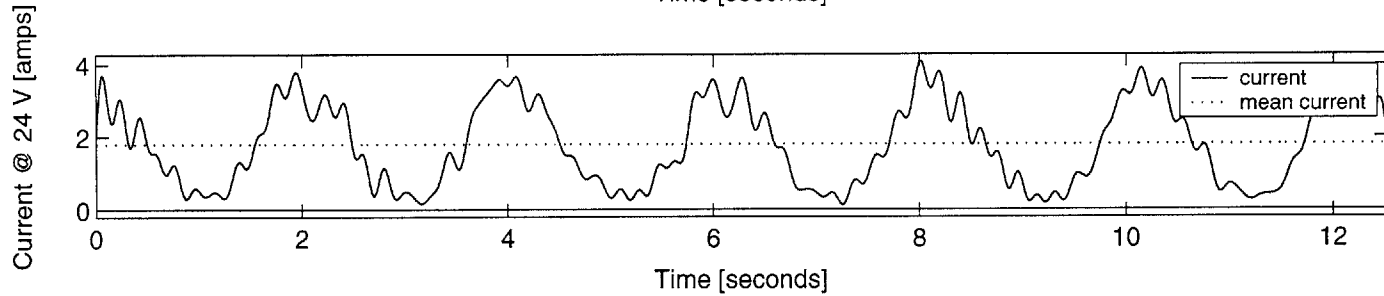
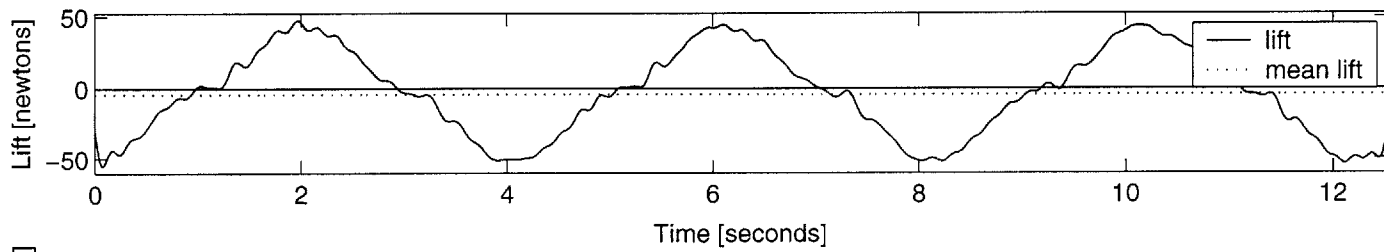
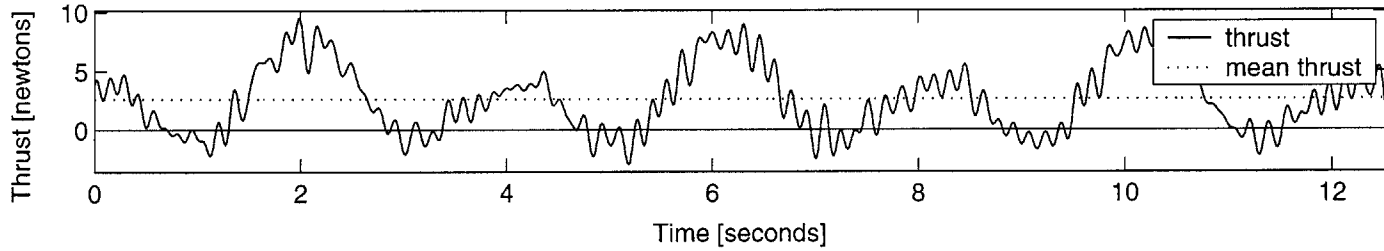




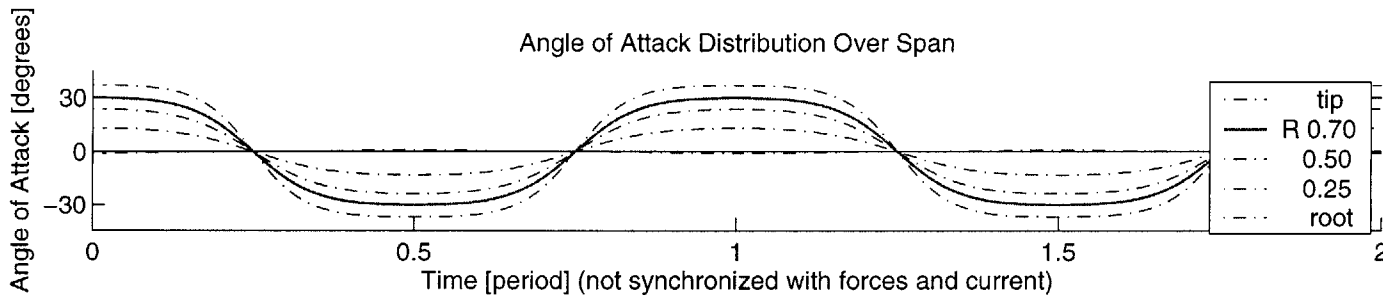
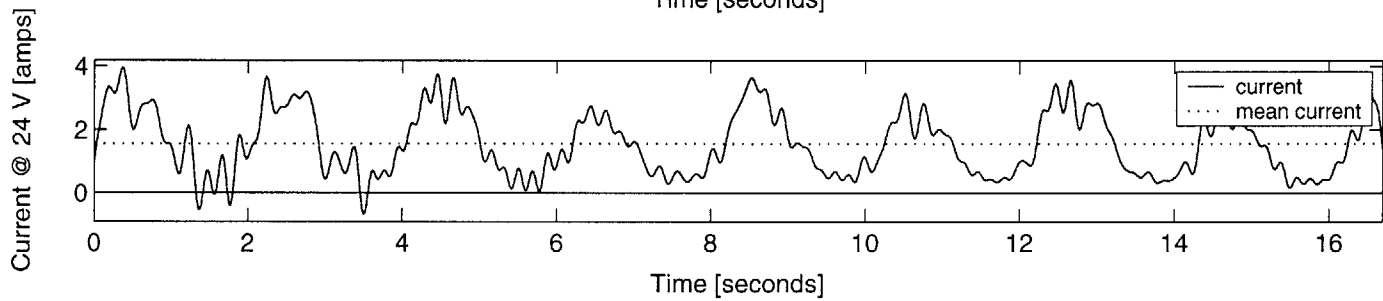
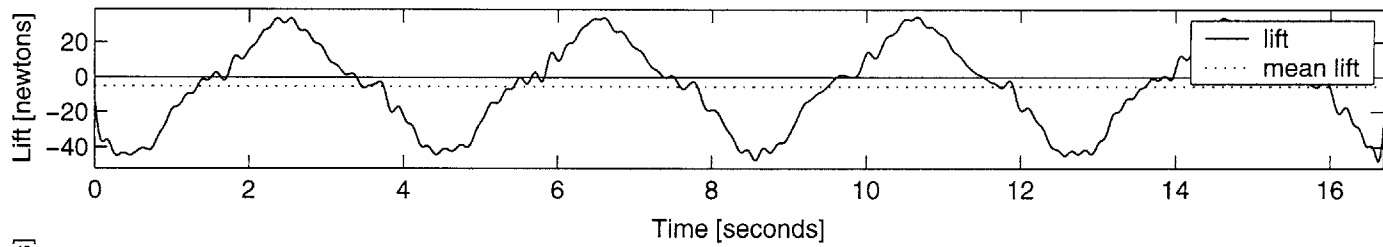
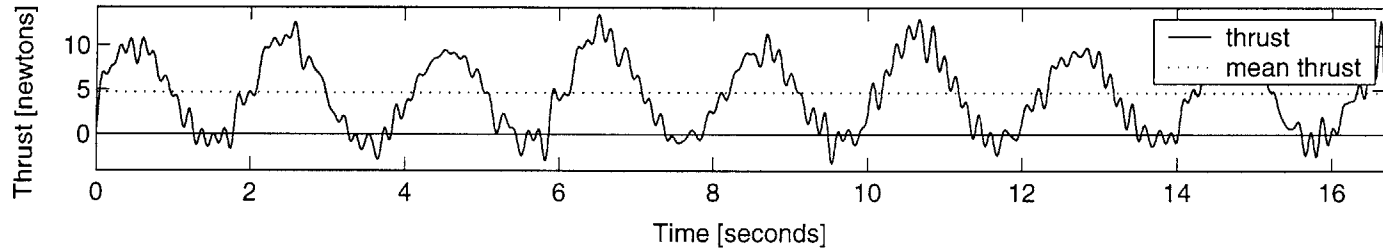
INPUT: U 0.5 [m/s], span 0.60 [m], chord 0.10 [m], roll 40 [deg], St 0.40, MaxAoa 50 [deg], run2 OUTPUT: Ct 0.2, efficiency 0.01



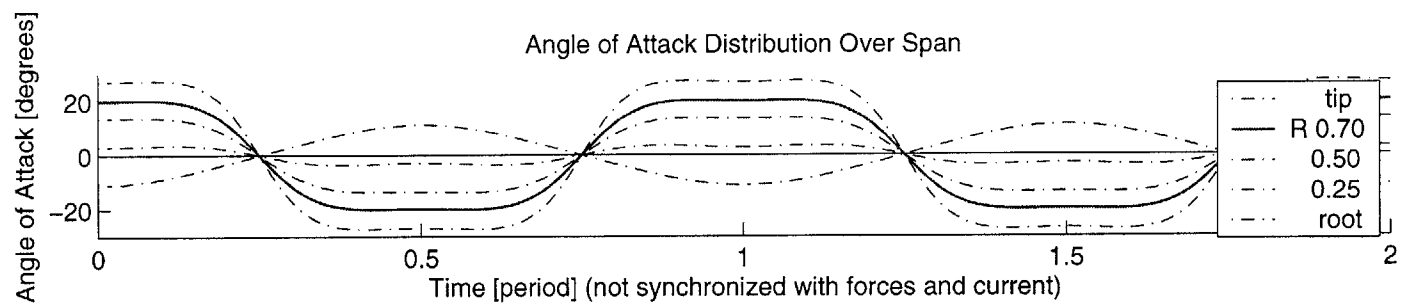
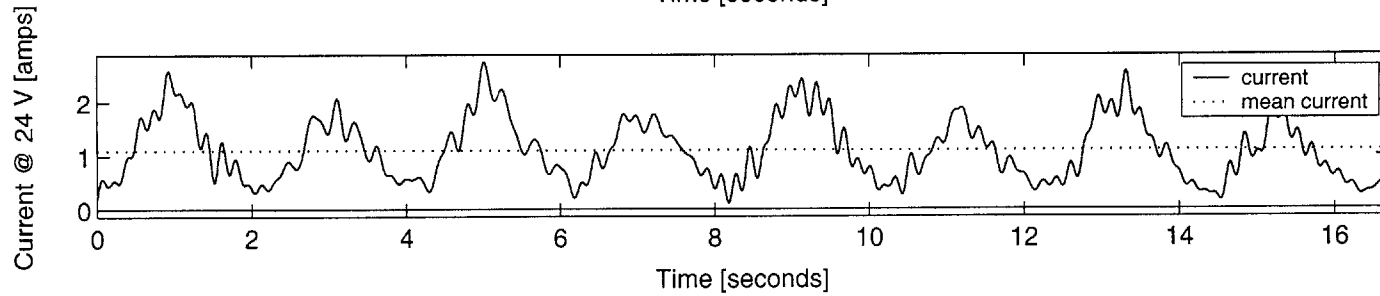
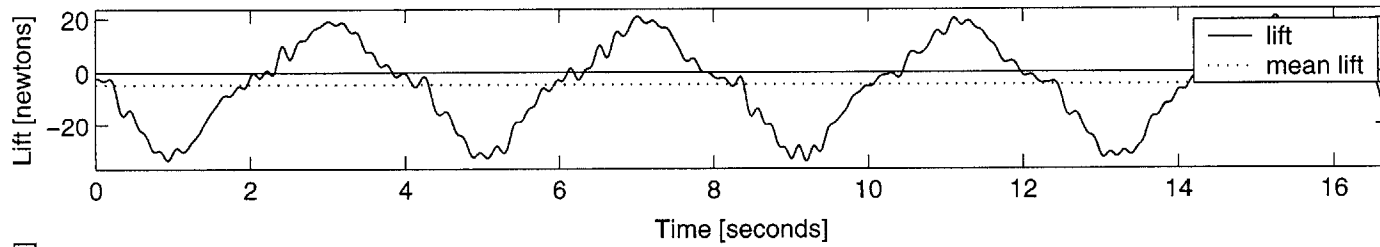
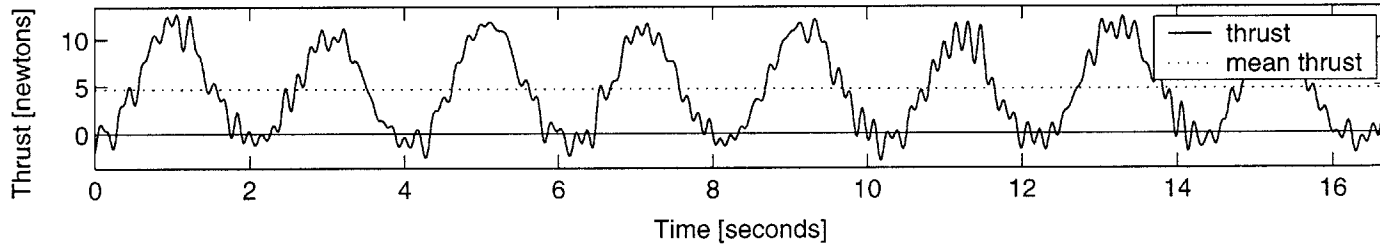
INPUT: U 0.5 [m/s], span 0.60 [m], chord 0.10 [m], roll 40 [deg], St 0.40, MaxAoa 40 [deg], run2 OUTPUT: Ct 0.3, efficiency 0.03



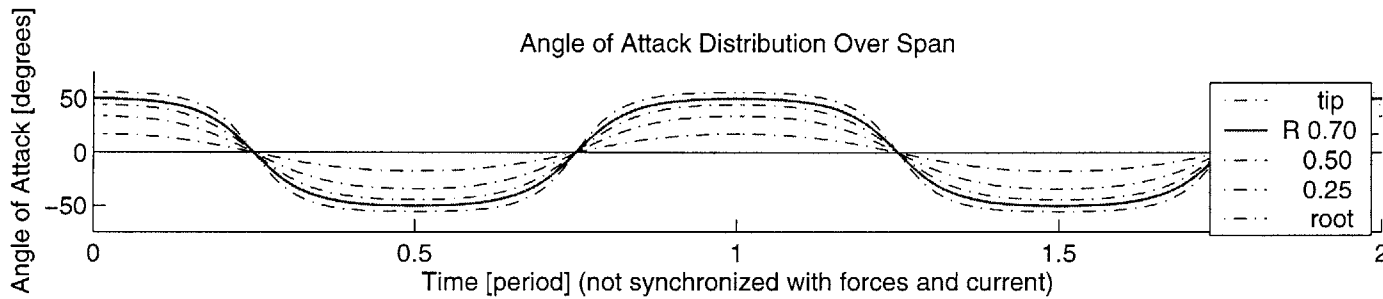
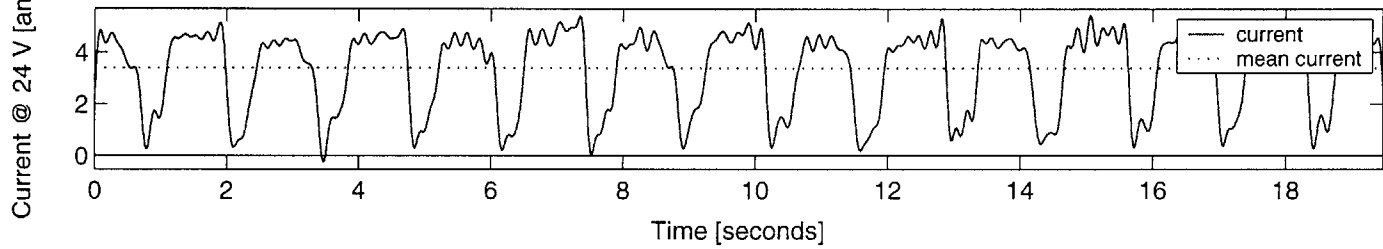
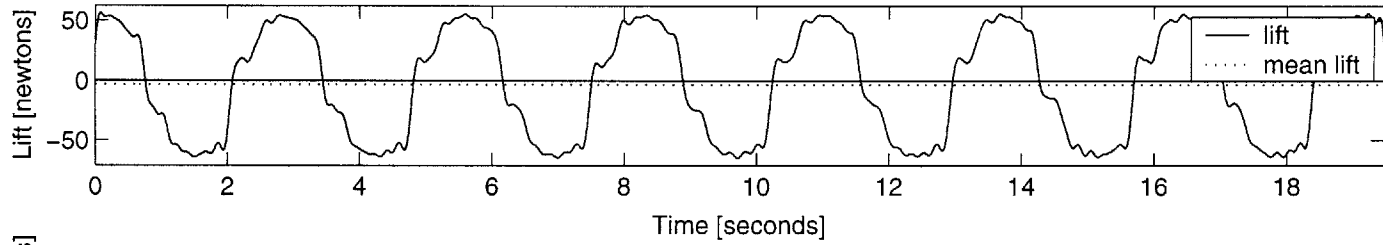
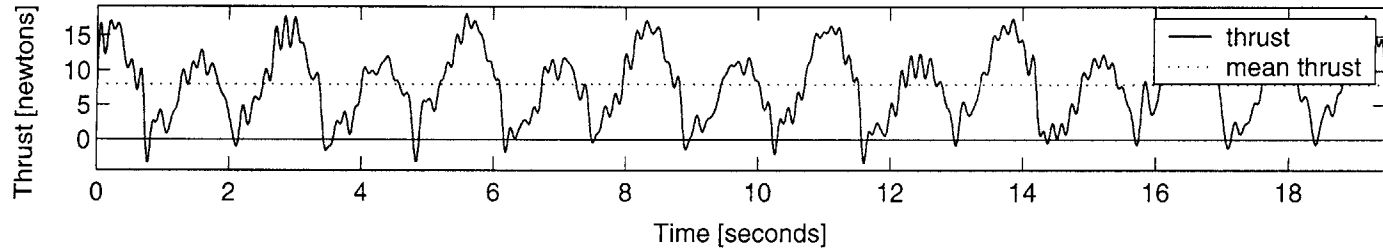
INPUT: U 0.5 [m/s], span 0.60 [m], chord 0.10 [m], roll 40 [deg], St 0.40, MaxAoa 30 [deg], run2 OUTPUT: Ct 0.6, efficiency 0.06



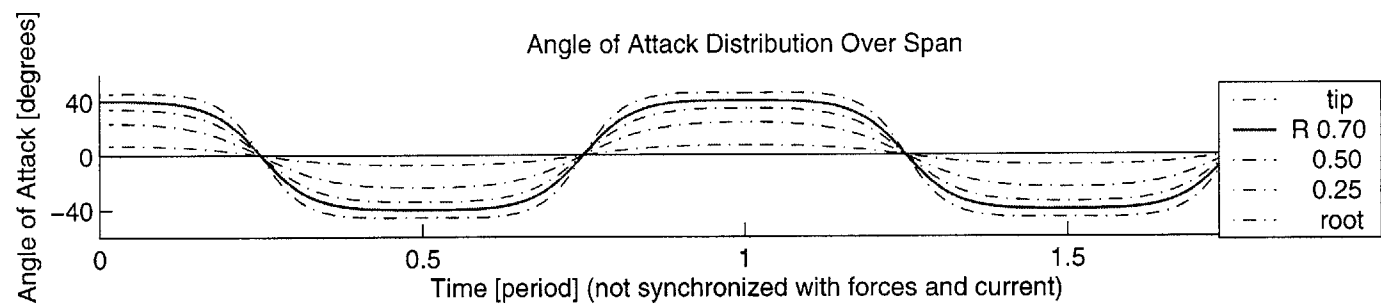
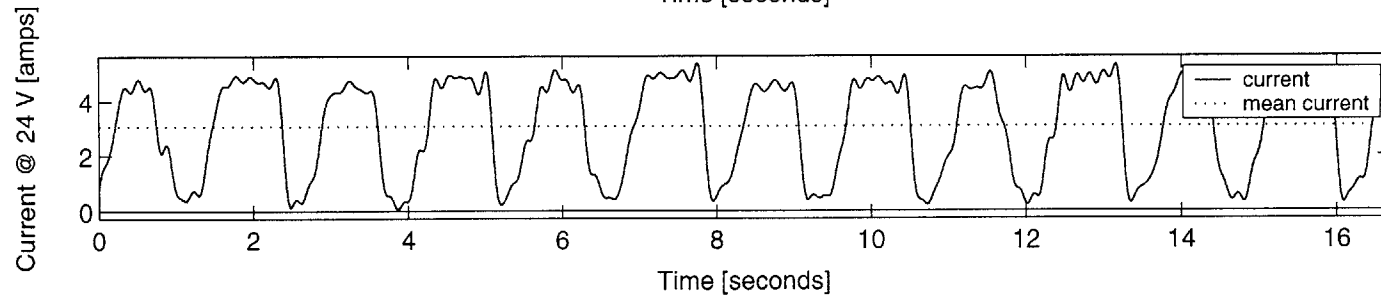
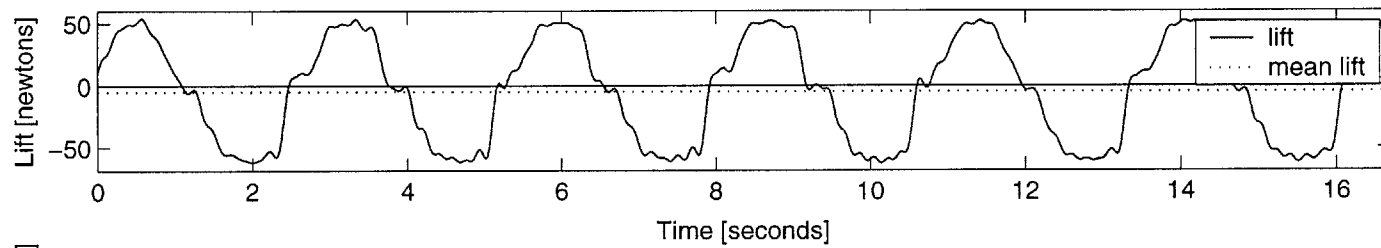
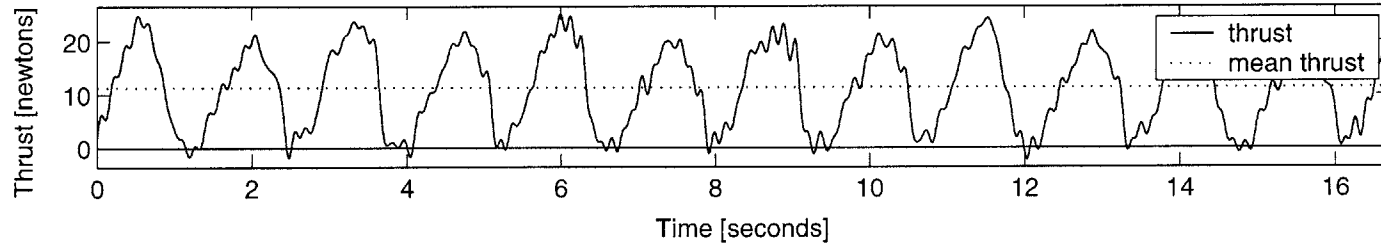
INPUT: U 0.5 [m/s], span 0.60 [m], chord 0.10 [m], roll 40 [deg], St 0.40, MaxAoa 20 [deg], run2 OUTPUT: Ct 0.6, efficiency 0.09



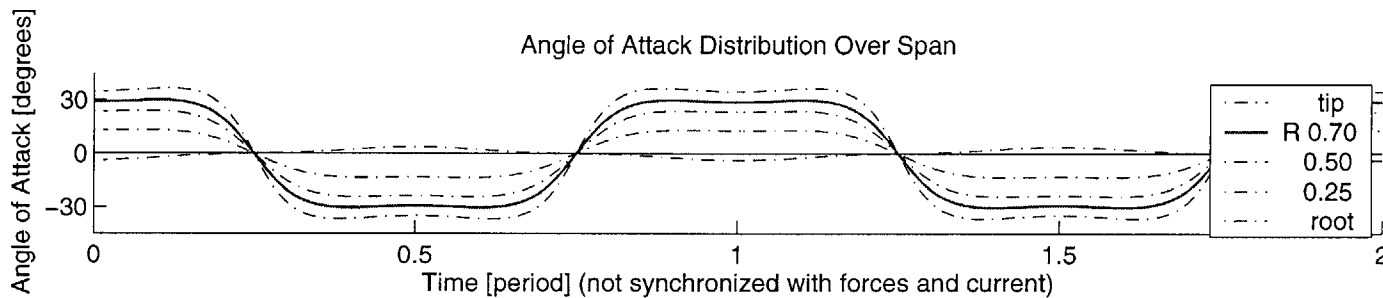
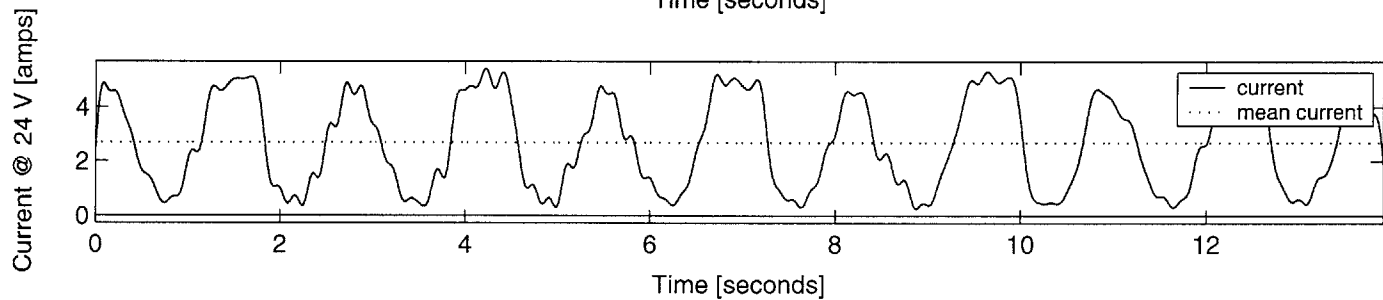
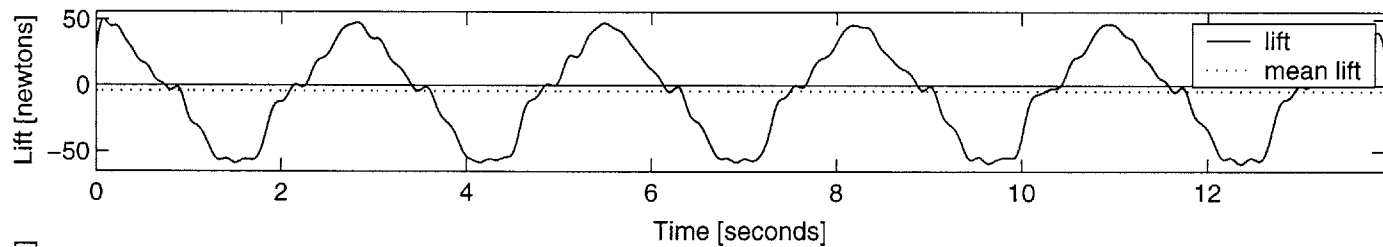
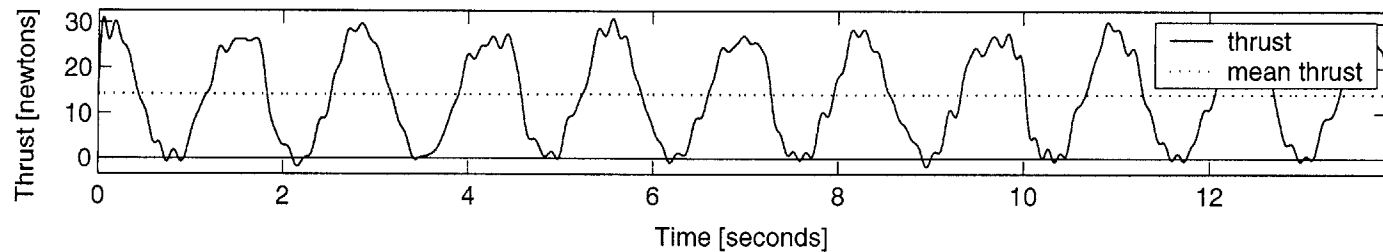
INPUT: U 0.5 [m/s], span 0.60 [m], chord 0.10 [m], roll 40 [deg], St 0.60, MaxAoa 50 [deg], run2 OUTPUT: Ct 1.1, efficiency 0.05



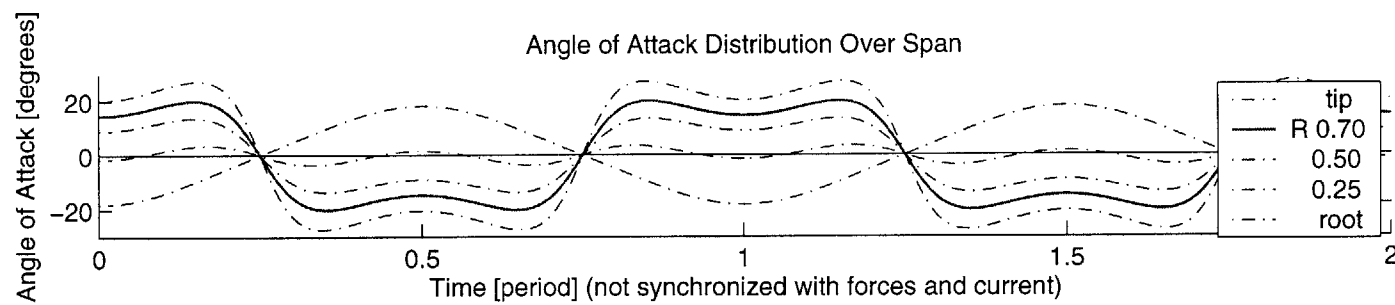
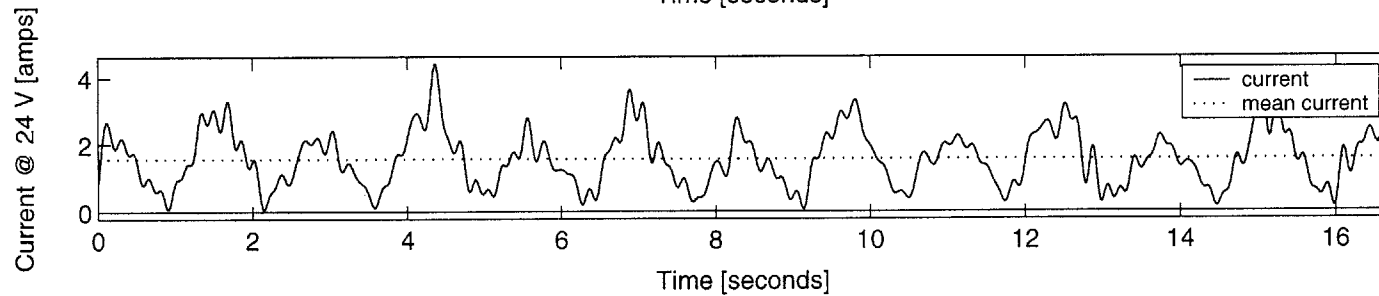
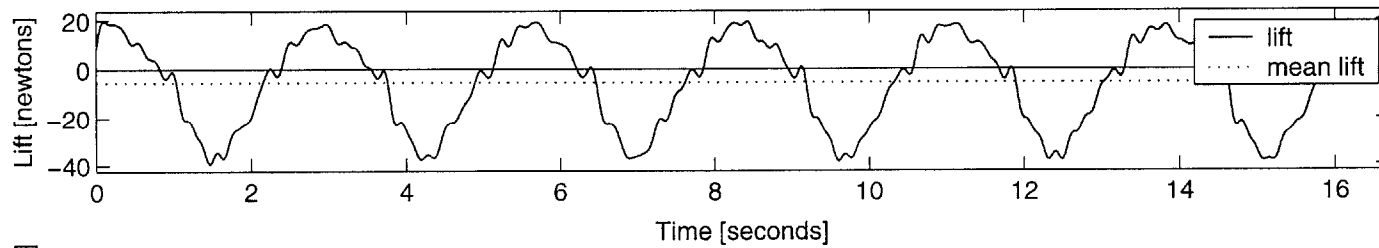
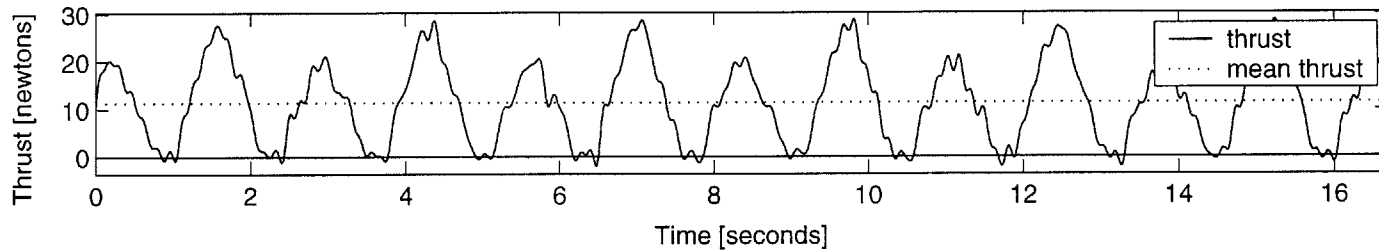
INPUT: U 0.5 [m/s], span 0.60 [m], chord 0.10 [m], roll 40 [deg], St 0.60, MaxAoa 40 [deg], run2 OUTPUT: Ct 1.5, efficiency 0.08



INPUT: U 0.5 [m/s], span 0.60 [m], chord 0.10 [m], roll 40 [deg], St 0.60, MaxAoa 30 [deg], run1 OUTPUT: Ct 1.9, efficiency 0.11

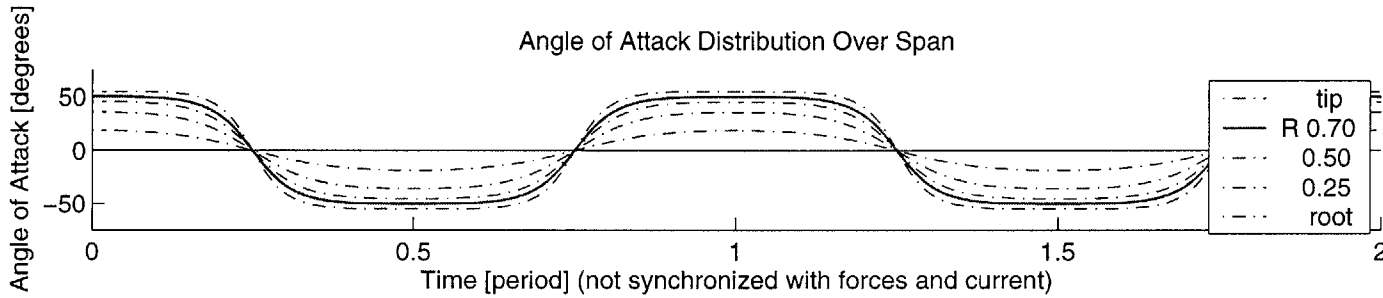
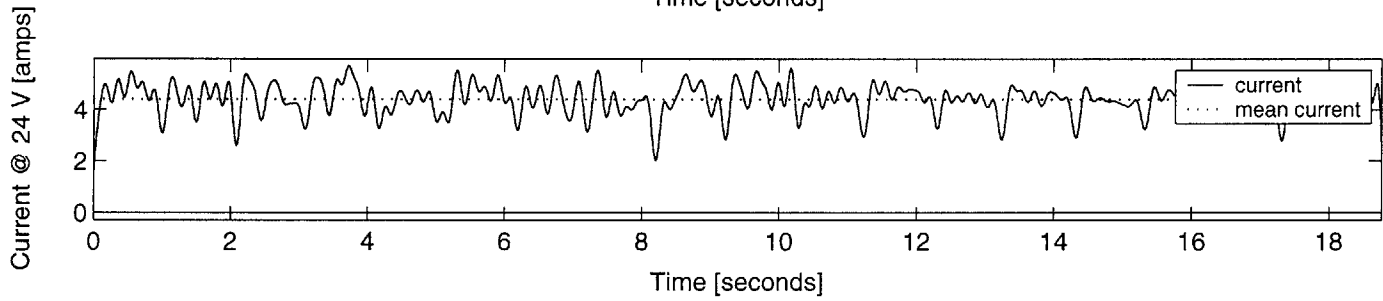
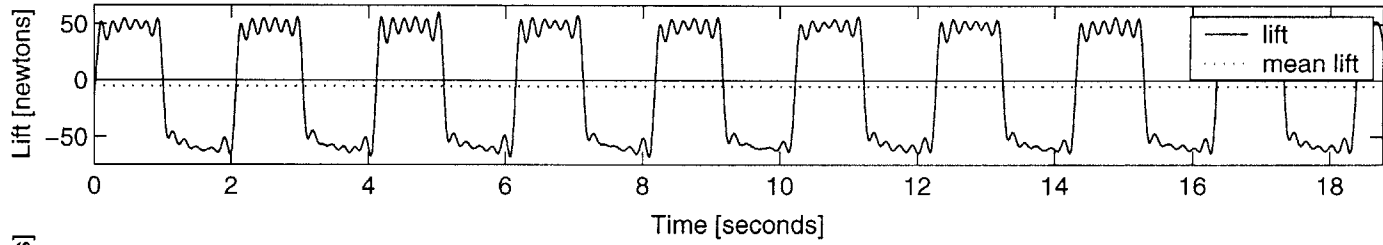
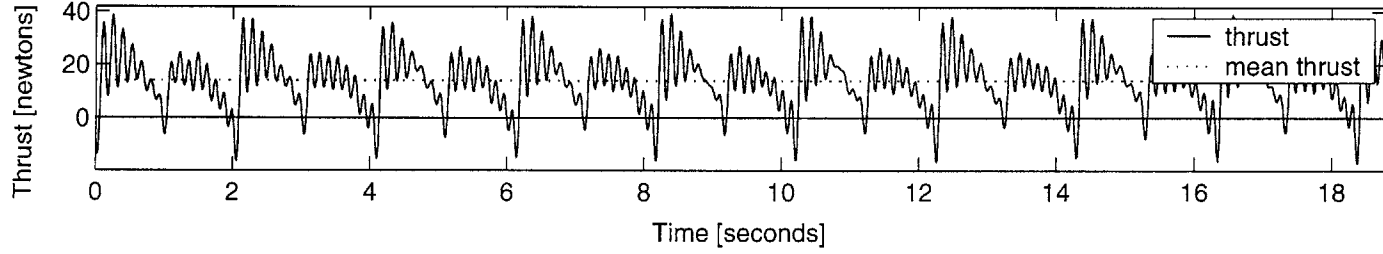


INPUT: U 0.5 [m/s], span 0.60 [m], chord 0.10 [m], roll 40 [deg], St 0.60, MaxAoa 20 [deg], run2 OUTPUT: Ct 1.5, efficiency 0.15

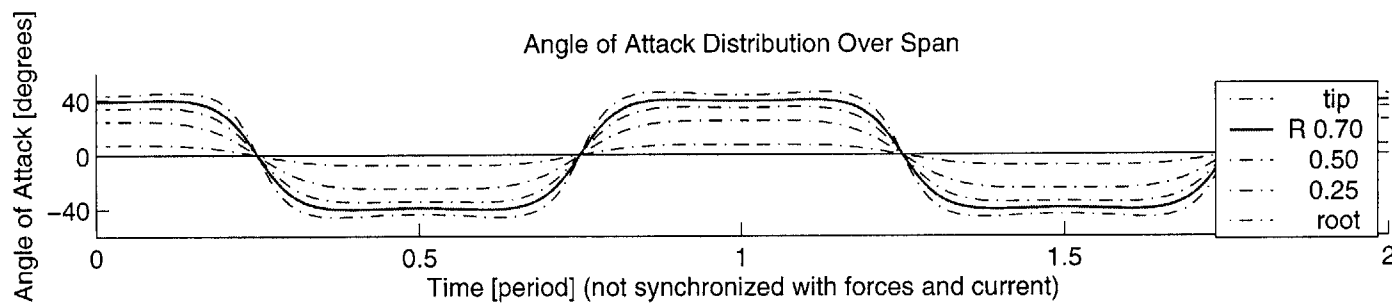
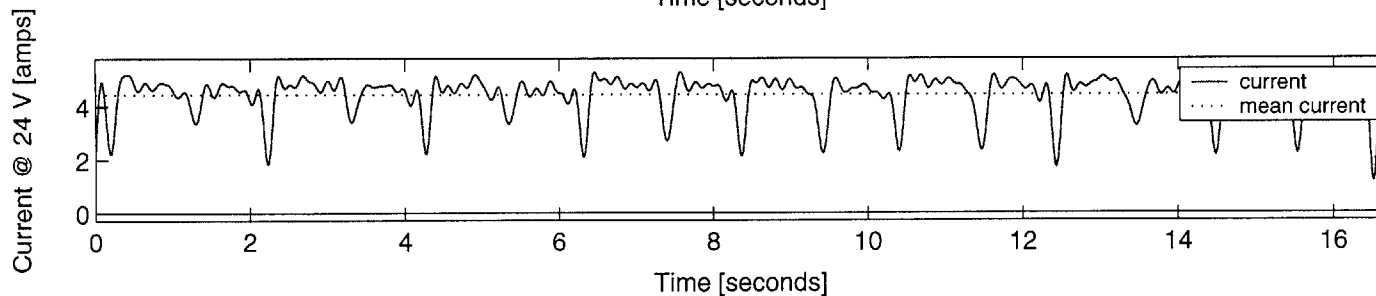
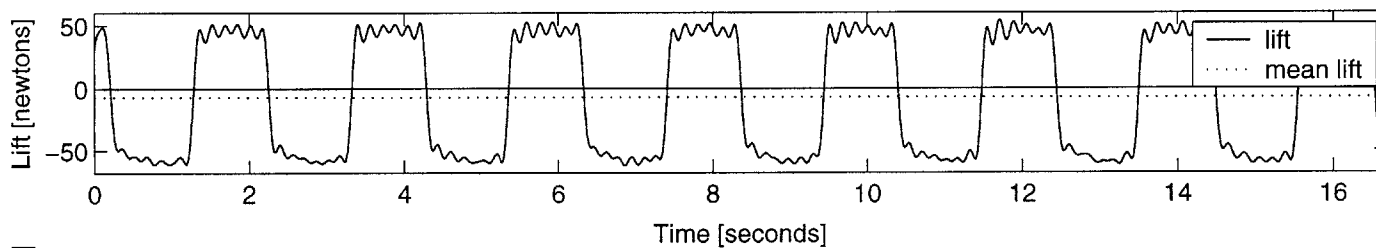
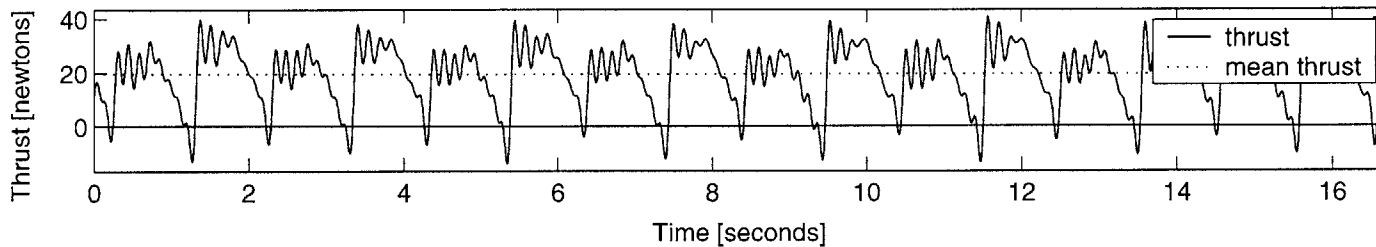




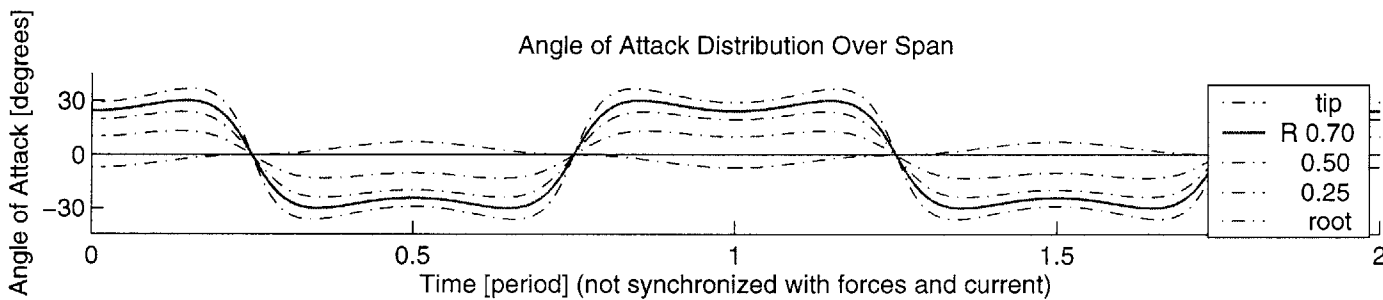
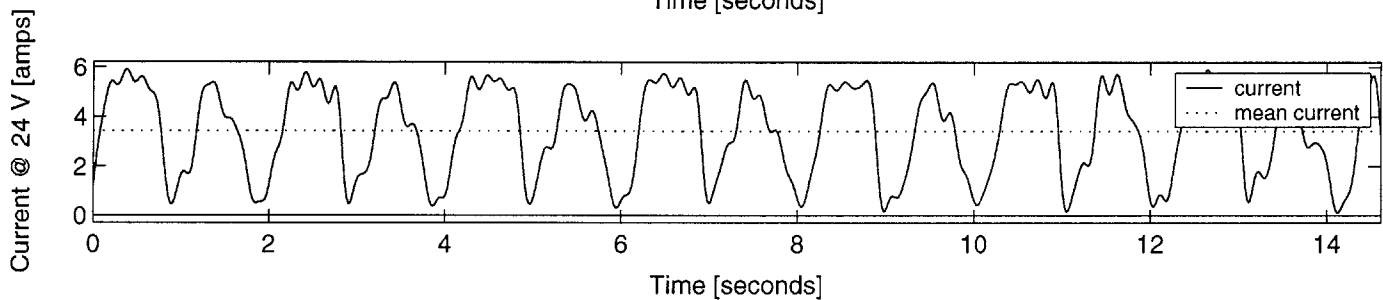
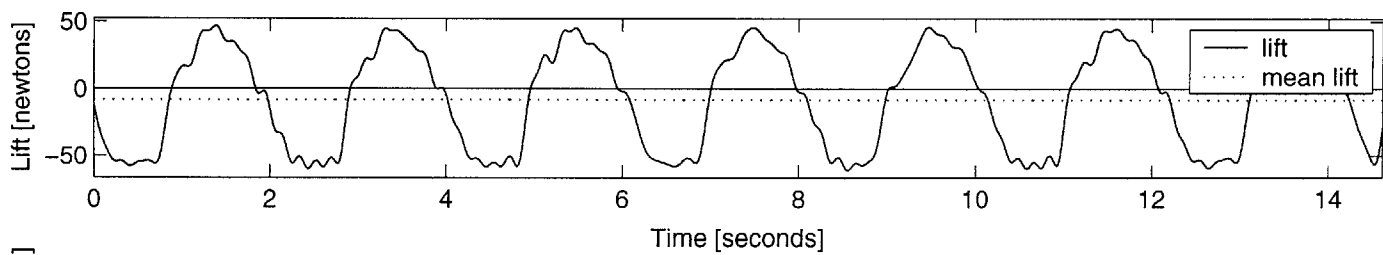
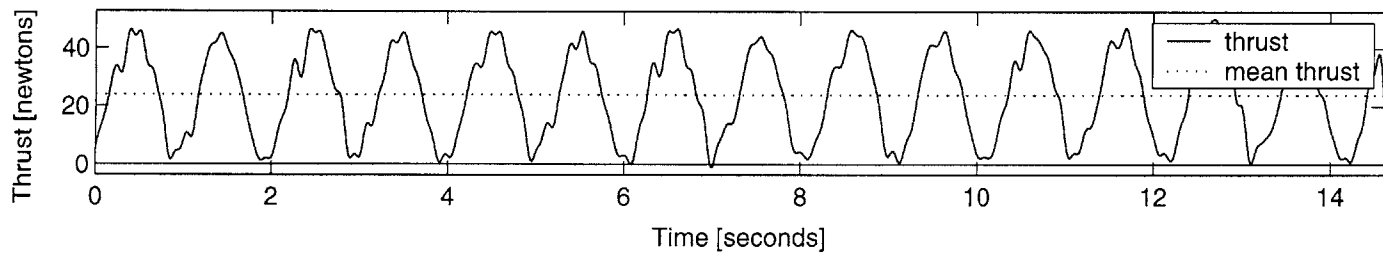
INPUT: U 0.5 [m/s], span 0.60 [m], chord 0.10 [m], roll 40 [deg], St 0.80, MaxAoa 50 [deg], run2 OUTPUT: Ct 1.8, efficiency 0.07



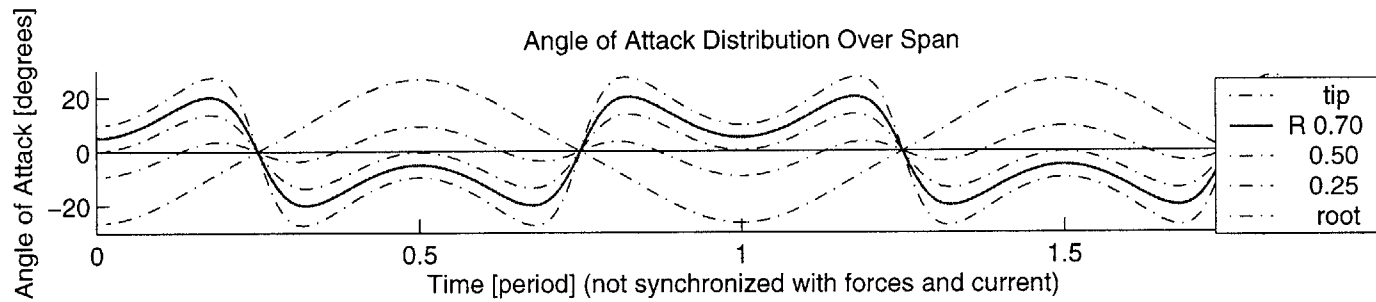
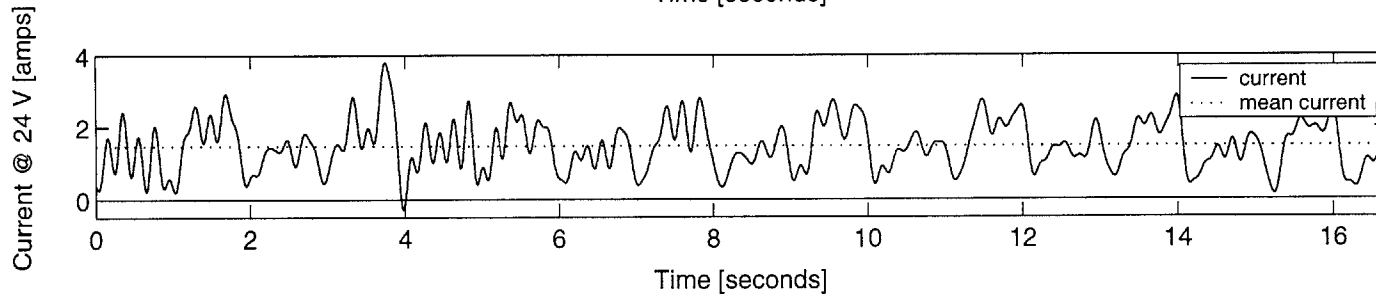
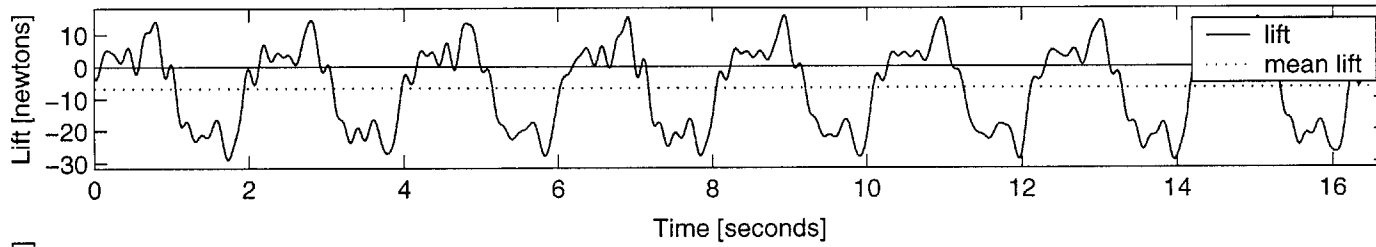
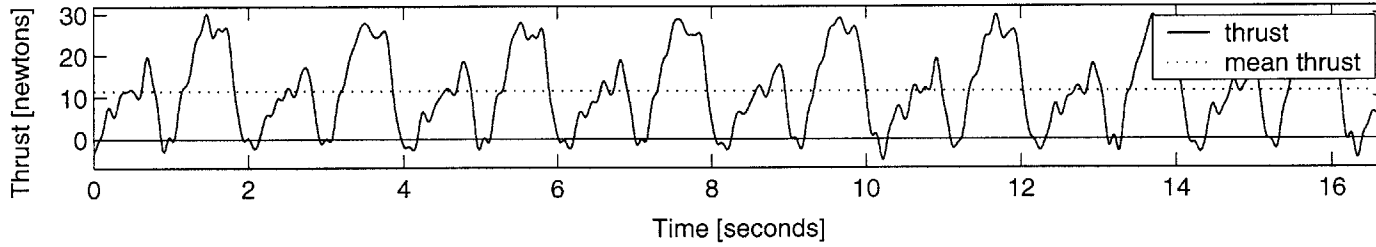
INPUT: U 0.5 [m/s], span 0.60 [m], chord 0.10 [m], roll 40 [deg], St 0.80, MaxAoa 40 [deg], run2 OUTPUT: Ct 2.6, efficiency 0.09



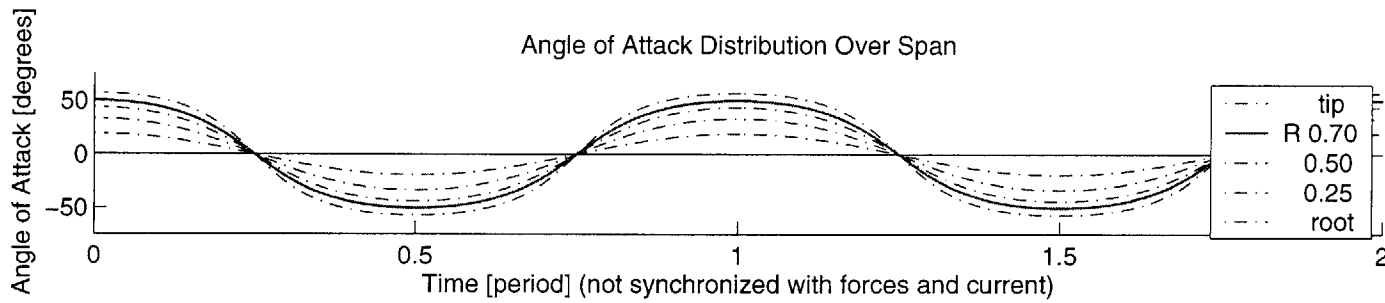
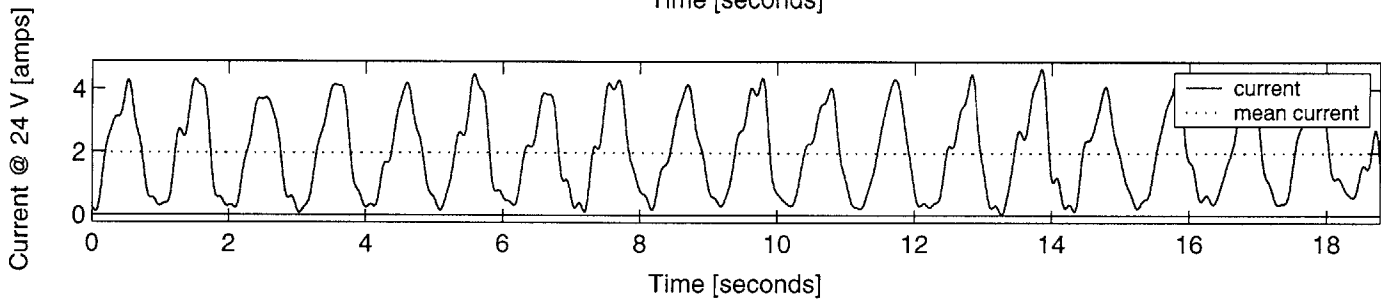
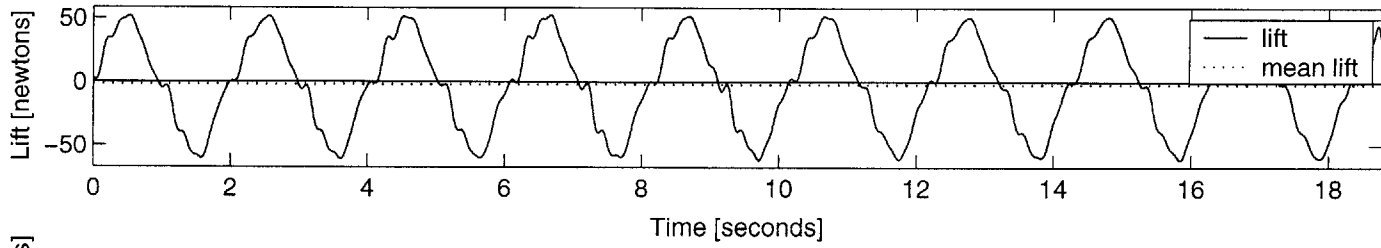
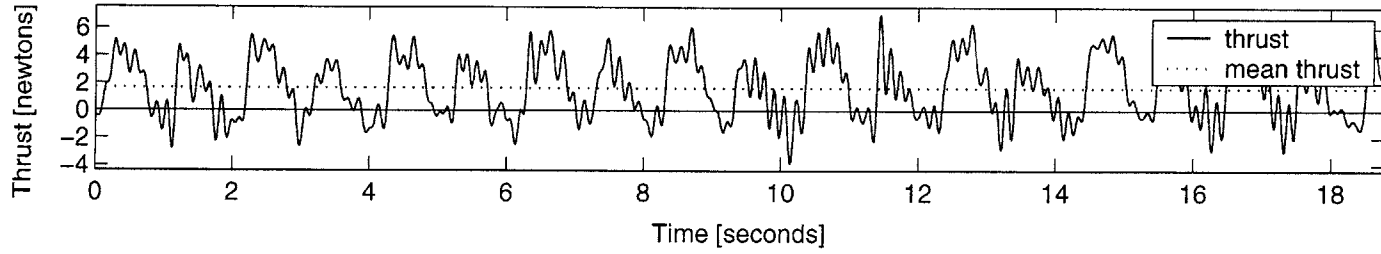
INPUT: U 0.5 [m/s], span 0.60 [m], chord 0.10 [m], roll 40 [deg], St 0.80, MaxAoa 30 [deg], run2 OUTPUT: Ct 3.2, efficiency 0.14



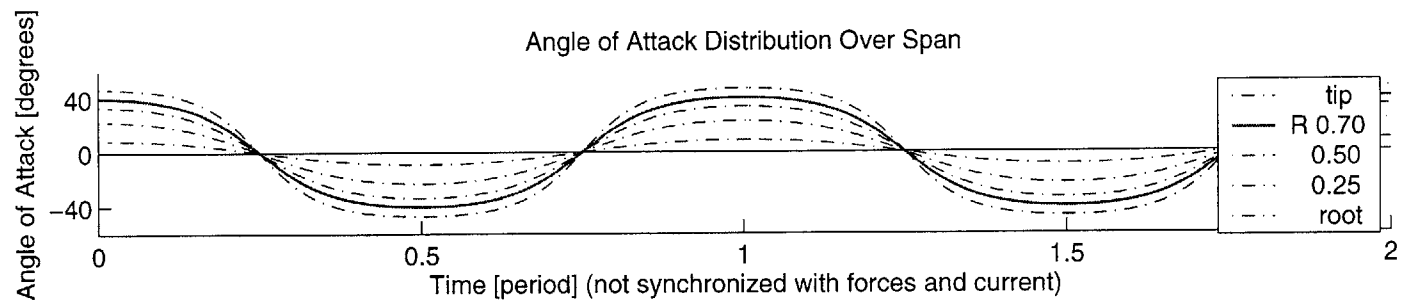
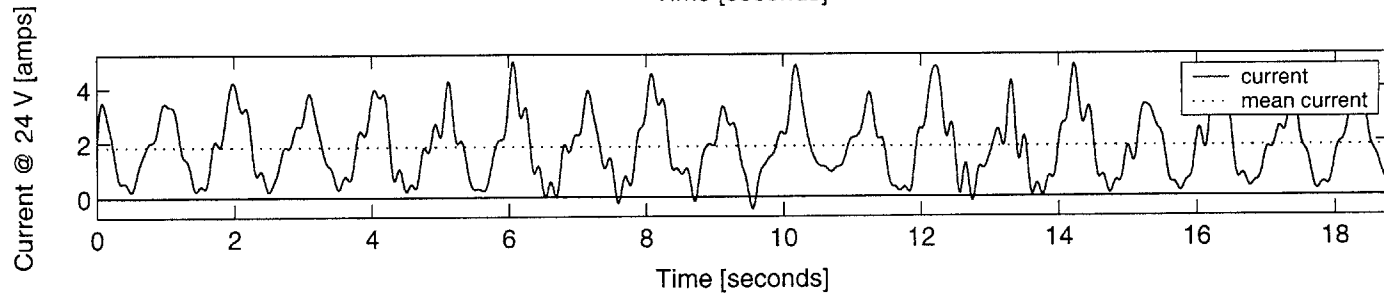
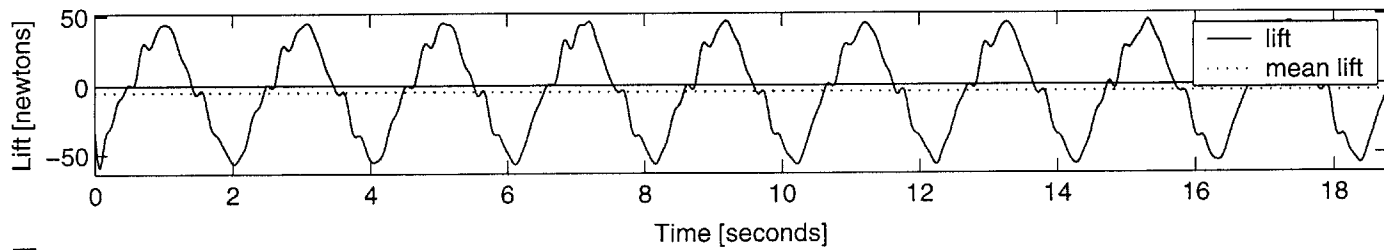
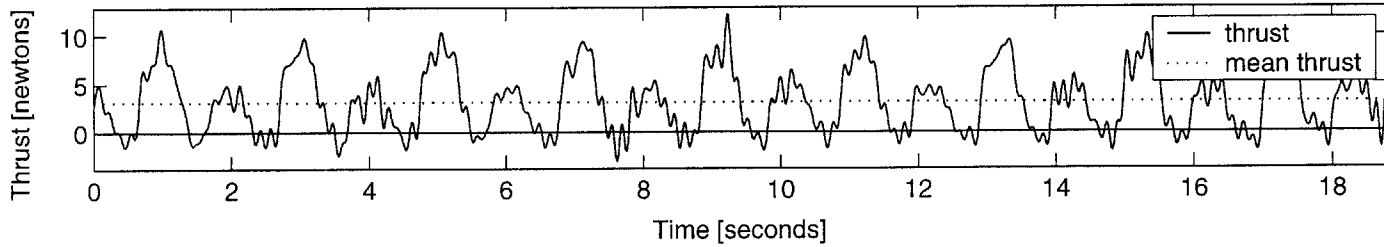
INPUT: U 0.5 [m/s], span 0.60 [m], chord 0.10 [m], roll 40 [deg], St 0.80, MaxAoa 20 [deg], run2 OUTPUT: Ct 1.5, efficiency 0.16



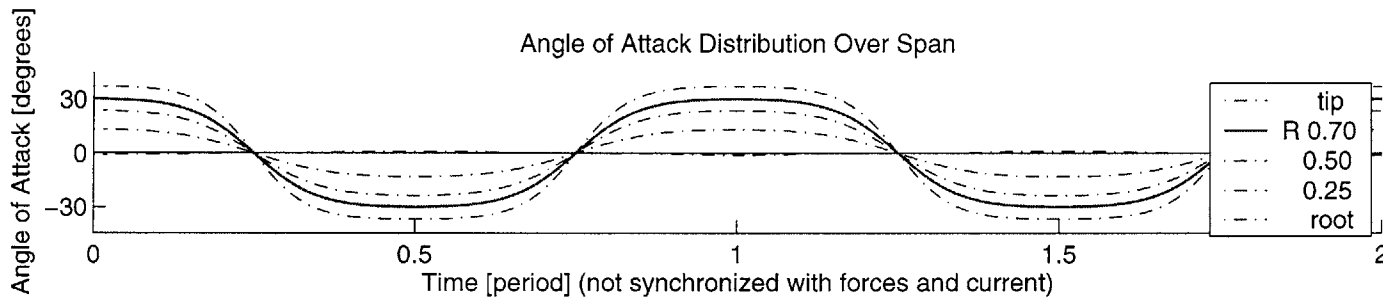
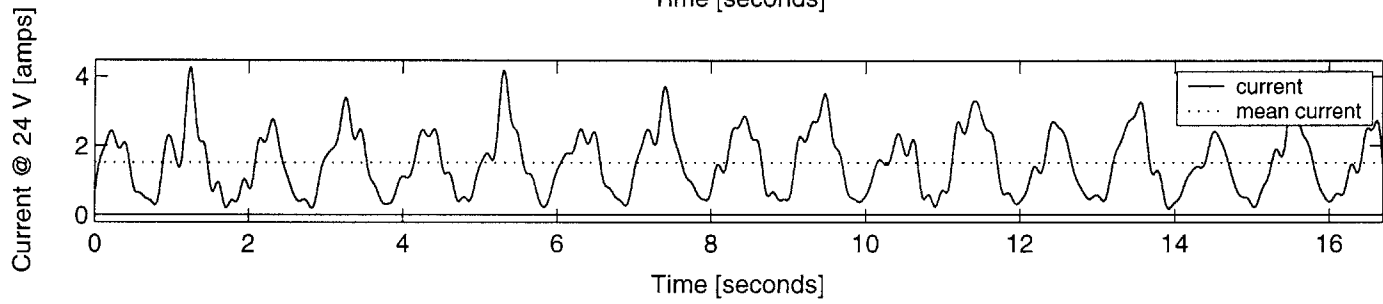
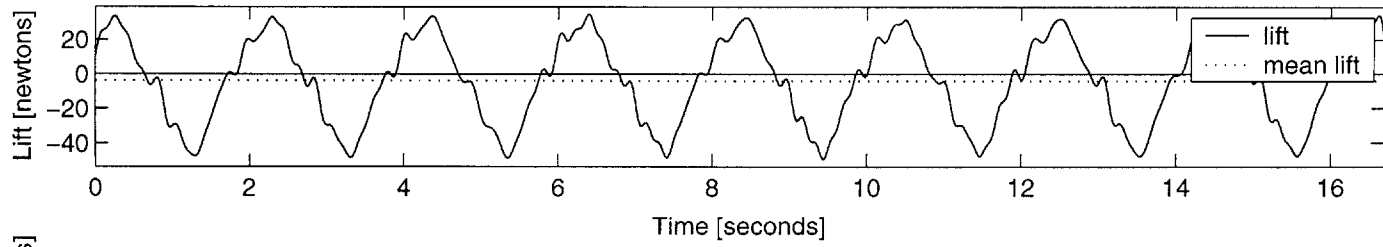
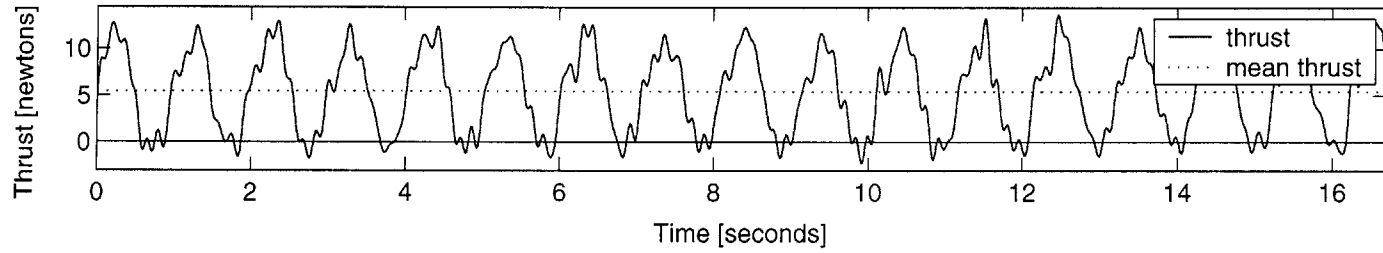
INPUT: U 0.5 [m/s], span 0.60 [m], chord 0.10 [m], roll 20 [deg], St 0.40, MaxAoa 50 [deg], run2 OUTPUT: Ct 0.2, efficiency 0.02



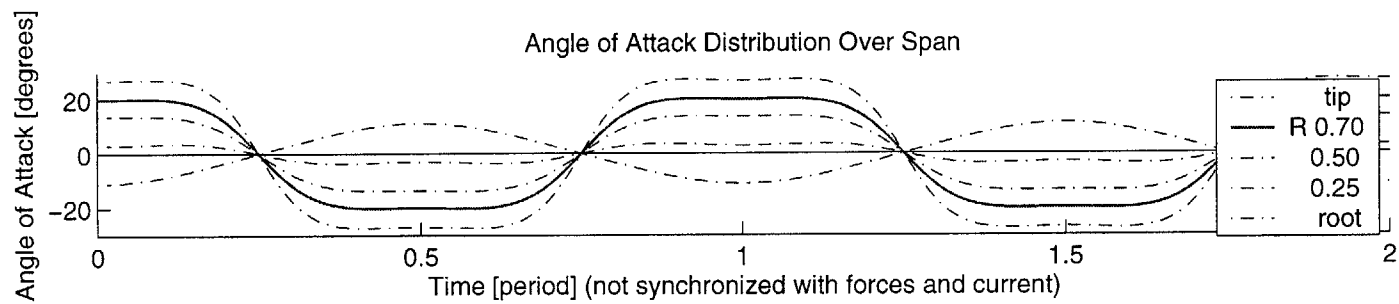
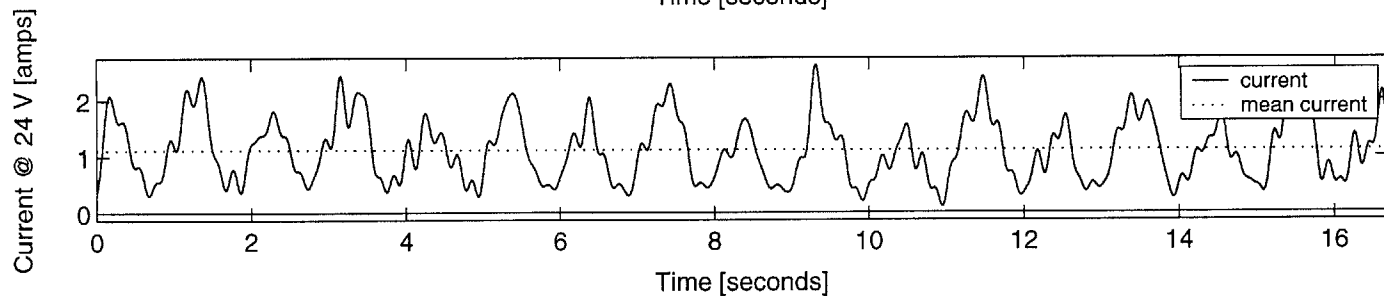
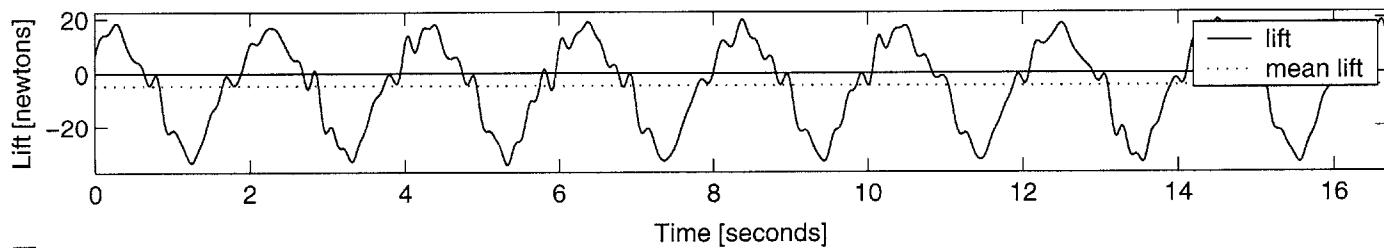
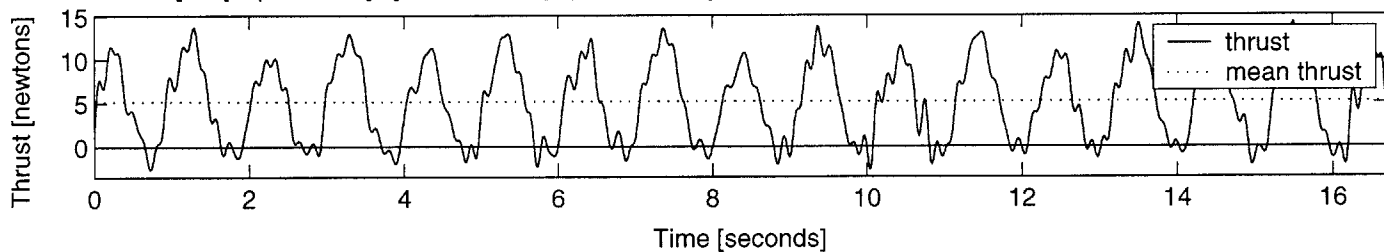
INPUT: U 0.5 [m/s], span 0.60 [m], chord 0.10 [m], roll 20 [deg], St 0.40, MaxAoa 40 [deg], run2 OUTPUT: Ct 0.4, efficiency 0.04



INPUT: U 0.5 [m/s], span 0.60 [m], chord 0.10 [m], roll 20 [deg], St 0.40, MaxAoa 30 [deg], run2 OUTPUT: Ct 0.7, efficiency 0.07

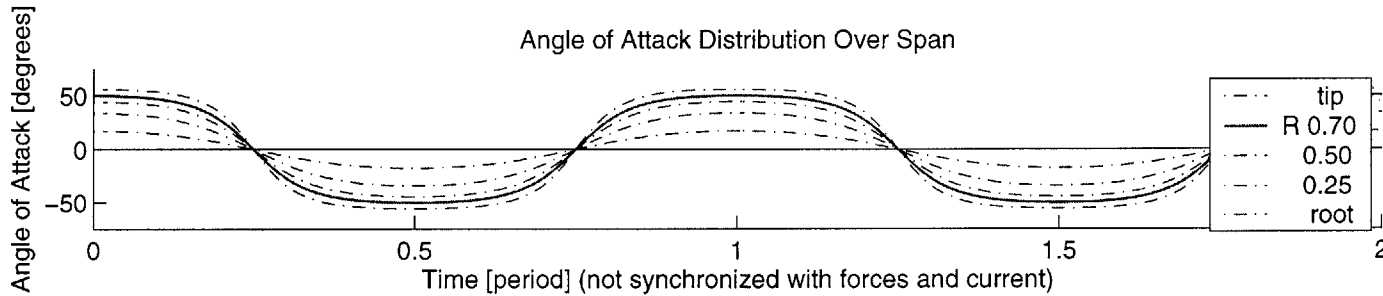
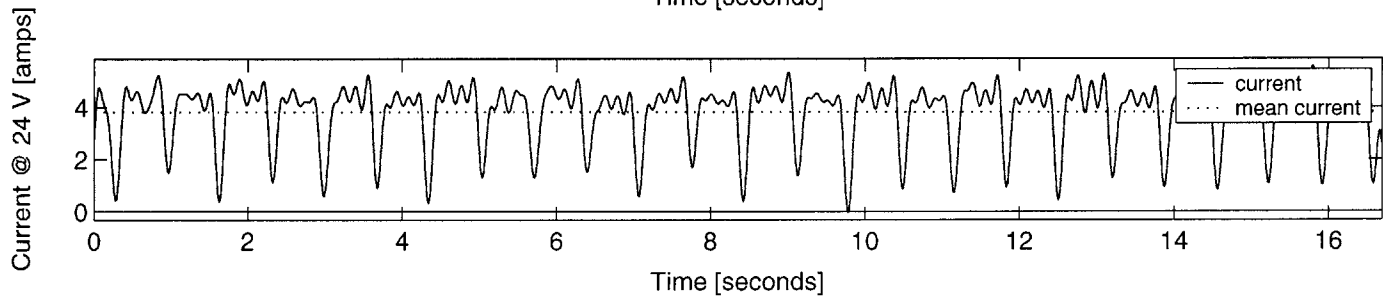
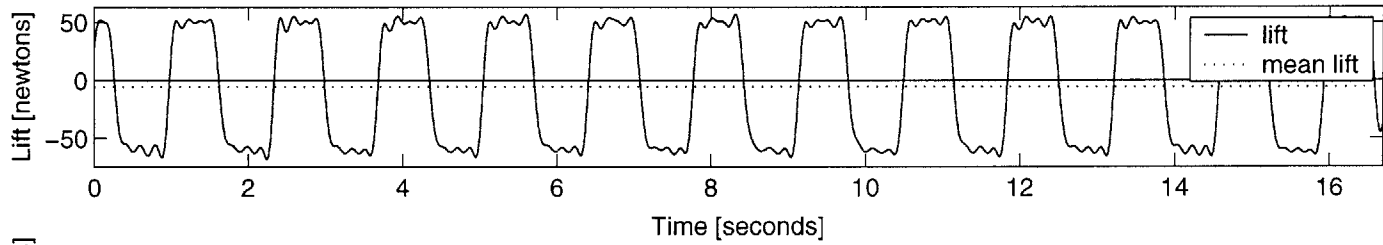
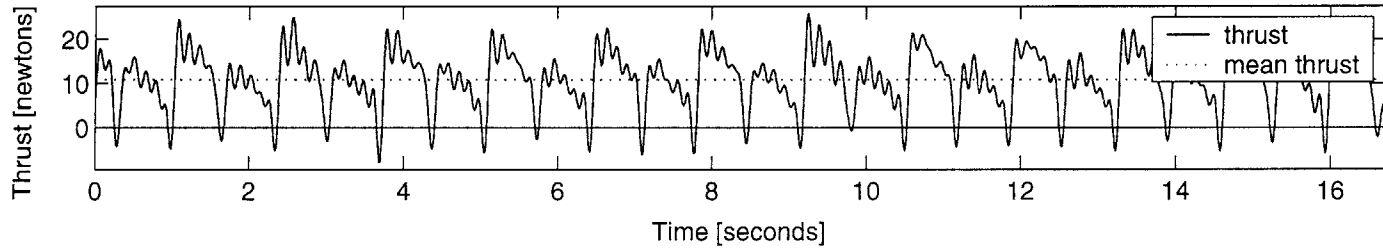


INPUT: U 0.5 [m/s], span 0.60 [m], chord 0.10 [m], roll 20 [deg], St 0.40, MaxAoa 20 [deg], run2 OUTPUT: Ct 0.7, efficiency 0.10

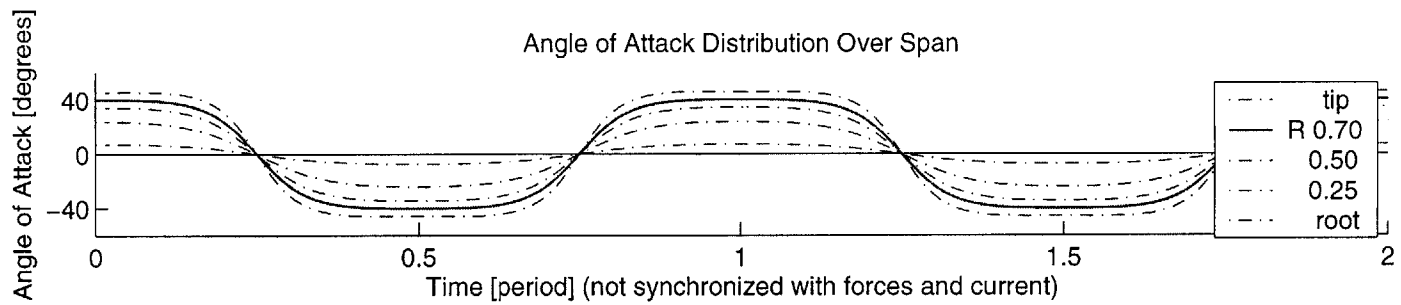
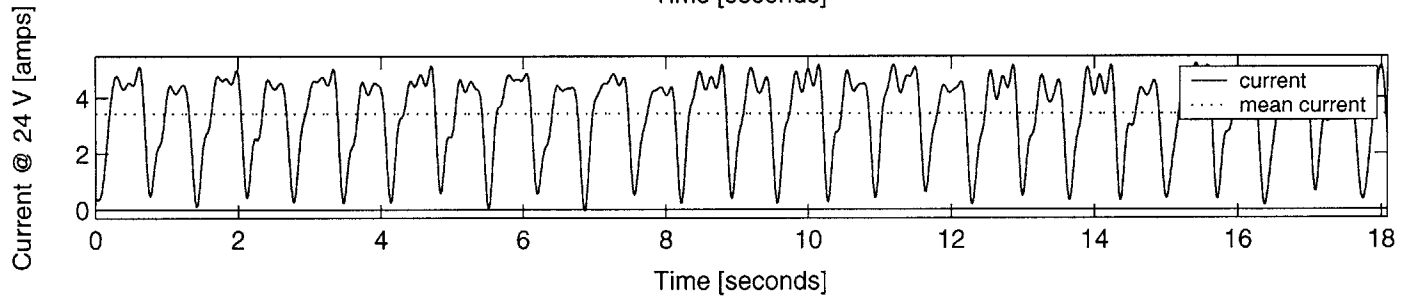
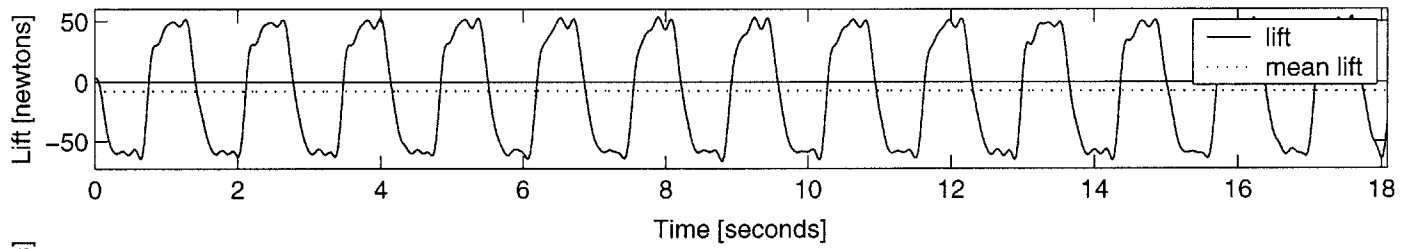
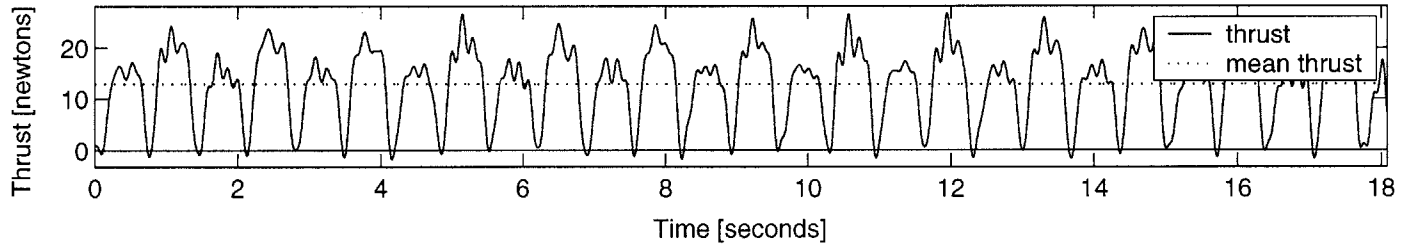




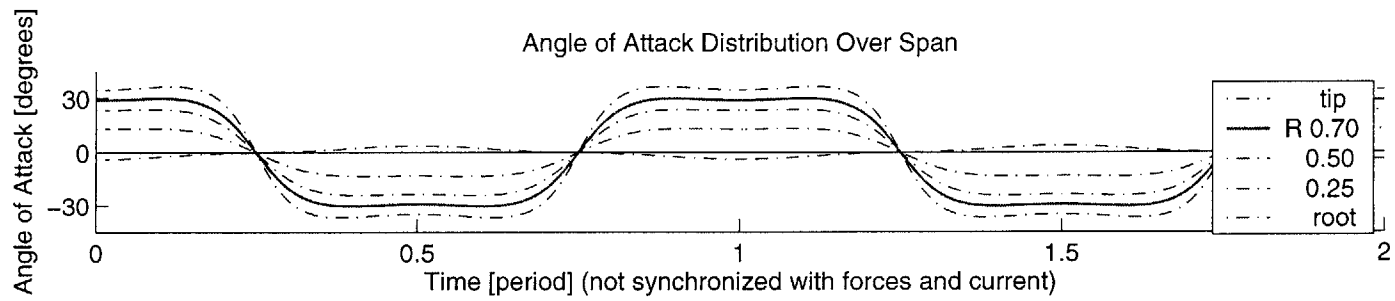
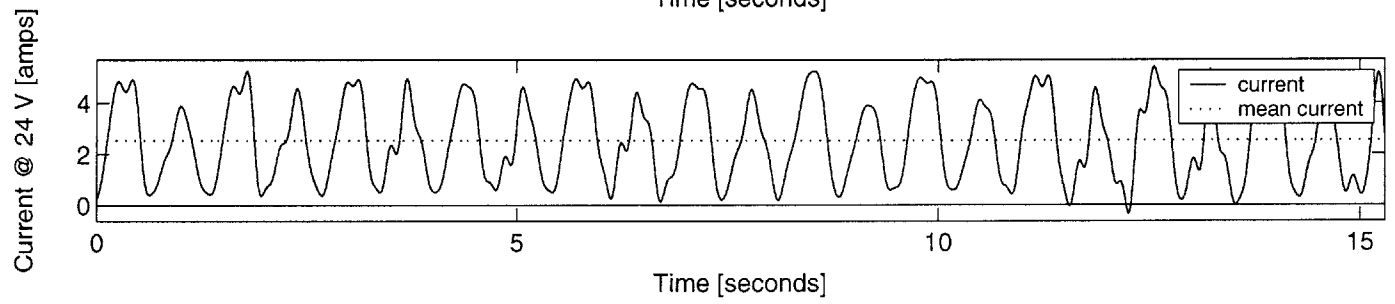
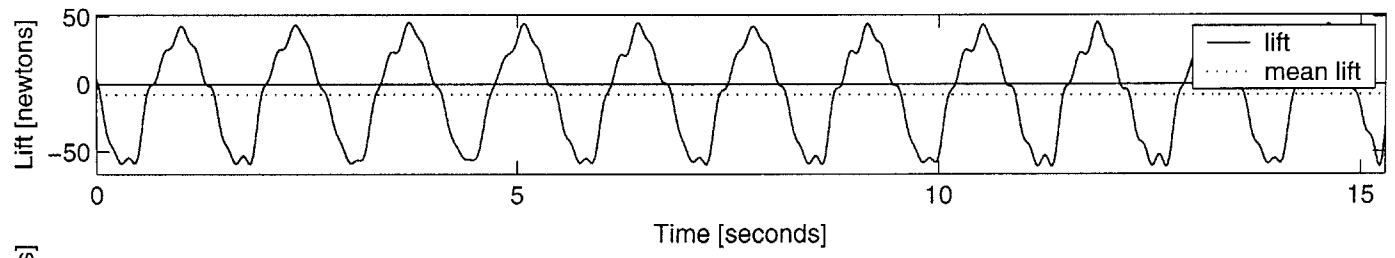
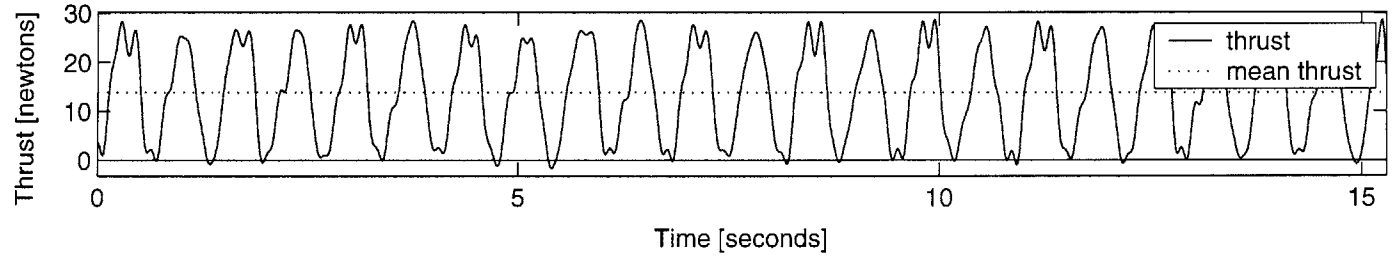
INPUT: U 0.5 [m/s], span 0.60 [m], chord 0.10 [m], roll 20 [deg], St 0.60, MaxAoa 50 [deg], run2 OUTPUT: Ct 1.4, efficiency 0.06



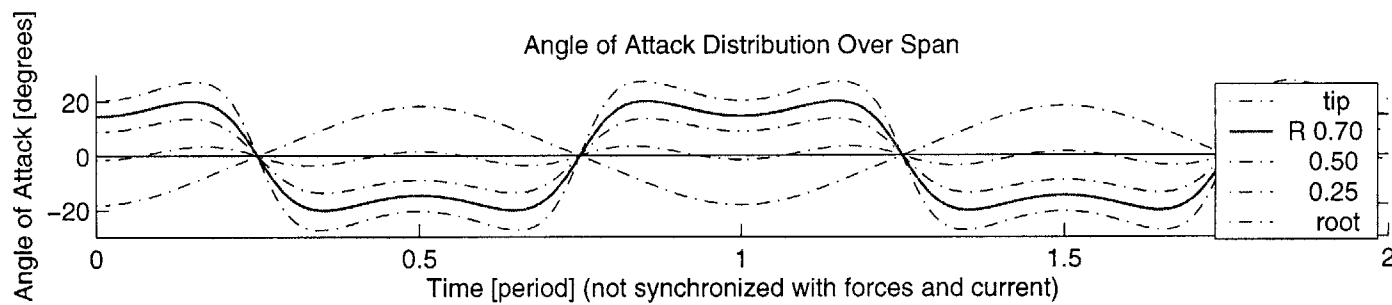
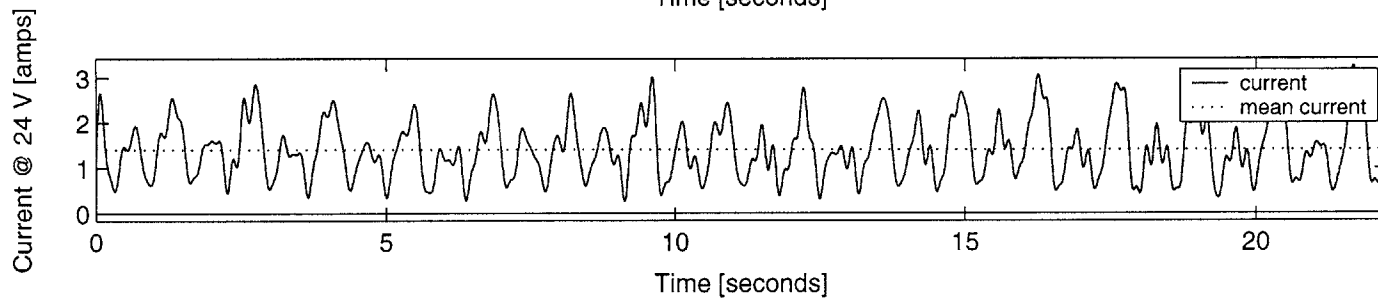
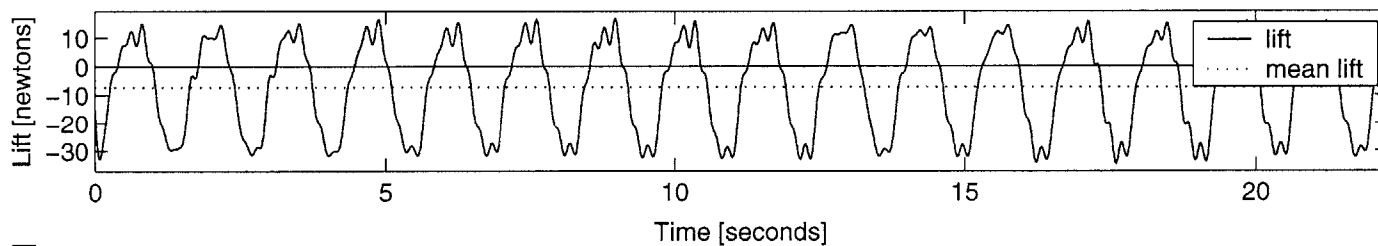
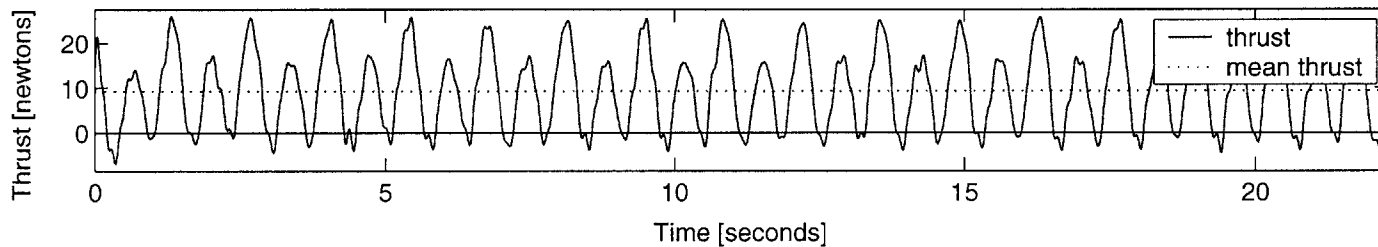
INPUT: U 0.5 [m/s], span 0.60 [m], chord 0.10 [m], roll 20 [deg], St 0.60, MaxAoa 40 [deg], run2 OUTPUT: Ct 1.7, efficiency 0.08



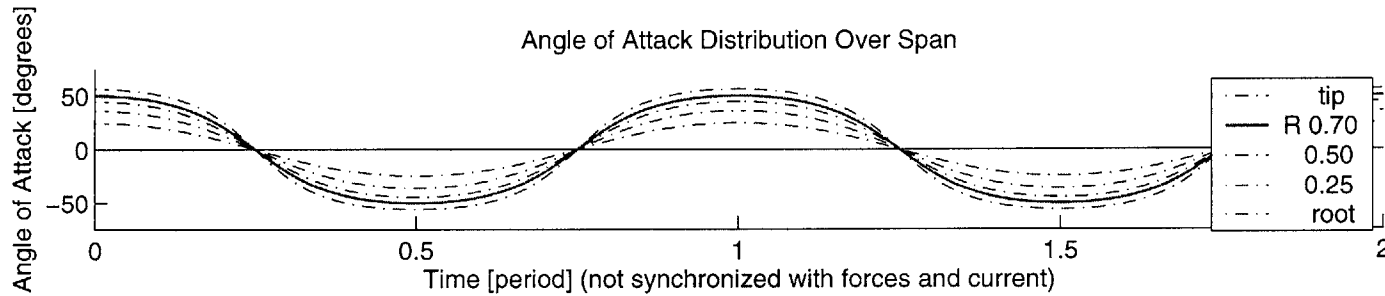
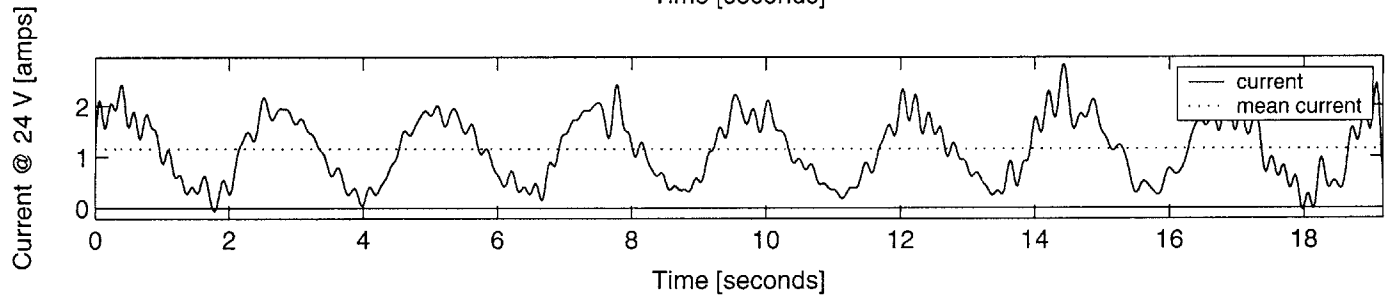
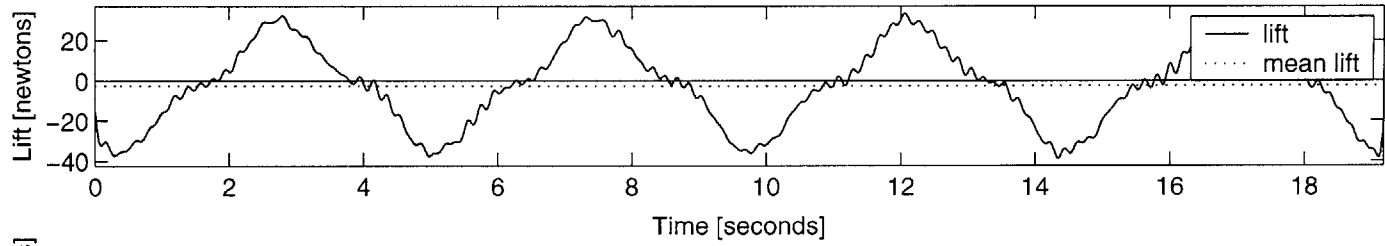
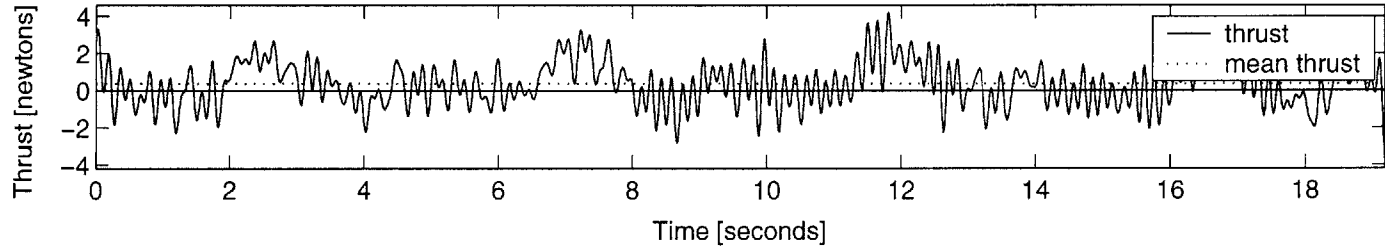
INPUT: U 0.5 [m/s], span 0.60 [m], chord 0.10 [m], roll 20 [deg], St 0.60, MaxAoa 30 [deg], run2 OUTPUT: Ct 1.8, efficiency 0.11



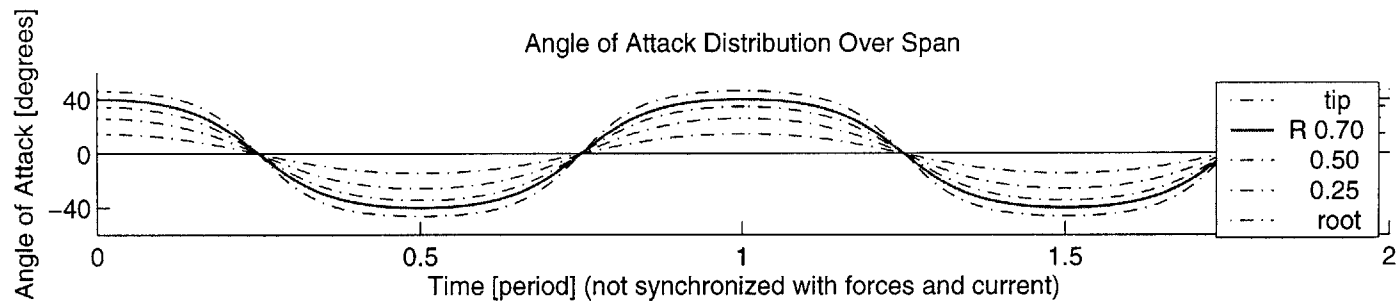
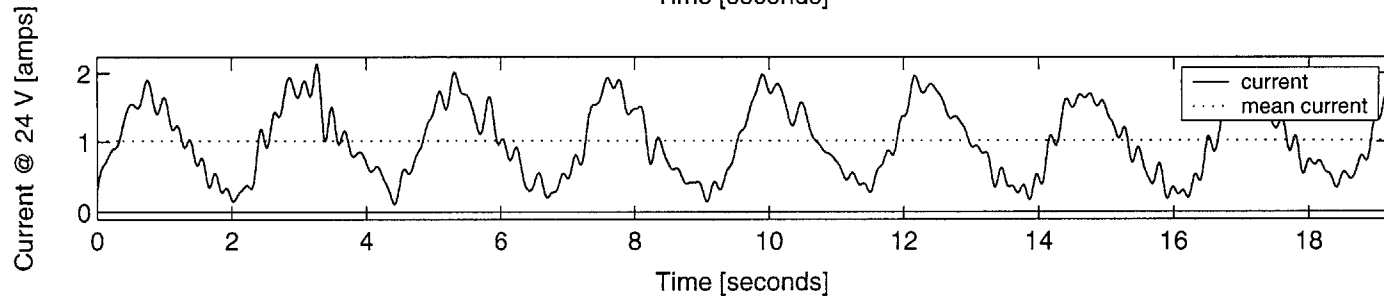
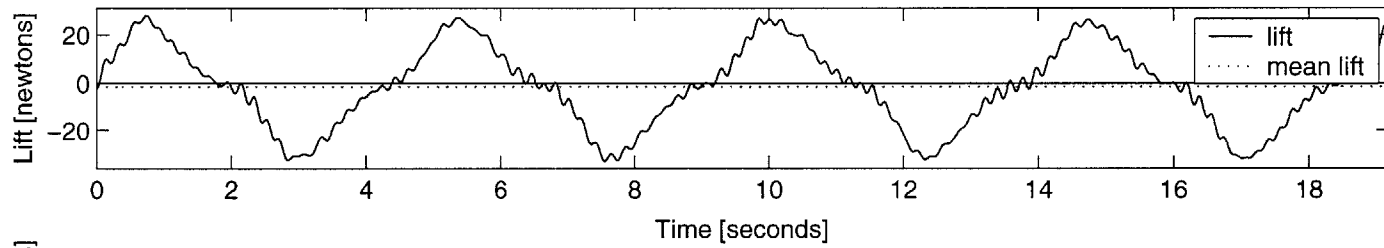
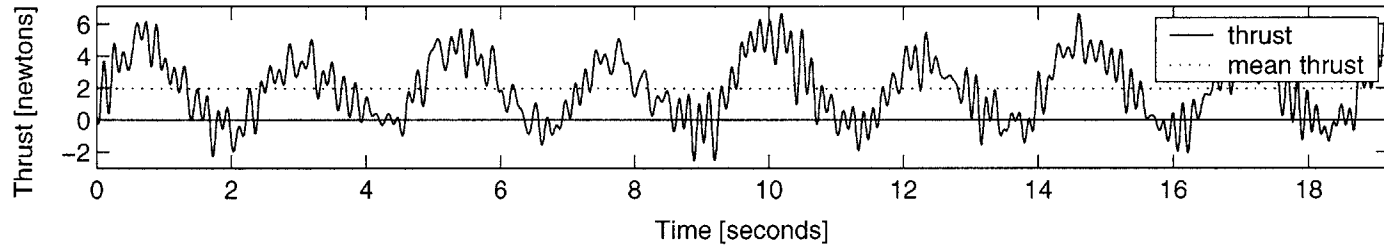
INPUT: U 0.5 [m/s], span 0.60 [m], chord 0.10 [m], roll 20 [deg], St 0.60, MaxAoa 20 [deg], run2 OUTPUT: Ct 1.2, efficiency 0.14



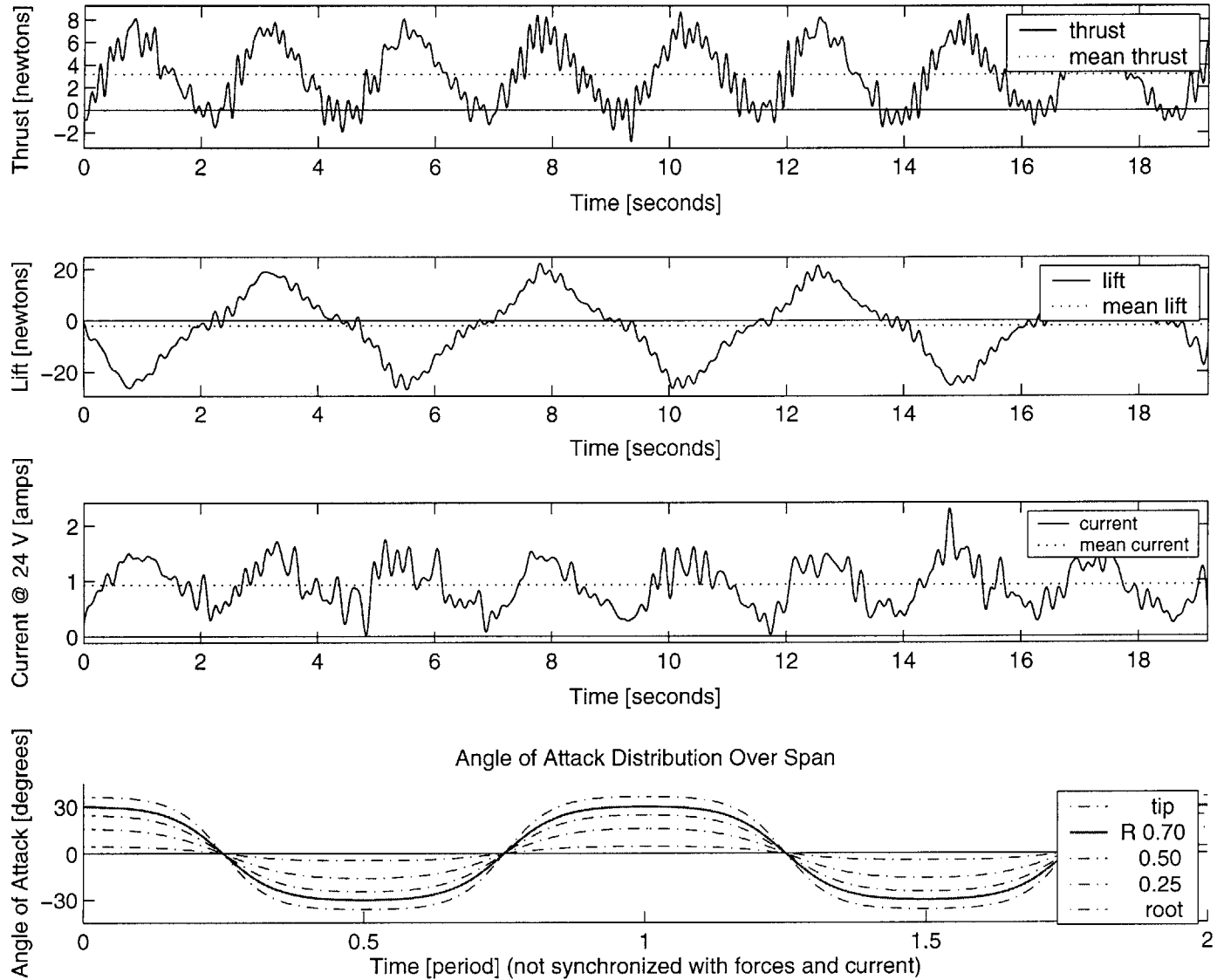
INPUT: U 0.5 [m/s], span 0.40 [m], chord 0.10 [m], roll 60 [deg], St 0.40, MaxAoa 50 [deg], run1 OUTPUT: Ct 0.1, efficiency 0.01



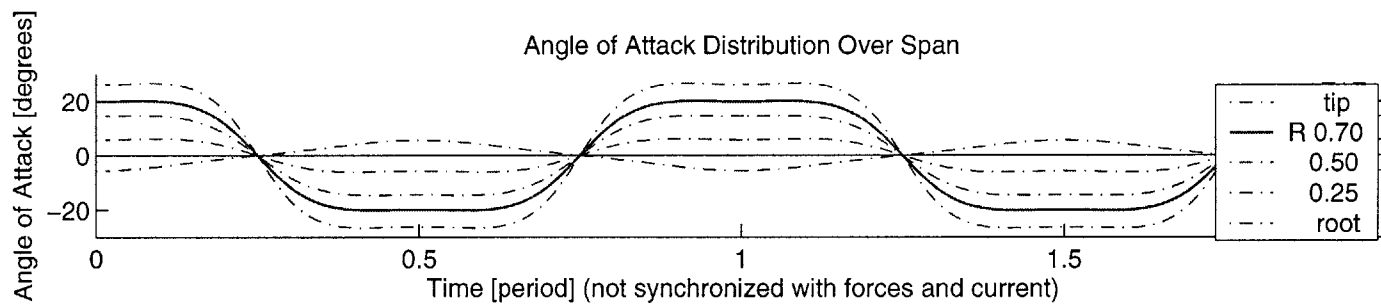
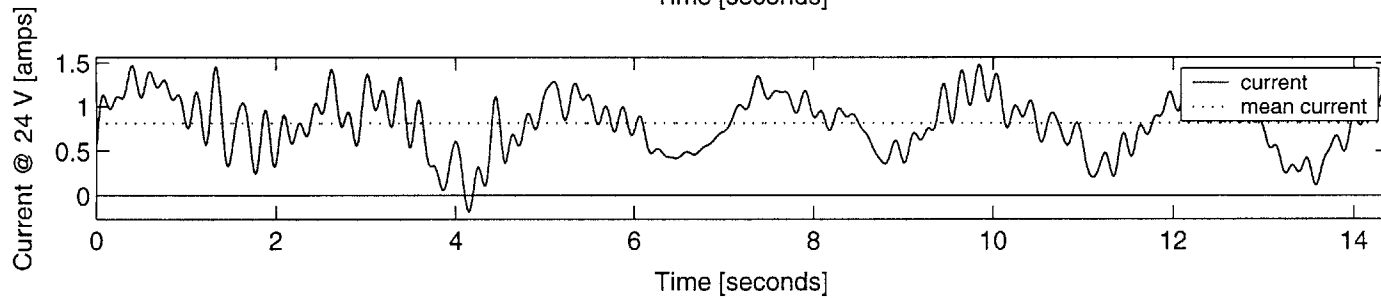
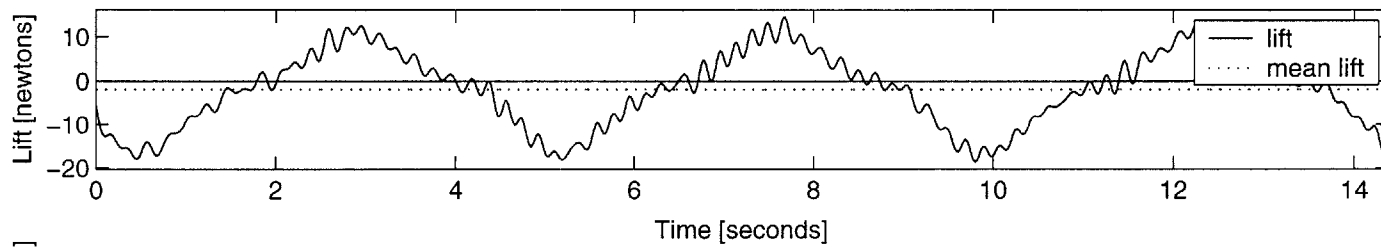
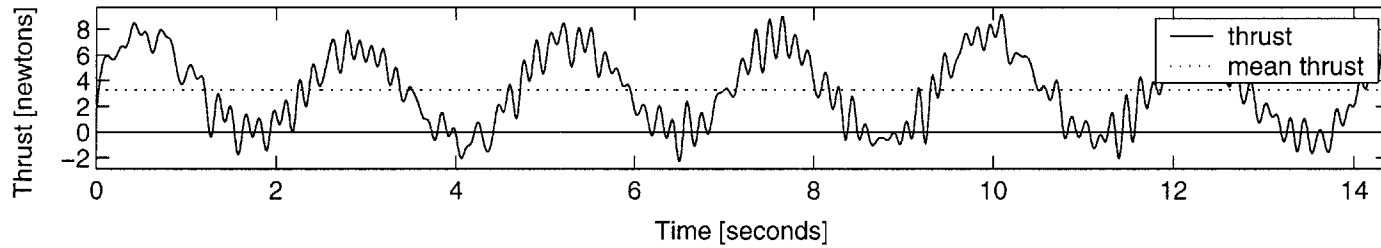
INPUT: U 0.5 [m/s], span 0.40 [m], chord 0.10 [m], roll 60 [deg], St 0.40, MaxAoa 40 [deg], run1 OUTPUT: Ct 0.4, efficiency 0.04



INPUT: U 0.5 [m/s], span 0.40 [m], chord 0.10 [m], roll 60 [deg], St 0.40, MaxAoa 30 [deg], run1 OUTPUT: Ct 0.6, efficiency 0.07

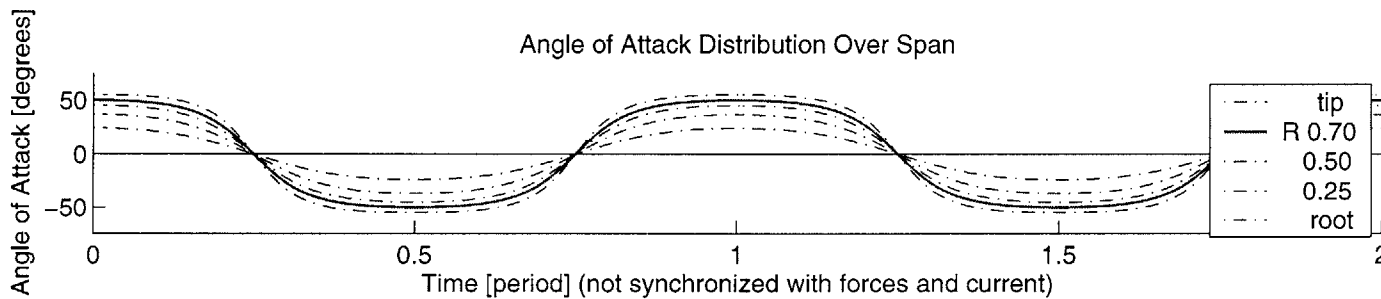
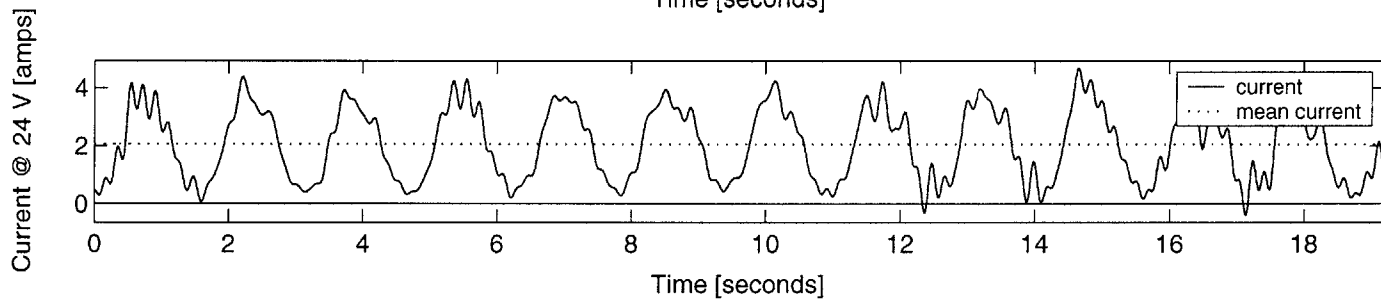
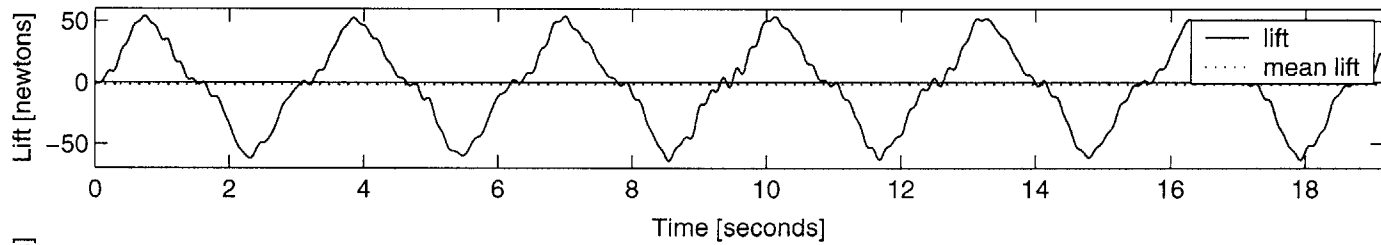
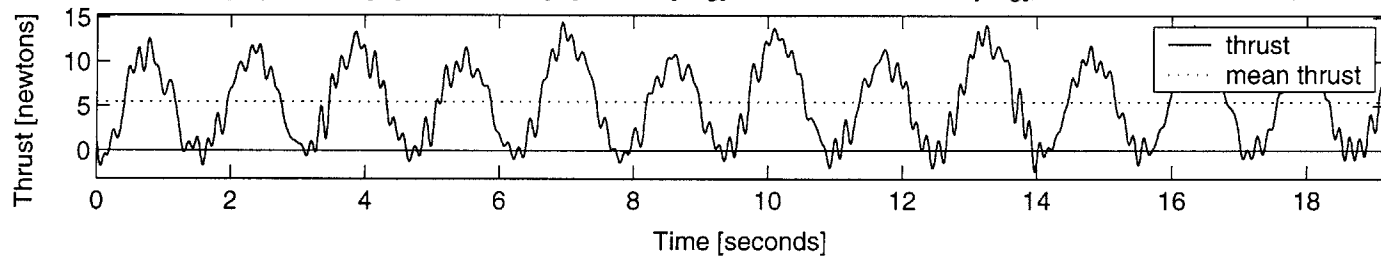


INPUT: U 0.5 [m/s], span 0.40 [m], chord 0.10 [m], roll 60 [deg], St 0.40, MaxAoa 20 [deg], run1 OUTPUT: Ct 0.7, efficiency 0.08

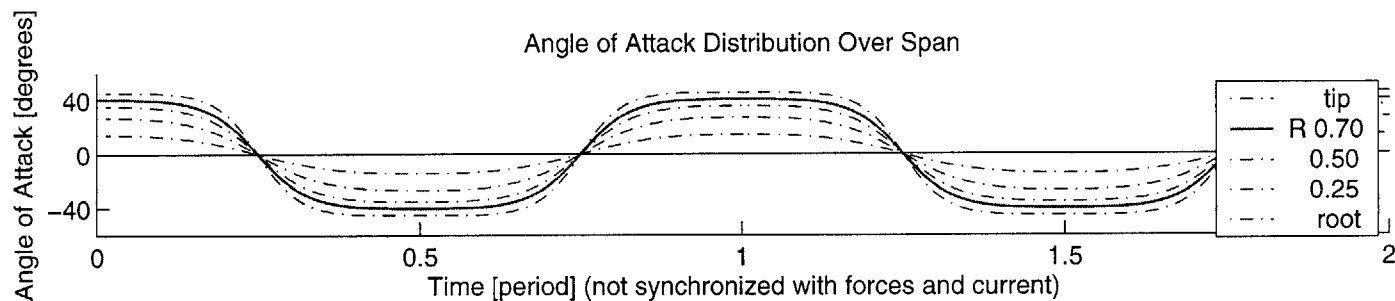
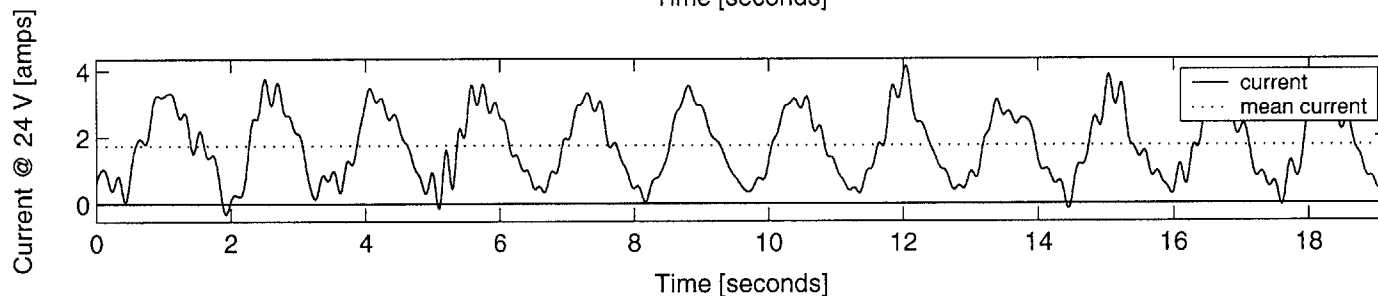
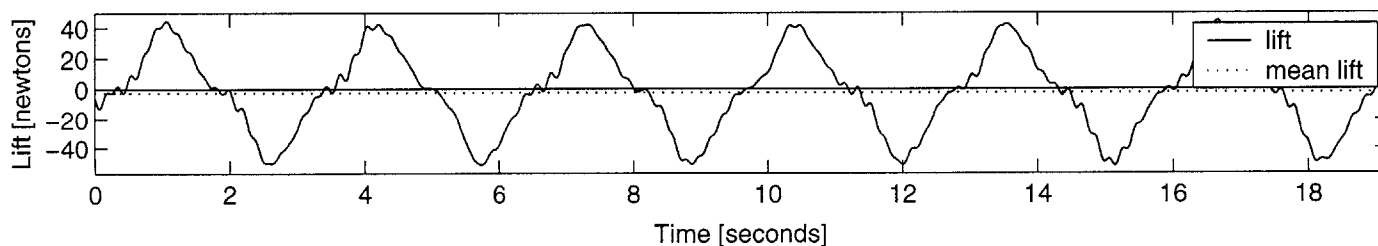
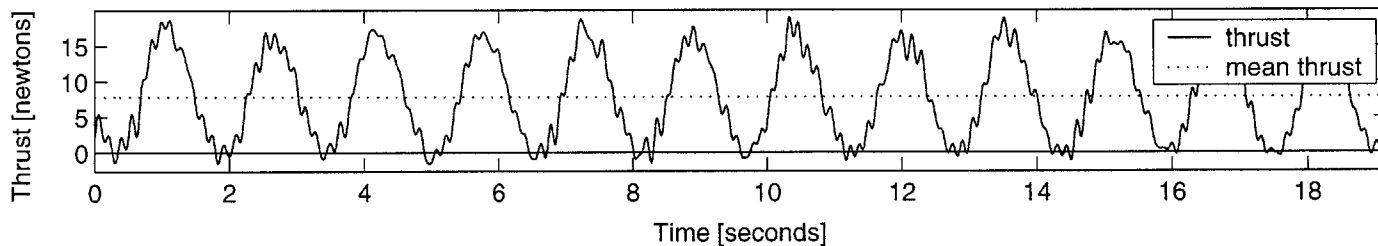




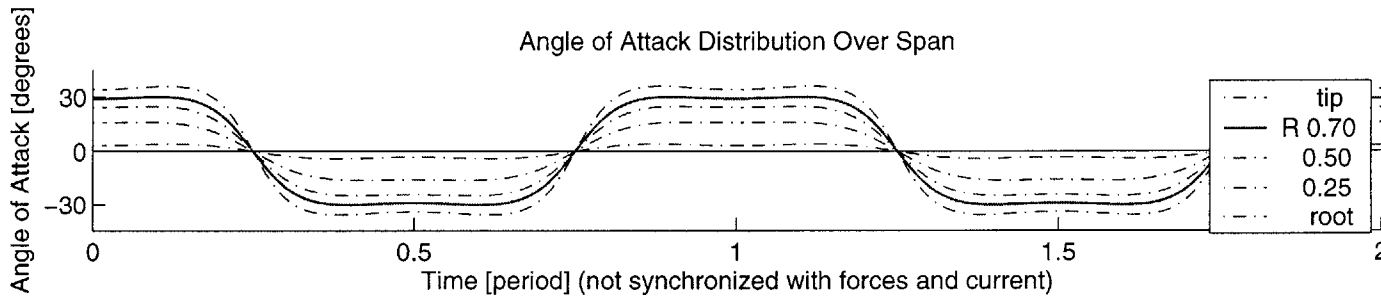
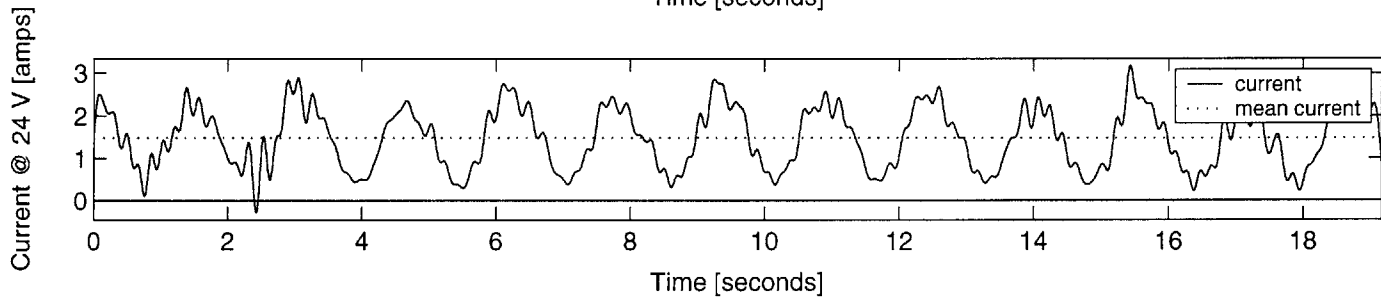
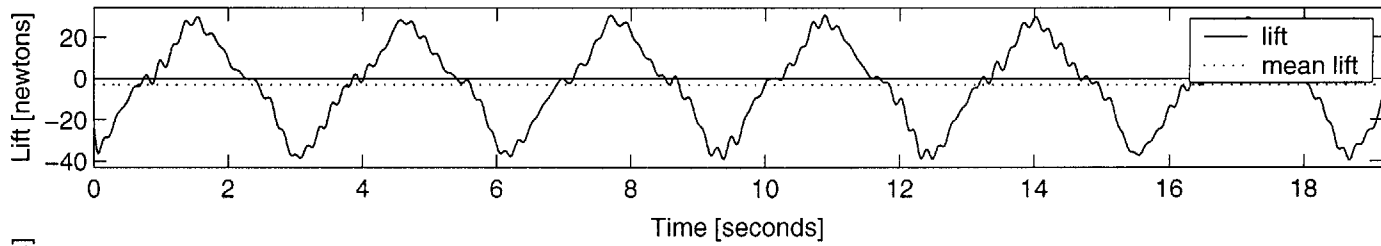
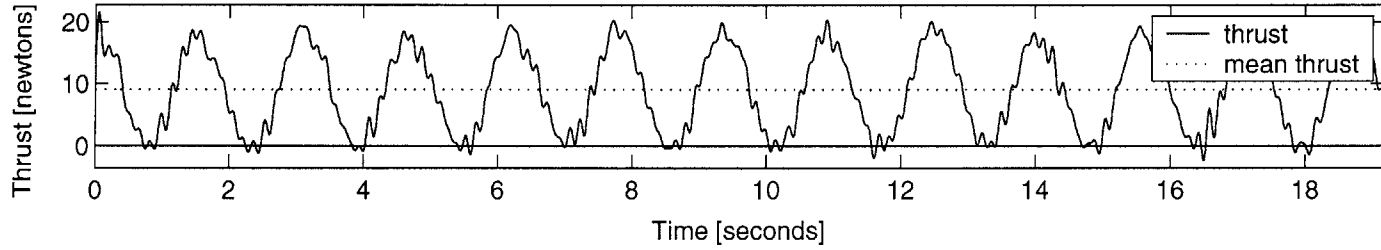
INPUT: U 0.5 [m/s], span 0.40 [m], chord 0.10 [m], roll 60 [deg], St 0.60, MaxAoa 50 [deg], run1 OUTPUT: Ct 1.1, efficiency 0.06



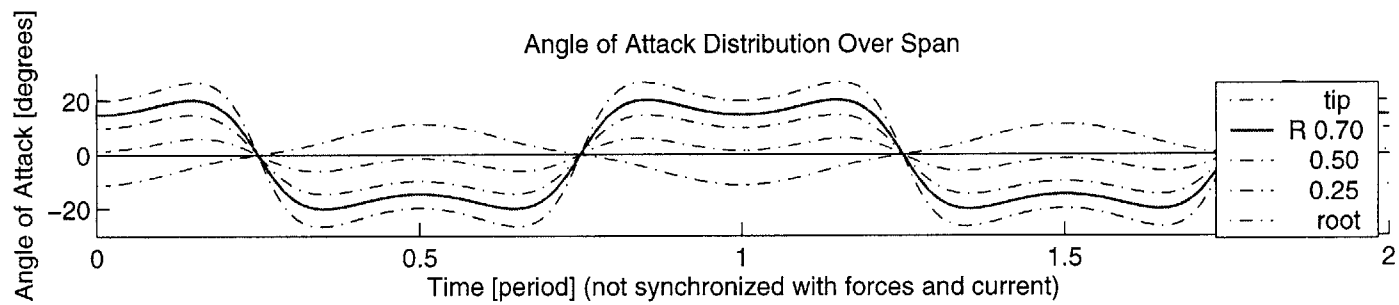
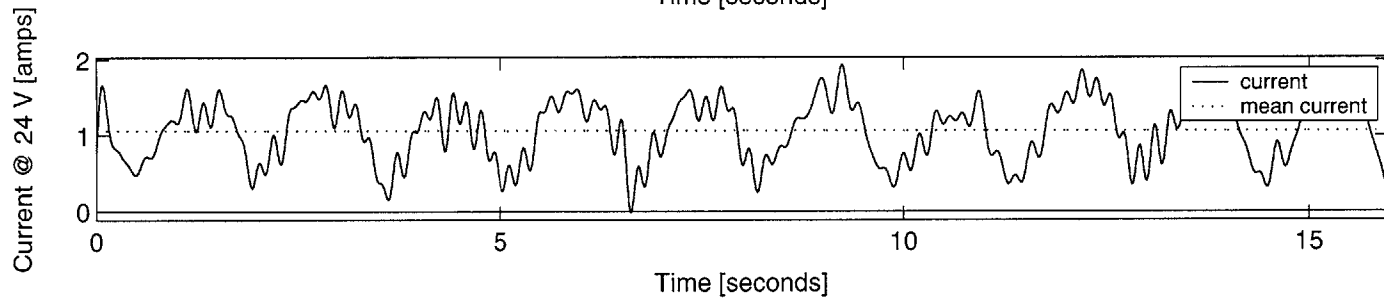
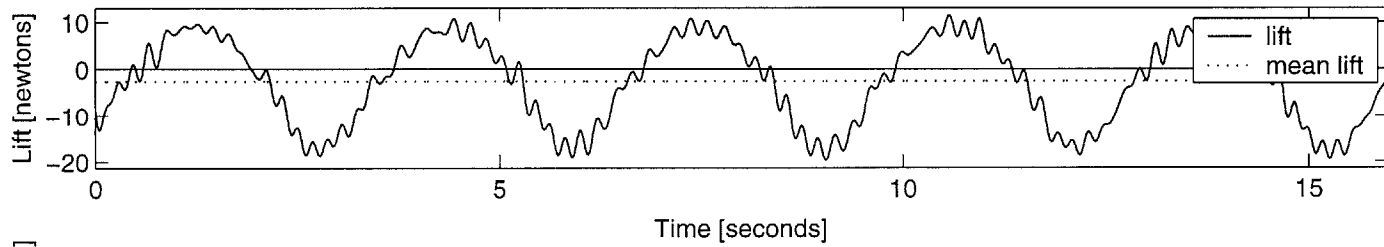
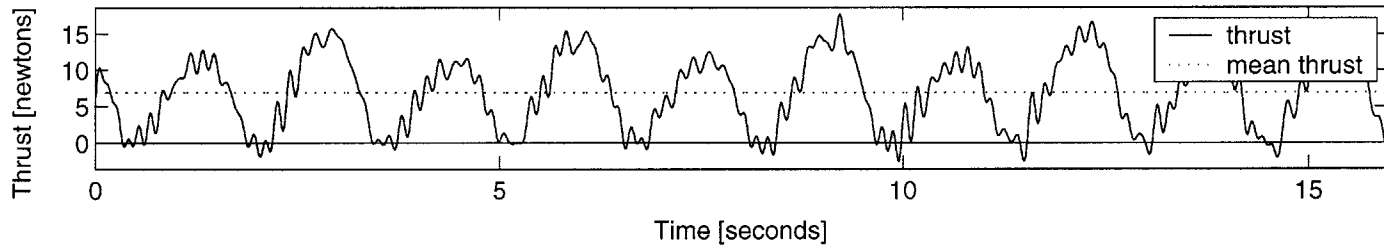
INPUT: U 0.5 [m/s], span 0.40 [m], chord 0.10 [m], roll 60 [deg], St 0.60, MaxAoa 40 [deg], run1 OUTPUT: Ct 1.6, efficiency 0.09



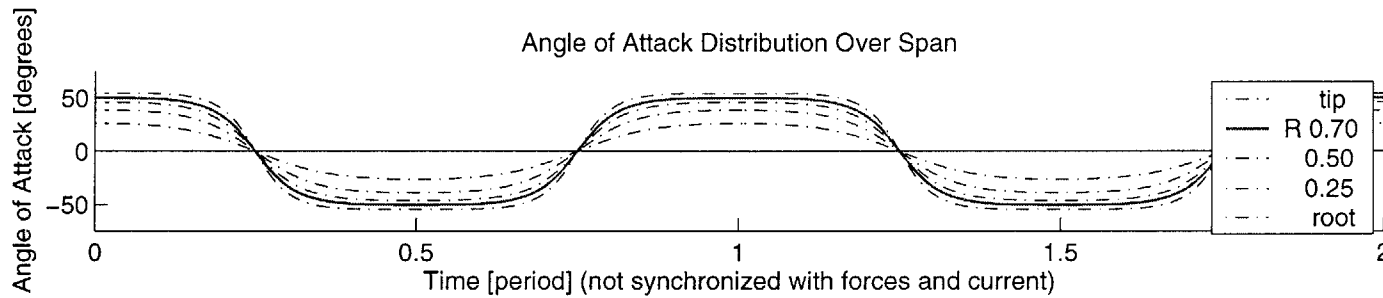
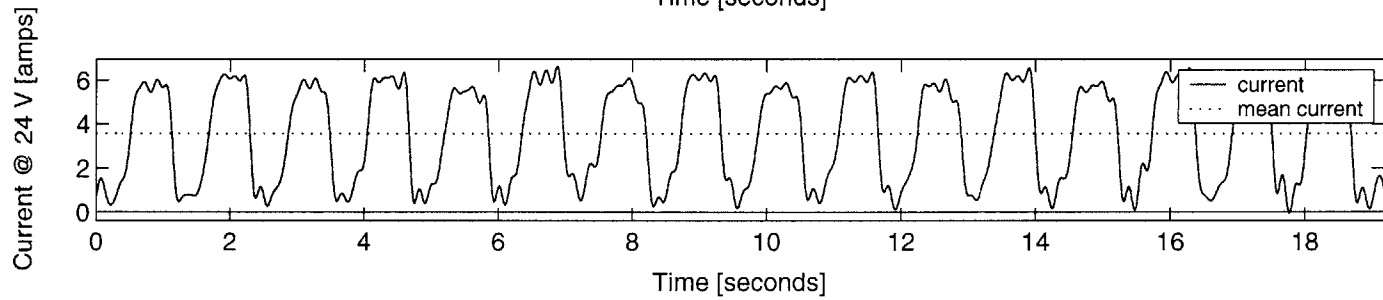
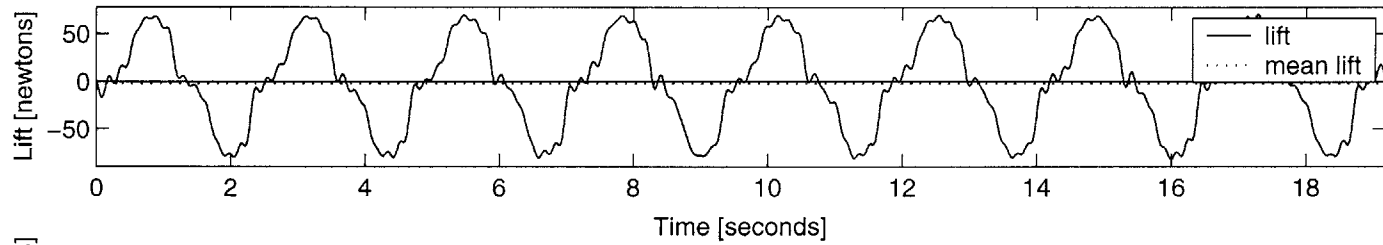
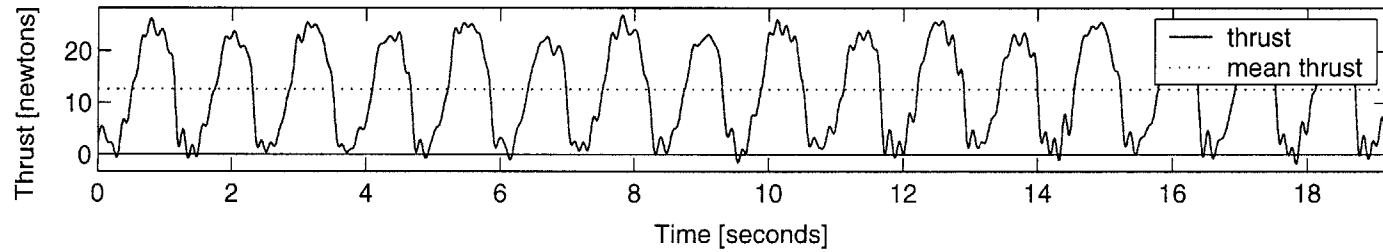
INPUT: U 0.5 [m/s], span 0.40 [m], chord 0.10 [m], roll 60 [deg], St 0.60, MaxAoa 30 [deg], run1 OUTPUT: Ct 1.8, efficiency 0.13



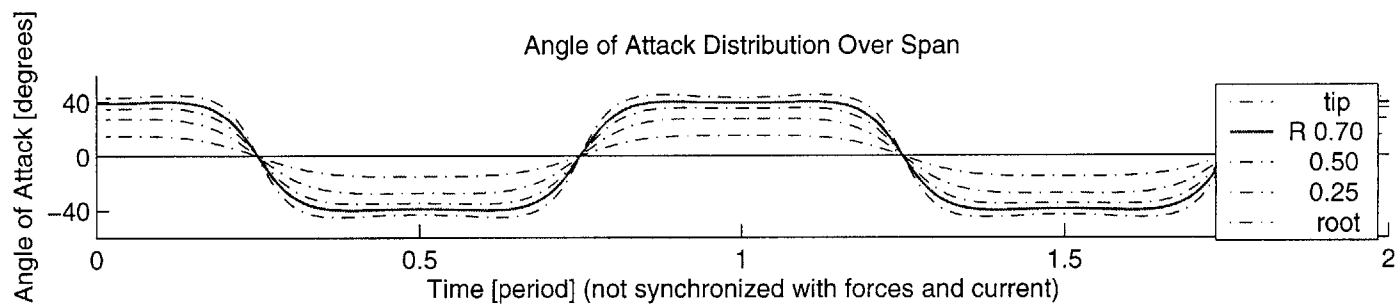
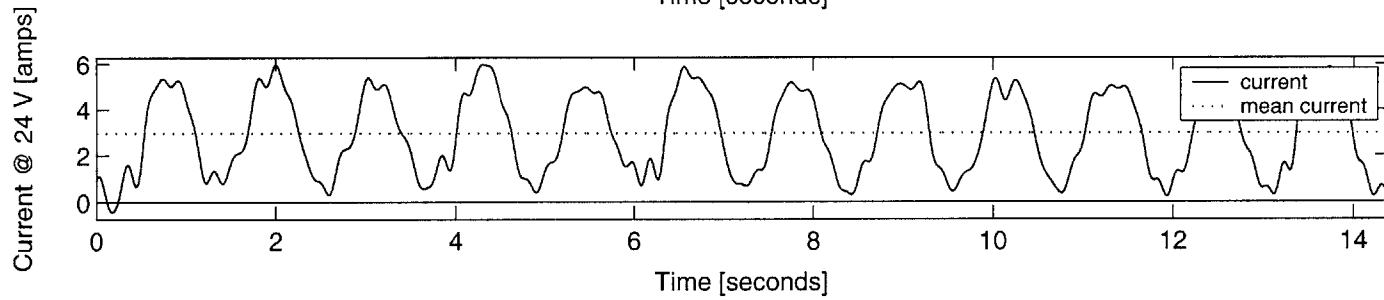
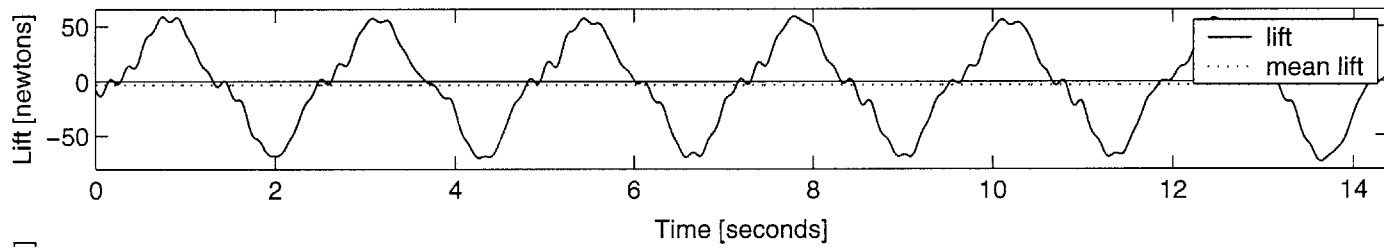
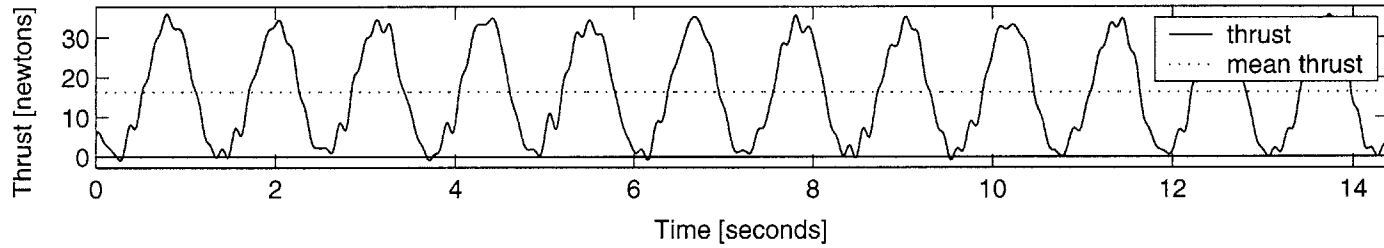
INPUT: U 0.5 [m/s], span 0.40 [m], chord 0.10 [m], roll 60 [deg], St 0.60, MaxAoa 20 [deg], run1 OUTPUT: Ct 1.4, efficiency 0.14



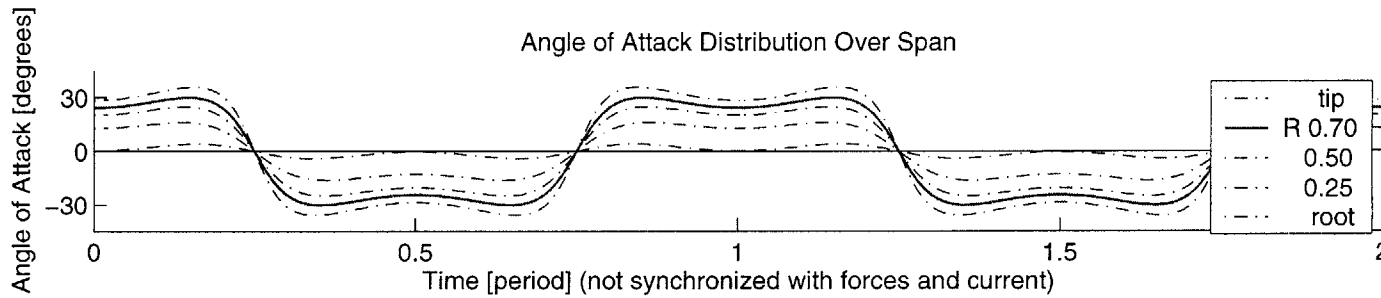
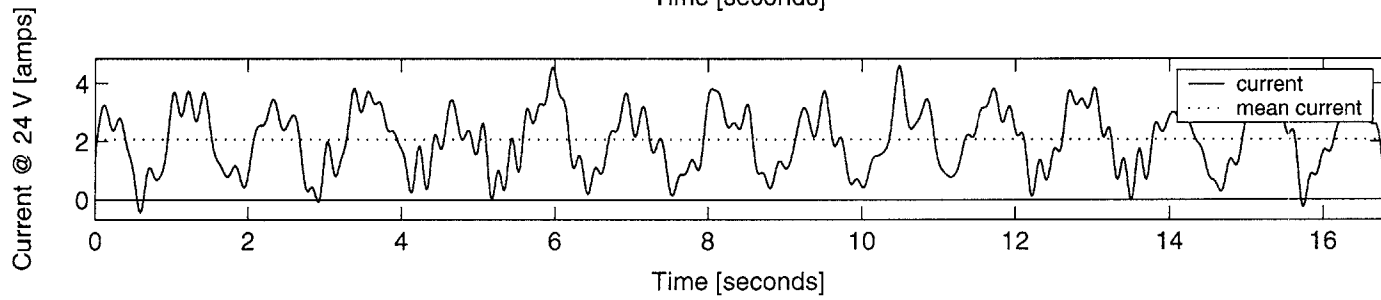
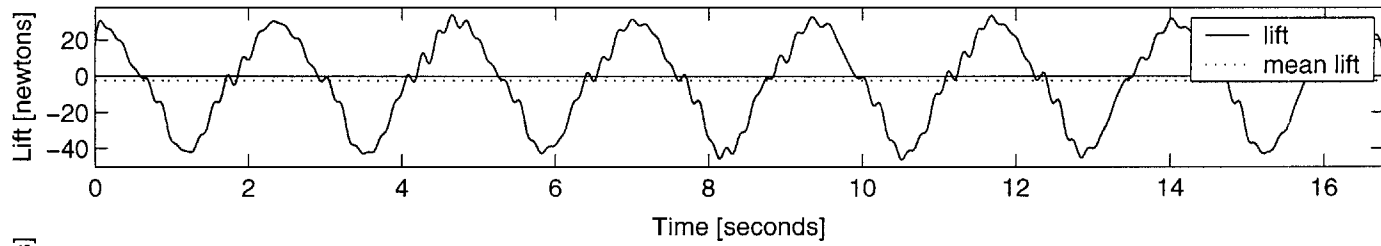
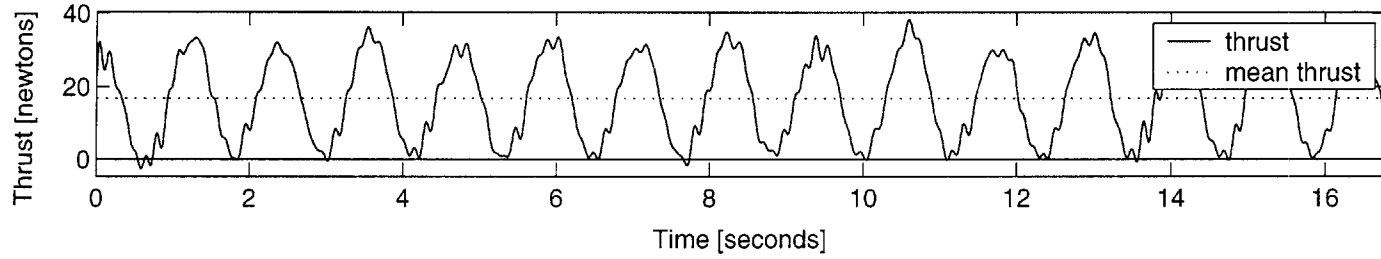
INPUT: U 0.5 [m/s], span 0.40 [m], chord 0.10 [m], roll 60 [deg], St 0.80, MaxAoa 50 [deg], run1 OUTPUT: Ct 2.5, efficiency 0.07



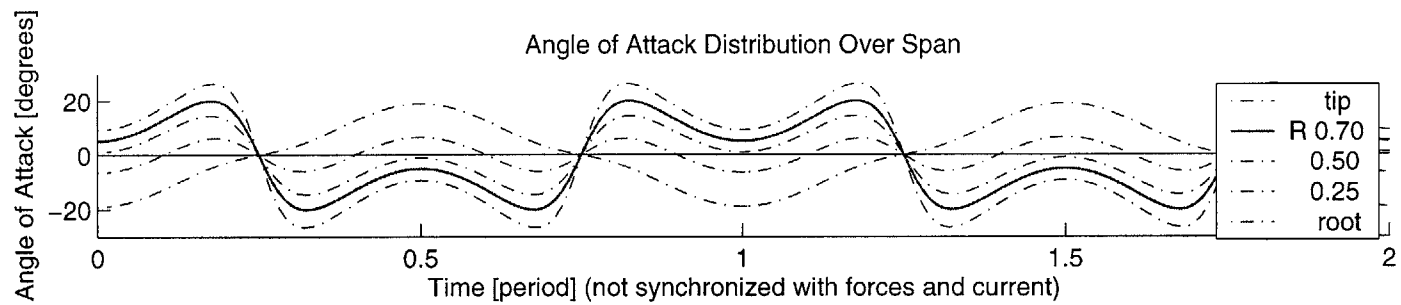
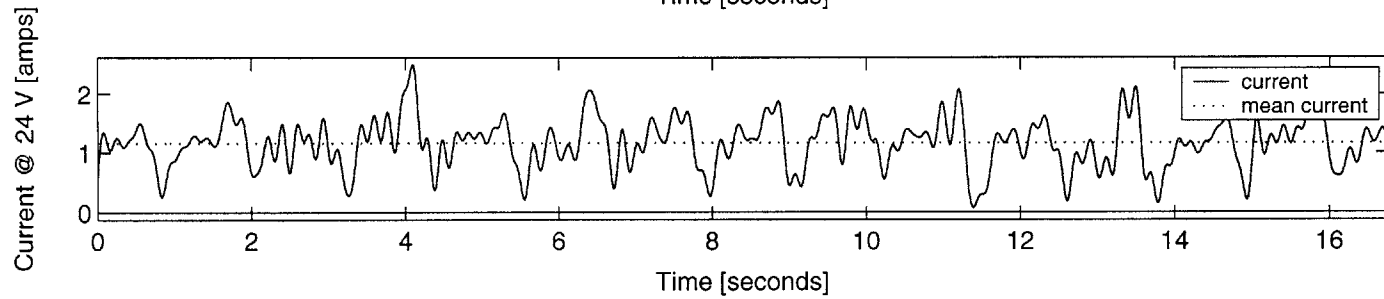
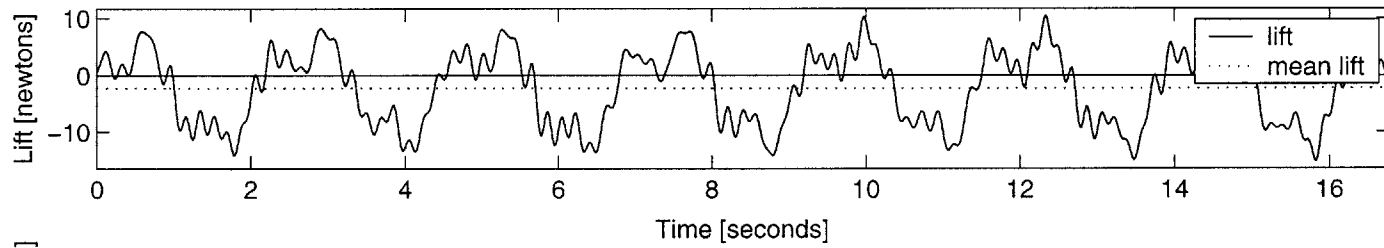
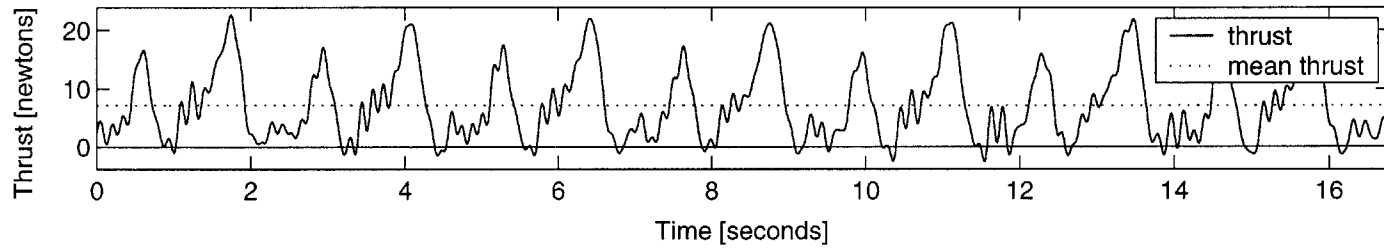
INPUT: U 0.5 [m/s], span 0.40 [m], chord 0.10 [m], roll 60 [deg], St 0.80, MaxAoa 40 [deg], run1 OUTPUT: Ct 3.3, efficiency 0.11



INPUT: U 0.5 [m/s], span 0.40 [m], chord 0.10 [m], roll 60 [deg], St 0.80, MaxAoa 30 [deg], run1 OUTPUT: Ct 3.4, efficiency 0.17

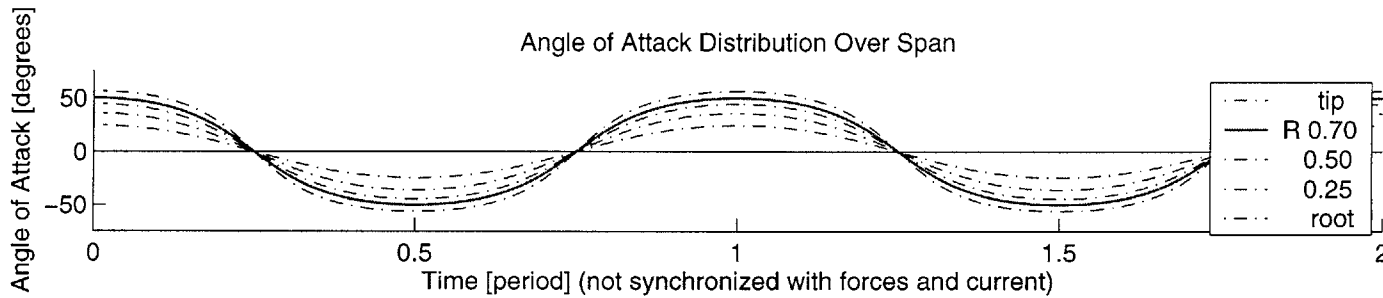
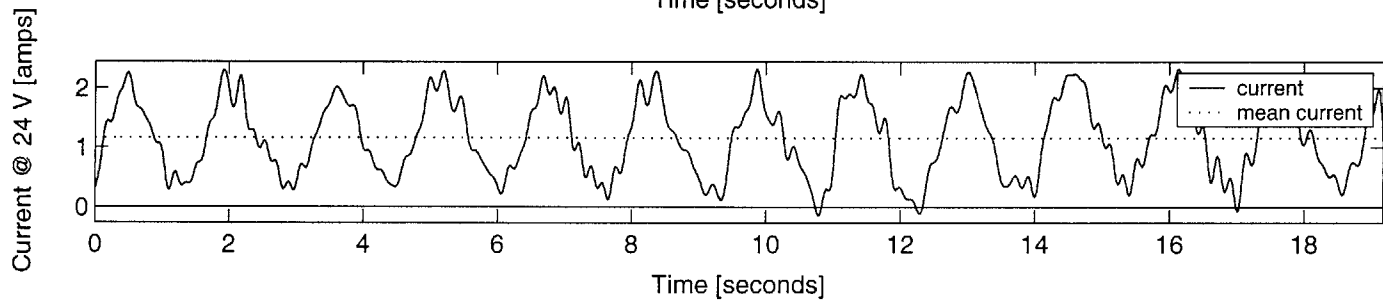
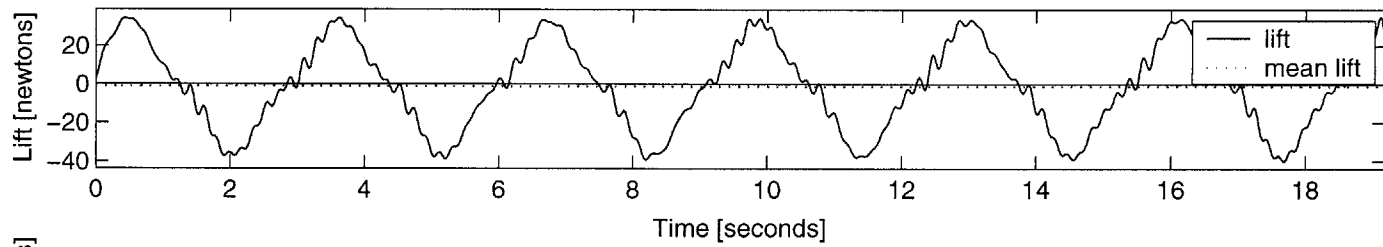
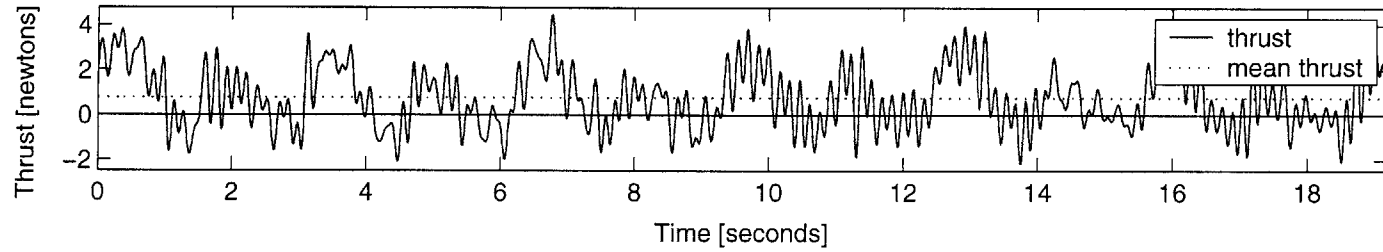


INPUT: U 0.5 [m/s], span 0.40 [m], chord 0.10 [m], roll 60 [deg], St 0.80, MaxAoa 20 [deg], run1 OUTPUT: Ct 1.4, efficiency 0.13

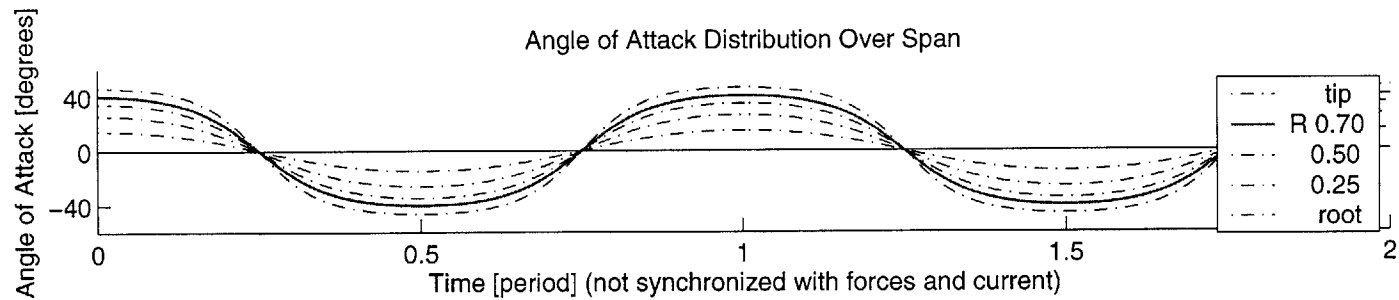
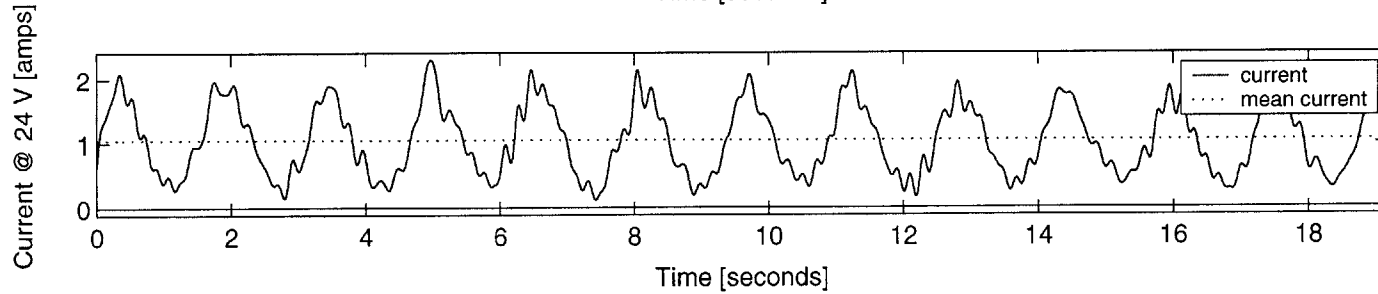
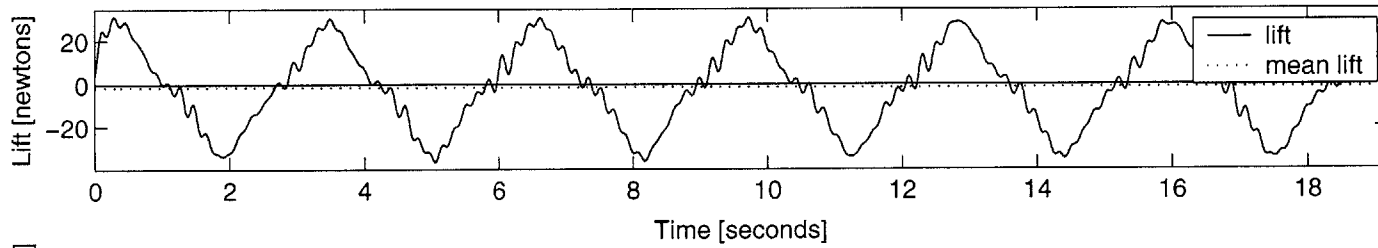
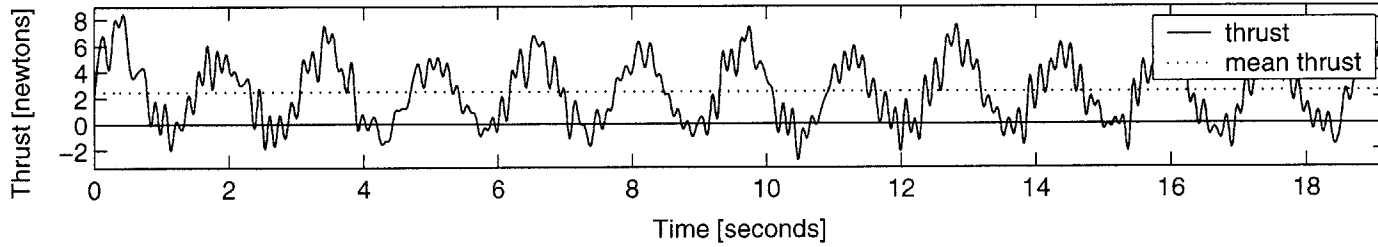




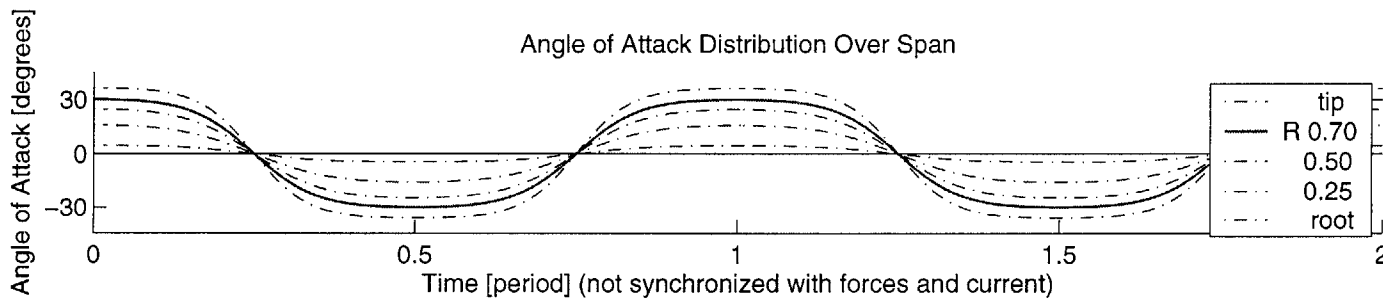
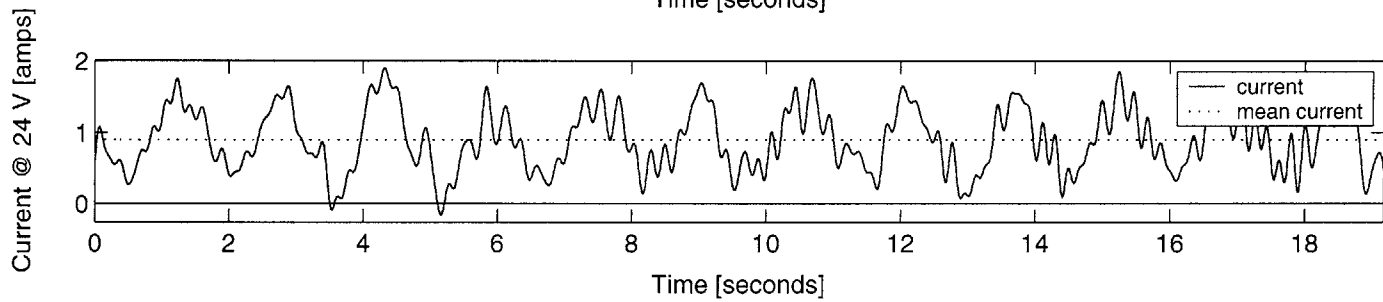
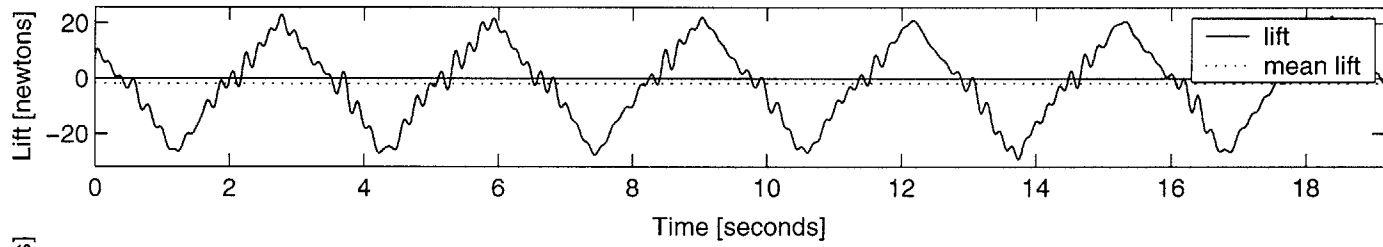
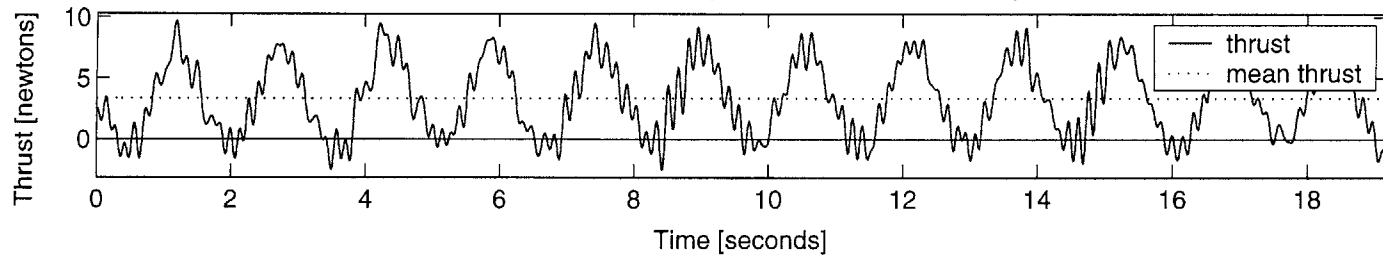
INPUT: U 0.5 [m/s], span 0.40 [m], chord 0.10 [m], roll 40 [deg], St 0.40, MaxAoa 50 [deg], run1 OUTPUT: Ct 0.2, efficiency 0.01



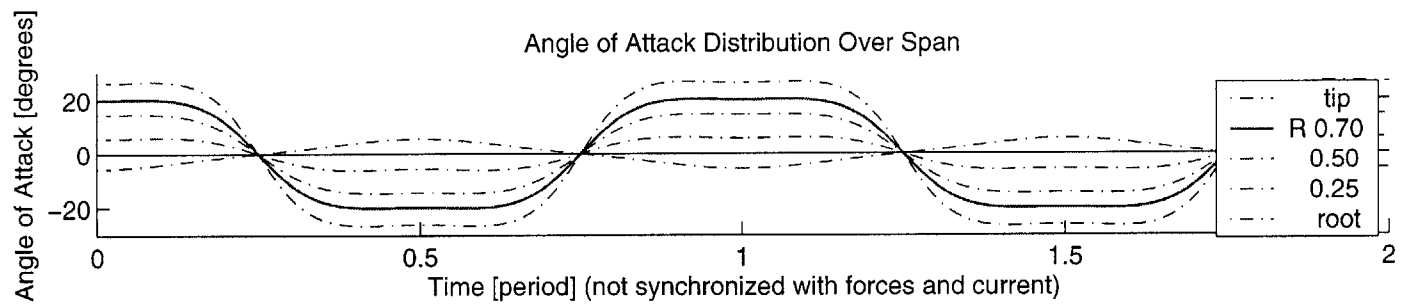
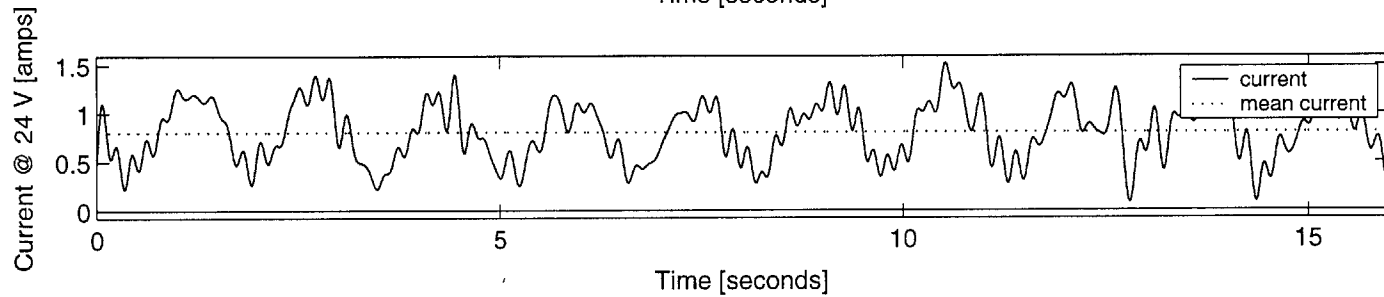
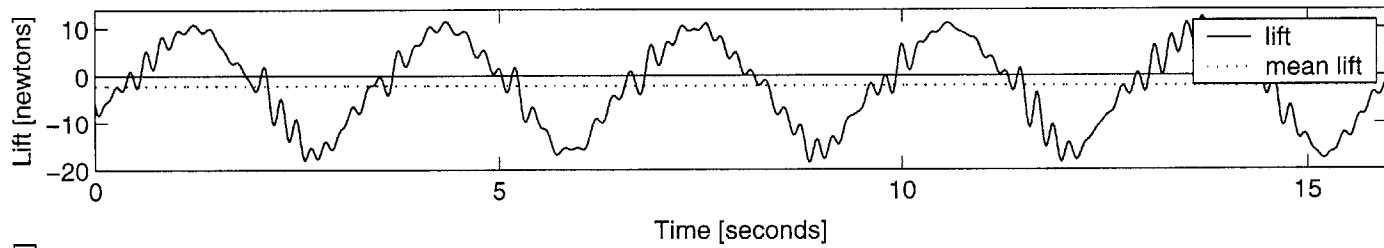
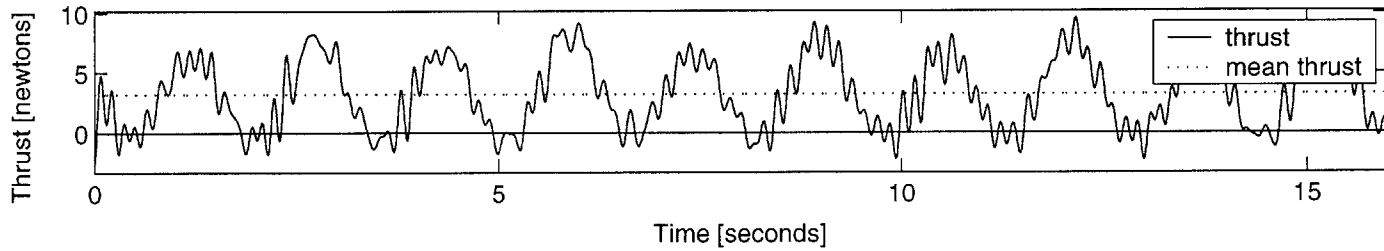
INPUT: U 0.5 [m/s], span 0.40 [m], chord 0.10 [m], roll 40 [deg], St 0.40, MaxAoa 40 [deg], run1 OUTPUT: Ct 0.5, efficiency 0.05



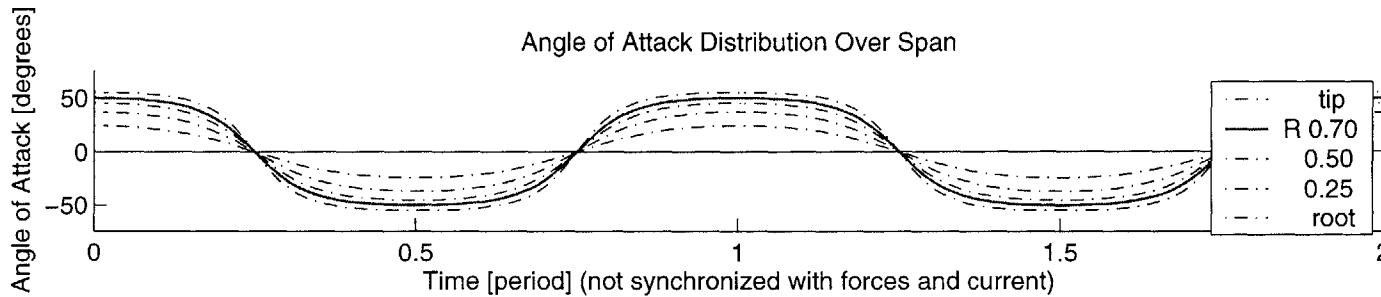
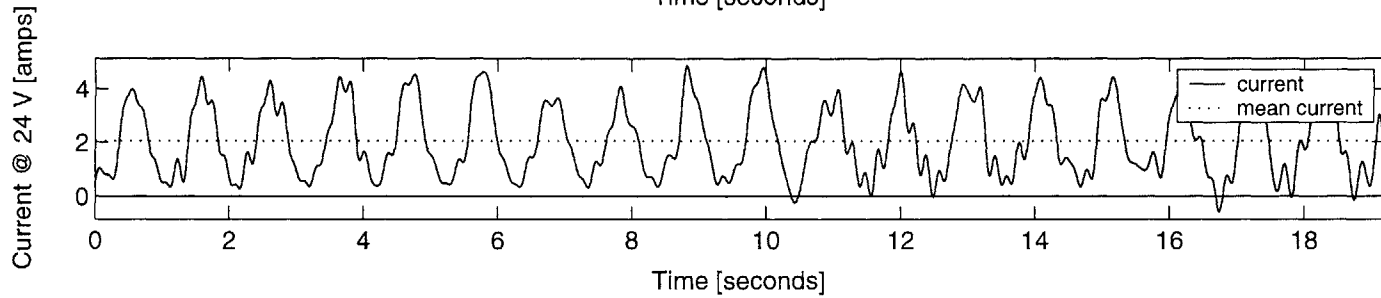
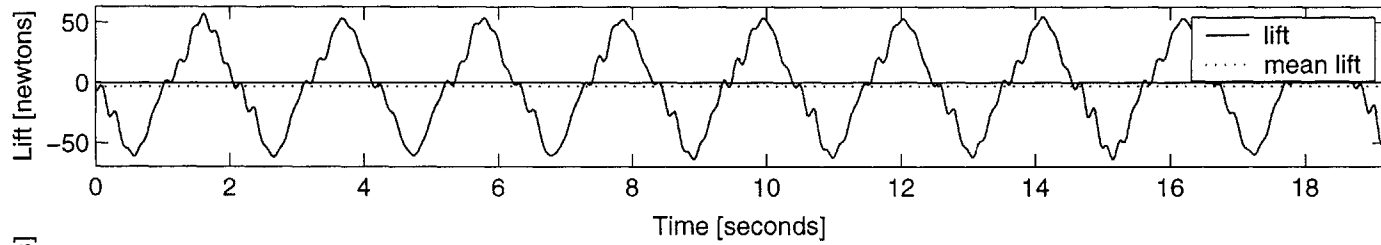
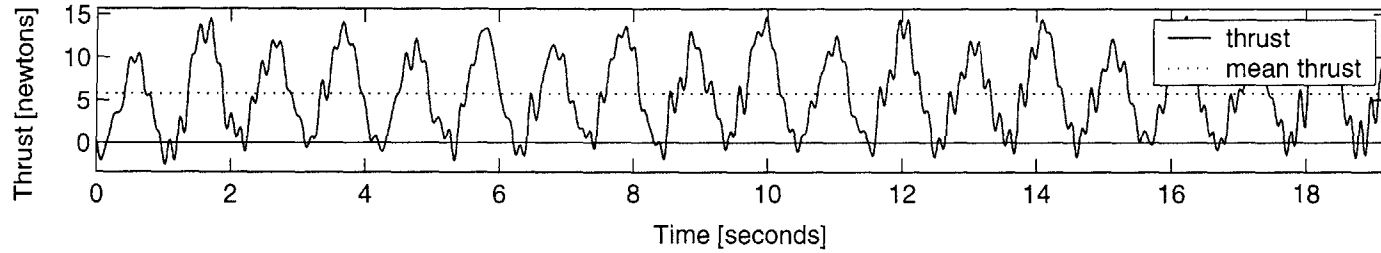
INPUT: U 0.5 [m/s], span 0.40 [m], chord 0.10 [m], roll 40 [deg], St 0.40, MaxAoa 30 [deg], run1 OUTPUT: Ct 0.7, efficiency 0.08



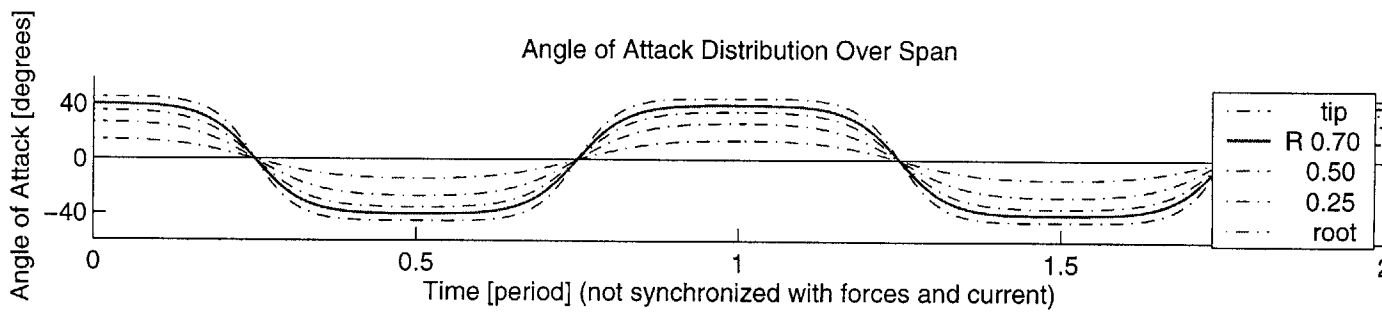
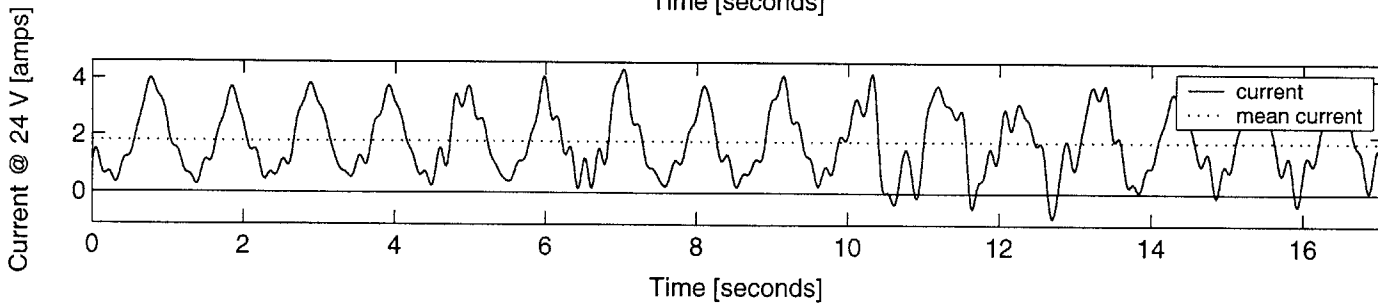
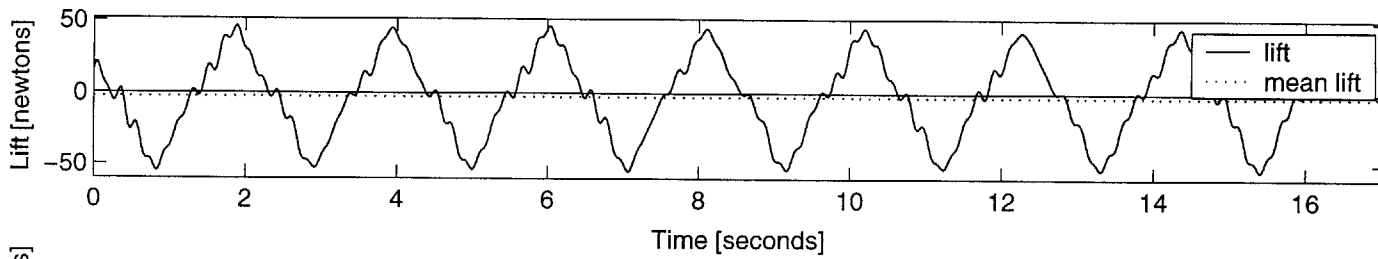
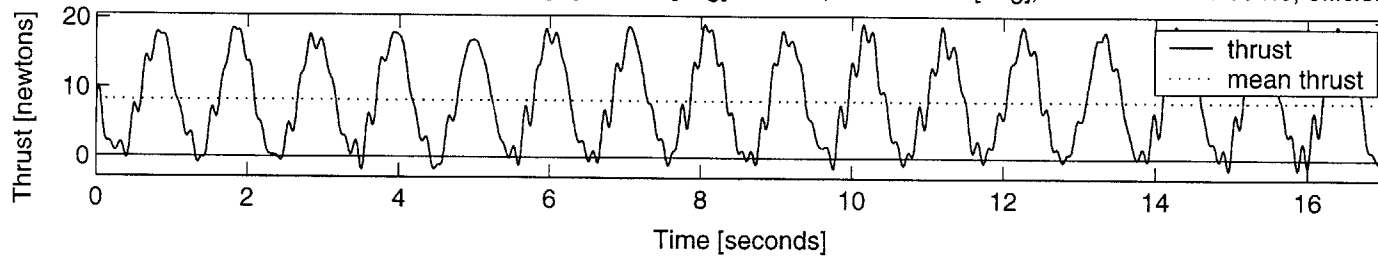
INPUT: U 0.5 [m/s], span 0.40 [m], chord 0.10 [m], roll 40 [deg], St 0.40, MaxAoa 20 [deg], run1 OUTPUT: Ct 0.6, efficiency 0.08



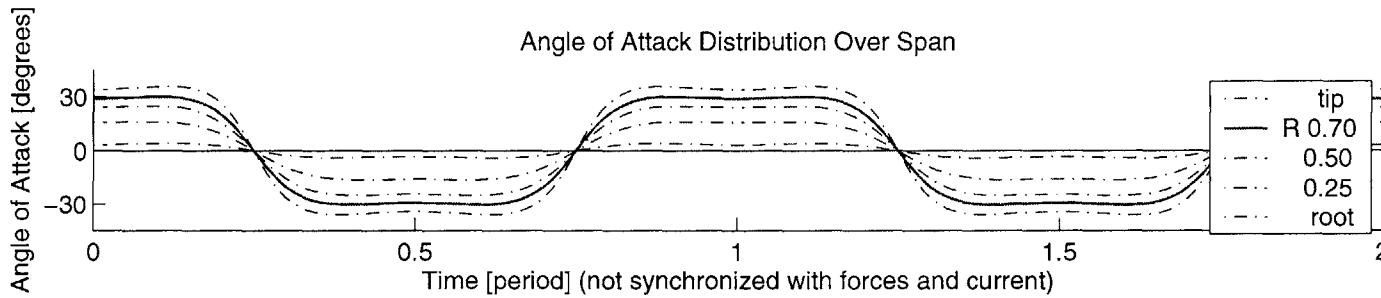
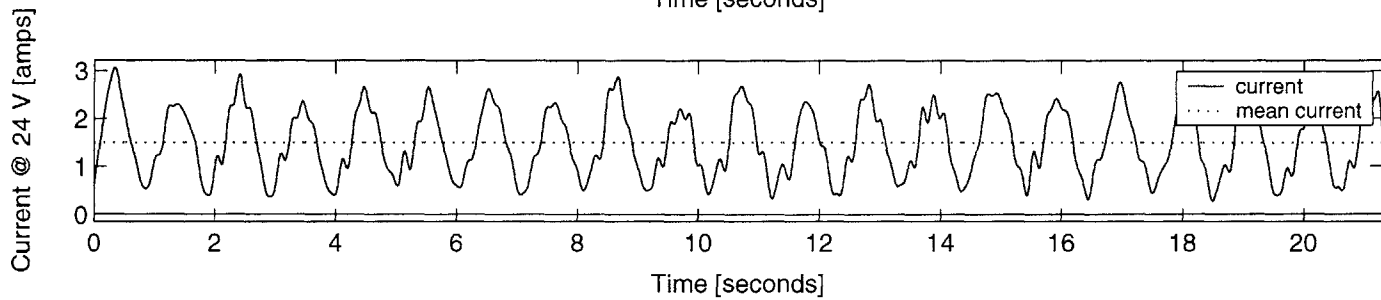
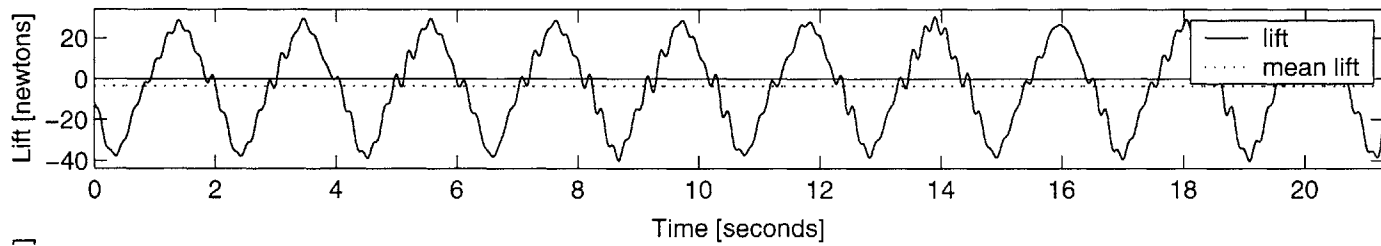
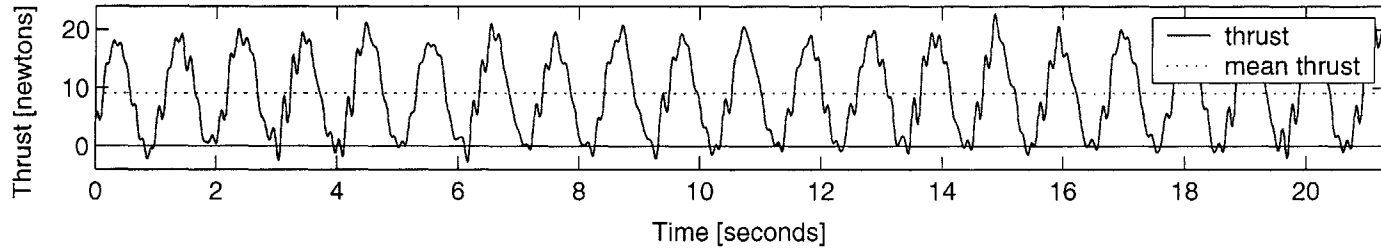
INPUT: U 0.5 [m/s], span 0.40 [m], chord 0.10 [m], roll 40 [deg], St 0.60, MaxAoa 50 [deg], run1 OUTPUT: Ct 1.2, efficiency 0.06



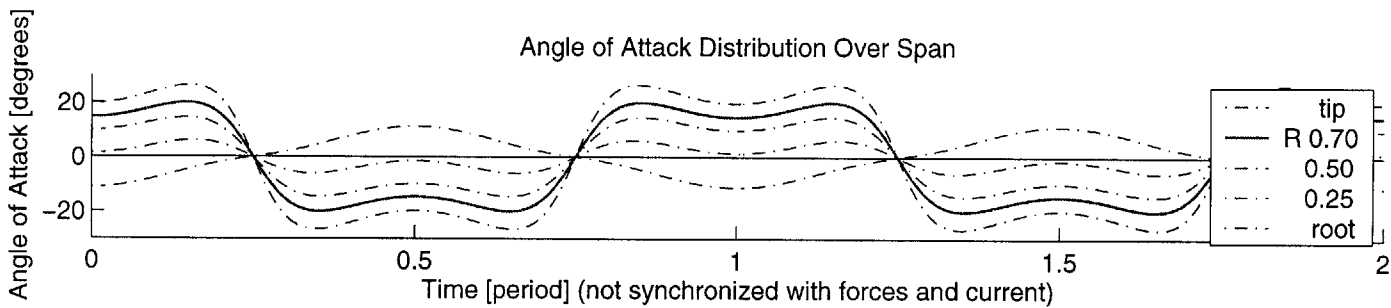
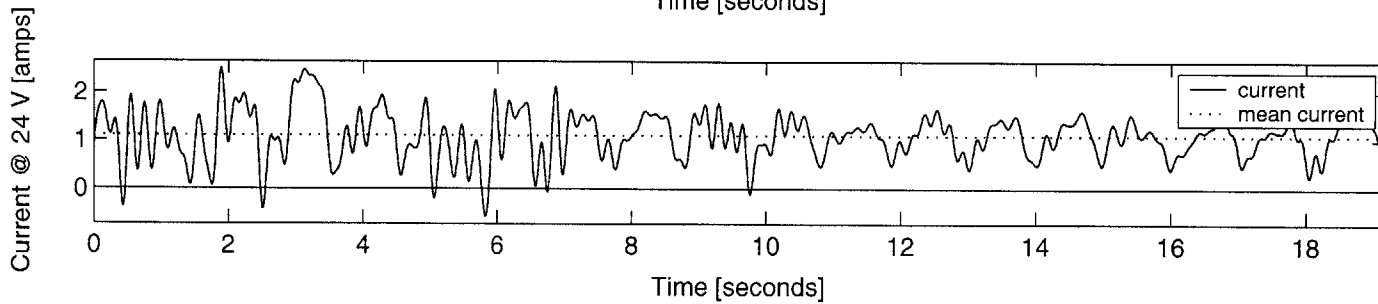
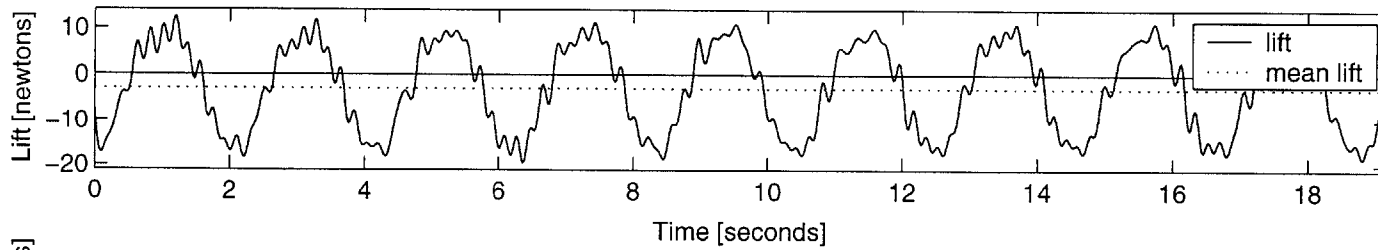
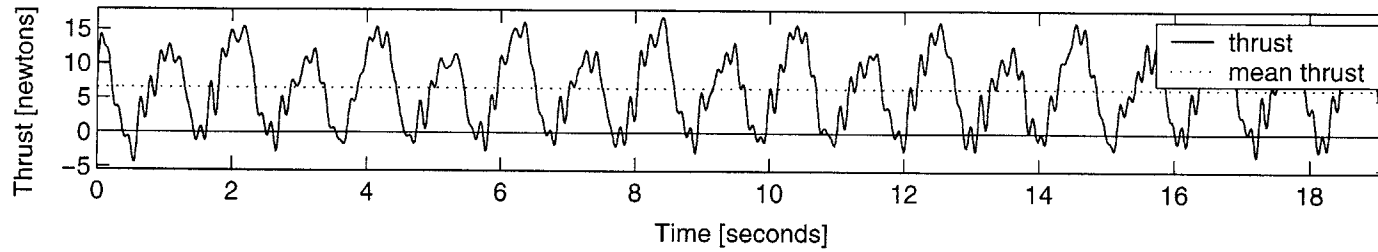
INPUT: U 0.5 [m/s], span 0.40 [m], chord 0.10 [m], roll 40 [deg], St 0.60, MaxAoa 40 [deg], run1 OUTPUT: Ct 1.6, efficiency 0.10



INPUT: U 0.5 [m/s], span 0.40 [m], chord 0.10 [m], roll 40 [deg], St 0.60, MaxAoa 30 [deg], run1 OUTPUT: Ct 1.8, efficiency 0.13

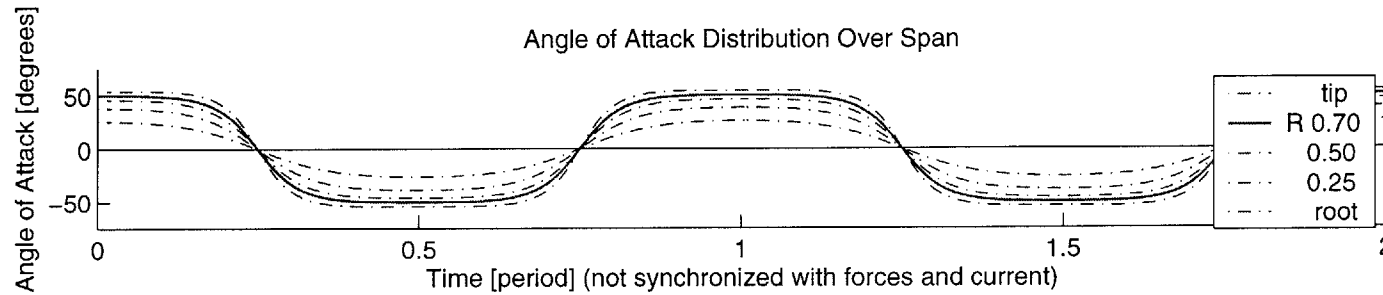
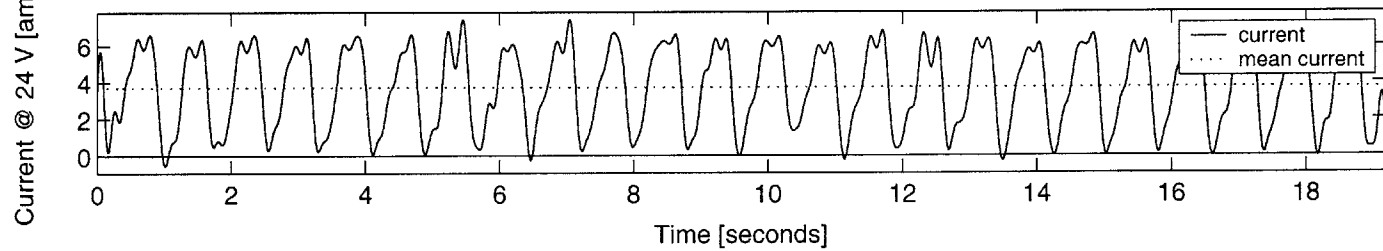
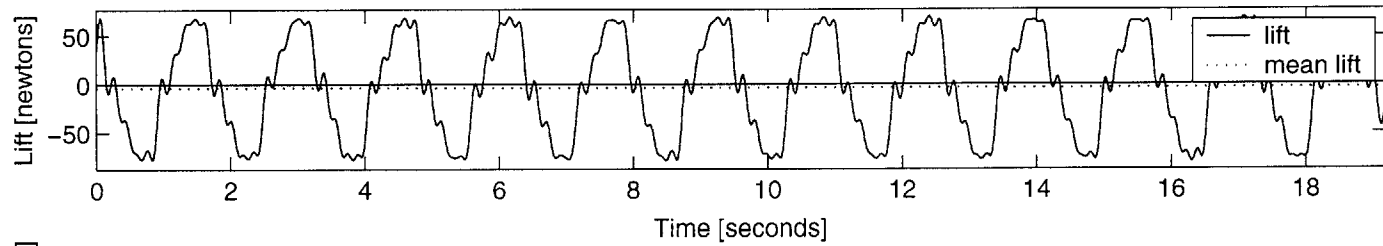
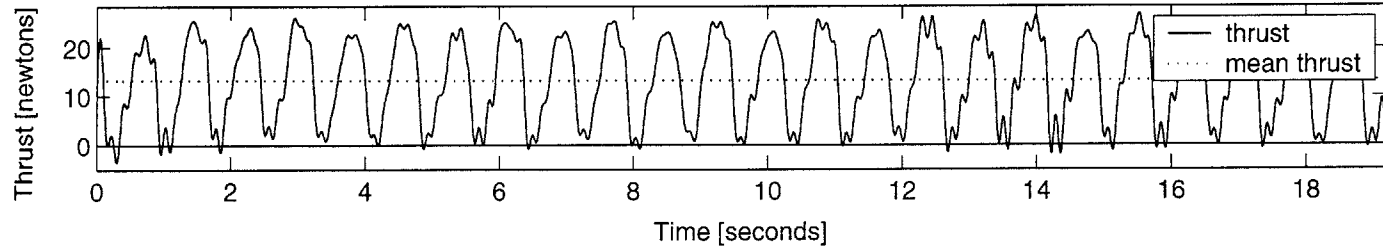


INPUT: U 0.5 [m/s], span 0.40 [m], chord 0.10 [m], roll 40 [deg], St 0.60, MaxAoa 20 [deg], run1 OUTPUT: Ct 1.3, efficiency 0.12

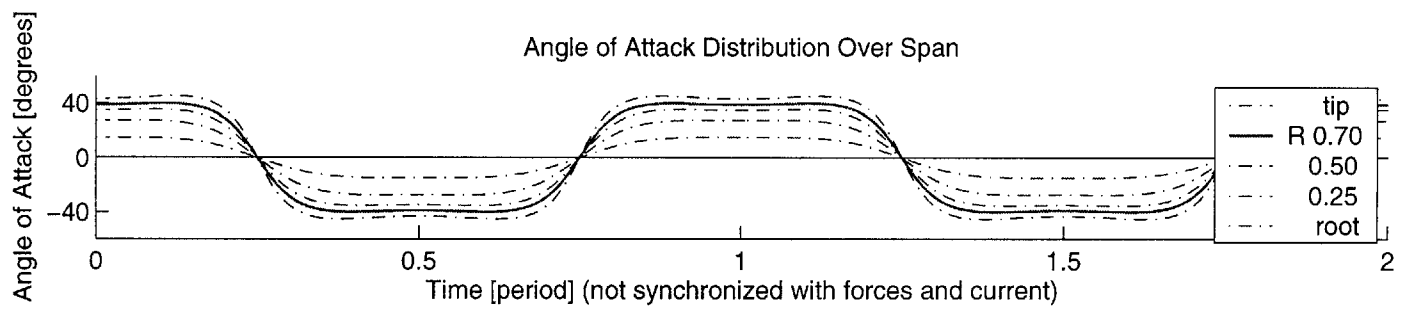
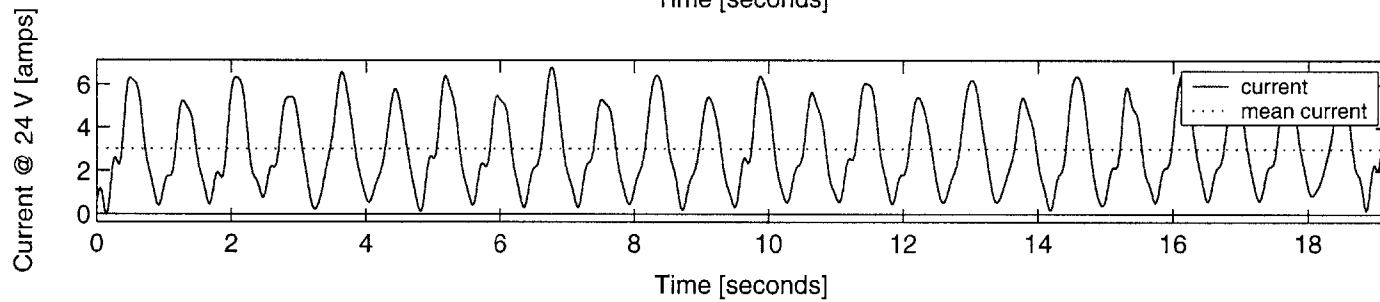
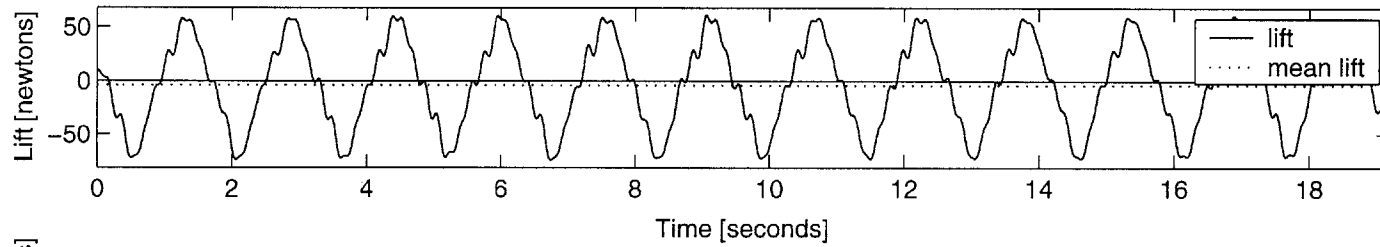
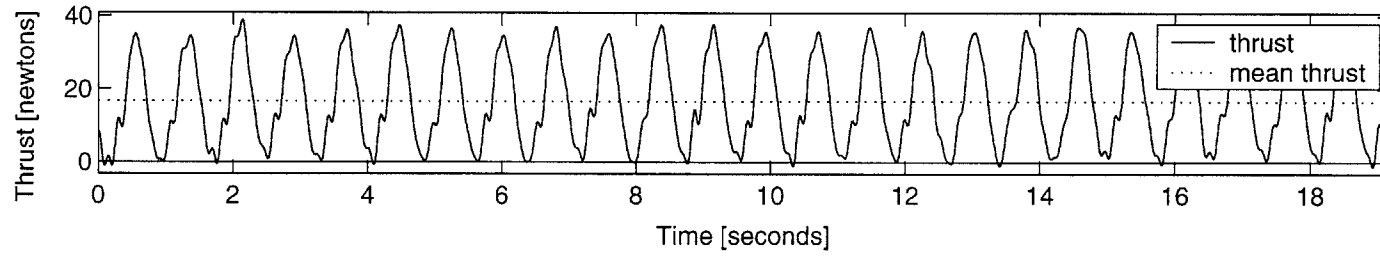




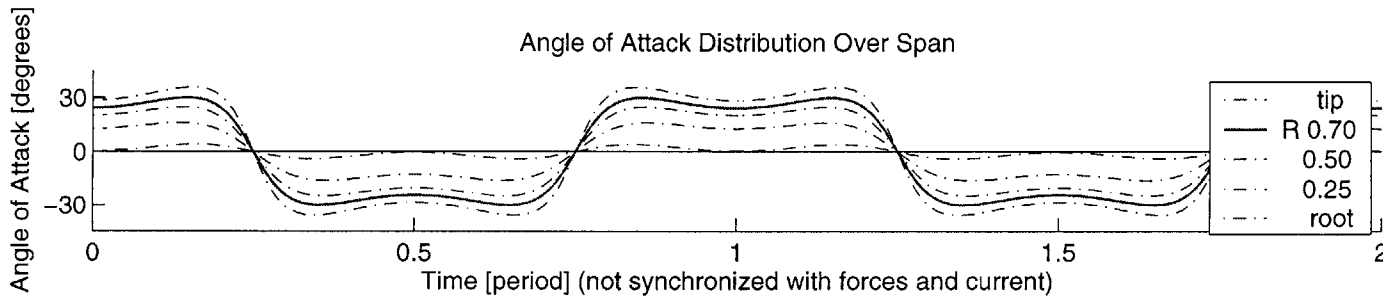
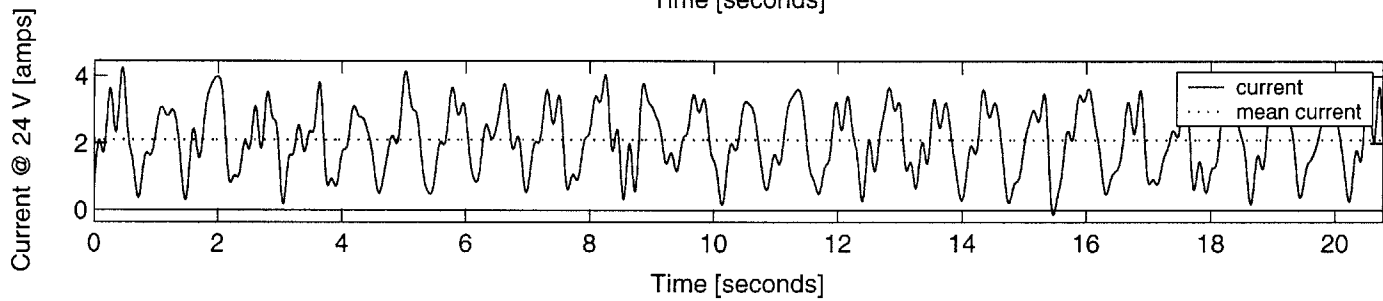
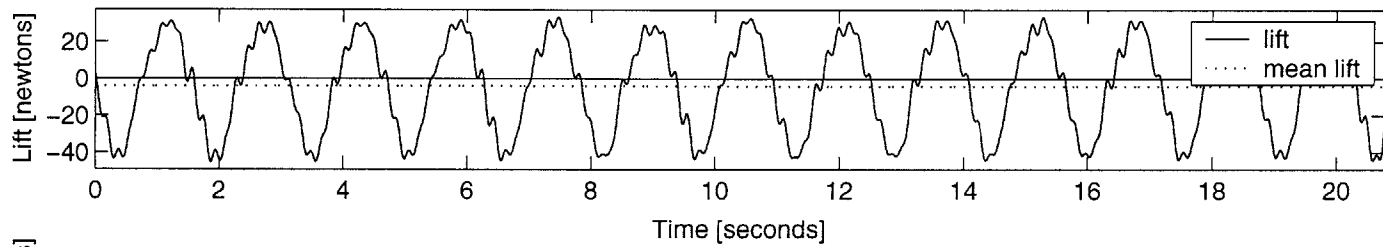
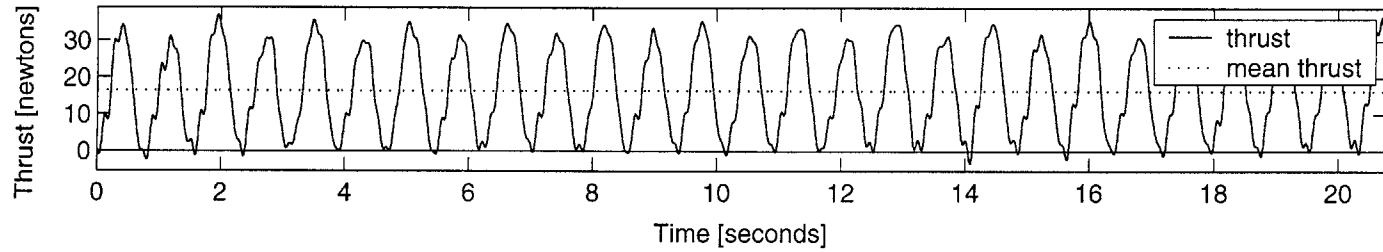
INPUT: U 0.5 [m/s], span 0.40 [m], chord 0.10 [m], roll 40 [deg], St 0.80, MaxAoa 50 [deg], run1 OUTPUT: Ct 2.6, efficiency 0.07



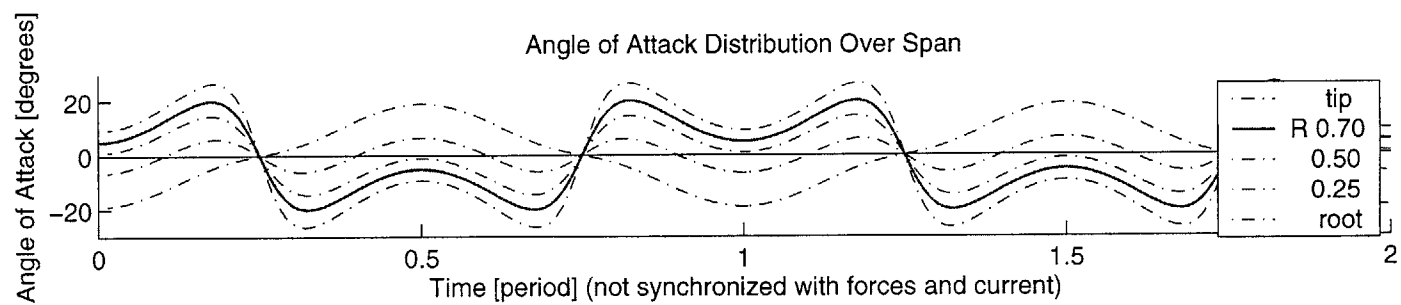
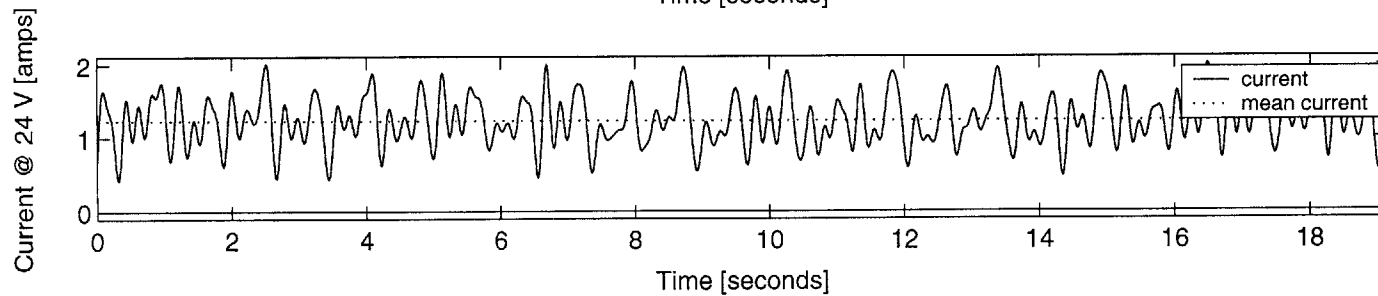
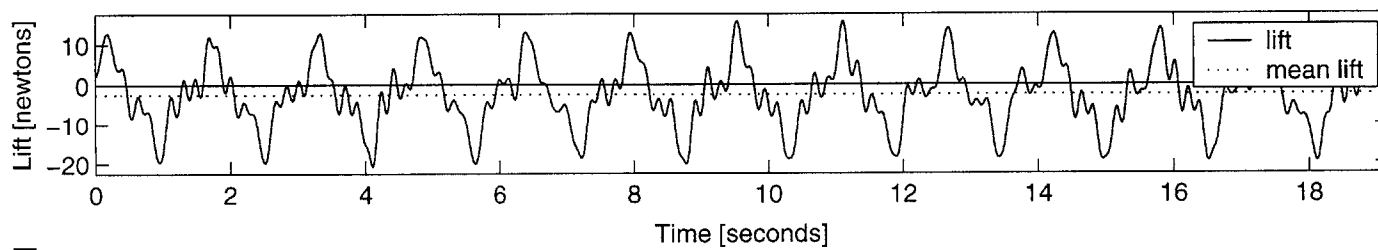
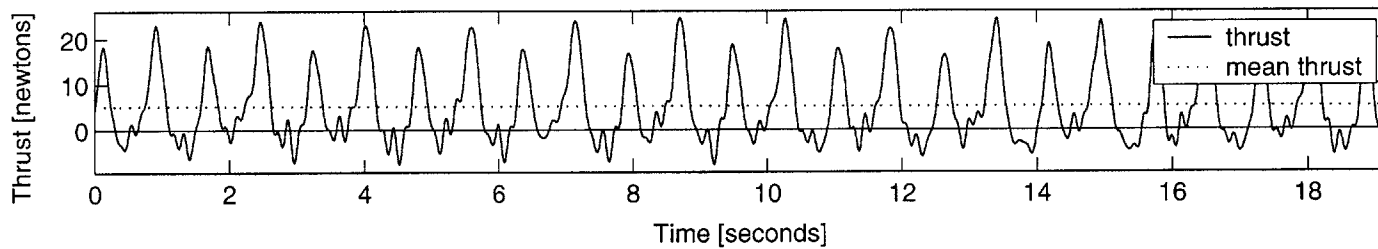
INPUT: U 0.5 [m/s], span 0.40 [m], chord 0.10 [m], roll 40 [deg], St 0.80, MaxAoa 40 [deg], run1 OUTPUT: Ct 3.3, efficiency 0.12



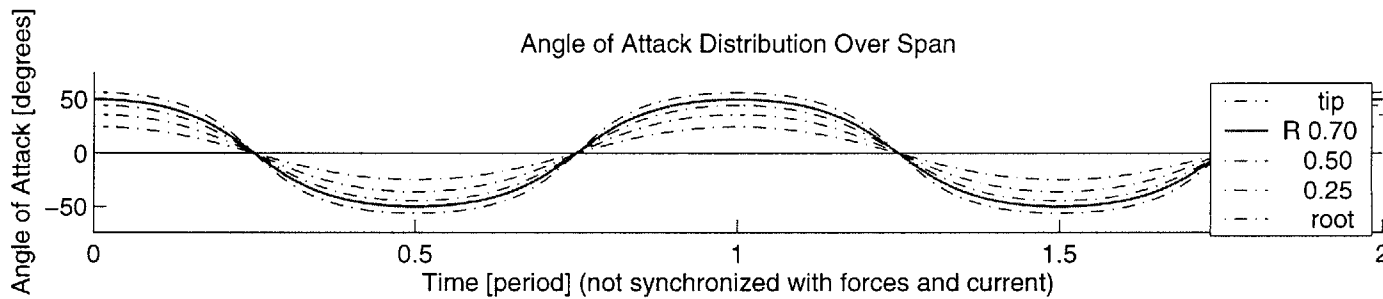
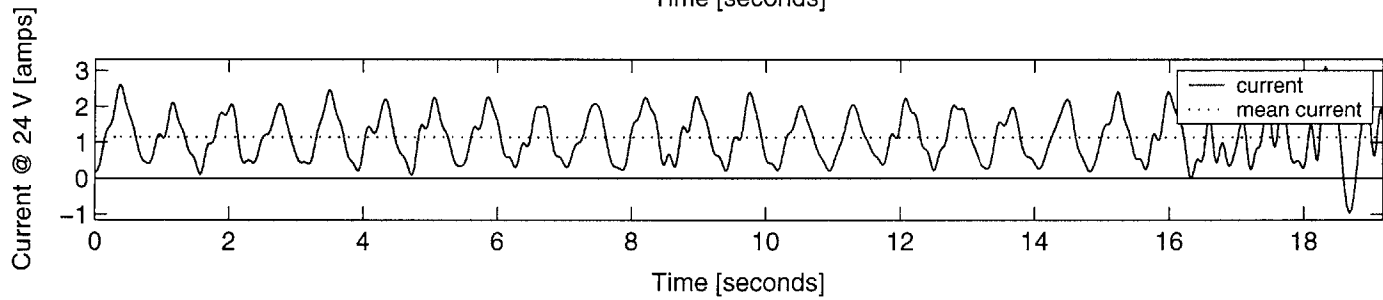
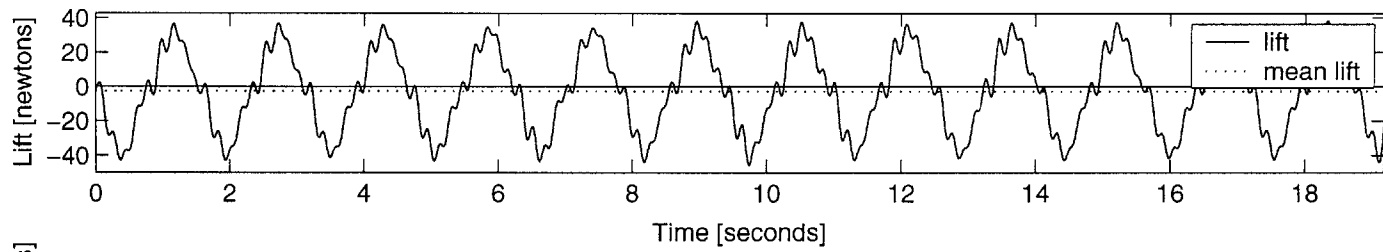
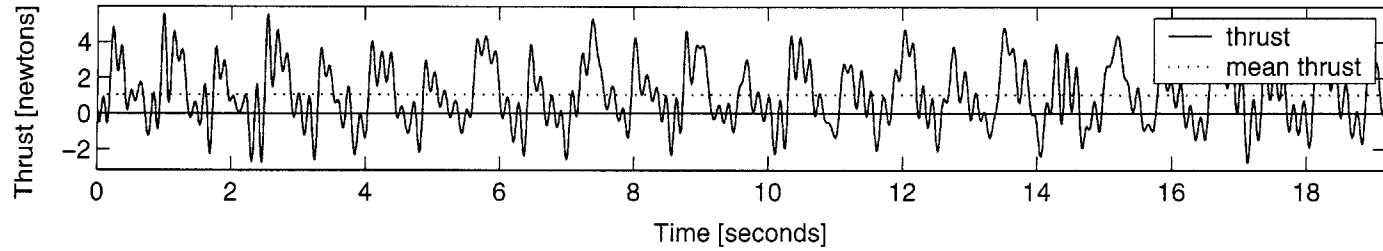
INPUT: U 0.5 [m/s], span 0.40 [m], chord 0.10 [m], roll 40 [deg], St 0.80, MaxAoa 30 [deg], run1 OUTPUT: Ct 3.3, efficiency 0.16



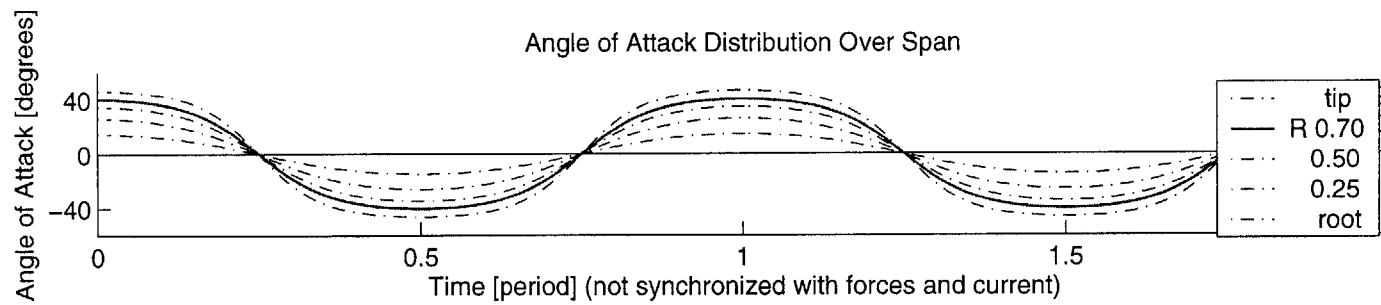
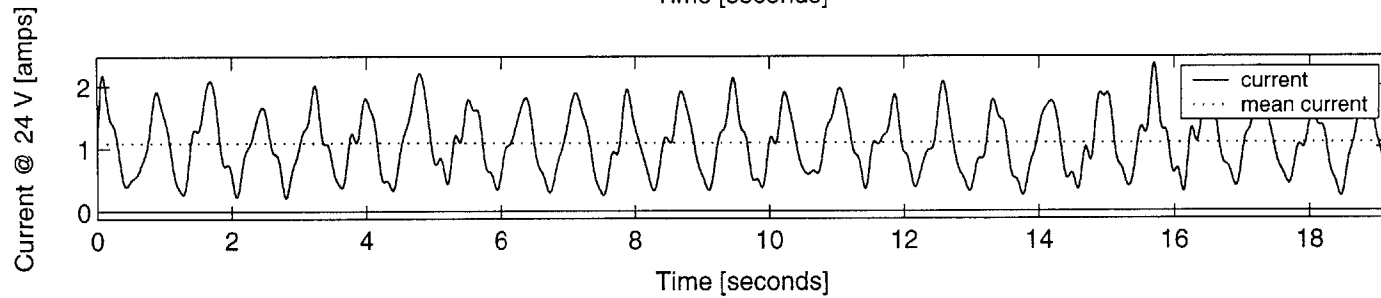
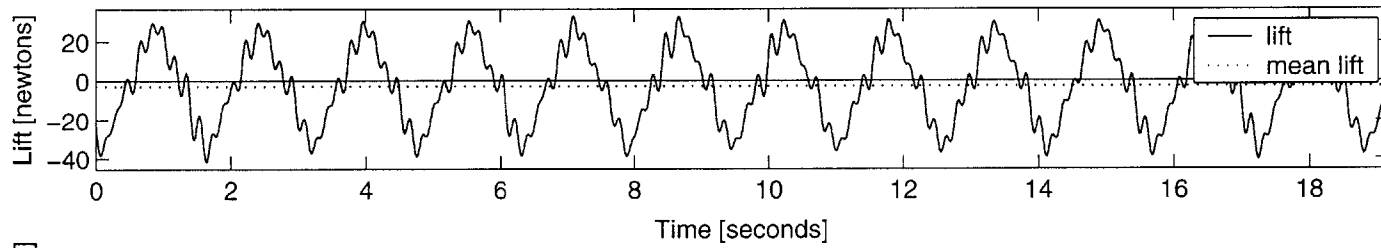
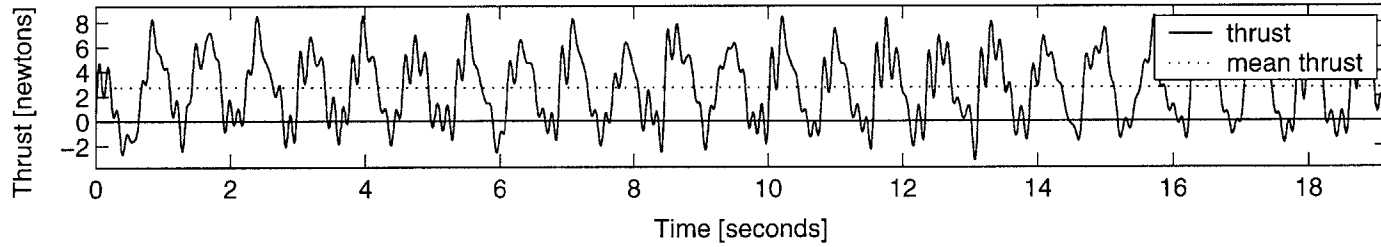
INPUT: U 0.5 [m/s], span 0.40 [m], chord 0.10 [m], roll 40 [deg], St 0.80, MaxAoa 20 [deg], run1 OUTPUT: Ct 1.0, efficiency 0.09



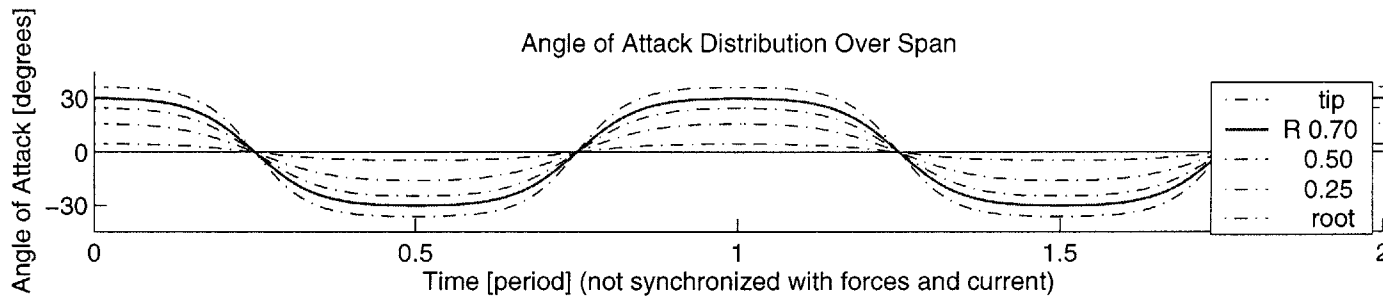
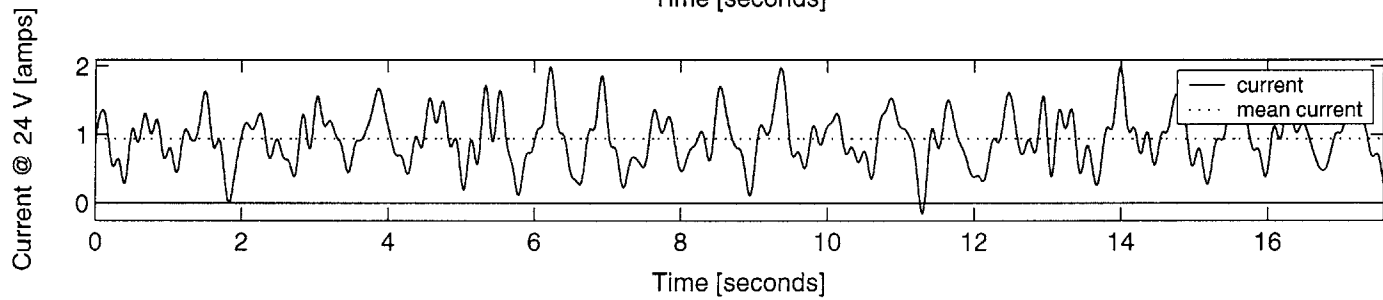
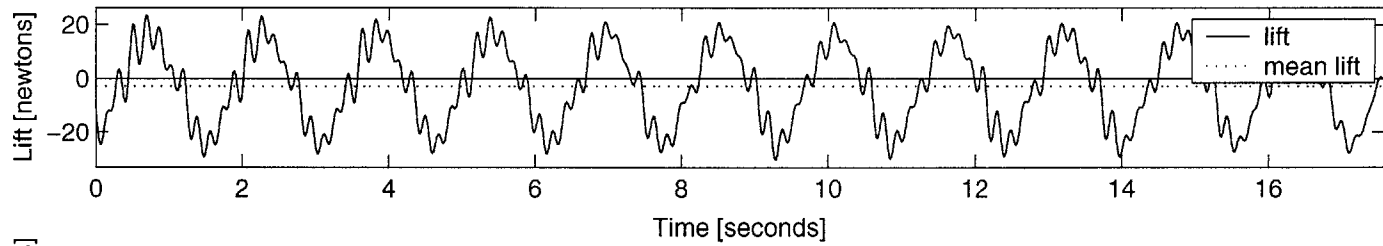
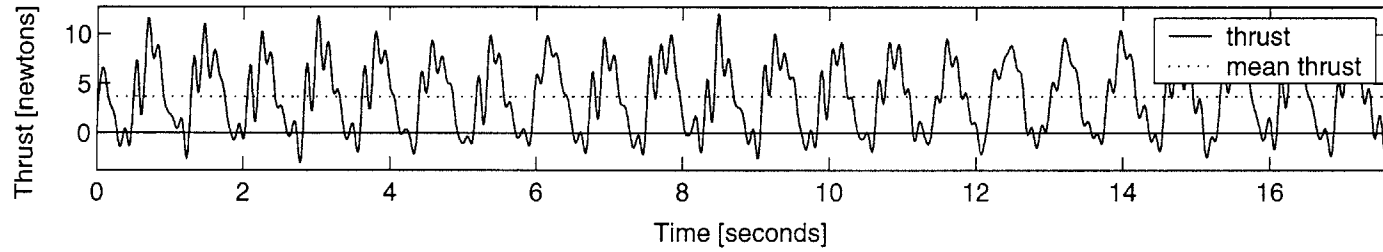
INPUT: U 0.5 [m/s], span 0.40 [m], chord 0.10 [m], roll 20 [deg], St 0.40, MaxAoa 50 [deg], run1 OUTPUT: Ct 0.2, efficiency 0.02



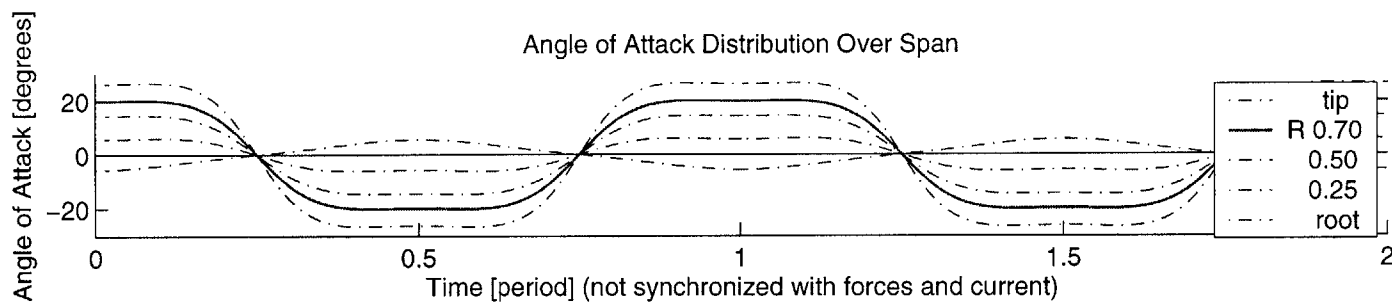
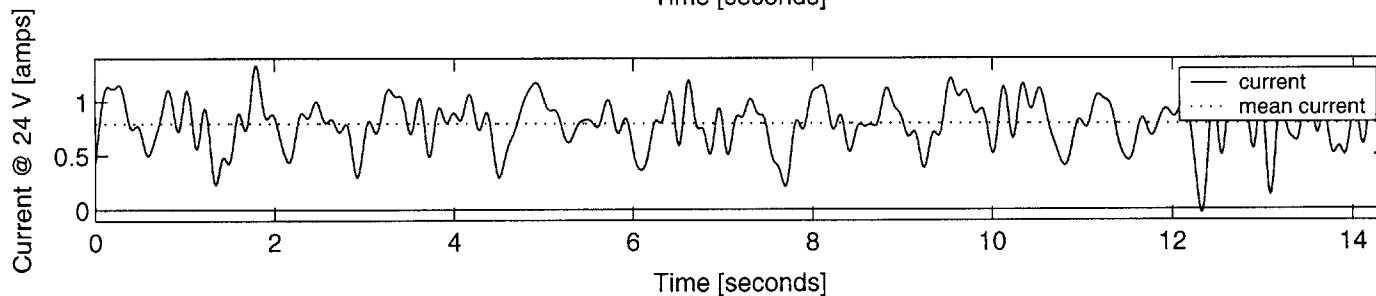
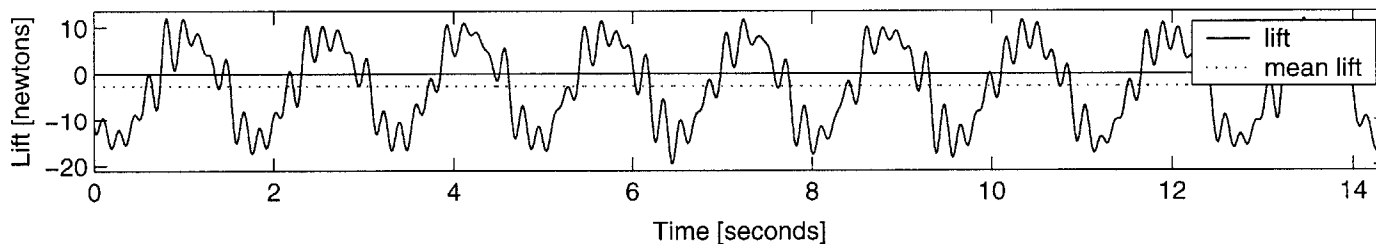
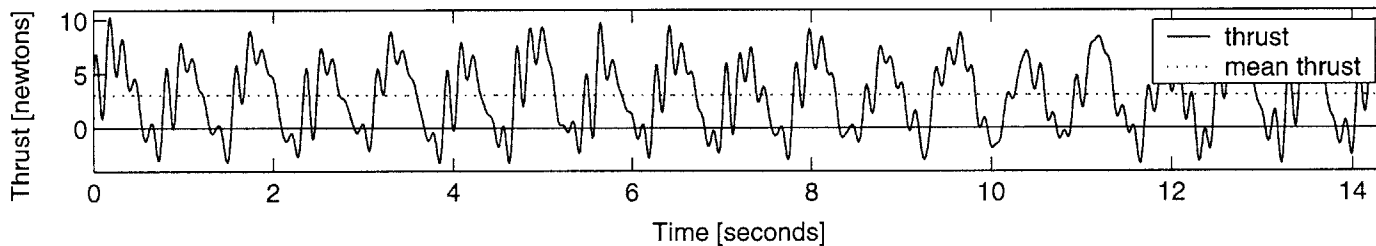
INPUT: U 0.5 [m/s], span 0.40 [m], chord 0.10 [m], roll 20 [deg], St 0.40, MaxAoa 40 [deg], run1 OUTPUT: Ct 0.5, efficiency 0.05



INPUT: U 0.5 [m/s], span 0.40 [m], chord 0.10 [m], roll 20 [deg], St 0.40, MaxAoa 30 [deg], run1 OUTPUT: Ct 0.7, efficiency 0.08

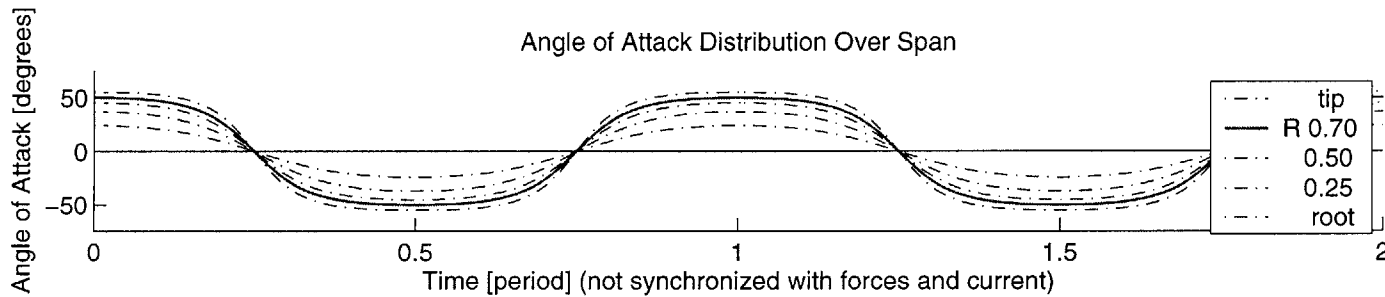
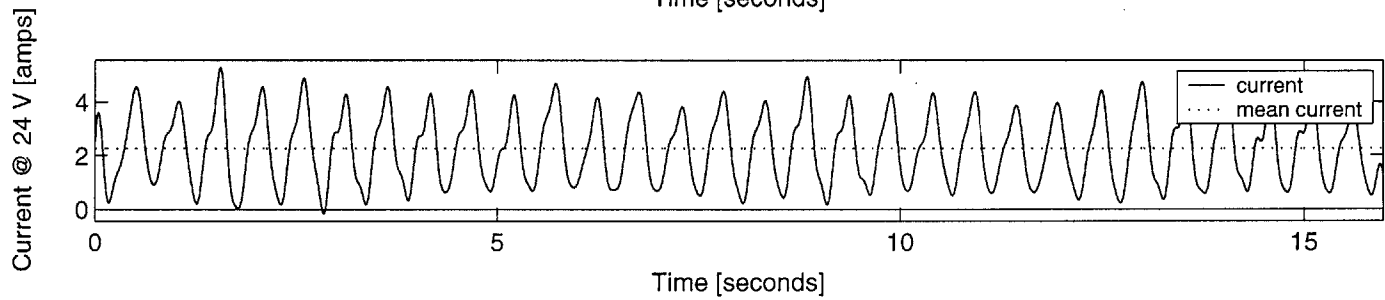
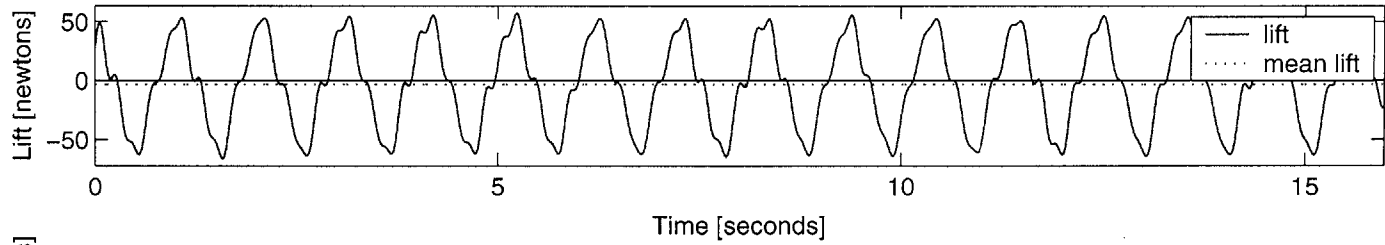
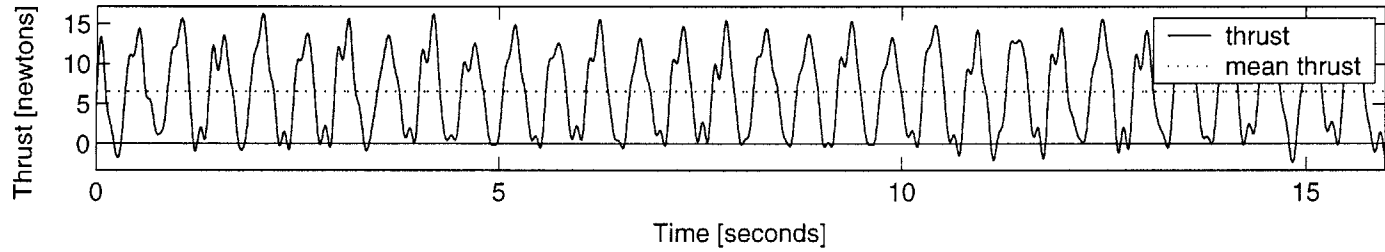


INPUT: U 0.5 [m/s], span 0.40 [m], chord 0.10 [m], roll 20 [deg], St 0.40, MaxAoa 20 [deg], run1 OUTPUT: Ct 0.6, efficiency 0.08

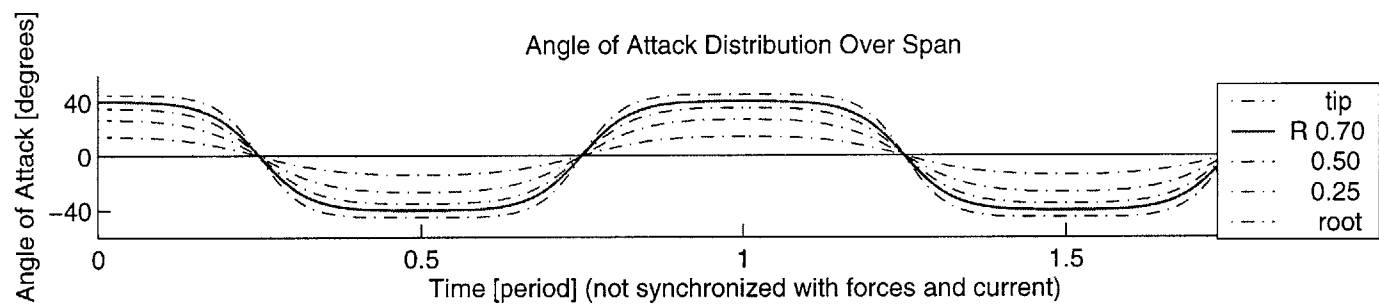
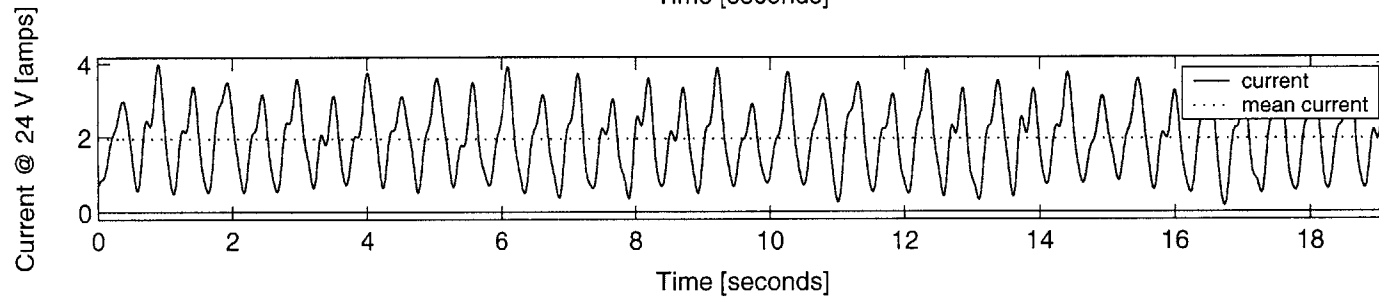
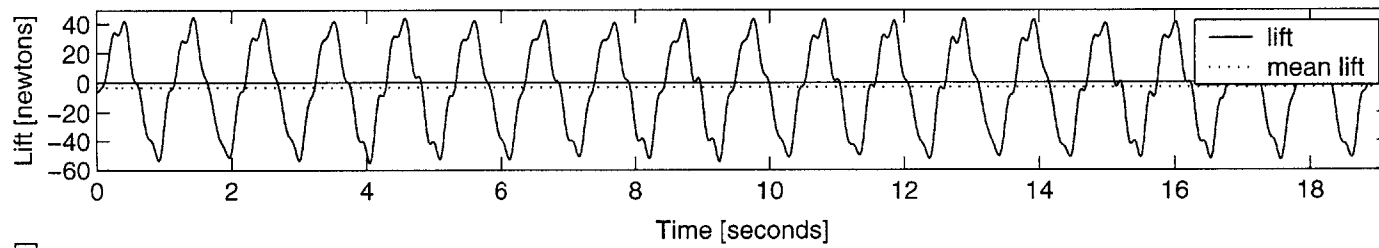
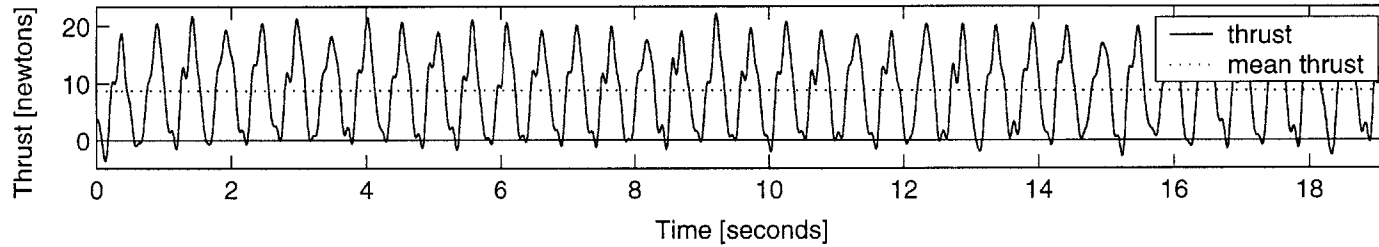




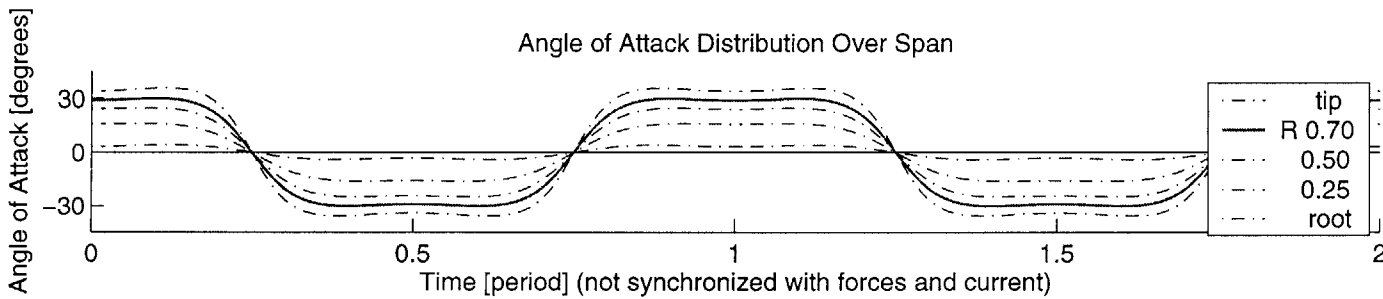
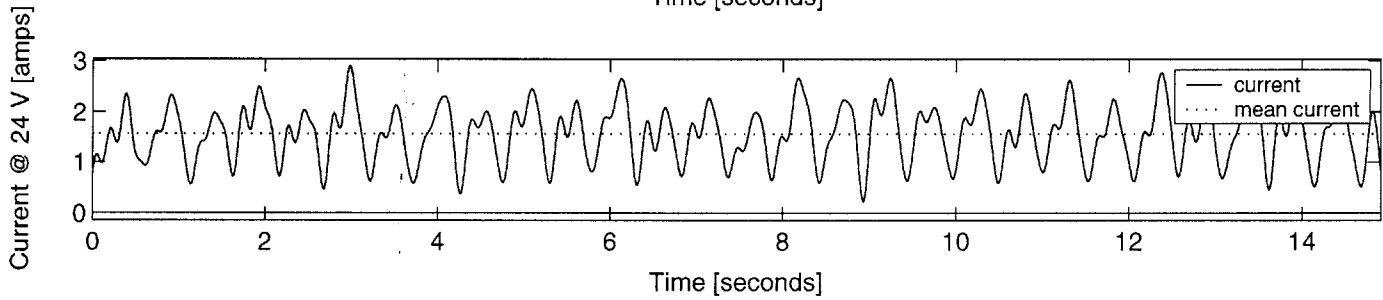
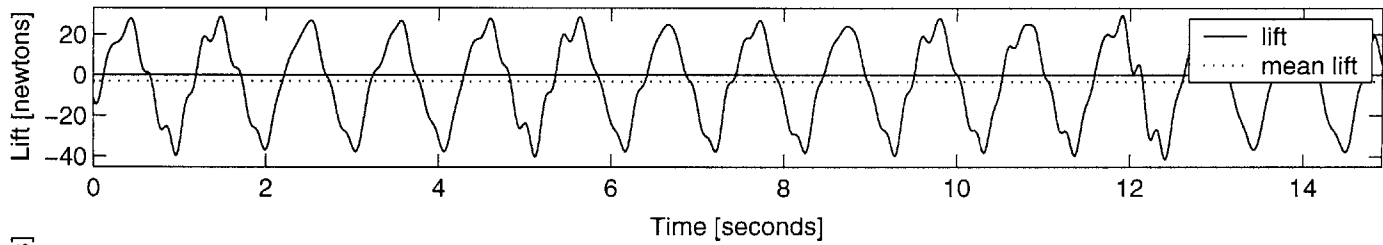
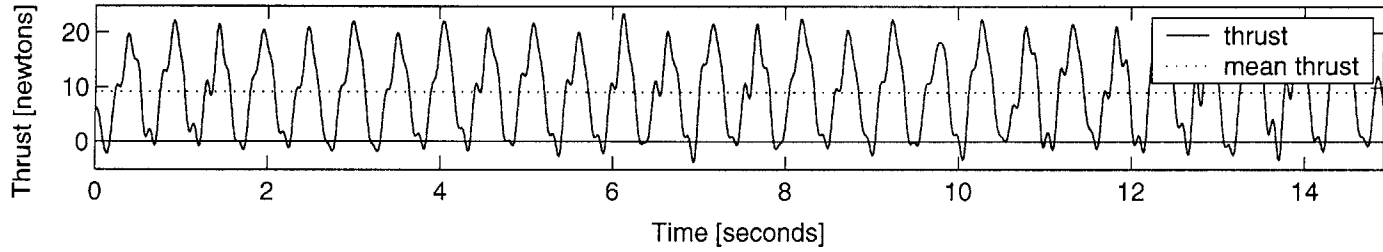
INPUT: U 0.5 [m/s], span 0.40 [m], chord 0.10 [m], roll 20 [deg], St 0.60, MaxAoa 50 [deg], run1 OUTPUT: Ct 1.3, efficiency 0.06



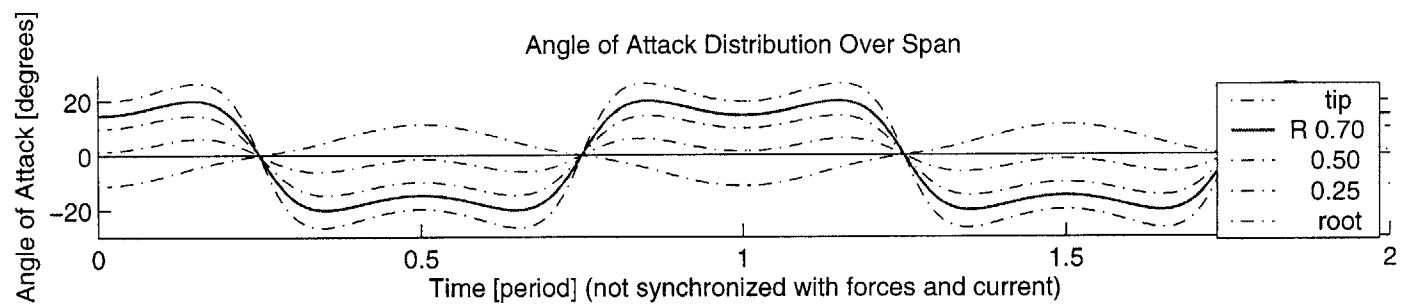
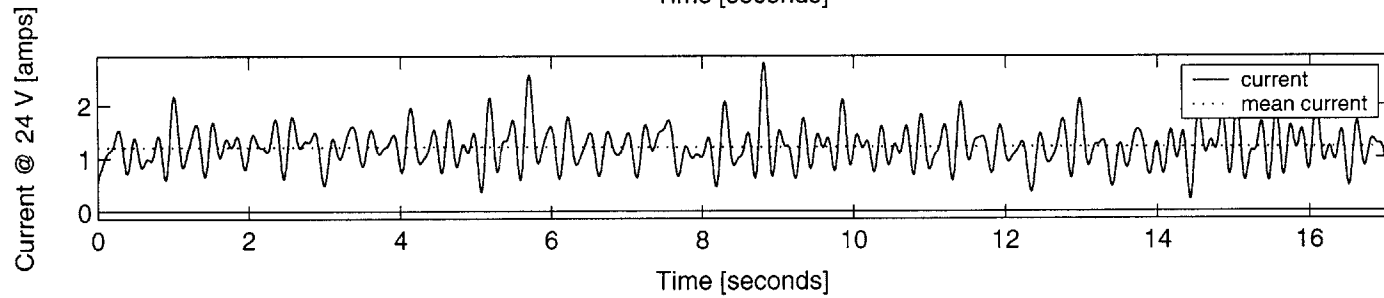
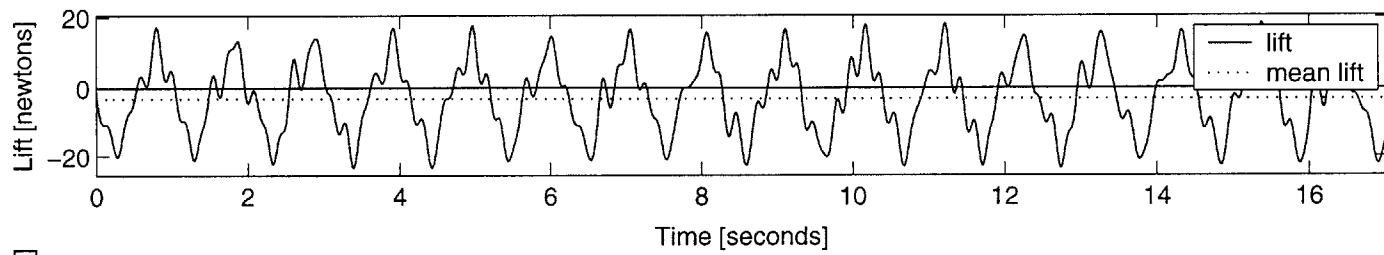
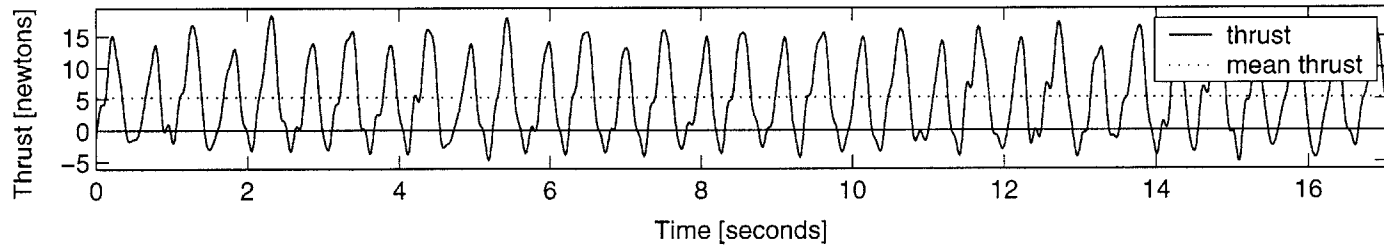
INPUT: U 0.5 [m/s], span 0.40 [m], chord 0.10 [m], roll 20 [deg], St 0.60, MaxAoa 40 [deg], run1 OUTPUT: Ct 1.8, efficiency 0.09



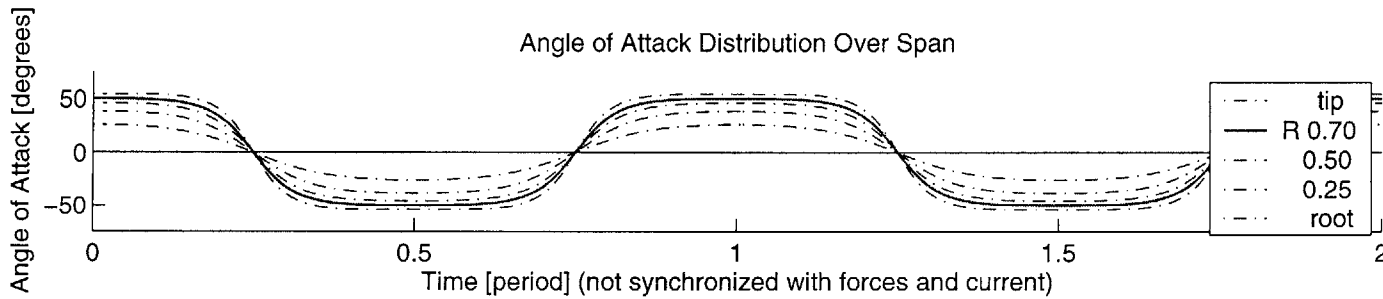
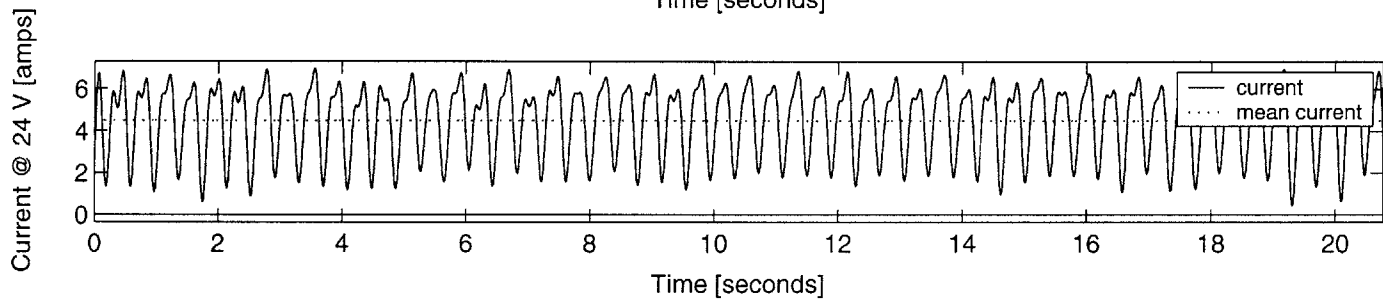
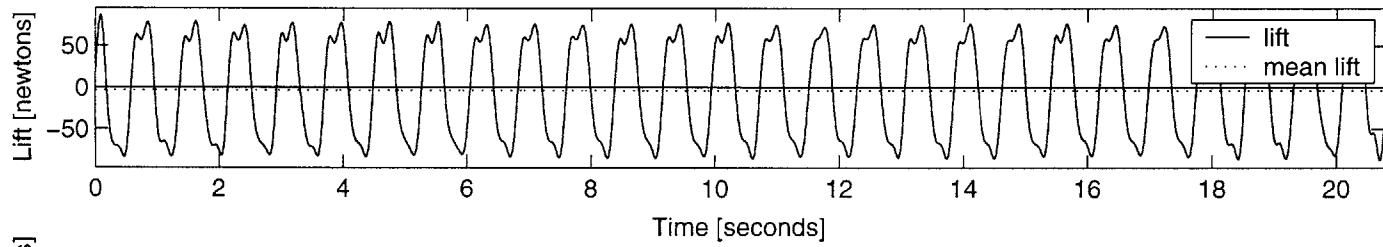
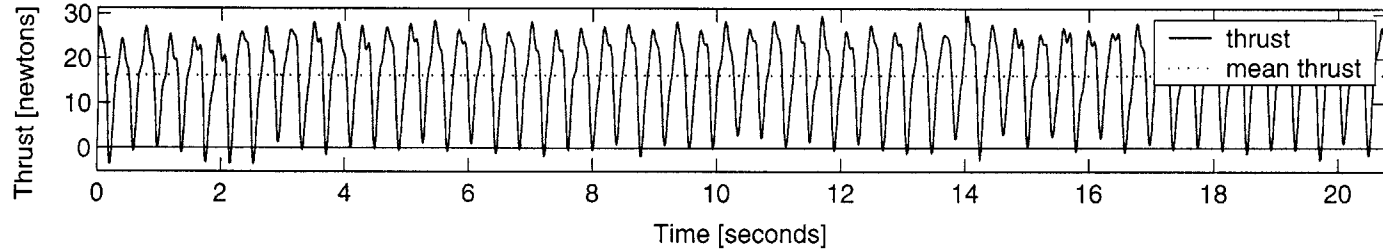
INPUT: U 0.5 [m/s], span 0.40 [m], chord 0.10 [m], roll 20 [deg], St 0.60, MaxAoa 30 [deg], run1 OUTPUT: Ct 1.8, efficiency 0.12



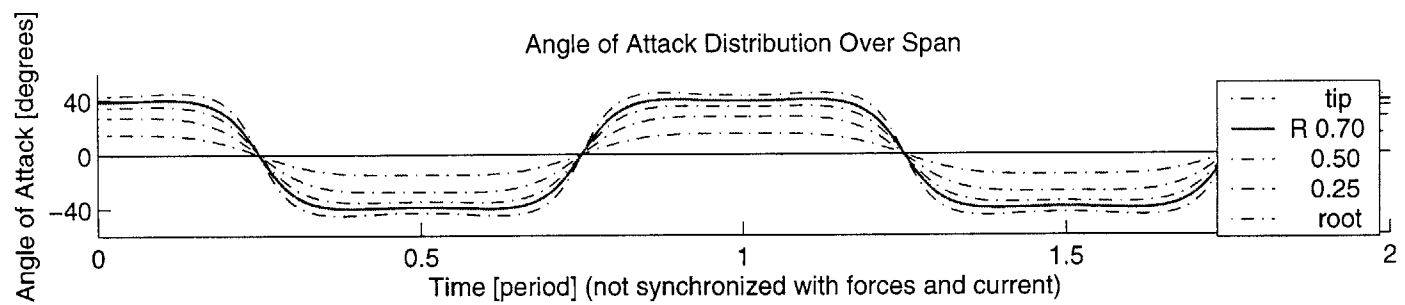
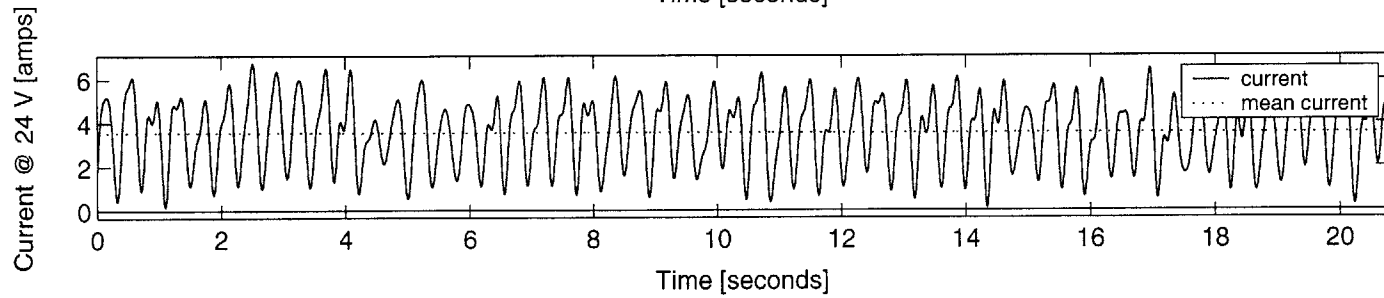
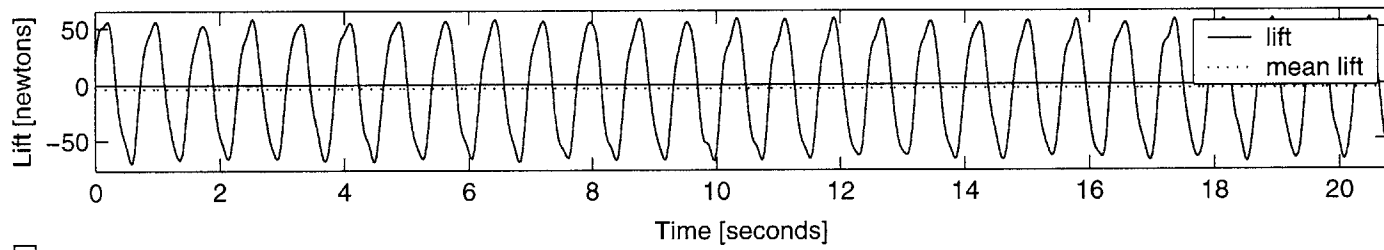
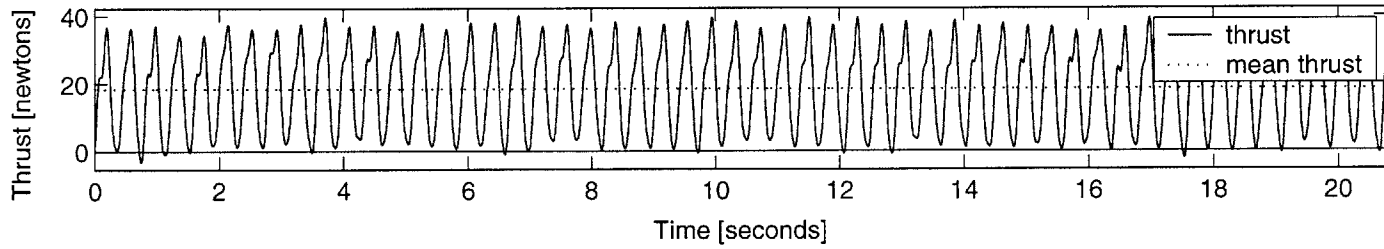
INPUT: U 0.5 [m/s], span 0.40 [m], chord 0.10 [m], roll 20 [deg], St 0.60, MaxAoa 20 [deg], run1 OUTPUT: Ct 1.1, efficiency 0.09



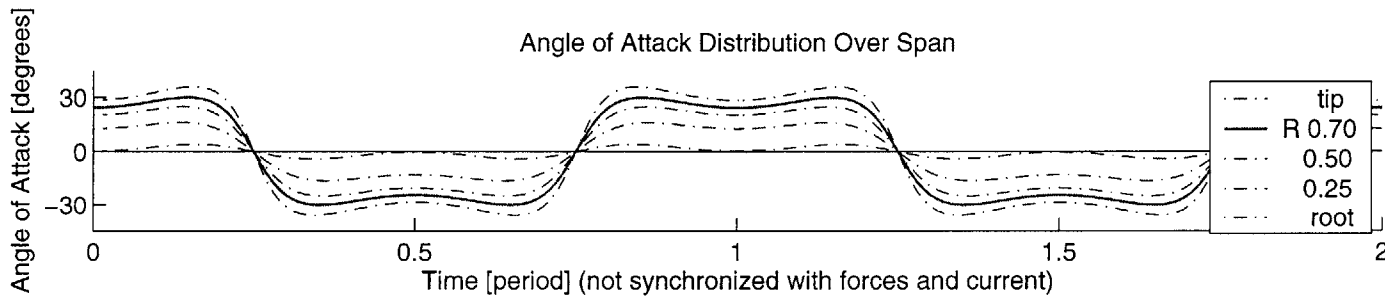
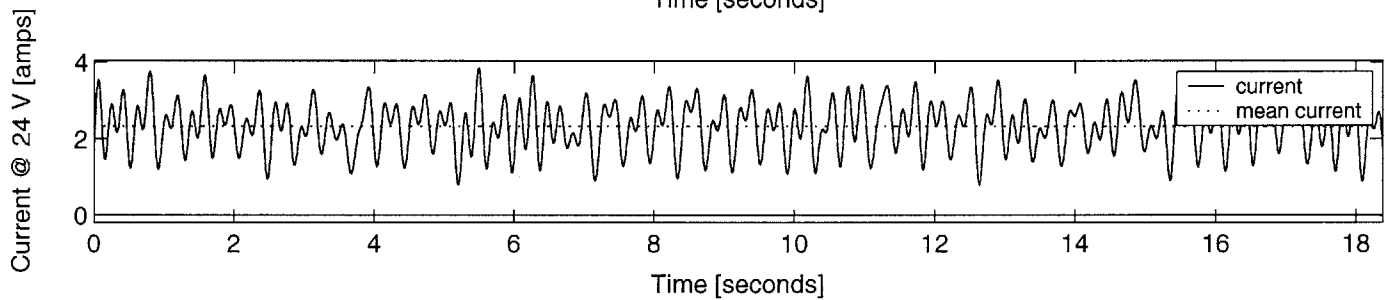
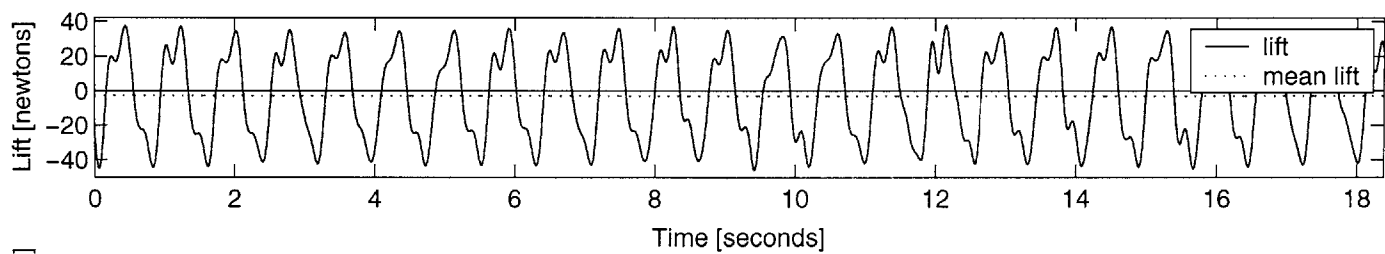
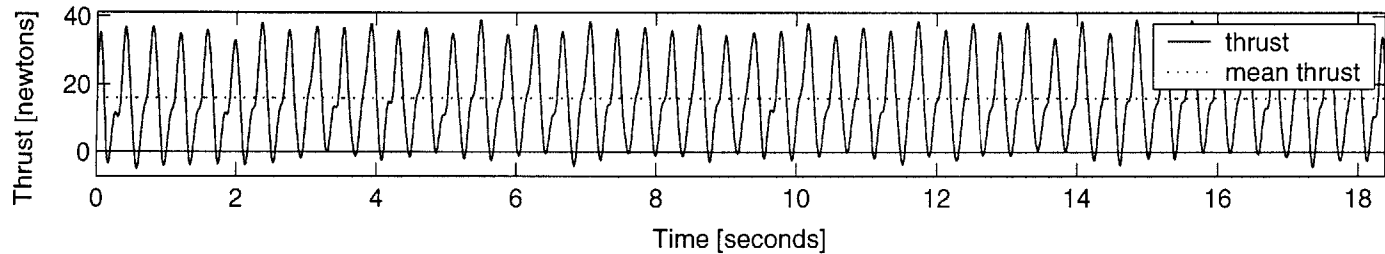
INPUT: U 0.5 [m/s], span 0.40 [m], chord 0.10 [m], roll 20 [deg], St 0.80, MaxAoa 50 [deg], run1 OUTPUT: Ct 3.2, efficiency 0.07



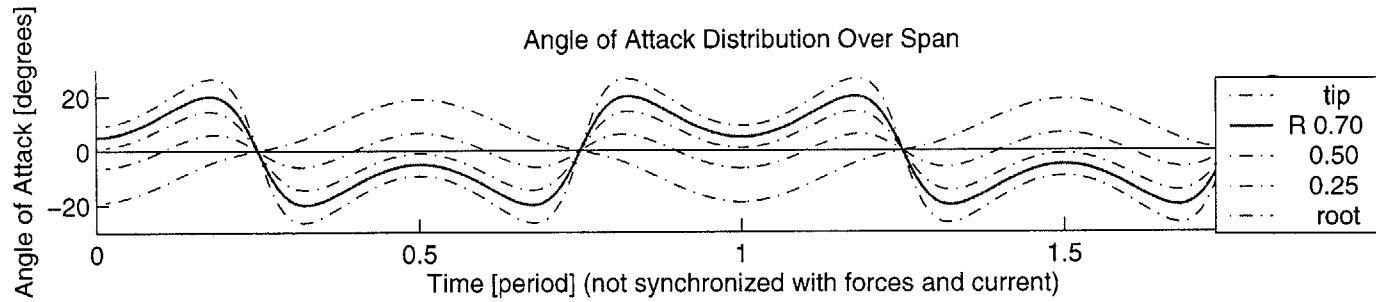
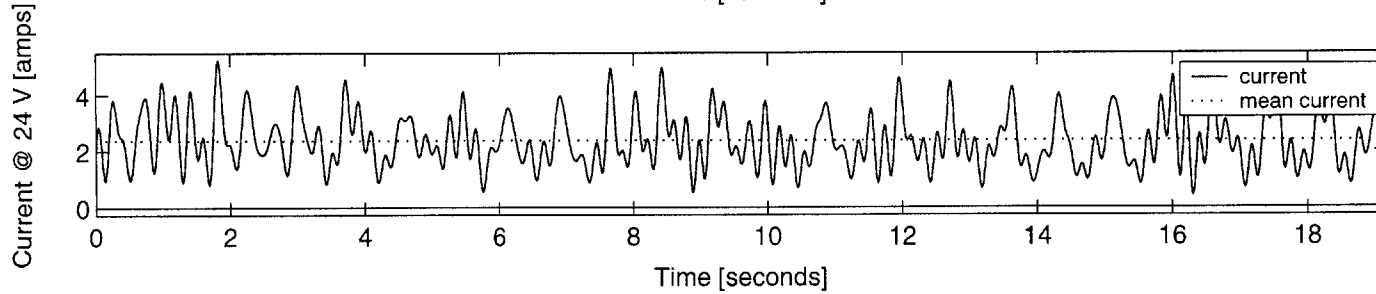
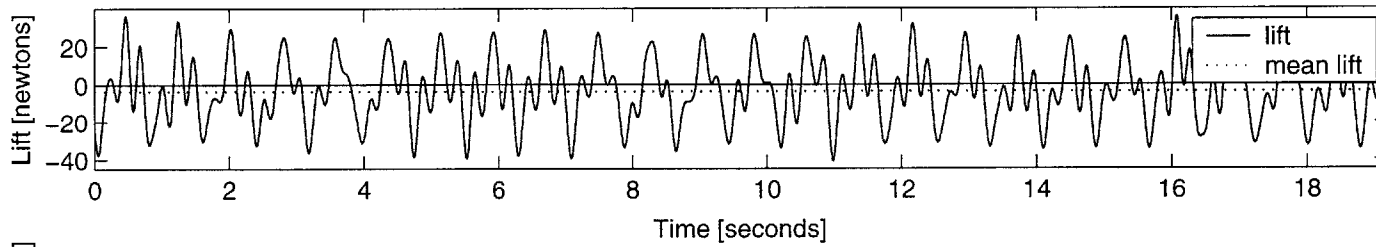
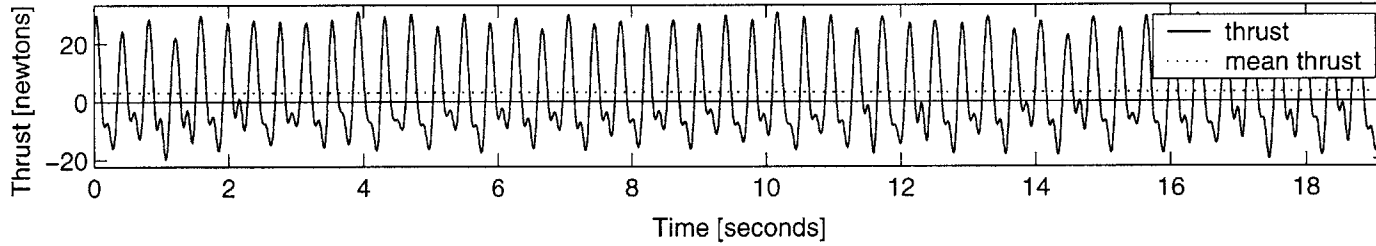
INPUT: U 0.5 [m/s], span 0.40 [m], chord 0.10 [m], roll 20 [deg], St 0.80, MaxAoa 40 [deg], run1 OUTPUT: Ct 3.7, efficiency 0.11



INPUT: U 0.5 [m/s], span 0.40 [m], chord 0.10 [m], roll 20 [deg], St 0.80, MaxAoa 30 [deg], run1 OUTPUT: Ct 3.2, efficiency 0.14



INPUT: U 0.5 [m/s], span 0.40 [m], chord 0.10 [m], roll 20 [deg], St 0.80, MaxAoa 20 [deg], run1 OUTPUT: Ct 0.6, efficiency 0.03





# Bibliography

- [1] I. L. Jones A. Balmford, A. L. R. Thomas. Aerodynamics and the evolution of long tails in birds. *Nature*, 361:628–631, 1993.
- [2] J. M. Anderson. *Vorticity Control for Efficient Propulsion*. PhD thesis, M.I.T., Cambridge, MA, 1996.
- [3] J. M. Anderson and N. K. Chhabra. Maneuvering and stability performance of a robotic tuna. *Integrative and Comparative Biology*, 42:118–126, 2002.
- [4] J. M. Anderson, K. Streitlien, D. S. Barrett, and M. S. Triantafyllou. Oscillating foils of high propulsive efficiency. *Journal of Fluid Mechanics*, 360:41–72, 1998.
- [5] P. R. Bandyopadhyay, J. M. Castano, J. Q. Rice, R. B. Phillips, W. H. Nedderman, and W. K. Macy. Low-speed maneuvering hydrodynamics of fish and small underwater vehicles. *Journal of Fluids Engineering*, 119:136–144, 1997.
- [6] D. S. Barrett. The design of a flexible hull undersea vehicle propelled by an oscillating foil. Master’s thesis, M.I.T., Cambridge, MA, 1994.
- [7] D. S. Barrett. *Propulsive Efficiency of a Flexible Hull Underwater Vehicle*. PhD thesis, M.I.T., Cambridge, MA, 1996.
- [8] D. N. Beal. *Propulsion Through Wake Synchronization Using a Flapping Foil*. PhD thesis, M.I.T., Cambridge, MA, 2003.
- [9] P. Domenici and R. W. Blake. *Biomechanics in Animal Behavior Chapter 1: Biomechanics in Behaviour*. BIOS Scientific Publishers Limited, Oxford, 2000.

- [10] F. E. Fish. Power output and propulsive efficiency of swimming bottlenose dolphins. *Journal of Experimental Biology*, 185:179–193, 1993.
- [11] Melissa Flores. Flapping motion of a three-dimensional foil for propulsion and maneuvering of underwater vehicles. Master’s thesis, M.I.T., Cambridge, MA, 2003.
- [12] P. Freymuth. Propulsive vortical signature of plunging and pitching airfoils. *AIAA*, 26:881–882, 1988.
- [13] Crawford H. Greenewalt. Dimensional relationships for flying animals. *Smithsonian Miscellaneous Collections*, 144(2), 1962.
- [14] Øyvind Haugstadal. Motion control of oscillating foils for steady propulsion and starting maneuvers. Master’s thesis, M.I.T., Cambridge, MA, 2000.
- [15] Michael V. Jakuba. Design and fabrication of a flexible hull for a bio-mimetic swimming apparatus. Bachelor’s thesis, M.I.T., Cambridge, MA, 2000.
- [16] Naomi Kato. Control performance in horizontal plane of fish robot with mechanical pectoral fins. *IEEE Journal of Oceanic Engineering*, 25(1), 2000.
- [17] J. M. Kumph. The design of a free swimming robot pike. Bachelor’s thesis, M.I.T., Cambridge, MA, 1996.
- [18] James C. Liao, David N. Beal, George V. Lauder, and Michael S. Triantafyllou. The Kármán gait: novel body kinematics of rainbow trout swimming in a vortex street. *Journal of Experimental Biology*, 206:1059–1073, 2003.
- [19] M. J. Lighthill. Aquatic animal propulsion of high hydromechanical efficiency. *J. Fluid Mechanics*, 44:265–301, 1970.
- [20] C. B. Martin. Design and performance evaluation of a biomimetic flapping foil. Master’s thesis, M.I.T., Cambridge, MA, 2001.
- [21] D. A. Read. Oscillating foils for propulsion and maneuvering of ships and underwater vehicles. Master’s thesis, M.I.T., Cambridge, MA, 2000.

- [22] Michael Sachinis. Pressure sensing of vorticity on the new robotuna. June 2000.
- [23] M. S. Triantafyllou and G. S. Triantafyllou. An efficient swimming machine. *Scientific American*, 272(3):64–70, March 1995.
- [24] M. S. Triantafyllou, G. S. Triantafyllou, and D. K. P. Yue. Hydrodynamics of fishlike swimming. *Annual Review of Fluid Mechanics*, 32:33–53, 2000.
- [25] John J. Videler. *Fish Swimming*. Chapman & Hall, London, 1993.
- [26] J. M. Wakeling and C. P. Ellington. Dragonfly flight: 2. velocities, accelerations and kinematics of flapping flight. *The Journal of Experimental Biology*, 200:557–582, 1997.
- [27] J. M. Wakeling and C. P. Ellington. Dragonfly flight: 3. lift and power requirements. *The Journal of Experimental Biology*, 200:583–600, 1997.